

Doctorate Program in Molecular
Oncology and Endocrinology
Doctorate School in Molecular
Medicine

XXIV cycle - 2008–2011
Coordinator: Prof. Massimo Santoro

**“New possible applications for
aptamers in targeted anti-
cancer therapies”**

Margherita Iaboni

Università degli Studi di Napoli Federico II
Dipartimento di Medicina Molecolare e Biotecnologie
Mediche

Administrative Location

Università degli Studi di Napoli Federico II
Dipartimento di Medicina Molecolare e Biotecnologie Mediche

Partner Institutions

Italian Institutions

Università degli Studi di Napoli “Federico II”, Naples, Italy
Istituto di Endocrinologia ed Oncologia Sperimentale “G. Salvatore”, CNR,
Naples, Italy
Seconda Università di Napoli, Naples, Italy
Università degli Studi di Napoli “Parthenope”, Naples, Italy
Università degli Studi del Sannio, Benevento, Italy
Università degli Studi di Genova, Genova, Italy
Università degli Studi di Padova, Padova, Italy
Università degli Studi “Magna Graecia”, Catanzaro, Italy
Università degli Studi di Udine, Udine, Italy

Foreign Institutions

Université Libre de Bruxelles, Bruxelles, Belgium
Universidade Federal de Sao Paulo, Brazil
University of Turku, Turku, Finland
Université Paris Sud XI, Paris, France
University of Madras, Chennai, India
University Pavol Jozef Šafárik, Kosice, Slovakia
Universidad Autonoma de Madrid, Centro de Investigaciones Oncologicas
(CNIO), Spain
Johns Hopkins School of Medicine, Baltimore, MD, USA
Johns Hopkins Krieger School of Arts and Sciences, Baltimore, MD, USA
National Institutes of Health, Bethesda, MD, USA
Ohio State University, Columbus, OH, USA
Albert Einstein College of Medicine of Yeshiwa University, N.Y., USA

Supporting Institutions

Dipartimento di Biologia e Patologia Cellulare e Molecolare “L. Califano”,
Università degli Studi di Napoli “Federico II”, Naples, Italy
Istituto di Endocrinologia ed Oncologia Sperimentale “G. Salvatore”, CNR,
Naples, Italy
Istituto Superiore di Oncologia, Italy

Italian Faculty

Salvatore Maria Aloj	Paolo Laccetti
Francesco Saverio Ambesi	Antonio Leonardi
Impiombato	Paolo Emidio Macchia
Francesco Beguinot	Barbara Majello
Maria Teresa Berlingieri	Rosa Marina Melillo
Bernadette Biondi	Claudia Miele
Francesca Carlomagno	Nunzia Montuori
Gabriella Castoria	Roberto Pacelli
Maria Domenica Castellone	Giuseppe Palumbo
Angela Celetti	Maria Giovanna Pierantoni
Lorenzo Chiariotti	Rosario Pivonello
Annamaria Cirafici	Giuseppe Portella
Annamaria Colao	Maria Fiammetta Romano
Sabino De Placido	Giuliana Salvatore
Gabriella De Vita	Massimo Santoro
Monica Fedele	Giampaolo Tortora
Pietro Formisano	Donatella Tramontano
Alfredo Fusco	Giancarlo Troncone
Domenico Grieco	Giancarlo Vecchio,
Michele Grieco	Giuseppe Viglietto
Maddalena Illario	Mario Vitale

**“New possible
applications for
aptamers in targeted
anti-cancer therapies”**

TABLE OF CONTENTS

LIST OF PUBLICATIONS	4
ABSTRACT	5
1. BACKGROUND	6
1.1 Cancer	6
1.2 Aptamers	7
1.2.1 SELEX Method	9
1.2.2 Post-SELEX modifications	12
1.2.3 Internalizing Aptamers	12
1.2.4 Molecular Chimeras	14
1.3 MicroRNAs	16
1.3.1 Role of microRNAs	18
1.3.2 MicroRNAs en route to the clinic	20
1.4 Breast cancer	22
1.4.1 Stem cells and cancer stem cells	24
1.4.2 Characterization of mammary stem cells	25
1.4.3 Clinical implications for “Cancer Stem Cell Hypothesis”	27
2. AIM OF THE STUDY	29
3. MATERIALS AND METHODS	30
3.1 Cell culture and transfection	30
3.3 Whole-Cell SELEX	30
3.3 RT-PCR, mutagenic and non-mutagenic PCR for cell-SELEX	31
3.4 Illumina sequencing	32
3.4.1 Illumina sequencing sample preparation	32
3.4.2 Illumina sequencing data processing	32
3.5 Chimeras treatment	33
3.6 Binding and internalization assays	33
3.7 Protein isolation and Western blotting	34
3.8 RNA extraction and RealTime-PCR	34
3.9 Proliferation assay and cell death quantification	35
4. RESULTS	36
4.1 AIM-1	36
4.1.1 Characterization of breast cancer stem cells (BCSCs) and breast cancer cells (BCCs)	36

4.1.2 Enrichment of selection for a complex target	38
4.1.3 Selection of the most enriched sequences	41
4.2 AIM-2	43
4.2.1 Selection of internalizing aptamers	43
4.2.2 Binding and internalization capability of GL21-miR212 chimeras	45
4.2.3 GL21-miR212 (2g) targets PED protein	47
4.2.4 GL21-miR212 (2g) inhibits cell viability	49
4.2.5 GL21-miR212 (2g) regulates TRAIL-induced cell death	50
5. DISCUSSION	52
6. CONCLUSIONS	58
ACKNOWLEDGEMENTS	59
REFERENCES	60

LIST OF PUBLICATIONS

This dissertation is based upon the following publications:

1) Incoronato MR, Garofalo M, Urso L, Romano G, Quintavalle C, Zanca C, **Iaboni M**, Nuovo G, Croce CM and Condorelli G. miR-212 increases TRAIL sensitivity in non-small cell lung cancer by targeting the anti-apoptotic protein PED. *Cancer Research* 2010;70(9):3638-46.

2) Quintavalle C, Incoronato MR, Puca L, Acunzo M, Zanca C, Romano G, Garofalo M, **Iaboni M**, Croce CM and Condorelli G. c-FLIPL enhances anti-apoptotic Akt functions by modulation of Gsk3 β activity. *Cell Death and differentiation* 2010;17(12):1908-16.

3) Quintavalle C, Garofalo M, Zanca C, Romano G, **Iaboni M**, del Basso De Caro M, Martinez-Montero JC, Incoronato M, Nuovo G, Croce CM, Condorelli G. miR-221/222 overexpression in human glioblastoma increase invasiveness by targeting the protein phosphates PTP μ . *Oncogene* 2011;31(7):858-68

4) Quintavalle C, Donnarumma E, **Iaboni M**, Roscigno G, Garofalo M, Romano G, Fiore D, De Marinis P, Croce CM, Condorelli G. Effect of miR-21 and miR-30b/c on TRAIL-induced apoptosis in glioma cells. *Oncogene* 2012. [Epub ahead of print]

5) Bettazzi F, Hamid-Asl E, Esposito CL, Quintavalle C, Formisano N, Laschi S, Catuogno S, **Iaboni M**, Marrazza G, Mascini M, Cerchia L, De Franciscis V, Condorelli G, Palchetti I. Electrochemical detection of miRNA-222 by use of a magnetic bead-based bioassay. *Anal Bioanal Chem.* 2013;405(2-3):1025-34.

ABSTRACT

In order of reducing the frequency of unwanted side effects of chemotherapy and recurrences in cancer, in the last ten years a major challenge has been the development of methods for the specific targeting to cancer cells. Aptamers are single-stranded RNAs able to form different three-dimensional structures, which allows them to specifically recognize their molecular targets. This makes aptamers attractive agents for targeted cancer therapy. Aptamers were first utilized for their ability to bind and inhibit the activity of their target protein, including extracellular ligands and cell surface proteins. More recently, aptamers were also used as delivery agents. Thanks to their ability to be endocytosed, aptamers may specifically bring a therapeutic cargo inside the cells.

In this thesis, I focused on different aspects regarding the aptamer-mediated targeting of cancer cells: 1) the selection of aptamers for a cancer stem cells-targeted therapy. In fact, as widely recognized, cancer stem cells are responsible for tumor recurrence, repopulating the tumor after a chemotherapeutic treatment. 2) The formation of aptamer-microRNA chimera molecules in which the aptamer is the delivery vehicle for a microRNA. The use of microRNAs represent a challenging approach in cancer therapy because they are able to regulate the expression of cellular proteins modulating different pathways. However, to date the absence of reliable means that permit the specific delivery of microRNAs to the appropriate tissue represents an obstacle to the success of this approach.

For the first purpose, I performed for the first time a SELEX (Systematic Evolution of Ligands by EXponential enrichment) method on human breast cancer stem cells, using in the counterselection step breast cancer differentiated cells. I selected putative aptamers specific for the stemness phenotype in breast cancer, useful to identify specific cell-surface targets, block molecular pathways and delivery therapeutics. For the second purpose, I selected an internalizing aptamer, GL21, that specifically binds to Axl receptor, overexpressed in many types of cancer cells. I linked this aptamer to miR-212. This microRNA is considered a tumour-suppressor miR because negatively regulates the anti-apoptotic protein PED found overexpressed in many tumors and involved in resistance to therapeutics. In A549 cells, TRAIL-resistant non-small cell lung cancer cells overexpressing Axl, this chimera was able to enter within the cells and carry the microRNA to the processing machinery. MiR-212, subsequently, targeted PED resulting in TRAIL sensitization.

In conclusion, in this thesis I studied new possible applications for aptamers aimed at avoiding therapeutic recurrences and at delivering “therapeutic” RNAs, as microRNAs, to the appropriate cells.

1. BACKGROUND

1.1 Cancer

Cancer is thought to reflect a multi-step process, resulting from an accumulation of inherited and or acquired defects in genes involved in the regulation of cell proliferation.

The development of a clinically recognizable human cancer may require the activation or inactivation of as many as four or five different genes.

Changes in the expression of key proteins of the cellular signaling pathways are the major molecular abnormalities found in cancer. In fact, an increasing number of proteins involved in cell growth, including growth factors, receptors, intracellular mediators and transcription factors have been found to be altered through multiple mechanisms of oncogene activation, such as enhanced or ectopic expression, deletions, single point mutations and generation of chimeric proteins, formed by chromosomal translocations.

Among these, many cell surface receptors with an intrinsic intracellular tyrosine kinase activity can act as oncogenes and cause cellular transformation (Kolibaba and Druker 1997).

Therefore, as major molecular determinants of cancer cells, all these proteins represent primary targets in the rational approach of the cancer mechanisms.

For this purpose, different types of molecules have been shown to be of potential utility for cancer diagnosis and therapy, including small chemical compounds, peptides, antibodies and nucleic acid ligands.

1.2 Aptamers

For a long time nucleic acids were mainly considered as linear carriers of information, whereas most cell functions were ascribed to protein molecules possessing complex three-dimensional structure.

It was found that single-stranded RNA molecules are able to form very different three-dimensional structures, which allows them to recognize specifically various molecular targets. They were called aptamers.

The term aptamer is derived from the Latin word “*aptus*”—which means fitting (Ellington and Szostak 1990) and the Greek word “*meros*” meaning particle.

Aptamers are short single-stranded nucleic acid oligomers (ssDNA or RNA) with a specific and complex three-dimensional shape characterized by stems, loops, bulges, hairpins, pseudoknots, triplexes, or quadruplexes. Based on their three-dimensional structures, aptamers can well-fittingly bind to a wide variety of targets from single molecules to complex target mixtures or whole organisms. Binding of the aptamer to the target results from structure compatibility, stacking of aromatic rings, electrostatic and van der Waals interactions, and hydrogen bindings, or from a combination of these effects (Hermann and Patel 2000).

The concept that nucleic acid ligands could modulate the activity of target proteins emerged from basic science studies of viruses. In the 1980s, research on HIV and adenovirus discovered that these viruses encode several small, structured RNAs that bind to viral or cellular proteins with high affinity and specificity. The observation that viruses utilize RNA ligands for their ends suggested to translational researchers in the late 1980s that RNA ligands might also be useful for therapeutic ends (Nimjee et al. 2005).

Aptamers realize their inhibiting function on a completely different mechanism with respect to miRNA and siRNA. Antisense, ribozymes, siRNAs, miRNAs recognize the target nucleic acid by complementary base pairing and, by activating an intracellular molecular machinery, impair the expression of the corresponding protein. Instead, aptamers act directly binding the target without interfering with its expression (Cerchia and de Franciscis 2006) (Fig.1).

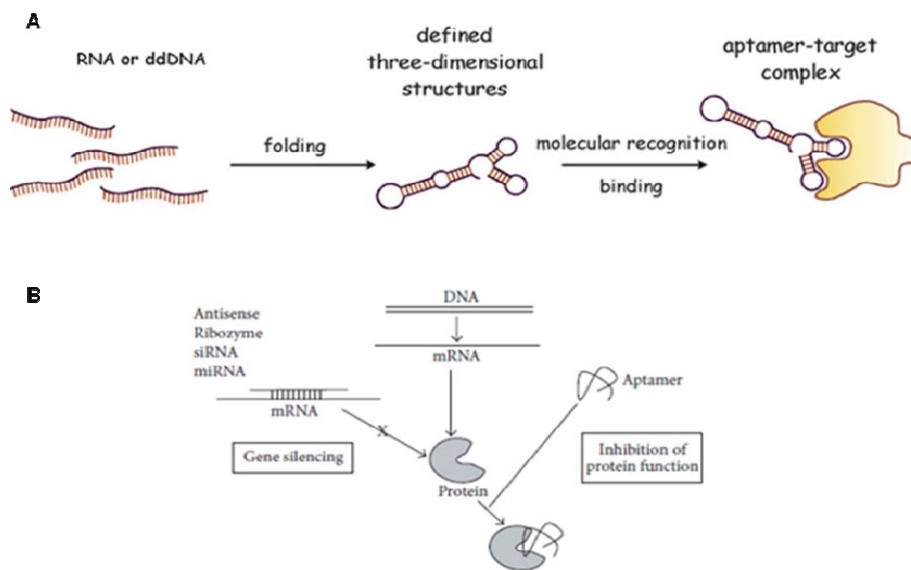


Fig.1: Aptamer functionality. A) Schematic representation of aptamer three dimensional structure and functionality and B) its mechanism of action compared to that of other ncRNAs.

Amongst drugs used for molecular targeting, monoclonal antibodies have made tremendous contributions in a wide range of applications. However, there are certain limitations associated with antibodies; monoclonal antibodies generally are incapable of membrane penetration due to larger size and hence are not ideal as carriers for targeted delivery of cytotoxic molecules inside the cells. Moreover, production of monoclonal antibodies is laborious, expensive, time consuming and suffers from batch-to-batch variations. They are also immunogenic, temperature sensitive, and their target binding kinetics cannot be easily modified.

Aptamers, generally considered being oligonucleotides analogous to antibodies, rival antibodies in many ways. These short, single stranded DNA/RNA molecules fold to form unique tertiary structures, allowing them to bind to target proteins with high specificity and affinity, often leading to modulation of the target protein activity. Aptamers generally range in size from 20 to 80 bases (6–26 kDa) which makes them larger than peptides but smaller than antibody fragments (scFv, Fab). Their small size enables them to access protein epitopes that might otherwise be inaccessible to bulky antibodies. It is also the small size, that provides aptamer a better chance of internalization than the antibodies, although this is possible only when it is bound to a target protein that undergoes internalization or the target is a cell surface receptor, to which it might act as a ligand. This feature allows aptamer to be used as

bifunctional ligands that, along with recognition, can also be employed as delivery vehicles. Once identified, aptamers can be chemically synthesized and stabilized to have a consistent structure-activity with little immunogenicity. These molecules are highly temperature-resistant and are stable over long term storage. Their targeted binding properties can be controlled and modified as desired, and the molecules can be derivatized easily for downstream applications (Fig.2). Due to these advantages, aptamers gained immediate attention for clinical development, and shortly after the advent of the technology, a substantial number of aptamers entered clinical trials for a wide range of applications (Dua et al 2011).

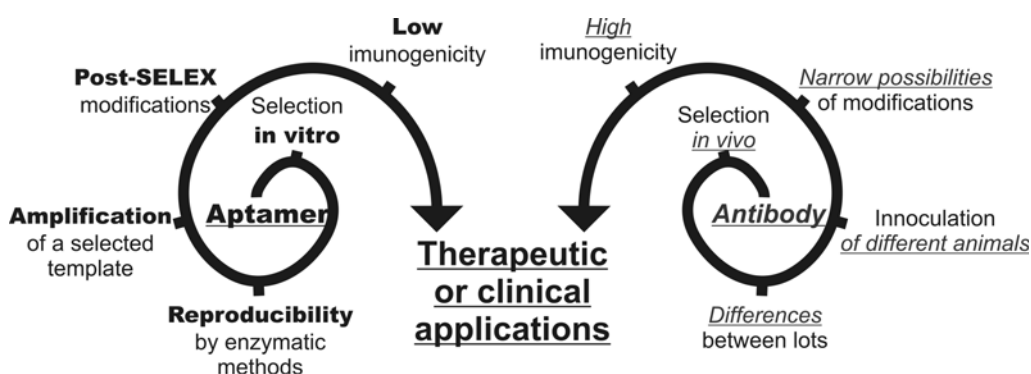


Fig.2: Comparison between aptamer and antibody features.

1.2.1 SELEX Method

The identification of nucleic acid sequences with unique properties from a random pool of sequences is achieved through iterative cycles of in vitro selection called SELEX (Systematic Evolution of Ligands by EXponential enrichment). The process was independently developed in 1990 by Larry Gold and Jack Szostak (Ellington and Szostak 1990; Tuerk and Gold 1990).

The starting material for the SELEX process is a DNA library obtained from combinatorial chemical synthesis. The library usually consists of random regions of 20–80 nucleotides (nt), flanked by defined constant 50 and 30 regions, 18–20 nt long. The complexity of the library and its molecular diversity is characterized by the length of the random region, providing each individual oligonucleotide with a unique sequence. A starting complexity of 10^{14} – 10^{15} is generally considered to be appropriate. A library containing 25 nt randomized nucleotides ($4^{25} = 10^{15}$) reaches the highest possible limit of

sequence diversity available for screening in a SELEX experiment. Further, all known single stranded oligonucleotide motifs can be built within this length. This suggests that libraries with short randomized regions are sufficient for a successful aptamer selection. Short libraries are better manageable, cost effective in chemical synthesis and involve lesser post-SELEX optimizations. However, longer randomized regions could provide greater structural complexity to the library and better opportunities for the identification of aptamers. The fixed region has a promoter region for T7/SP6 RNA polymerase and primers for reverse transcription (RT) and polymerase chain reaction (PCR). This DNA library is the basic starting material for selecting RNA/DNA/ ssDNA/chemically modified aptamers. High affinity aptamers have been successfully generated from both DNA-SELEX and RNA-SELEX. The initial double-stranded oligonucleotide library is converted into single-stranded DNA (ssDNA) (in the case of DNA-SELEX) or transcribed to RNA via in vitro transcription (in the case of RNA-SELEX) (Fig.3).

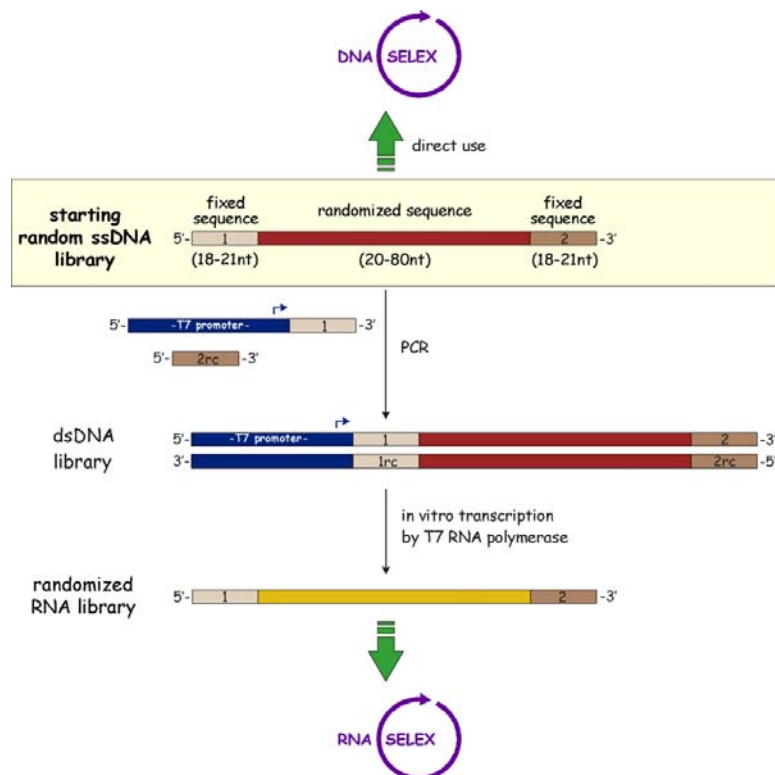


Fig.3: Starting random DNA oligonucleotide library. The two fixed sequences, termed 1 and 2, act as primer binding sites in the PCR. Two special primers are needed for the PCR. The antisense primer, termed 2rc, is reverse complementary to the fixed sequence at 3'-end of the library. The sense primer, termed T7 promoter-1, is derived from the fixed sequence at the 5'-end and is modified by an extension containing the T7promoter sequence.

The pool of random single stranded molecules is allowed to adopt secondary structures and is then incubated with the target protein in a binding buffer at an appropriate temperature. In the initial binding step, only a very small fraction of the pool will bind to the target, which is separated from the unbound fraction through a suitable partitioning technique.

The target-bound aptamers are isolated and amplified using PCR (or RT-PCR in the case of RNA-SELEX) to obtain an enriched pool, which is then used for the next round of SELEX. This repetitive selection/amplification cycle results in selective enrichment of sequences that physically interact with the target in high affinity. The enrichment efficiencies of the binders are governed by the stringency of selection, which can be obtained using suitable competitors during incubation, limiting target concentration, and by increasing the stringencies of the post-incubation washes.

The progress of binder enrichment during SELEX can be monitored using binding assays.

After reiterating these steps (the number of rounds of selection necessary is determined by both the type of library used as well as by the specific enrichment achieved per selection cycle), the resulting oligonucleotides are subjected to DNA sequencing. The sequences corresponding to the initially variable region of the library are screened for conserved sequences and structural elements indicative of potential binding sites and, subsequently, tested for their ability to bind specifically to the target molecule.

Initially the SELEX method was focused on purified membrane proteins to identify cell surface targets, but the selection was done in not-physiological conditions. A modification of the traditional SELEX procedure is cell-SELEX, in which whole live cells are used as targets, aim at generating aptamers able to discriminate within the same tumor between two strictly related phenotype (Cerchia et al. 2009) and to discovery unknown targets that could be used as biomarkers. Compared with the traditional SELEX method using a single target protein, cell-SELEX usually requires more selection cycles (>20) and longer processing times for efficient enrichment of an aptamer population.

Unlike SELEX with purified targets, cell-SELEX faces a major problem of the selection of ligands that recognize multiple surface proteins along with the target of interest. To avoid the parallel selection of aptamers for unintended targets, 'Counter-SELEX' or 'negative selection' is critical. It consists in a previous step on cells with different characteristics compared to the goal of the selection. Non-bound sequences from the negative step are added to the target, and the selection proceeds as usual.

1.2.2 Post-SELEX modifications

Aptamers generated by the different SELEX schemes have many limitations for direct use in downstream applications. Natural, unmodified oligonucleotides, especially RNAs, are unstable in biological fluids. To protect RNA from digestion by nucleases, chemically modified nucleotides are incorporated into the oligonucleotide backbone. Various modifications at the 2'-carbon of the ribose sugar have been shown to render RNA resistant to nucleases. The endonucleases that target RNA in biological fluids are generally specific for pyrimidines; therefore, the introduction of modified pyrimidine residues is sufficient to stabilize it towards nucleases. The most commonly employed functional group modifications are 2'-F, OMe, or NH₂ modifications of the pyrimidine nucleotides, all of which can be introduced at either the pre- or post-SELEX step.

Even with extensive nucleotide modifications to hinder nuclease attack, aptamers can be cleared from the circulation within minutes (Hicke et al. 2006). To increase the plasma half-lives of these molecules, it is important to increase aptamer size via conjugation with bulky groups. While several strategies have been attempted, including tagging with cholesterol (Rusconi et al. 2002) and attachment to liposomes (Willis et al. 1998), most efforts have concentrated on covalent conjugation with polyethylene glycol (PEG) (Farokhzad et al. 2004). PEGylation has been shown to significantly improve the serum half-lives of aptamers without substantially affecting their binding affinities.

1.2.3 Internalizing Aptamers

The negatively charged phosphate backbone of the nucleic acid molecule is the primary cause for its inadequate and inefficient cellular association, owing to electrostatic repulsion from the negatively charged cell surface. Moreover, oligonucleotides longer than 25 bases are difficult to import into cells because of their size and predisposition to self-hybridize (Patil et al. 2005). Though efforts have been made to incorporate aptamers into liposome vesicles (Mann and Dzaou 2000) or other delivery vector systems (Chaloin et al. 2002; Good et al. 1997), it is highly desirable, augmenting the cell-specific aptamer selections described above, to select aptamers that not only recognize a cell, but also are endocytosed.

In literature, are described few exceptions of internalizing aptamers, between these: DNA anti-PTK7 aptamer (Xiao et al. 2008) and RNA aptamers against

PSMA (Lupold et al. 2002), CD4 (Zhou Q et al. 2012) and HIV gp120 (Khati et al. 2003).

Another published internalizing RNA aptamer is GL21. It emerged from a whole cell-SELEX on U87MG cells, a malignant human glioma cell line, using in the counter-selection step less malignant human T98G glioma cells. Cerchia et al. (2009) found that GL21 aptamer is able to bind and inhibits the signaling of Axl receptor, belonging to the TAM family of tyrosine kinase receptors (RTKs) that also includes Sky (Tyro3, Dtk) and Mer. They are characterized by an extracellular domain consisting of two immunoglobulin-like domains followed by two fibronectin type 3-like domains. Axl-family members are activated by Growth-arrest-specific gene 6 (Gas6), a member of the vitamin K-dependent protein family that resembles blood coagulation factors rather than typical growth factors (Fig.4).

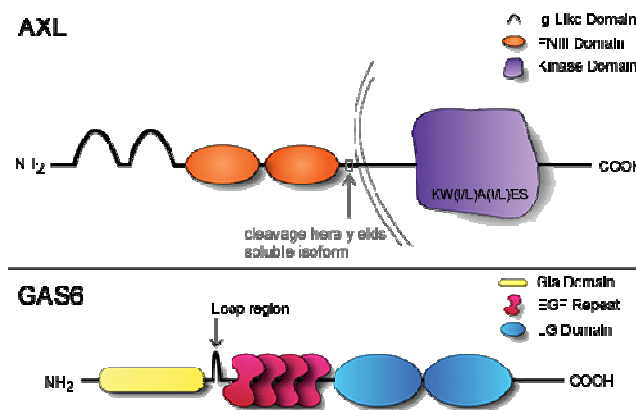


Fig.4: Axl receptor and Gas6 structures.

Axl overexpression has been reported in many human cancers and is associated with invasiveness and/or metastasis in lung (Shieh et al. 2005), prostate (Sainaghi et al. 2005), breast (Zhang et al. 2008), gastric (Wu et al. 2002) and pancreatic cancers (Koorstra et al. 2009), renal cell carcinoma (Chung et al. 2003) as well as glioblastoma (Hutterer et al. 2008). Furthermore, by a phosphoproteomic approach based on the profiling of phosphotyrosine signaling, activated Axl protein was detected in ~5% primary tumors of non-small-cell lung cancer (Rikova et al. 2007). Using a rational approach based on its predicted secondary structure they designed a 34-mer truncated version of the 92-mer original molecule, named GL21.T, which contains the active site of GL21 and preserves high binding affinity to the U87MG cells. Determining the cell type specificity, GL21.T didn't bind other human cancer cell types including neuroblastoma, lung and breast without Axl receptor, while bound A549 cells, a non-small cell lung cancer (NSCLC) cell line, that, instead, presents the receptor on the cellular surface. It is also able to be endocytosed

into target cells, getting ~30% of cell internalization following 15-minute incubation and reached ~60% following 2 hours of aptamer treatment (Cerchia et al. 2012).

1.2.4 Molecular Chimeras

Instead of directly interrupting a disease process, as would do a function-blocking aptamer, endocytosed aptamers could work as delivery agents into cells. They were called by Hicke et al. “escort aptamers” (Hicke and Stephens 2000). Escort aptamers have been successfully adapted for the targeted delivery of active drug substances both in vitro and in vivo, including anti-cancer drugs, toxins, enzymes, radionuclides, virus, and siRNAs. The cargoes are attached to the aptamers either through their assembly with functionalized groups linked to the aptamer and cargos, or through direct conjugation to the aptamer, creating a molecular chimera, as in the case of oligonucleotides (Zhou and Rossi 2010.).

Aptamer-mediated targeted delivery can enhance the therapeutic efficacy and reduce the toxic effects of drugs.

The three RNA aptamers above-named have been exploited for the creation of a molecular chimera for siRNA delivery (Fig.5).

1) Anti-PSMA RNA aptamer-mediated RNAi

Three independent groups have successfully employed the anti-PSMA RNA aptamers to specifically deliver siRNAs to target cells.

- In Chu et al. work (2006) two biotinylated siRNAs and two aptamers were non-covalently assembled via a streptavidin platform.
- Giangrande and colleagues conjugated the RNA aptamer to the sense strand of the siRNA followed by annealing of the complementary siRNA sense strand to complete the chimeric molecule (McNamara et al. 2006). In a subsequently work they inverted sense and antisense strands. A 2 nucleotide (UU)-overhang and a polyethylene glycol tail were added to the 3'-end of the guide strand and to the 5'-end of passenger strand, respectively (Dassie et al. 2009).
- Wullner et al. (2008) generated bivalent anti-PSMA aptamer-siRNA chimera using the siRNA itself as a linker to join the two aptamers.

2) Anti-CD4 RNA aptamer-mediated RNAi

In which the anti-CD4 aptamer or siRNAs were non-covalently joined via phi29 RNAs (ncRNA molecules of the bacteriophage phi29) containing complementary loop domains. Two pRNA molecules were respectively fused with siRNAs and the anti-CD4 aptamer. Through the interaction of right and left interlocking loops, the two chimeric pRNAs could precisely dimerized into a stable nanovector of approximately 25 nm in diameter (Guo et al. 2005).

3) Anti-gp120 RNA aptamer-mediated RNAi

27-mer Dicer substrate RNA duplex and the aptamer were attached with complementary 'sticky' sequence. After a simple annealing, they formed stable base pairs (Zhou et al 2009).

In this design format, one pair of complementary GC-rich sticky bridge sequences was chemically attached to the 3' end of the aptamer. The complement to this sequence was attached to one of the two siRNA strands and the aptamer and siRNA were joined by Watson-Crick base pairing. A flexible three-carbon atom hinge (C3) was added as a spacer between the adhesive (sticky) sequence and the aptamer to allow spatial and structural flexibility. Importantly, this sticky bridge-based strategy can be used to facilitate the effective interchange of different siRNAs with a single aptamer, which is required to avoid viral resistance to the siRNA component.

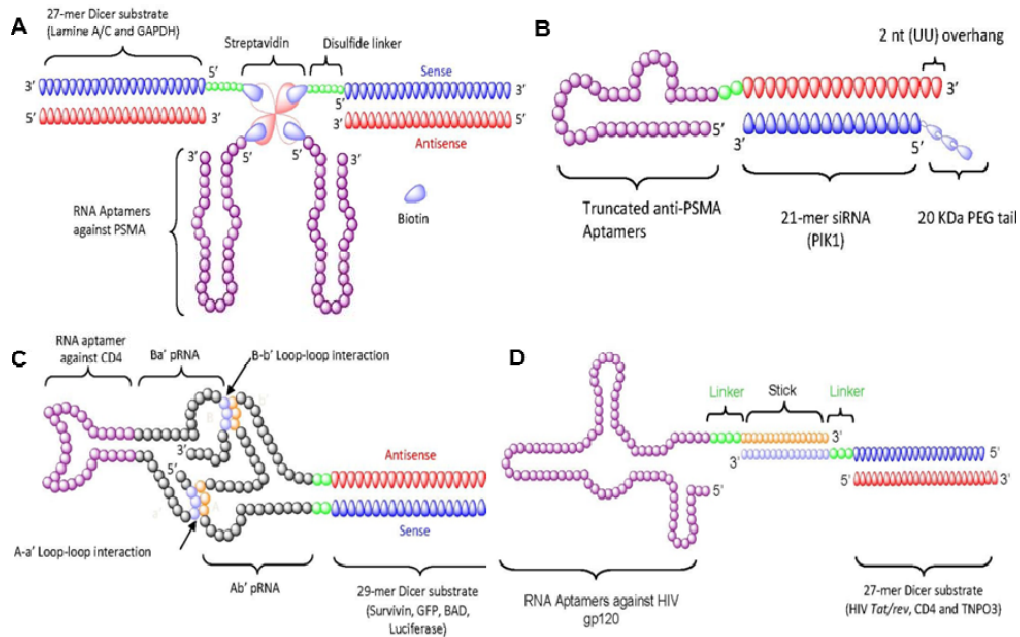


Fig.5: Representations of molecular chimeras: A) Anti-PSMA RNA aptamer-mediated RNAi (Chu et al.); B) Anti-PSMA RNA aptamer-mediated RNAi (Dassie et al.); C) Anti-CD4 RNA aptamer-mediated RNAi; D) Anti-gp120 RNA aptamer-mediated RNAi.

1.3 MicroRNAs

Short non coding RNAs, as small interfering RNAs and microRNAs, for their ability to inhibit the expression of complementary RNA transcripts are being exploited as a new class of therapeutics for a variety of diseases.

Since their discovery nearly two decades ago, microRNAs (miRNAs, miRs) have been one of the most investigated families of molecules. In fact, a recent PubMed search found nearly 18,000 miRNA-related articles in the literature (Nana-Sinkam and Croce 2013).

MicroRNAs (miRNAs) are small non-protein-coding molecules that regulate gene expression by a post-translational repression mechanism. MiRNAs are members of a family of small RNAs, typically 19-30 nucleotides, which includes small nuclear RNA (snRNA) involved in mRNA splicing, small nucleolar RNA (snoRNA) which direct modification of ribosomal RNA and short interfering RNA (siRNA) produced from long double-stranded RNA precursors. Similar to miRNA, siRNA also functions to regulate gene expression.

miRNAs are endogenous RNAs highly conserved in the genomes of animals, plants, fungi and viruses. In humans, miRNAs are transcribed as long primary transcripts (pri-miRNA) over 1 kb in size, which have a stem-loop structure, are capped at the 5'-end and have a 3'-poly (A) tail. Pri-miRNA transcripts undergo to a two steps maturation process to produce functional miRNA. The first step occurs in the nucleus and is facilitated by Drosha, an endonuclease RNase III, and the double-stranded RNA-binding domain (dsRBD) protein DGCR8. Drosha cleaves both strands of the pri-miRNA transcript in a staggered manner, producing a stem-loop precursor molecule (pre-miRNA), approximately 70 nucleotides in length.

These pre-miRNA molecules are, then, transported from the nucleus to the cytoplasm, a process mediated by Exportin-5, a nuclear transport receptor, and the nuclear protein Ran-GTP.

The final processing step is facilitated by the RNA III enzyme Dicer and a dsRBD protein TRBP, which cuts both strands of the pre-miRNA at the base of the stem-loop. This produces a duplex molecule approximately 22 nucleotides long. The duplex molecule contains the single-stranded mature miRNA and a fragment termed miRNA*, which is derived from the opposite complementary arm of the pre-miRNA. The miRNA: miRNA* molecule is then incorporated into a large protein effector complex called the RNA-induced silencing complex (RISC). The RISC is activated upon unwinding of the miRNA: miRNA* duplex. The miRNA* strand is subsequently degraded, whilst the miRNA molecule guides the RISC complex to the target mRNA. It is the interaction of the miRNA/RISC and its target mRNA that results in gene regulation.

The interaction between a miRNA and its target is restricted to the 5'-end of the miRNA. Sequence complementarity between nucleotides 2-8 is vital for target sequence recognition. The degree of complementarity between the 3'-UTR region of the target mRNA and this so called "seed region" in the 5'-end of the miRNA determines the mechanism by which the miRNA regulates the target. If the miRNA bears sufficient sequence complementarity (near perfect) to the target mRNA, then regulation is carried out by a process called RNA interference, in which the RISC complex is directed to cleave the target mRNA.

If there is insufficient complementarity, which is generally the case in mammals, regulation is achieved by repression of translation, the exact mechanism of which is still under debate (Lynam-Lennon et al. 2009) (Fig.6).

To date, at least six models of translational repression have been proposed: (i) RISC induces deadenylation which causes decrease of translational efficiency by blocking target mRNA circularization; (ii) RISC blocks cap function by interacting with either the cap or eIF4E; (iii) RISC blocks a late step in initiation of translation such as recruitment of 60S ribosomal subunit; (iv) RISC blocks a post-initiation step such as elongation and/or ribosome drop-off; (v) RISC induces proteolysis of nascent peptides during translation; or (vi) RISC recruits target mRNAs to processing bodies, in which mRNA is degraded and/or stored in a translationally inactive state. These models do not necessarily exclude each other (Kwak et al 2010).

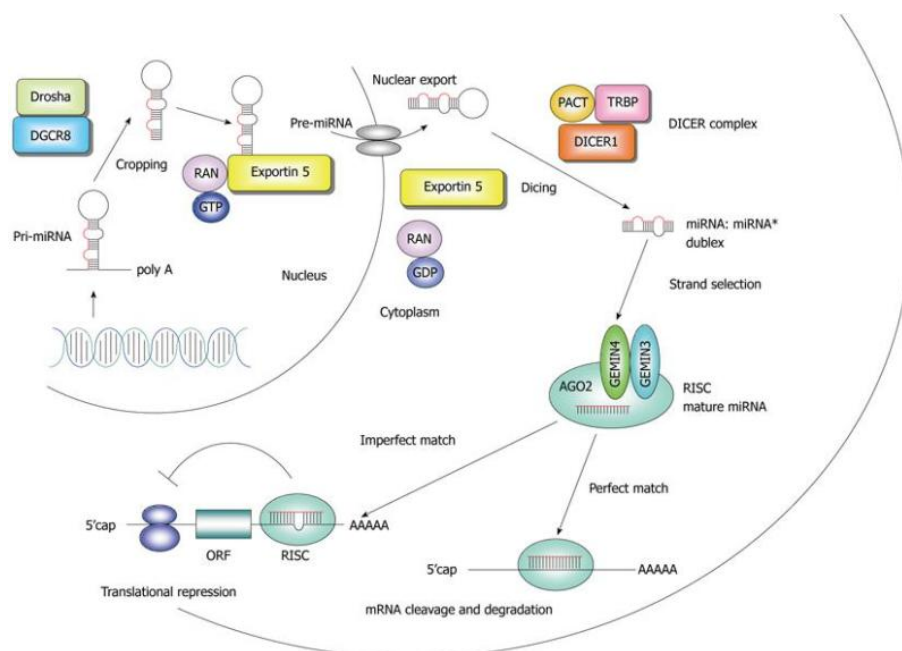


Fig.6: MiRNA biogenesis and mechanisms of gene expression regulation.

MiRNA regulation appears to be an extremely dynamic process. Since the perfect complementarity to the target is not required for regulation, a single miRNA can regulate a number of target genes and, inversely, a single gene can be targeted by different miRNAs. This ultimately makes the identification of target genes much more difficult, the result of which is that the functions of many miRNAs are still unknown.

1.3.1 Role of microRNAs

As master gene regulators, miRNAs are able to impact a variety of cellular pathways and functions. Since their discovery in *C.elegans* more than a decade ago (Lee et al. 1993), thousands of miRNAs have been identified to date in a variety of organisms. For example, over 1000 human miRNAs are reported in miRBase version 18 (<http://mirbase.org>) (Mo 2012).

Early studies have shown that miRNAs are critical to developmental timing, cell death, cell proliferation, immunity and patterning of the nervous system. Deregulation of miRNAs can lead to a variety of human disease. Thus, it is critical to understand how miRNAs are regulated in normal cellular processes as well as during disease processes.

The first evidence for miRNA involvement in human cancer came from a study by Calin et al. (2002) examining a recurring deletion (65% of patients) at chromosome 13q14 in the search for a tumor suppressor gene involved in chronic lymphocytic leukemia (CLL). In this study was found that the region of deletion encodes two miRNA: miR-15a and miR-16-1. Subsequent investigations have confirmed the involvement of these two miRNAs in the pathogenesis of CLL (Calin et al. 2005; Cimmino et al. 2005).

To date, a lot of miRNAs have been characterized for their function in cancer. Several experiments and clinic analysis suggest that miRNAs may function as a novel class of oncogenes or tumor suppressor genes. Oncogenic miRNAs, called “oncomirs”, may promote tumor development by negatively inhibiting tumor suppressor genes and/or genes that control cell differentiation or apoptosis. On the other hand, some tumor suppressor miRNAs may prevent tumor development by negatively inhibiting oncogenes and/or genes that control cell differentiation or apoptosis. Their expression is decreased in cancerous cells (Zhang et al. 2007).

The identified mechanisms for this observed alteration include impaired miRNA processing, chromosomal alterations, effects of environmental factors (e.g., cigarette smoke and infection), transcriptional enhancers or repressors, epigenetic regulation, and polymorphisms.

A tumor-suppressor miRNA is miR-212.

It belongs to miR-132/212 family. They are two miRNAs sharing close sequences highly conserved among vertebrates. miR-132 and miR-212 were first reported to be transcribed in rats and in mice from regions in the non-coding transcripts. Similarly to their rodent orthologues, hsa-miR-132 and hsa-miR-212 share the same primary transcript. In addition, in human, they are found in an intergenic region located on chromosome 17p13.3. MiR-132 and miR-212 exhibit similar mature sequences and share the same seed region. They may therefore target the same mRNAs (Wanet et al. 2012).

Regarding its transcriptional regulation, the miR-212/132 locus was first identified in neuronal cells as a target of the cAMP-response element binding (CREB) protein transcription factor. In non-neuronal cells the miR-212/132 locus is under the control of the transcriptional repressor Repressor Element 1 silencing transcription factor/neuron-restrictive silencer factor (REST/NRSF) (Wu and Xie 2006).

Given their involvement in neuronal development and functions, it is not surprising that deregulated expression patterns of miR-132 and miR-212 have been associated with developmental defects as well as brain-related disorders. For example, a down-regulation of miR-212 has been identified in fetuses with anencephaly (Zhang et al. 2010)). Moreover, miR-132 and miR-212 are both deregulated in the prefrontal cortex of individuals affected by schizophrenia and bipolar disorders (Perkins et al. 2007; Kim et al. 2010). MiR-212 was also found to be down-regulated in Alzheimer's disease patients, and its expression modulation correlates with the density of neurofibrillary tangles, a characteristic lesion of Alzheimer's disease (Wang et al. 2011). In the last 5 years, several groups, performing miRNA expression profiling in diverse immune-related contexts, came to highlight the induction of miR-132 (and miR-212) in several cell types including monocytes, macrophages, mast cells and lymphatic endothelial cells. So, besides their numerous roles in neuronal development, functions and related diseases, increasing evidences point towards an important involvement of miR-132 and miR-212 in mediating inflammatory processes. Indeed, miR-132 was recently designated as a 'NeurimmiR', a class of miRNAs regulating both neuronal and immune functions and was suggested to function as a cross-talk between both systems (Soreq and Wolf 2011).

Despite their neurimmiR functions, miR-212/132 are shown to be deregulated in different cancer types. For example, miR-212 down-regulation has been associated with the resistance/bad response to several anti-cancer treatments (Hatakeyama et al. 2010). Other reports suggest that miR-212 would negatively affect gastric cancer cells proliferation (Wada et al. 2009).

In non-small cell lung carcinoma, miR-212 negatively regulates the anti-apoptotic protein PED/PEA15 (Fig.7). PED (Phosphoprotein Enriched in Diabetes) is a death-effector-domain (DED) family member of 15 kDa found overexpressed in a number of different tumors including gliomas, squamous carcinoma, thyroid, breast, lung cancer, and B-cell chronic lymphocytic leukemia. It inhibits the assembly of a functional death-inducing signaling

They are similar to protein-coding genes in that they regulate many survival-signaling pathways, are themselves subject to mutagenesis and often have conflicting roles in various disease states. They differ, however, in their therapeutic potential. In essence, miRNA replacement therapies may do what protein-coding gene replacement therapies have tried to do, but with fewer obstacles to overcome. MiRNA are much smaller and less antigenic than their protein-coding counterparts and, as such, cellular delivery is possible without the use of potentially harmful viral-based delivery mechanisms that are needed for the cellular uptake of larger protein-coding genes.

Likewise, effective tools for systemically silencing miRNAs have been developed, that specifically and safely target miRNAs. These antagomirs act as small sponges that soak-up miRNAs, resulting in subsequent miRNA degradation and, thus, the upregulation of predicted targets with an *in vivo* effect that can be sustained for over 3 weeks. This is in contrast to standard antisense miRNA targeting, which has a limited ability to suppress miRNA functions and often leads to toxicity. Thus far, antagomirs have proven to efficiently silence miRNA function with limited side effects.

Although the initial proof-of-principle studies using miRNAs as therapeutics took advantage of adenoviral-based and lentiviral-based delivery methods, translation into clinical practice requires the development of safer delivery vehicles. These include packaging mature miRNAs into lipid-based nanoparticles (neutral or charged) that can be delivered locally to the tumor tissue or systemically, in which case they have been found to accumulate and to therapeutically regulate their targets in the lung, pancreas and prostate. Expanding on this, physical and chemical moieties of the particles that facilitate the targeted distribution and the controlled and sustained release of miRNA – including liposomes, polymers and dendrimer conjugates – are under clinical investigation.

Certainly, we must be cautious of the possible side effects of these molecules in human trials, independently of the side effects that could be associated with the delivery agents. Even in situations in which the miRNA is delivered directly to the tumour, miRNA could escape from the tumor cells and become systemic, either through microvesicle exocytosis or secretion of miRNA-Argonaute2 complexes. It is plausible that miRNA overexpression could lead to the saturation of the miRNA machinery and non-specific effects. Furthermore, increasing the cellular concentration of miRNAs may suppress lower-affinity targets that might not be targeted at endogenous miRNA levels. Similarly to current chemotherapies, concentration and dose schedules need to be evaluated for efficacy and toxicity, and the long-term effects following treatment must be assessed (Nana-Sinkam and Croce 2012).

Given all these problems, fewer studies using directed miRNA targeting have reached clinical trial. MiR-122 is the one miRNA that has successfully reached clinical trials as a targeted therapy (Elmén et al. 2008). The hepatic-specific miR-122 has been shown to drive HCV viral load through directed targeting of HCV. Investigators eventually translated these largely *in vitro* findings to large

animal models, demonstrating that systemic delivery of antimiR-122 could reduce HCV viral load in a chimpanzee model of chronic HCV infection with minimal toxicity (Lanford et al. 2010). Santaris Pharma subsequently conducted a human phase IIa trial demonstrating safety and antiviral function using miravirsen (a locked nucleic acid-modified miR-122 antagonist).

1.4 Breast Cancer

Breast cancer is a leading cause of cancer mortality among women, second only to lung carcinoma, and fifth most common cause of cancer death (after lung cancer, stomach cancer, liver cancer, and colon cancer).

The mammary gland is not like most vertebrate organs that are formed during embryogenesis and maintain their basic structure throughout adult life. In males, it is present in a rudimentary and generally non-functional form. In females, it is a highly dynamic organ that undergoes dramatic morphogenetic changes during puberty, pregnancy, lactation and regression.

The adult human mammary gland consists of a branching system of ducts surrounded by a collagenous and fatty stroma. An inner layer of luminal epithelial cells lines the system of ducts and lobules and an outer layer of contractile myoepithelial cells surrounds the luminal cells (Clayton et al. 2004) (Fig.8).

Ducts form before birth, by branching and invading the mammary fat pad.

During puberty, ductal outgrowth rapidly increases under hormonal stimulation, resulting in side branching (Rudland et al. 1997; Hennighausen and Robinson 2001). The final differentiation stage is achieved in the mammary gland during pregnancy and lactation, when numerous lobulo-acinar structures containing the milk-secreting alveolar cells are formed through extensive proliferation, followed by terminal differentiation.

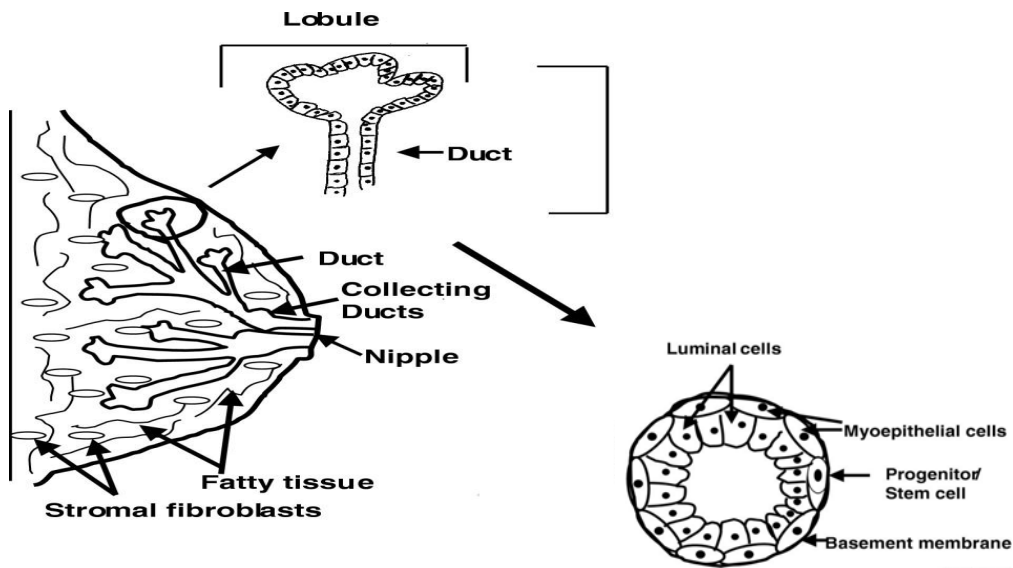


Fig.8: Mammary gland structure.

Although the adult breast is often called ‘resting’ (outside pregnancy and lactation), proliferation and apoptosis occur during each menstrual cycle. Thymidine labeling has shown that proliferation occurs mainly in the luminal cells, is maximal during the second half of the cycle and declines with age (Potten et al. 1988). In addition, most breast cancers arise from luminal epithelial cells (Gusterson et al. 1982)

Therefore, a compartment of cells with high proliferative potential and differentiation ability is needed in order to sustain numerous pregnancies, a description that fits the definition of stem cells or early progenitor cells (Dontu et al. 2003).

In the 19th century, the developments in surgical procedures led to the establishment of the radical mastectomy that was used for almost a century, until the 1970s, when conservative procedures started being explored together with the use of radiotherapy. There is now no doubt that estrogenic hormones of ovarian origin promote the growth of human breast cancer. This confirmation prompted the search for hormones that would antagonize the effects of estrogen, which led to the discovery of tamoxifen in 1966. Tamoxifen was quickly validated, and it was also shown that the mechanism of action of tamoxifen is to block the activity of the estrogen receptor (ER) in tumor cells, therefore blocking their growth (Vivanco 2010).

1.4.1 Stem Cells and Cancer Stem Cells

Stem cells, as classically defined, are cells with the ability to self-renew and to generate daughter cells that can differentiate down different cell lineages to form all the cell types that are found in the mature tissue.

In order to maintain this ability indefinitely, they must be able to perform asymmetric cell divisions. Each cell, therefore, generates one that is identical to it as well as another which is different, in that it is more committed towards a certain differentiation pattern. The identical cell maintains the stem cell compartment through time; the distinct cell undergoes a series of divisions and differentiation steps that result in the generation of terminally differentiated cell populations. The cells in intermediate states between the stem cell and the terminally differentiated cell are usually referred to as progenitors, transit cells or transit amplifying cells. Although both stem cells and transit amplifying cells divide and produce similar end products (a range of differentiated progeny), they differ in their ability to proliferate and maintain an undifferentiated state for an extended period of time (Cariati and Purushotham 2008).

In contrast to the ‘stochastic’ model of oncogenesis, where transformation results from random mutations and subsequent clonal selection, experimental and clinical data have accumulated to support the hypothesis that cancer may arise from mutations in stem cell populations (Cancer Stem Cell Hypothesis) (Reya et al. 2001) (Fig.9). As a matter of fact, about 10 years ago, John Dick’s team provided evidence that leukemia growth and propagation are driven by a small population of leukemia cells that have the ability to perpetually self-renew. They called this cell population as cancer stem cells (CSC) (Bonnet and Dick 1997). Since then, putative CSC have been isolated from many other tumors including breast, brain, colon, pancreas, prostate, lung and head and neck tumors.

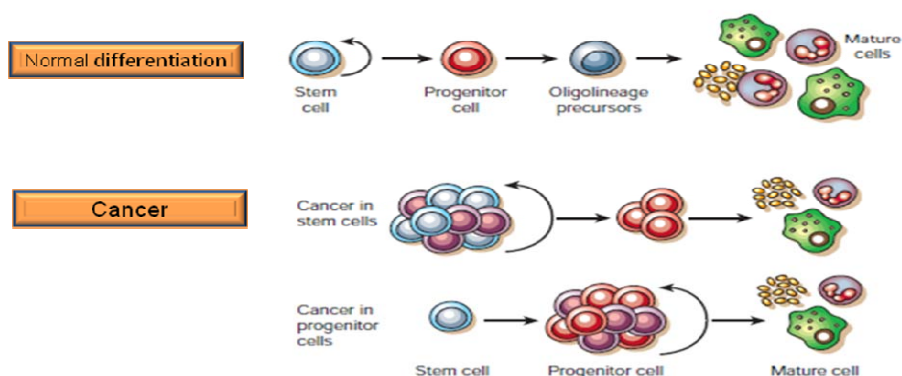


Fig.9: Schematic representation of normal differentiation and “cancer stem cell hypothesis”.

The basic arguments supporting the idea that tissue stem cells may be primary targets for transformation can be summarized as follows: (i) stem cells are long-lived, slowly dividing cells that persist in tissues long enough to accumulate multiple genetic alterations required for neoplastic transformation, while somatic cells are constantly replaced through periodic cell turnover; moreover, long-lived cells are exposed to genotoxic insults much longer than are short-lived ones; (ii) molecular pathways, which play a critical role in governing stem cell self-renewal (i.e. Wnt, Notch, Sonic Hedgehog, PTEN) are often deregulated in a number of tumors; (iii) normal stem cells and tumor cells share a number of phenotypic features, such as: a relatively undifferentiated state, the ability to self-renew, the activation of cytoprotective mechanisms (i.e. telomerase activity, overexpression of anti-apoptotic proteins, increased transmembrane molecule efflux capability) as well as a remarkable competence for migration (Ponti et al. 2006).

Mutations, probably regarding dysregulation of self-renewal pathways, can hit normal stem cells, but also strike more developmentally advanced, although still immature, early progenitor cells. So cancer may derive from different “cells of origin” (Visvader 2011).

This leads to expansion of this cell population that may undergo additional genetic and epigenetic changes. The nature of these genetic and epigenetic changes, the microenvironment and the type of progenitor they target, probably contribute to the cellular heterogeneity found in tumors (Charafe-Jauffret 2008).

1.4.2 Characterization of mammary stem cells

Given the paucity of normal stem cells in adult tissues and the lack of universal morphologic traits, their isolation represents a major hurdle for their study.

The purification and characterization of normal adult stem cells specific for the mammary gland could therefore be extremely helpful for understanding normal mammary development, as well as carcinogenesis.

The existence of self-renewing, multipotent mammary stem cells was first suggested decades ago by the work of Daniel et al. Their studies in mice and rats (Daniel et al. 1971; Kim et al. 2000) demonstrated that an entire mammary gland can be generated from serially transplanted random fragments of epithelium. Generally, senescence occurred after the fourth transplant, but in about 25% of cases, seven and eight serial transplantations were achieved. This indicates that mammary stem cells are dispersed throughout the entire gland and have a potent, although limited, self-renewal capacity. More recently, Kordon and Smith (1998), using mammary epithelium marked with mouse mammary tumour virus (MMTV) showed that clonal dominant populations

were responsible for the generation of a new gland in recipient animals. Serial transplantation of the clonally derived outgrowth recapitulated the entire functional repertoire of the gland, demonstrating the existence of self-renewing and multipotent mammary stem cells.

Propagation of mammary gland cells in an undifferentiated state in vitro could help to escape difficulties. In fact, a major advance in neural stem cell research was achieved when it was found that an undifferentiated multipotent population of neural cells can be grown in suspension as neurospheres (Reynolds and Weiss 1996; Weiss et al. 1996). Neurospheres were shown to consist of 4%–20% stem cells, the rest of the population representing progenitor cells in various stages of differentiation.

Analogous to primary neural cells, Dontu et al. (2003) found that also human mammary epithelial cells form spherical colonies, termed “nonadherent mammospheres,” when cultured on nonadherent surfaces in the presence of growth factors and in absence of serum. They demonstrate that nonadherent mammospheres are enriched in cells with functional characteristics of stem/progenitor cells: self-renewal and multi-lineage differentiation. In fact, mammosphere-derived cells are able to form new spheres, containing multipotent cells. They have also shown that mammospheres contain cells capable of clonally generating functional ductal alveolar structures in reconstituted three-dimensional culture systems in Matrigel. When combined with human mammary fibroblasts they are able to reconstitute the mammary tree in the cleared mammary fat pad of NOD/SCID mice (Liu et al. 2005) (Fig.10). Successively, Ponti et al. demonstrated that also cancer stem cells are able to form mammospheres in vitro (Ponti et al. 2005).

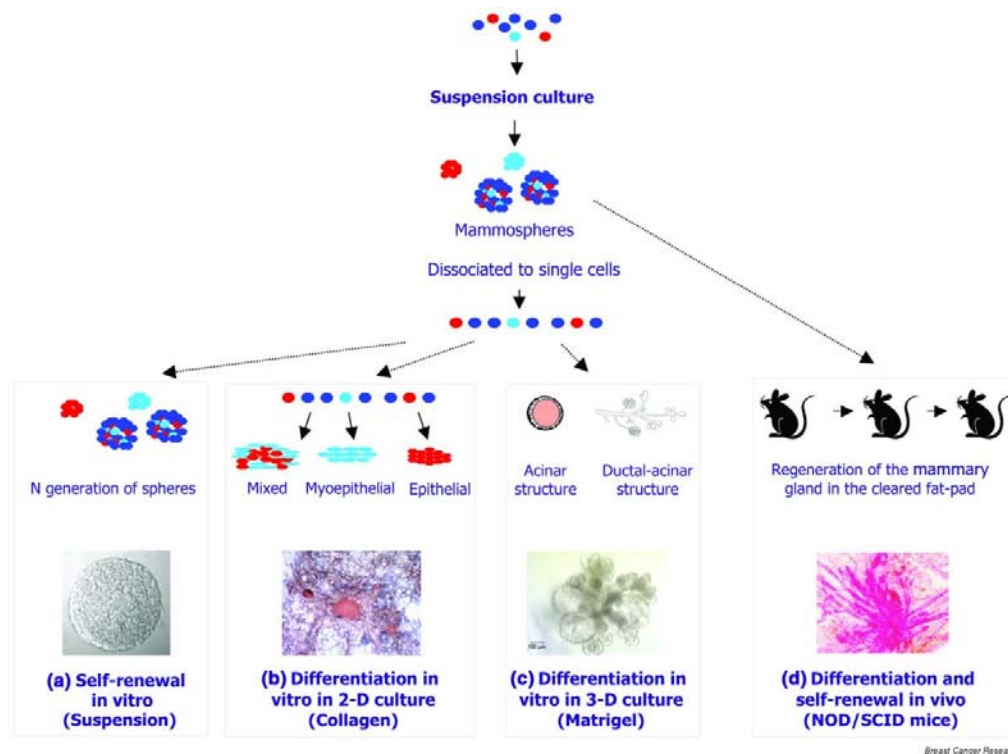


Fig.10: Experimental design for assessing the differentiation and self-renewal potential of cells grown as mammospheres. A) Self-renewal is tested by evaluating the ability of mammosphere-derived cells to form new spheres, containing multipotent cells; B) Differentiation into ductal and myoepithelial cells is assessed on cells cultivated on collagen in the presence of serum; C) Differentiation into ductal, myoepithelial, and alveolar cells is tested in the same conditions as in b with the addition of matrigel as an overlayer; D) Differentiation and self-renewal is assessed combining cells with human mammary fibroblasts. They are able to reconstitute the mammary tree in the cleared mammary fat pad of NOD/SCID mice.

1.4.3 Clinical implications for “Cancer Stem Cell Hypothesis”

The cancer stem cell model has fundamental implications in clinic. Tumor response is usually defined in the clinic as the shrinkage of a tumor by at least 50%. However, if cancer stem cells exist, then shrinkage of tumors may reflect the effects of these agents on the differentiated cells in a tumor rather than the cancer stem cell component. This may explain why in clinical trials for

advanced cancers, tumor regression often does not translate into clinically significant increases in patient survival.

By virtue of their fundamental importance in organogenesis, normal stem cells have evolved mechanisms that promote their survival and resistance to apoptosis, maintained by cancer stem cells. There are several molecular mechanisms that may account for the resistance to apoptosis. These include: (a) cell cycle kinetics. Many cancer stem cells are not cycling and are in G0 and thus resistant to cell cycle-specific chemotherapy agents. (b) DNA replication and repair mechanisms. Stem cells may be resistant to DNA-damaging agents by virtue of being able to undergo asynchronous DNA synthesis in addition to displaying enhanced DNA repair. (c) During asynchronous DNA synthesis, the parental “immortal” DNA strand always segregates with the stem cell and not the differentiating progeny. This process may be regulated by P53. This prevents the stem cell compartment from accumulating mutations associated with replication or from being affected by DNA damaging agents. (d) Antiapoptotic proteins. Stem cells express higher levels of antiapoptotic proteins, such as members of the Bcl-2 family and inhibitors of apoptosis, compared to differentiated cells. (e) Transporter proteins. Stem cells express high levels of transporter proteins, such as ABCG2 (BCRP1), as well as P-glycoprotein (Wicha et al. 2006).

Therefore, eradication of cancers may require the targeting and elimination of cancer stem cells. Thus, one must devise strategies that can selectively kill these cancer stem cells while sparing normal stem cells.

2. AIM OF THE STUDY

The present work aims at investigate new possible applications for aptamers in targeted anti-cancer therapies.

- AIM-1: Selection of aptamers for a cancer stem cell-targeted therapy.

In fact, one of the limits of the conventional treatment in cancer therapy is the lack of efficacy to eradicate tumor cells. So, the existence of cancer stem cells has significant implications in cancer treatment.

We wanted to select aptamers able to bind with high affinity and specificity breast cancer stem cells.

- AIM-2: Aptamers as delivery vehicles for “therapeutic” RNAs.

Knowing the specific surface molecule targeted, aptamers could be used to block specific molecular pathways or, if internalized, as delivery vehicles, conjugating them to “therapeutic” RNA. In particular, “therapeutic” RNAs could be considered microRNAs for their capability to regulate expression of many cellular proteins. So, we created a molecular chimera linking GL21 aptamer, which specifically binds Axl receptor and is endocytosed within the cell, and miR-212. This miR negatively regulates the anti-apoptotic protein PED and modulates response to therapy.

3. MATERIALS AND METHODS

3.1 Cell culture and transfection

Breast cancer stem cells (BCSCs) and breast cancer differentiated cells (BCCs) used for SELEX method were provided by Matilde Todaro and Giorgio Stassi's lab (Department of Surgical and Oncological Sciences, Cellular and Molecular Pathophysiology Laboratory, University of Palermo, Palermo, Italy). BCCs were trypsinized and counted and the same amount of BCSCs was dissociated to obtain single cells using trypsin 0.05% - EDTA for the SELEX cycle performed the day after.

A549 cells were grown in RPMI 1640, while U87MG and MCF7 cells were grown in DMEM. All the cells came from American Type Culture Collection. Their media were supplemented with 10% heat-inactivated fetal bovine serum (FBS) 10%, 2mM Glutamine and 100 U/mL penicillin/streptomycin. For miRs transient transfection, cells were transfected using Oligofectamine (Invitrogen) with 100nM (final concentration) of pre-miR-212 or scrambled (Applied Biosystem). For siRNA-PED transient transfection, A549 were transfected using Lipofectamine 2000 (Invitrogen) with 100nM of si-RNA PED or an empty vector (Ribok, Euroclone).

3.2 Whole-Cell SELEX

The SELEX cycle was performed essentially as described (Fitzwater and Polisky 1996). Transcription was performed in the presence of 1 mM 2'-F pyrimidines and a mutant form of T7 RNA polymerase (2.5 u/ml T7 R&DNA polymerase, Epicentre Biotechnologies) was used to improve yields. 2'-F-Py RNAs were used because of their increased resistance to degradation by seric nucleases. 2'-F-Py RNAs (1100-500 pmol) were heated at 85°C for 5 min in 1.5 ml of DMEM-F12 serum free, snap-cooled on ice for 2 min, and allowed to warm up to 37°C. Before incubation in the cells, 13.5 ml of medium were added to RNA to reach a final volume of 15 ml.

Counterselection step against BCCs. To avoid selection for aptamers non-specifically recognizing BCSCs surface, the pool was first incubated for 30 min (up to round 8) or for 15 min (for the following rounds) at 37°C with 1.5×10^6 BCCs (100-mm cell plate), and unbound sequences were recovered for

the selection phase. This step was meant to select sequences recognizing specifically the BCSCs.

Selection step against BCSCs. The recovered sequences were incubated with 3×10^6 for the first three cycles or 1.5×10^6 BCSCs (for the following rounds) at 37°C in a 50 ml tube with gentle shaking. Sequences were recovered after several washings with 4 ml of DMEM-F12 serum free by total RNA extraction (Ambion).

During the selection process, we progressively enhanced the selective pressure by increasing washings number (from one for the first cycle up to three for the last cycles) and by decreasing the incubation time (from 30 to 15 min from round 9). It was also increased the number of counterselection steps from one to two from cycle 10 and was introduced the use of $100 \mu\text{g/ml}$ polyinosine, as a nonspecific competitor (Sigma).

To follow the evolution of the pool we performed a binding assay for the starting and final cycles.

At the end of SELEX method, sequences of the pools were subjected to Illumina sequencing. The sequences have been analyzed for multiple alignment (ClustalW) (Thompson et al. 1997) and structural elements (MFOLD) (Zuker 2003) indicative of potential binding sites.

For cycles of internalization, 1.5×10^6 U87MG were incubated with 1000 pmol (for the first round) and 500 pmol (for the second round) and treated with $0.5 \mu\text{g/ml}$ proteinase K (Roche). Following 30- and 15-minute treatment for the first and second round, respectively, the amount of RNA internalized was recovered. Sequences were either cloned with TOPO-TA cloning kit (Invitrogen) and subjected to Illumina sequencing and analyzed.

3.3 RT-PCR, mutagenic and non-mutagenic PCR for cell-SELEX method

RNA extracted from each SELEX cycle was retro-transcribed using MuLV (Murine Leucemia Virus) reverse Transcriptase (Roche) according to the manufacturer's protocol. The retro-transcription reaction was as follow: 90°C for 3min, 42°C for 15min and 50°C for 30min. The product was used for mutagenic PCR, characterized by higher concentration of MgCl_2 and dNTP, using $0.5 \text{ U}/\mu\text{l}$ of Taq DNA-polymerase (Roche) and $2 \mu\text{M}$ primers:

P10: 5' TAATACGACTCACTATAGGGAGACAAGAATAAACGCTCAA

P20: 5' GCCTGTTGTGAGCCTCCTGTTCGAA

The mix was prepared by adding MgCl_2 and dNTP to a final concentration of 7.5 mM and 1 mM , respectively. The reaction was as follow: 93°C for 3min, 10 cycles of 93°C for 1 min, 53°C for 1min and 72°C for 1 min, and a final extension of 72°C for 5min.

The PCR product was, then, amplified through a non-mutagenic PCR using 0.1 U/ μ l of Taq DNA-polymerase (Roche) and 200 μ M dNTP, not adding MgCl₂ to that contained in the Taq Buffer. The reaction was as follow: 95°C for 3min, 8 cycles of 95°C for 30 sec, 60°C for 1min and 72°C for 30 sec, and a final extension of 72°C for 5min.

Amplified DNA was purified using Amicon Ultra Centrifugal Filters (Millipore).

3.4 Illumina sequencing

3.4.1 Illumina sequencing sample preparation

The DNA pools for selection rounds 0, 3, 5, 7, 10, 12, 13, 15 were amplified using High Fidelity PLUS Taq (Roche) in presence of p10 and p20 primers. The protocol is as follows. The DNA pool was heated at 95°C for 3 min, followed by 10 cycles of heating at 95°C for 30 sec, annealing at 60°C for 1 min and extending at 72°C for 30 sec and a final extension step at 72°C for 5min. The PCR product was run on an 8% acrylamide gel and the appropriate band (~100bp) was excised, gel purified and DNA quantitated using a Nanodrop spectrophotometer (Thermo Scientific). Samples were submitted for ILLUMINA® NEXT GENERATION SEQUENCING (NGS) (San Raffaele Hospital, Milan, Italy – Unità Funzione del Genoma) where samples were processed by TruSeq DNA Sample Prep v2 kit (Illumina®), controlled on an Agilent Technologies 2100 Bioanalyzer and sequenced by Illumina MiSeq System.

3.4.2 Illumina sequencing data processing

Illumina sequencing data were pre-processed and filtered by a multiple sequence alignment algorithm to identify the variable region sequences. Total sequences of a given round were compared to total rounds to extract those more representative and to examine their enrichment evolution.

3.5 Chimeras treatment

GL21-miR212 (2g) long strand, miR-212 (2g) short strand, miR-212 (1g) short strand were purchased from Chemgenes as 2'-fluoropyrimidine RNAs:

- GL21-miR212 (2g) long strand:

5' GGAUGAUCAAUCGCCUCAAUUCGACAGGAGGCUCACGGUACCU
UGGCUCUAGACUGCUUACUUU

- miR-212 (2g) short strand:

5' AGUAACAGUCUCCAGUCACGGCCACC

- miR-212 (1g) short strand:

5' UAACAGUCUCCAGUCACGGCC

while GL21scr-miR212 long strand and GL21-miR212 (1g) long strand were previously amplified and, then, transcribed in presence of 2'-fluoropyrimidines.

- GL21scr-miR212 long strand:

5' GGGTTCGTACCGGGTAGGTTGGCTTGCACATAGAACGTGTCAGG
CCGTGACTGGAGACTGTTA

- GL21-miR212 (1g) long strand:

5' GGGATGATCAATCGCCTCAATTCGACAGGAGGCTCACGGCCGTG
ACTGGAGACTGTTA

The amplification was done using:

- GL21scr-miR212 forward primer:

5' TAATACGACTCACTATAGGGTTCGTACCGGGT

- GL21-miR 212 (1g) forward primer:

5' TAATACGACTCACTATAGGGATGATCAATCGC

- GL21-miR212 (1g)/GL21scr-miR212 reverse primer:

5' AATAACAGTCTCCAGTCACG

The reaction was as follow: 94°C for 4 min, 20 cycles of 94°C for 30 sec, 55°C for 30 sec and 72°C for 30 sec, and a final extension of 72°C for 3 min.

Before each treatment, the RNA long strand was denatured at 98°C for 20 minutes, the RNA short strand at 55°C for 10 minutes and annealed each other using Binding Buffer 10X (200 mM Hepes, pH 7.4, 1.5 M NaCl, 20 mM CaCl₂).

3.6 Binding and internalization assays

Binding to BCSCs of the starting and final pools was performed in 2ml tubes in triplicate with 5'-[³²P]-labeled RNA. 3.5x10⁴ cells per tube were incubated with the pools (200 nM as final concentration) in 200 µl of DMEM-F12 serum

free for 15 minutes at 37°C with gentle shaking and in the presence of 100 µg/ml polyinosine, as a nonspecific competitor (Sigma). After two washings with 500 µl of medium, bound sequences were recovered in 100 µl of SDS 1% and the amount of radioactivity recovered was counted. The background value obtained with the starting pool was subtracted from the value obtained with the final pool.

For chimeras binding assay, A549 and MCF7 cells were plated in 24 multi-well in triplicate. RNAs were 5'-[³²P]-labeled and incubated on cells at a final concentration of 200nM at 37°C for 15 minutes and the amount of radioactivity recovered was counted. To check the endocytosis rate, after the incubation with radiolabeled chimeras, cells were incubated with High Salt PBS (0.5M NaCl). Following 5 minutes-treatment at 4°C, the amount of RNA internalized was recovered and counted. In both assays, results were normalized for cells number.

3.7 Protein isolation and Western blotting

Cells were washed twice in ice-cold PBS and lysed in JS buffer (50 mM HEPES pH 7.5 containing 150 mM NaCl, 1% Glycerol, 1% Triton 100X, 1.5 mM MgCl₂, 5 mM EGTA, 1 mM Na₃VO₄ and 1X protease inhibitor cocktail). Protein concentration was determined by the Bradford assay (BioRad) using bovine serum albumin as the standard and equal amounts of protein were analyzed by SDS-PAGE (15% acrylamide). Gels were electroblotted onto nitrocellulose membranes (Millipore). For immunoblot experiments, membranes were blocked for 1 hr with 5% non-fat dry milk in Tris Buffered Saline (TBS) containing 0.1% Tween-20 and incubated at 4°C over night with primary antibody. Detection was performed by peroxidase-conjugated secondary antibodies using the enhanced chemiluminescence system (Amersham-Pharmacia Biosciences). Primary antibodies used were: anti-PED (Condorelli et al. 1998), anti-Axl (R&D Systems), anti-Caspase-8 Cell Signalling) and anti-βactin (Sigma).

3.8 RNA extraction and RealTime-PCR

Total RNAs (miRNA and mRNA) were extracted using Trizol (Invitrogen) according to the manufacturer's protocol. Reverse transcription of total miRNA was performed starting from equal amounts of total RNA/sample (1µg) using

miScript reverse Transcription Kit (Qiagen). Quantitative analysis of miR-212 and RNU6B (as an internal reference) were performed by RealTime-PCR using specific primers (Qiagen) and miScript SYBR Green PCR Kit (Qiagen). The reaction for detection of miRNAs was performed as follow: 95°C for 15min, 40 cycles of 94°C for 15sec, 55°C for 30sec and 70°C for 30sec. All reactions were run in triplicate. The threshold cycle (CT) is defined as the fractional cycle number at which the fluorescence passes the fixed threshold. For quantization the $2^{(-\Delta\Delta CT)}$ method was used as previously described (Livak and Schmittgen 2001). Experiments were carried out in triplicate for each data point and data analysis was performed by using software (Bio-Rad).

3.9 Proliferation assay and cell death quantification

A549 and MCF7 cells were treated with GL21-miR212 (2g) and GL21scr-miR212 for 3 hours and then plated in 96 multi-well plates in triplicate for 24, 48, 72 and 96 hours. Alternatively, A549 cells were transfected with siPED RNA and an empty vector and plated in 96 multi-well plates in triplicate for 24, 48 and 72 hours. Cell viability was assessed with CellTiter 96 Aqueous One Solution Cell Proliferation Assay (Promega). Metabolically active cells were detected by adding 20 μ l of MTS to each well and plates analyzed in a Multilabel Counter (BioTek).

For cell death quantification, cells treated were incubated with TRAIL at a final concentration of 50 ng/ml for 24h.

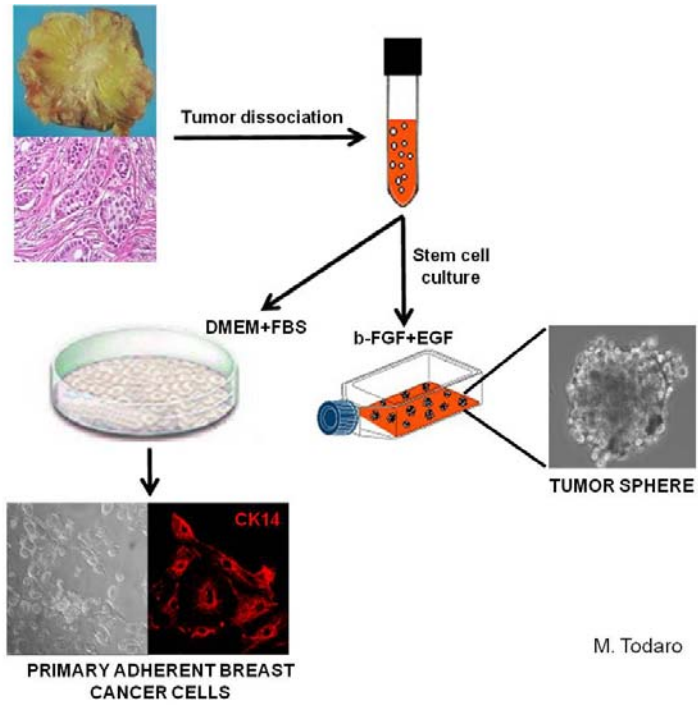
4. RESULTS

4.1 AIM-1

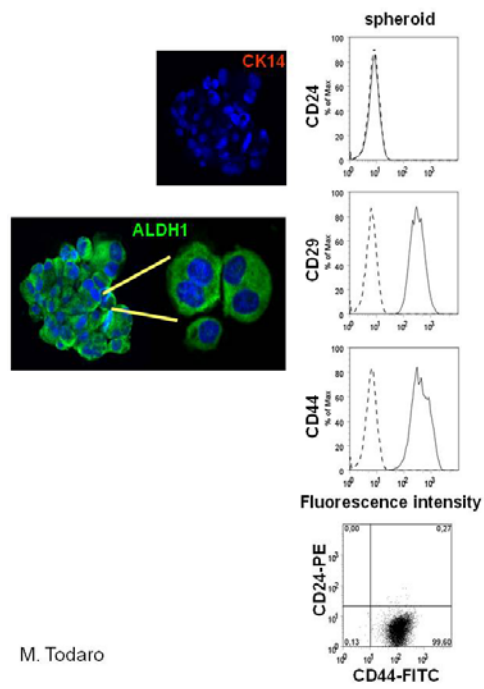
4.1.1 Characterization of breast cancer stem cells (BCSCs) and breast cancer cells (BCCs)

Stemness phenotype includes the capability to propagate in an undifferentiated state in non-adherent conditions as spheres, to differentiate and to express some stemness markers. Both BCSCs and BCCs were obtained by dissociating a breast cancer sample from a patient who had undergone surgery. A part of the cells was plated in suspension in a medium containing growth factors, such as EGF and bFGF, and in the absence of serum, observing mammosphere formation, typical of BCSCs. The rest of the cells were, instead, plated in adherence in the presence of serum, forming a culture of primary adherent BCCs. Both types of cells were assessed for markers of stemness and differentiation. BCCs were analyzed by immunofluorescence for the expression of CK14 (differentiation marker). On the other hand, BCSCs were evaluated by fluorescence-activated cell sorting (FACS) resulting in CD24(-/low)/CD44+ (Al-Hajj et al. 2003), CK14- and expressing ALDH1 by immunofluorescence (Ginestier et al. 2007). Moreover, to evaluate differentiation property, mammospheres were dissociated and plated in adherence with serum, obtaining a culture assessed for differentiation markers. Indeed, the obtained BCCs were analyzed by immunofluorescence showing an increase in the expression of CK8/18 and CK14 (differentiation markers) and a reduction of CK5 (stemness marker) (Fig.11).

A



B



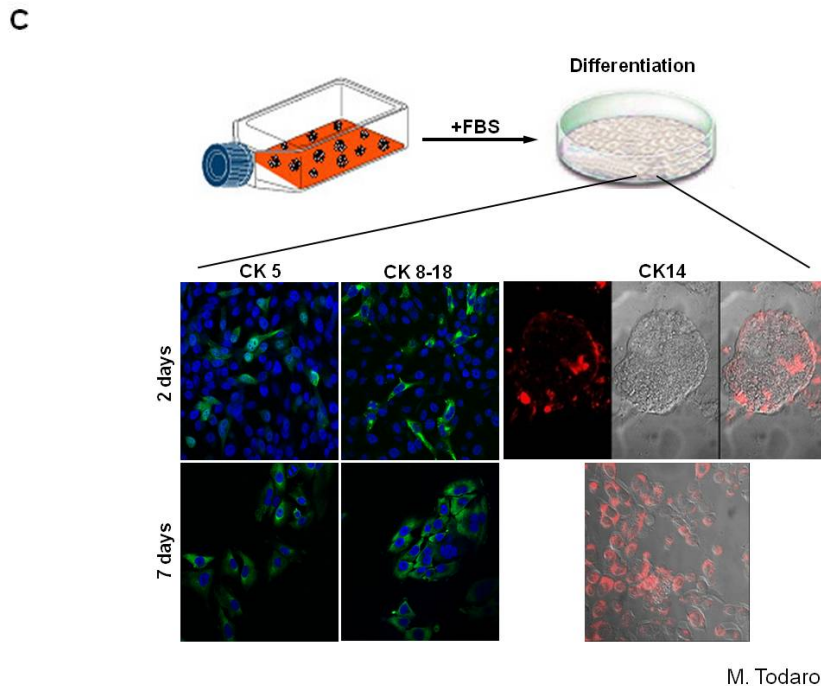


Fig.11: In vitro propagation and characterization of BCSCs and BCCs from a human sample. A) BCSCs and BCCs were obtained plating cells from a breast tumor in suspension (with EGF and bFGF and in absence of serum) and in adherence (in presence of serum), respectively. BCCs resulted CK14+ (fluorescent red) by immuofluorescence; B) characterization of BCSCs for stemness markers resulting CD24(-/low)/CD44+ by FACS (right panel), CK14- and ALDH1+ by immunofluorescence (fluorescent green) (left panel); C) analysis of BSCSs capability to differentiate in BCCs. BCSCs were plated in adherence with serum and differentiation markers were evaluated after 2 and 7 days. Cells showed an increase of CK8/18 (fluorescent green) and CK14 (fluorescent red), while a reduction of CK5- (fluorescent green) by immunofluorescence.

EGF=epidermal growth factor, bFGF=basic fibroblast growth factor, CK=cytokeratin, ALDH1= aldehyde dehydrogenase 1.

4.1.2 Enrichment of selection for a complex target

In order to isolate cell specific ligands for a given tumor condition, I used as target in the selection steps BCSCs and in the counterselection steps BCCs from the same patient. For the SELEX cycle it was used a library of RNAs formed by a central degenerated sequence of 45 nucleotides flanked by two

fixed regions recognized by T7-RNA Polymerase. The library is modified with 2'Fluoro-Pyrimidines (2-F-Py) to resist to nuclease degradation. At each round, the selection step on BCSCs was preceded by one or two counterselection steps against BCCs. All the unbound sequences were, then, recovered and incubated on BCSCs (Fig.12).

During the selection process, I progressively increased the selective pressure by changing both incubation and washing conditions (Table 1). After several washings of the cells with DMEM serum free, the bound RNAs was recovered by total RNA extraction. Sequences enriched by the selection step were amplified by RT-PCR followed by mutagenic PCR (in presence of high concentration of nucleotides and magnesium) to increase library variability and by in vitro transcription, before a new cycle of selection. In total I performed 15 cycles.

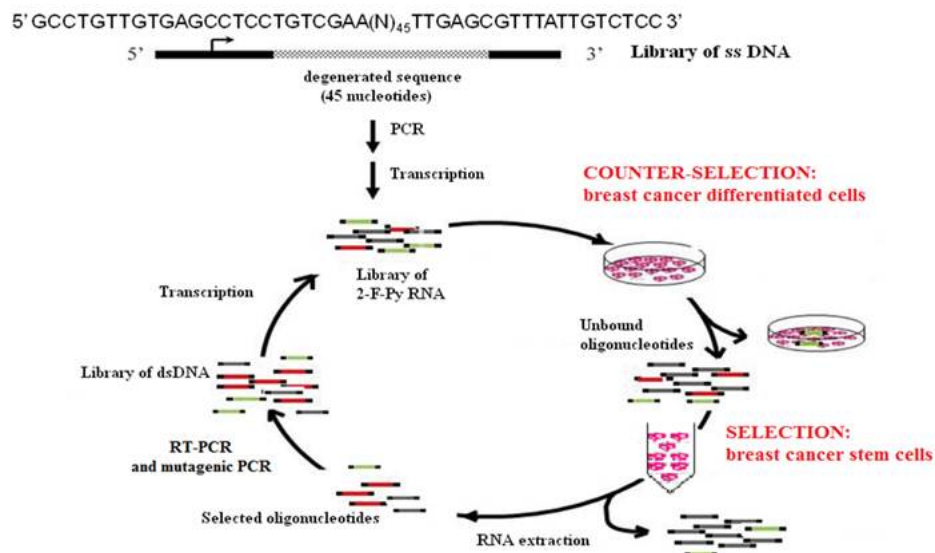


Fig.12: SELEX method scheme. A library of ssDNAs, formed by a degenerated central region of 45 nt flanked by two fixed region, was amplified and transcribed in presence of 2'-fluoropyrimidines (2-F-Py). The 2-F-Py RNA library was incubated on BCCs (counterselection step). Unbound sequences were, then, incubated on BCSCs. Bound sequences were recovered by RNA extraction and RT-PCR, amplified by mutagenic PCR to increase library variability and used for the next SELEX cycle.

Round number	Cell number (x10 ⁶)	RNA amount (x100pmol)	Washing number	Incubation time (min)	Counter selection step number	Poli-I Competitor (40ng/ml)
1	3	11	1	30	1	-
2	1,7	5	2	30	1	-
3	3	10	3	30	1	-
4	1,5	5	4	30	1	-
5	1,5	5	4	30	1	-
6	1,5	5	3	30	1	-
7	1,5	5	3	30	1	-
8	1,5	5	3	30	1	-
9	1,5	5	3	15	1	-
10	1,5	5	3	15	2	-
11	1,5	5	3	15	2	+
12	1,5	5	3	15	2	+
13	1,5	5	3	15	2	+
14	1,5	5	3	15	2	+
15	1,5	5	3	15	2	+

Table 1: Conditions used for each of 15 SELEX cycles.

At the end of SELEX cycles, to evaluate the enrichment of the library for the desired target we compared the binding capacity of the final pool (cycle 15), named B15, to the naive starting one (B0). For the binding assay both pools were 5'-[³²P]-labeled and, then, incubated on BCSCs for 15 minutes at 37°C with gentle shaking. Finally, bound sequences were recovered and the amount of radioactivity counted. B15 showed a higher capacity to bind BCSCs respect to B0, 1.6 times more (Fig.13). So, the final pool was enriched for aptamers that preferentially bind to BCSCs.

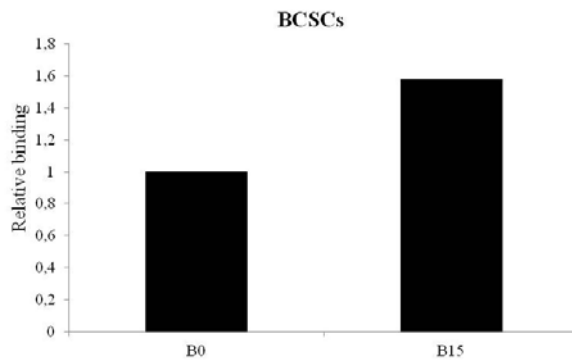
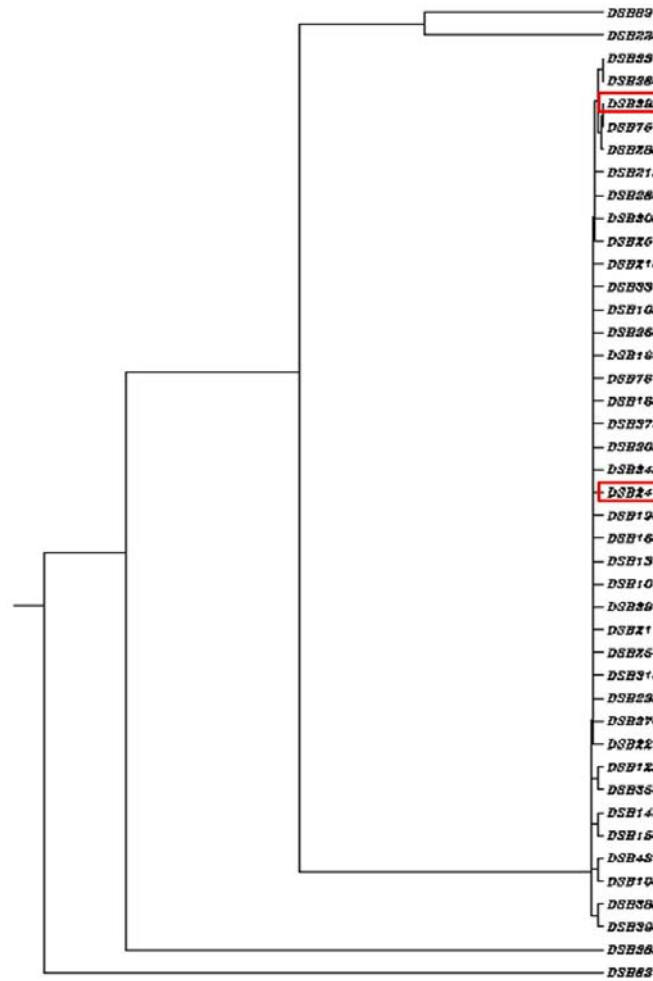


Fig.13: Binding assay for B15 pool on BCSCs. B0 and B15 were radiolabeled and incubated on BCSCs. The binding affinity of the final pool was compared to B0, the starting one.

4.1.3 Selection of the most enriched sequences

In order to isolate individual aptamers that may distinguish BCSCs from BCCs, I performed Illumina sequencing on DNA pools for selection rounds 0, 3, 5, 7, 10, 12, 13, 15. A total of 8 Gigabyte sequences reads were obtained from the sequencing experiments. To count and align sequences, we designed a multiple sequence alignment algorithm. The first step of the algorithm was to extract the raw Illumina data. The sequences were, then, size selected with a distribution of lengths up to 45 nucleotides, which corresponds to the random region of aptamers. By this algorithm, I noted that there was a tendency through the cycles. Indeed, the maximum enrichment was observed in the 7th cycle with a reduction in the following ones. 386 sequences were extracted from the sequencing analysis of each SELEX cycle. Among these sequences, 43 showed a higher enrichment index and were, therefore, analyzed for alignment and structure prediction. Sequences corresponding to variable regions were aligned using ClustalW and aptamers grouped in families based on their primary sequence similarity. I found a big family of 39 sequences that were divided in 2 groups on the base of their structure prediction. Two representative aptamers of each group with the most elevated enrichment index were selected. They will be used for further analysis (Fig.14).

A



B

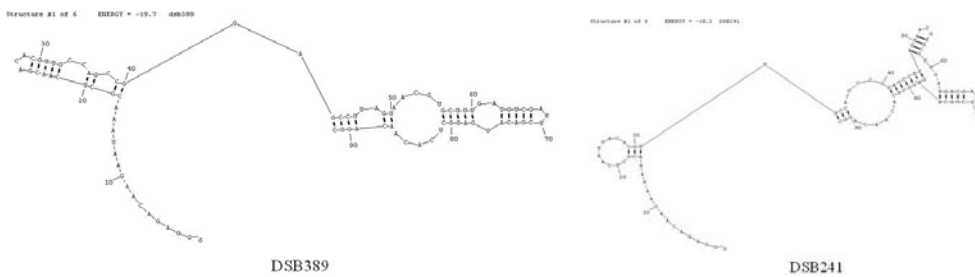


Fig.14: Analysis of enriched sequences. A) Dendrogram (obtained by using ClustalW program) for visual classification of similarity among 43 individual sequences with a higher enrichment index obtained by Illumina sequencing. Red squares indicate the most enriched sequences, DSB389 and DSB241; B) their predicted structure (by using RNA structure 5.3 program).

4.2 AIM-2

4.2.1 Selection of internalizing aptamers

GL13 pool, an enriched pool of aptamers after 13 rounds of SELEX against U87MG, a malignant glioblastoma cell line, was used to find internalizing sequences. Two rounds of internalization were done. Cells were incubated with GL13 and, then, treated with proteinase K, able to destroy surface proteins, for 30 min (first round) or 15 min (second round) at 37°C. The bound aptamers were discarded and the internalized aptamers were recovered by RNA extraction (Fig.15).

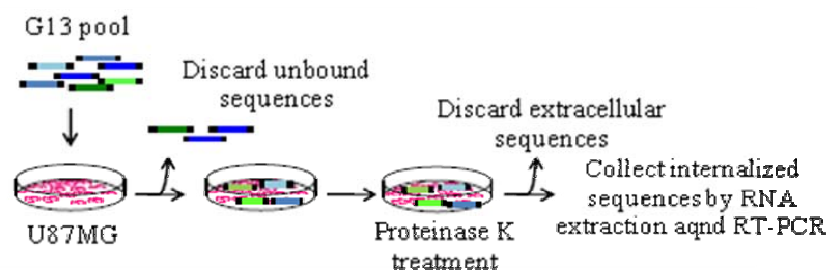
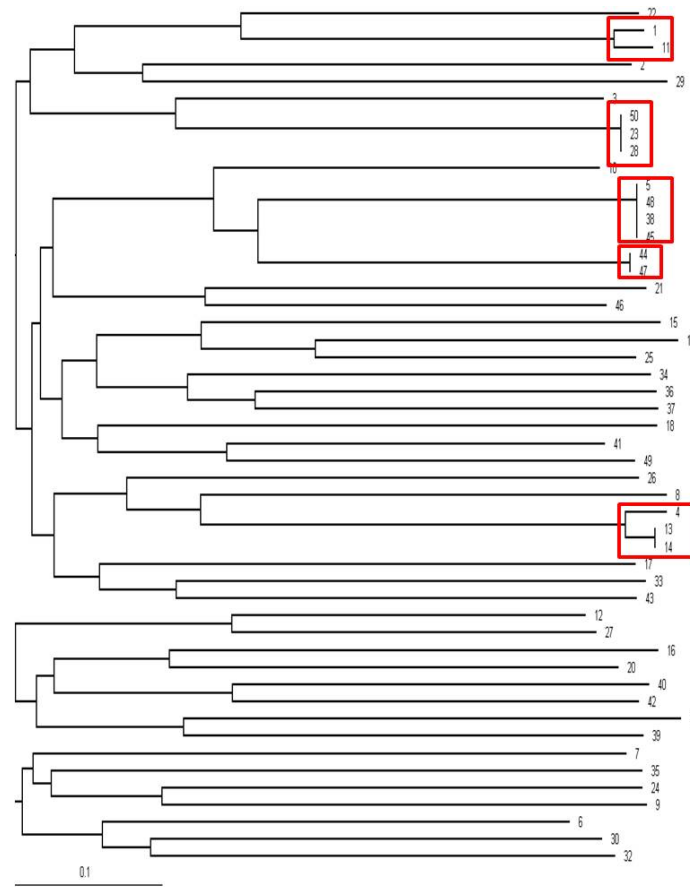


Fig.15: Schematic representation of both rounds of internalization.

The resulting GL13i2 pool enriched for internalizing aptamers was analyzed to obtain individual sequences. 50 sequences were cloned, aligned using ClustalW and grouped in families based on their primary sequence similarity (Fig16-A). I identified 5 principle families and, in one of these, I found a sequence, M13, identical to GL21 analyzed in a previous work (Cerchia et al. 2009). It was used for further analysis and was found that M13/GL21 is able to bind Axl receptor expressed on the surface of U87MG, but also of other cell lines expressing Axl, as A549 of NSCLC (Cerchia et al. 2012).

Each round of the two cycles of internalization was also subjected to Illumina sequencing. Most 100 enriched individual sequences were extracted through the same algorithm used for Illumina sequencing in AIM-1 and the enrichment reported in graphic (Fig16-B). Comparing Cloning and Illumina sequencing results, I found a little correspondence. In fact Gi-98, -71 and -13, that showed the highest enrichment index, presented identical sequence of M23, M28, M50 family; M5, M45, M48, M38 family and M7 sequence, respectively (Table 2).

A



B



Fig.16: Representation of internalizing aptamers: two cycles of internalization were performed on U87MG cells and individual sequences were obtained through Cloning and Illumina sequencing. A) Dendrogram for visual classification of sequences obtained by cloning. Families were indicated with red squares; B) visual representation for enrichment of sequences obtained by Illumina sequencing.

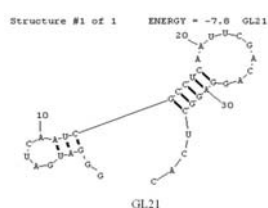
Illumina sequencing	Cloning
Gi-13	M7
Gi-71	M5, M38, M45, M48
Gi-98	M23, M28, M50

Table 2: Corrispondance between most enriched sequences coming from Cloning and Illumina sequencing.

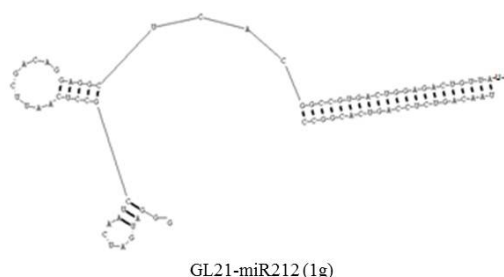
4.2.2 Binding and internalization capability of GL21-miR212 chimeras

Based on the demonstration that A549 cells express Axl receptor and PED protein targeted by miR-212, we designed two different chimeras (1g and 2g), in which we joined GL21 aptamer to miR-212. A scrambled chimera, GL21scr-miR212, was also designed, in which the portion regarding GL21 had a no-related sequence. In the first generation chimera, GL21-miR212 (1g), the aptamer is covalently linked to antisense strand of mature miR-212 hybridized to 21-mer sense strand. Instead, in the second generation chimera, GL21-miR212 (2g), both antisense and sense strands are longer and not completely complementary. In fact, antisense strand is modified in the way to present an imperfect pairing with the sense strand, making structure more similar to that of a pre-miR. In both types of chimera the antisense strand presents two overhanging bases (UU) at 3' end necessary for Dicer processing (Fig.17).

A



B



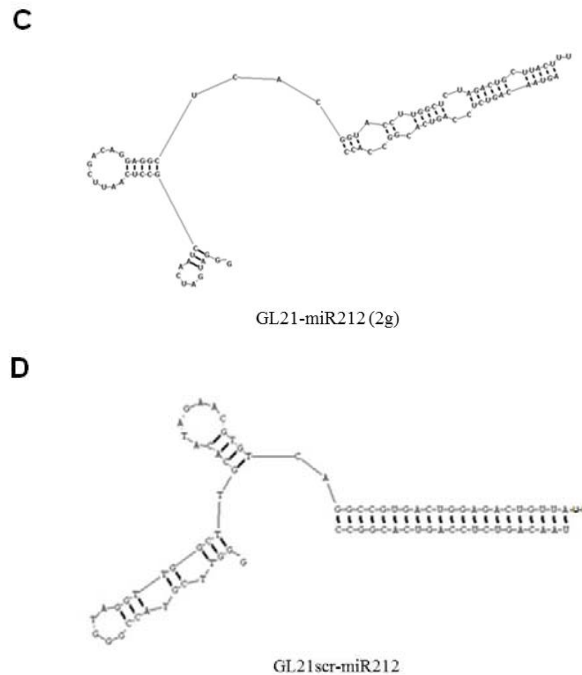


Fig.17: Chimeras structure prediction: A) GL21; B) GL21-miR212 (1g); C) GL21-miR212 (2g); D) GL21scr-miR212. They were designed with RNA structure 5.3 program.

Even if by structure prediction GL21 seems to maintain its three-dimensional conformation within chimera, it was necessary to assure that GL21-miR212 chimeras were able to bind and internalize into A549 cells. So, I performed a binding and an internalization assay in A549, using MCF7 cells as control. In fact, the latter do not express Axl receptor while expresses PED protein. Chimeras were 5'-[³²P]-labeled and incubated on cells at 37°C for 15 minutes and the amount of radioactivity recovered was counted. Instead, for the internalization assay after incubation with radiolabeled chimeras, cells were treated with High Salt PBS C for 5 minutes at 4°.

I found that GL21-miR212 (1g) and GL21-miR212 (2g) were both able to bind and internalize into A549. This was not obtained in MCF7 cells that do not express Axl. Comparing results for both assays, GL21-miR212 (2g) showed a lower binding affinity to A549 cells, but a higher internalization rate than GL21-miR212 (1g) (Fig.18).

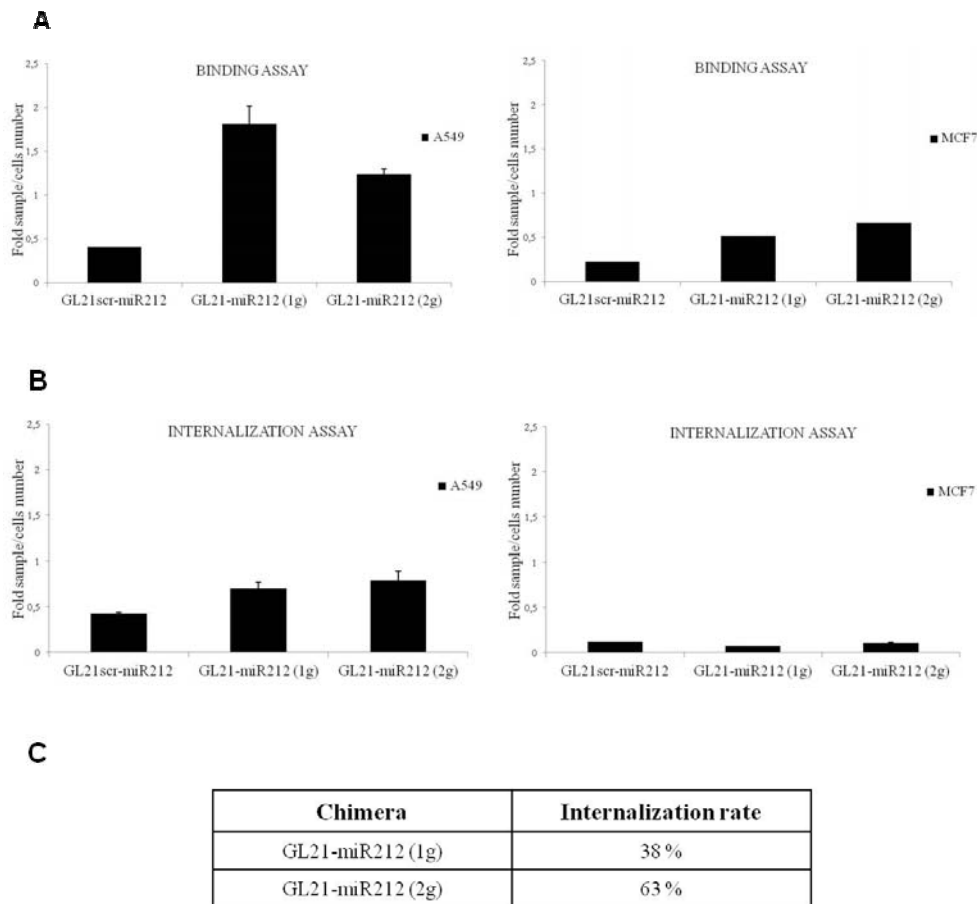


Fig.18: Binding and internalization analysis of the two generations of chimeras. A) Binding assay and B) internalization assay for chimeras on A549 (left panels) and MCF7 cells (right panels). Results were normalized over cells number; C) percentage of internalization rate respect to the bound amounts.

4.2.3 GL21-miR212 (2g) targets PED protein

First of all, we wanted to test the best chimera secondary structure that was processed by miRNA machinery and that was, therefore, functional. So, I treated A549 cells with both chimeras using GL21scr-miR212 and GL21 aptamer as negative control. The treatment was at a final concentration of 400 nM for 48h. Although both chimeras were able to internalize into A549 cells, as previously demonstrated, only GL21-miR212 (2g) targeted PED, downregulating its protein level. This means that only the second generation chimera is correctly processed by Dicer on the base of its structure. On the

other hand, either GL21scr-miR212 or the aptamer alone are unable to target PED (Fig.19).

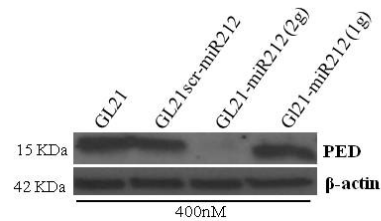


Fig.19: Comparison of functionality between two generations of chimeras. PED protein levels in A549 cells, treated at a final concentration of 400nM, were evaluated by western blot. Cell lysates were immunoblotted with anti-PED antibody. To confirm equal loading, the membrane was immunoblotted with anti-β-actin antibody.

Relying on literature (McNamara et al. 2006), I started the experiments using a final concentration of 400 nM for chimera treatment, but I performed a dose-response assay to evaluate if chimera worked at lower doses. So, A549 cells were treated with different final concentrations (50, 100, 200, 300 and 400 nM) of GL21-miR212 (2g) and its control, GL21scr-miR212. By western blot, we observed that PED disappearance was already appreciable at 200 nM (Fig.20).

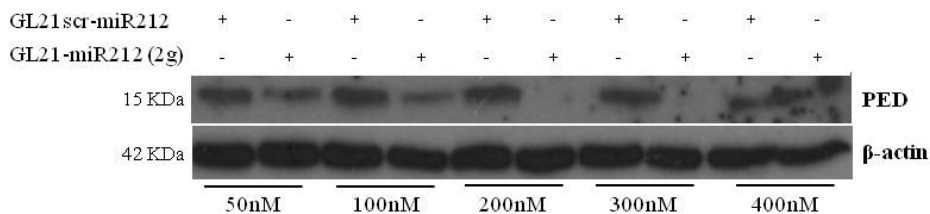
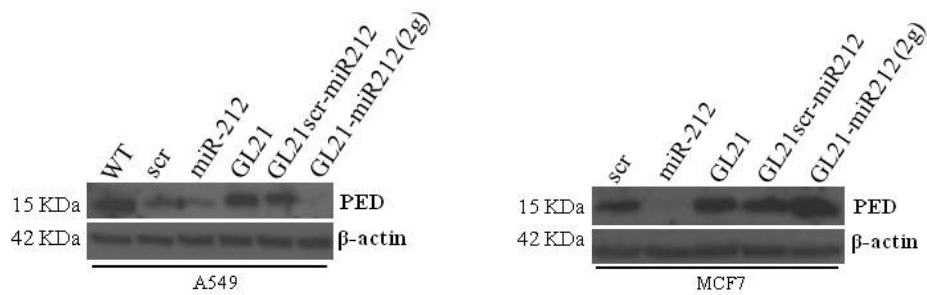


Fig.20: Dose-response effect of GL21-miR212 (2g) chimera treatment. A549 cells were treated with different final concentrations (50, 100, 200, 300, 400 nM) of chimera and scrambled chimera for 48h.

In order to assess if the effects of GL21-miR212 (2g) were specific for cell type, we treated both A549 and MCF7 cells. Chimeras treatment was realized at a final concentration of 300nM, an intermediate condition on the base of the dose-response assay. MiR-212 and GL21 were used as positive and negative controls, respectively. GL21-miR212 (2g) chimera downregulated PED as miR-212 in A549 cells, while no effects were observed in MCF-7 cells (Fig.21-A). To confirm that the results on PED protein levels were correlated with

miR-212 RNA levels, the same samples were monitored by RT-PCR (Fig.21-B). It showed that GL21 efficiently delivered miR212 inside the target cells, resulting in PED downregulation.

A



B

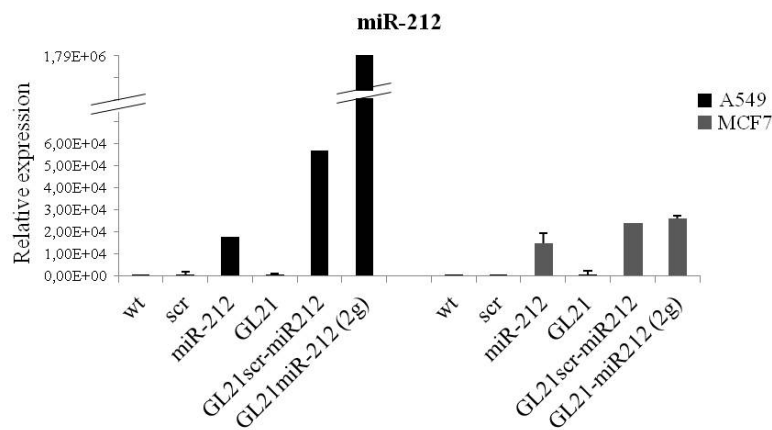


Fig.21: PED and miR-212 expression levels. A549 and MCF7 cells were treated with GL21-miR212 (2g) for 48h. GL21scr-miR212 and GL21 were used as negative controls, while transfection with pre-miR-212 as positive control. Control scrambled was used to assure transfection efficiency. The same samples were subjected to western blot (A) for PED protein levels and to RT-PCR (B) for miR-212 expression levels.

4.2.4 GL21-miR212 (2g) inhibits cell viability

In order to verify if PED targeting had effects on cell viability, A549 and MCF7 cells were plated in triplicate and treated with GL21scr-miR212 and GL21-miR212 (2g) for 24, 48, 72 and 96 hours at 300 nM as final

concentration. Cell viability was evaluated using an MTT assay. A decrease in A549 cell vitality was observed already at 24 hours of treatment and viability decreased during time, compared to scrambled chimera (Fig.22-A). Instead no effects were observed on MCF7 cells. To confirm that the effect was directly due to PED downregulation, I transfected A549 cells with a siRNA for PED and a control vector, and an MTT assay was performed after 24, 48 and 72 hours. PED silencing confirmed a miR-212-mediated decrease in cell viability after chimera treatment (Fig.22-B).

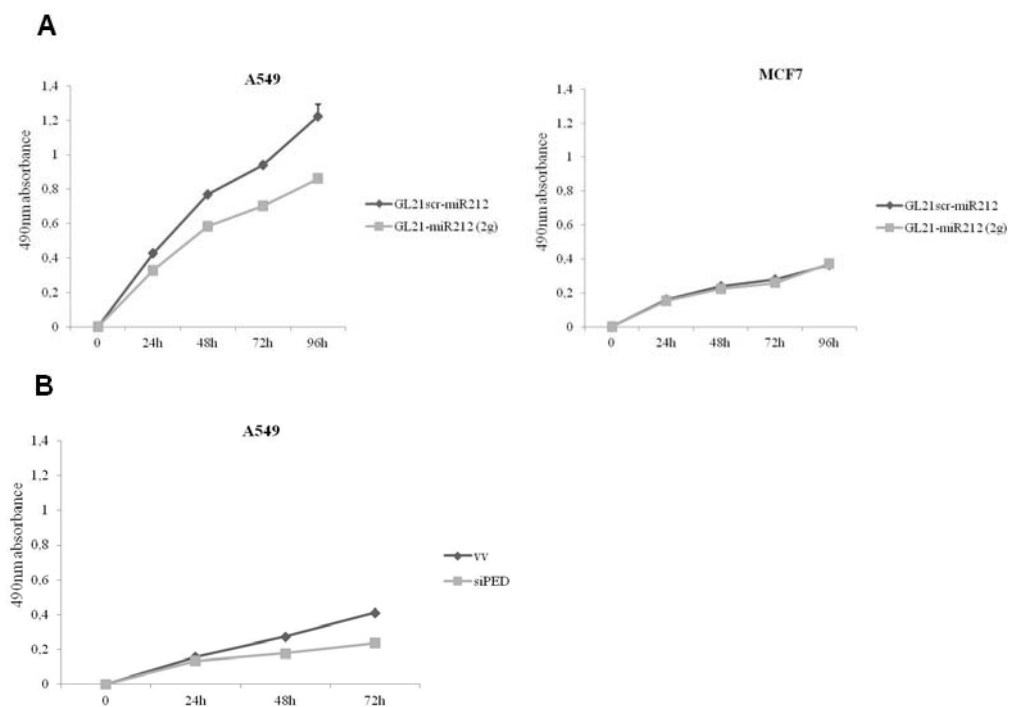


Fig.22: GL21-miR212 (2g) effects on cell viability. A) A549 (left panel) and MCF7 cells (right panel) were treated with GL21-miR212 (2g) and scrambled chimera for 24, 48, 72 and 96 hours. Cell viability was evaluated with an MTT assay. B) A549 cells were transfected with a siRNA for PED and an empty vector. MTT assay was performed at 24, 48 and 72 hours.

4.2.5 GL21-miR212 (2g) regulates TRAIL-induced cell death

To verify that chimera sensitizes to TRAIL-induced apoptosis owing to PED targeting by miR-212 (Incoronato et al. 2010), A549 and MCF7 cells were treated with GL21scr-miR212 and GL21-miR212 (2g) for 48 hours and were exposed to TRAIL for 24 hours at 50 ng/mL as final concentration. After this

time, cell viability was assessed using an MTT assay. A549 cells underwent to TRAIL-induced cell death when treated with the chimera, while MCF7 cells remained insensitive, as expected (Fig.23-A). To confirm this data, I analyzed caspase-8 activation. I treated A549 cells with GL21-miR212 (2g) using GL21scr-miR212 and transfection with pre-miR-212 as negative and positive controls, respectively. Caspase-8 activation was then evaluated following treatment with TRAIL for 3 hours (Fig.23-B). As shown, cleavage of caspase-8 was evident in cells treated with GL21-miR212 (2g) or, alternatively, transfected with pre-miR-212. So, the presence of exogenous miR-212 internalized by the chimera led to caspase-8 activation, resulting in induced-cell death only in target cells.

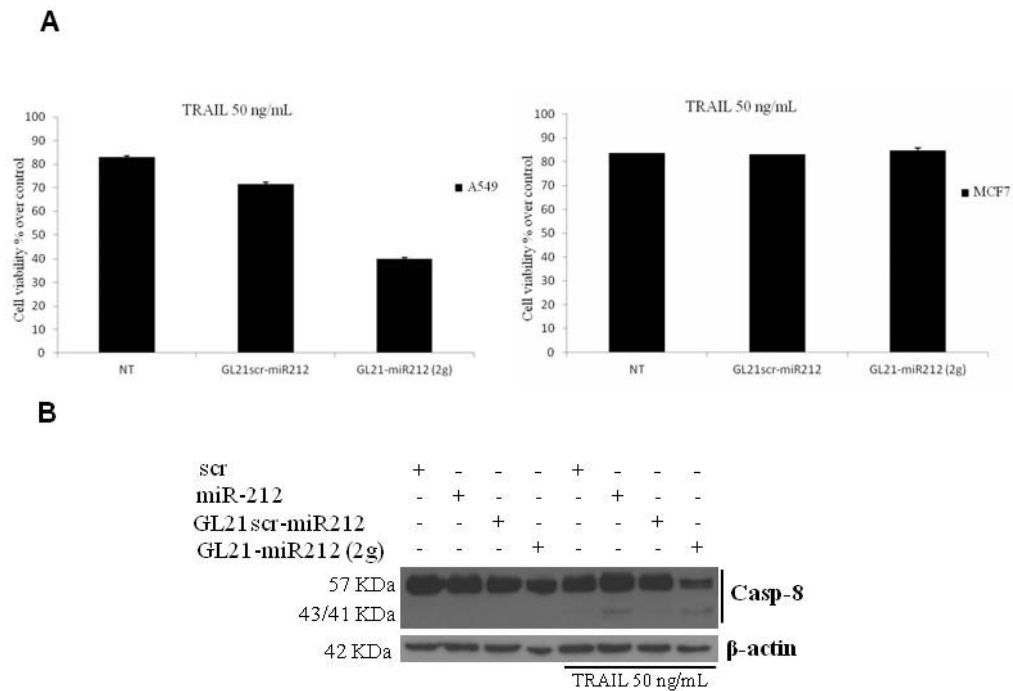


Fig.23: TRAIL sensitization. A) A549 (left panel) and MCF7 cells (right panel) treatment with TRAIL 50 ng/mL for 24h. Cell viability was evaluated with MTT assay. B) A549 cells were transfected with pre-miR-212 or alternatively treated with GL21-miR212 (2g). Control scrambled and scrambled chimera were used as negative controls. Cells were treated for 3h with TRAIL 50 ng/mL and cell lysates were immunoblotted with anti-caspase-8 antibody.

5. DISCUSSION

Since their discovery more than a decade ago, aptamers are emerging as new tools in the scenario of targeted anti-cancer therapy. In fact, considerable interest has been shown in developing novel treatments that target only cancer cells, thus avoiding the toxicity of conventional therapies, as chemotherapy and radiotherapy, against normal tissues adjacent to the tumor. Moreover, conventional therapies are initially effective in controlling tumor growth, but still many patients relapse over time.

Here we show new applications for aptamers in anti-cancer targeted therapies, as tools for cancer stem cell-targeted therapy and as possible molecular vehicles for microRNAs.

For recurrences, at least two major explanations exist. The first is that all cancer cells acquire resistance, resulting in decreased sensitivity to therapy over time. In this case, the relative proportion of cells in residual tumors with tumorigenic properties would be expected to be similar before and after treatment. The second explanation is that a rare subpopulation of cells with tumorigenic potential is intrinsically resistant to therapy. In this case, the relative proportion of cells in residual tumors with tumorigenic properties would be expected to increase after treatment. Consistent with this hypothesis, it has been previously shown that the gene expression pattern of residual tumor cells is different from that of cells of the initial tumor, in particular with differential expression of genes involved in cell cycle arrest and survival pathways (Chang et al. 2005). So, although the majority of cells in the original tumor may be killed by chemotherapy, the most important target, a small population of therapy-resistant cancer cells that possess tumorigenic capacity, is spared, thereby allowing tumor regrowth. It is well established that this tumorigenic subpopulation of cancer cells is represented by cancer stem cells (Li X et al. 2008). This hypothesis provided a unified explanation for the successes and failures of cytotoxic chemotherapy.

The starting point for a targeted therapy is the identification of cancer-specific biomarkers, which may be used to assess changes in expression states of certain proteins or genes within a primary tumor.

In breast cancer some markers for stemness phenotype were identified, as the expression of CD44 (CD44+) but low or no of CD24 (CD24-/low) and a panel of nonepithelial lineage markers (Lin-). This subpopulation can form mammospheres in vitro and was shown to be enriched for tumorigenic cells by its ability to form xenograft tumors in immunocompromised mice (Al-Hajj et al. 2003). The tumorigenicity of CD44+/CD24^{-/low} cells has been confirmed in subsequent studies (Ponti et al. 2005; Patrawala et al. 2006). This subpopulation is found enriched in residual breast cancer after conventional therapy, so it is responsible for recurrence (Phillips et al. 2006; Creighton et al. 2009).

During time, other markers were identified for breast stem cells, as expression of epithelial specific antigen or ALDH1, but no of sialomucin (MUC-/ESA+) (Gudjonsson et al. 2002, Ginestier et al 2007). However, mammary gland is very heterogeneous and stem cells need to be better characterized. Therefore, finding molecular probes capable of identifying CSCs with specificity is an important challenge for making the elimination of CSCs a long-term success treatment. Aptamers respond to many necessities because they can distinguish among thousand proteins and do so in a short period. They can detect small differences between proteins that are otherwise quite similar in structure, an essential property if proteins are differentiated on the cell surface.

Here, for the first time it has been set up a differential SELEX protocol to target whole living human cancer stem cells. In particular, I performed 15 cycles using breast cancers stem and differentiated cells coming from the same patient. Firstly, the aptamers library was incubated on the BCCs and unbound sequences were recovered for the selection phase, on breast cancer stem cells. The use of living cells as targets for SELEX has been already described. Indeed, it has been demonstrated that it is possible to obtain aptamers for a given transmembrane tyrosine kinase receptor (RET), if an appropriate protocol is adopted. This provided the first evidence for the possibility to use SELEX to distinguish between cells that differ for a single (or few) membrane epitope (Cerchia et al. 2005). Then, a similar approach was adopted to distinguish between closely related tumor cell lines by targeting unknown epitopes on the cell surface (Cerchia et al. 2009). Here I adopted a similar approach to distinguish among two different cancer cell states: stem and differentiated. Three works already exist on the selection of aptamers for stem surface epitopes. The first one identified aptamers for the epithelial cell adhesion molecule EpCAM (also known as CD326 or ESA) and the second one for the cancer stem cell marker CD133 (Shigdar et al. 2011; Shigdar et al. 2013). In both cases, SELEX was done on purified protein and, then, aptamers were tested on cells. However, this strategy presents some limitations. In fact, aptamers have the potential of being used in living systems, especially within human biological conditions, so it becomes important select aptamers in their native conformation and condition. Cell-SELEX, performed here, uses whole living cells to avoid the disadvantage of selecting physiologically nonfunctional aptamers. A third work exist to discovery aptamers for cancer stem cells. In this one, the authors identified DNA aptamers for prostate cancer stem cells. However, although DNA aptamers have some advantages over RNA aptamers, as simpler chemical modifications in order to grant nuclease resistance, secondary structures formed by ssDNA are less stable than those of RNA molecules (Harada and Frankel 1995).

In this study, after 15 cycles of cell-SELEX on BCSCs I performed Illumina sequencing on DNA pools for many selection rounds. Analyzing results with an algorithm, the maximum enrichment was reached in the 7th cycle with a reduction in the following cycles. This result reflects the enrichment found in the binding assay. In fact, 5'-[³²P]-labeled B15 and B0 cycles were compared

for their binding affinity to BCSCs, showing a fold change of ≤ 1.6 . This not so high rate probably is due to the fact that, after the maximum enrichment, the method has begun to select also less specific sequences for the stemness phenotype. So, it is important to set up the appropriate SELEX protocol for the selection goal.

A panel of 386 sequences was obtained. Among these, 43 sequences were extracted on the base of the enrichment index and grouped for their primary sequence similarity. I identified a big family of 39 sequences showing a high grade of similarity. This family was, then, regrouped on the base of structure prediction and the two most representatives sequences were extracted for future analysis. This two sequences will be assessed for their binding capability and specificity to discover the specific surface epitope, identifying new possible biomarkers for stemness phenotype in breast cancer. Then, these aptamers will be analyzed for their ability to block signal transduction of cancer stem cells. In fact, aptamers act in the same way as antibodies by folding into a three-dimensional structure to bind to their target, but in a advantageous way. First of all, both DNA and RNA ligands bind their targets with dissociation constants (Kd) in the low picomolar (1×10^{-12} M) to low nanomolar (1×10^{-9} M) range. This makes binding of an aptamer a highly specific interaction, with the ability to discriminate between related proteins that share common sets of structural domains. Aptamers also display low to no immunogenicity when administered in preclinical doses 1000-fold greater than doses used in animal and human therapeutic applications. Bioavailability and pharmacokinetics can also be modified in order to render aptamers resistant to nuclease degradation or to reduce renal clearance (Nimjee et al. 2005).

It is possible also to select aptamers that not only recognize a cell, but are also endocytosed. It is a competitive application for developing targeted delivery vehicles. Here I have set up a SELEX protocol for a rapid internalization of aptamers within cells identifying many individual sequences, as GL21 aptamer. Since their discovery, escort aptamers have been successfully adapted for the targeted delivery of active drug substances forming a molecular chimera.

This approach aims at combining an aptamer with another non-aptamer moiety (biomacromolecules, drug, or dyes), where one molecule engages with the target and the other one has a functional effect on the target molecule. It is difficult to know beforehand whether the joining may diminish the activity of one or both of the recombining partners (Burke and Willis 1998). However, with the progress of research in this field, as discussed here, it is very clear that chimeras are highly stable and efficient in activity.

I have developed and characterized an aptamer-miRNA chimera that target specific cells and act as substrate for Dicer, thereby triggering cell type-specific gene silencing. In this study, I have targeted an anti-apoptotic gene, PED, with a tumor suppressor microRNA specifically in cancer cells expressing the cell-surface receptor Axl. To date, all published RNA chimeras are made with siRNAs, so the conjugation of an aptamer with a microRNA is a new concept.

Due to their relatively small molecular weight (~6,000) and the endogenous power of targeting broad-range regulators, miRNAs have emerged as promising therapeutics. However, although synthetic miRNAs might be locally or systemically (intravenously) administered, negatively charged miRNAs have difficulty in penetrating hydrophobic cellular membranes, therefore requiring assisted cellular delivery. Moreover, miRNAs target a broad range of target genes in a context-dependent manner leading to unexpected effects in certain cells or tissues. So, it is very challenging to deliver tumor cell-specific miRNA therapeutics via an affordable and convenient approach.

One approach was the use of lentiviral or adenoviral vectors expressing miRNA precursors or inhibitors (antagomirs) (Kumar et al. 2008). However, the safety issue of viral vectors is a concept to consider in clinical applications. Other delivery approaches include nanoparticles or liposomes (Babar et al. 2012; Wu et al. 2011). In comparison with these approaches, an aptamer-microRNA chimera responds to many necessities, first of all that regarding the specific delivery, thus avoiding side effects. Moreover, an aptamer-miRNA chimera is a molecule totally composed by RNA sequences. This may have important advantages in terms of cost and production, flexibility regarding chemical modification and safety. Notably, the approach developed here is compatible with chemical synthesis of RNAs. Short RNA aptamers (25–35 bases) that bind various targets with high affinities have been described (Pestourie et al. 2005). Chimeras designed with such short aptamers would have a long strand of 45–55 bases, a length that can currently be produced with chemical synthesis. In contrast, protein reagent production in cell culture is considerably more complex and difficult to control. Moreover, chemically synthesized RNA is amenable to various modifications such as pegylation that can be used to modify its in vivo half-life and bioavailability. Of course, in the case of aptamer-miRNA chimeras, such modifications would need to be tested to determine whether they interfere with mechanisms such as uptake and processing by Dicer. An additional, notable advantage of the chimera over alternative approaches is its simplicity. As above mentioned, the chimera consists only of RNA, and any nonspecific side effects may, therefore, be limited to those already produced by the miRNAs themselves. Finally, as RNA is believed to be less immunogenic than protein, the chimeric RNAs would also be expected to produce less nonspecific activation of the immune system than protein-mediated delivery approaches. This fact may be important especially in case of following repeated administrations. In light of these reasons, microRNAs bioconjugated with aptamers are more advantageous compared to other approaches already existing.

Here I have generated two chimeras with distinct secondary structures, but they were not equally functional. In fact, the production of mature miRNAs is dependent on endogenous miRNA processing machinery. In first generation chimera, GL21-miR212 (1g), the aptamer is covalently linked to antisense strand of mature miR-212 hybridized to 21-mer sense strand. Instead, in second generation chimera, GL21-miR212 (2g), 26-mer antisense and sense strand are

not completely complementary, but they present an imperfect pairing making structure more similar to a pre-miR. Despite in both generations the antisense strand presents two overhanging bases (UU) at 3' end necessary for Dicer processing, between them only the second generation chimera is able to downregulate the miRNA target. The reason resides in the fact that Dicer-mediated processing of RNAs may result in more efficient incorporation of resulting miRNAs as well as siRNAs into RISC (Kim et al. 2005)). This suggestion is based on the observation that longer double-stranded RNAs (~29 bps), which are processed by Dicer, deplete their cognate mRNAs at lower concentrations than 19- to 21-bp miRNAs, which are not processed by Dicer. Thus, it is tempting to speculate that, because second generation chimera is correctly processed by Dicer, may be more potent in terms of gene-silencing ability than dsRNAs of 19–21 bps that are not processed.

GL21-miR212 (2g) was designed on the experience of Dassie et al. (2009) for A10-Plk1 chimera, in which A10 truncated aptamer recognizes PSMA receptor on the surface of prostate cancer cells and vehicles siPlk1 to RISC complex. So, I used the truncated version of GL21 aptamer consisting of 34 nucleotides of the 92mer original molecule. It maintains the active site of GL21 and preserves high binding affinity to cells expressing Axl, a receptor overexpressed in many human cancers. Chimera designed with the short aptamer has a long strand of 62 bases, a length that can be efficiently produced with chemical synthesis. Moreover, the aptamer is covalently linked to antisense strand to enhance loading of the guide strand into RISC. Optimal loading of the guide strand into RISC is thought to reduce off-target effects that result from inappropriate incorporation of both miRNA strands into the silencing complex (Sledz et al. 2003). Although we cannot rule out potential off-target effects mediated by the guide strand itself, these effects would likely be restricted to the tumor, as the miRNAs are targeted to Axl expressing cancer cells.

GL21-miR212 (2g) is able to bind and internalize into A459 cells, non-small cell lung cancer cell line, in a specific way. In fact, a scrambled chimera, GL21scr-miR212, which has a not-related structure in the aptamer portion, is unable to bind and internalize. In the same way, chimeras does not bind and internalize if assays are performed on MCF7, breast cancer cells not expressing Axl receptor.

Because chimera is totally made of RNA that is prone to degradation by nucleases into the blood, it was already synthesized with 2'-fluoropyrimidines to increase in vivo stability. So I performed experiments to mimic physiological conditions. This modification is well characterized in humans and is reported to be well tolerated with little toxicity (Behlke 2008). RNA oligonucleotides with this modification have already been approved for use in humans (Macugen), with many more quickly moving through the clinical pipeline (Katz and Goldbaum 2006). Although we cannot completely rule out potential intracellular toxicity of 2' fluoropyrimidines-modified RNAs leading to nonspecific immunostimulation, experiments in vivo demonstrated that

problematic toxicity in humans is not expected (Dassie et al. 2006). To reduce this possibility, however, I tested different concentrations of chimera from 50 up to 400 nM to determine the minimum concentration that had effect on miR target.

In the chimera the aptamer is linked to miR-212. It is a tumor suppressor miRNA because negatively modulates PED/PEA-15 expression, a protein with a broad antiapoptotic action. As known, apoptosis is the predominant mechanism by which cancer cells die in response to cytotoxic drugs, but deregulation of apoptosis-related proteins can led to resistance to drug treatments.

The anti-apoptotic action of PED is accomplished, at least in part, through its DED domain, which acts as a competitive inhibitor for pro-apoptotic molecules during the assembly of a functional death-inducing signaling complex (DISC) and inhibiting the activation of caspase 8, which take place following treatment with different apoptotic cytokines (CD95/FasL, TNF-alfa and TRAIL).

PED is found overexpressed in a number of different human tumors, including non-small cell lung cancer, which represents about 80% of all lung cancer and is mostly diagnosed at an advanced stage (either locally advanced or metastatic disease).

Because of resistance to therapeutic drugs, standard treatment of this tumor has only a 20% to 30% positive clinical response. In the last years, the discovery of the pivotal role in tumorigenesis of the Epidermal Growth Factor Receptor (EGFR) has provided a new class of targeted therapeutic agents: the EGFR tyrosine kinase inhibitors (EGFR-TKIs). Since their introduction in therapy, in advanced NSCLC patients harboring EGFR mutations, the use of EGFR TKIs in first-line treatment has provided an unusually large progression-free survival (PFS) benefit with a negligible toxicity when compared with cytotoxic chemotherapy. Nevertheless, resistance invariably occurs (Sgambato et al. 2012). TRAIL (ApoL/TNF-related apoptosis-inducing ligand) is a relatively new member of the tumor necrosis factor (TNF) ligand family, which induces apoptosis in a variety of cancers, both in vitro and in vivo, without producing significant effects in normal cells. This unique property makes TRAIL an attractive candidate for cancer therapy. However, a significant proportion of cancer cell lines is resistant to TRAIL-induced apoptosis. As already published by Incoronato et al. (2010), miR-212 targeting PED is able to increase TRAIL sensitivity. Here, I demonstrated that GL21-miR212 (2g) chimera is not only correctly processed by miRNA machinery, but is also functional. In fact, exogenous miR-212 delivered by GL21 aptamer led to TRAIL sensitization through caspase-8 activation in TRAIL-resistant cells, as A549.

6. CONCLUSIONS

In conclusion, in this study I have explored new possible applications for aptamers in targeted anti-cancer therapies. Through an appropriate SELEX protocol, I demonstrated that it is possible to select specific aptamers for the stemness phenotype in human breast cancer. Knowing that stem cells are responsible for tumor recurrences, aptamers could have important clinical benefits to overcome therapy resistance. At the same time, I also set up a SELEX protocol to identify aptamers able to be rapidly internalized within cells. I demonstrated that internalized aptamers can be used to create bioconjugates with “therapeutic” RNAs, as miRNAs. This strategy is advantageous over others already existing for miRNAs delivering, because summarizes many positive aspects: the specific delivery of miRNAs aptamer-mediated to avoid side effects, the clinical potential of miRNAs themselves and advantages in terms of cost, production, flexibility regarding chemical modification and safety of all made-RNA molecules.

ACKNOWLEDGMENTS

I would greatly to thank my supervisor Prof. Condorelli for the opportunity of this Ph.D, for her help during these years solving many problems and making me more confident in science.

Dr Vittorio de Franciscis and Laura Cerchia for their guidance, advices and encouragement.

Dr Paloma Giangrande giving hospitality to me twice in her lab at University of Iowa. She has transmitted to me her enthusiasm for this job and, also outside lab, she is a special person.

Dr Matilde Todaro and Giorgio Stassi providing me all the human breast samples.

All my lab friends, starting from Dr Cristina Quintavalle, my post-doc, for her help in scientific experiments and thank you to everybody for their friendship having spent so much time together. I can't forget Dr Ciro Zanca who suggested me for the position available in the lab.

Dr de Franciscis' lab and in particular Dr Carla Lucia Esposito for the continuous collaboration.

I would especially thank my parents. I don't have enough words to show my gratitude all days of my life.

Raffaella Fontanella has shared my difficulties in the last two years supporting me.

Barbara Trisciuglio, you are simply my best friend.

Finally, I would like to thank the Department of Molecular and Cellular Biology and Pathology L. Califano. It has provided the support and equipment I have needed to produce and complete my thesis.

REFERENCES

Al-Hajj M , Wicha MS , Benito-Hernandez A , Morrison SJ , Clarke MF . Prospective identification of tumorigenic breast cancer cells . Proc Natl Acad Sci U S A 2003 ; 100 (7): 3983 – 3988.

Babar IA, Cheng CJ, Booth CJ, Liang X, Weidhaas JB, Saltzman WM, Slack FJ. Nanoparticle-based therapy in an in vivo microRNA-155 (miR-155)-dependent mouse model of lymphoma. Proc Natl Acad Sci U S A. 2012;109(26):E1695-704.

Behlke MA. Chemical modification of siRNAs for in vivo use. Oligonucleotides 2008;18(4):305-19.

Bonnet D, Dick JE. Human acute myeloid leukemia is organized as a hierarchy that originates from a primitive hematopoietic cell. Nat Med 1997;3:730–737.

Burke DH, Willis JH. Recombination, RNA evolution, and bifunctional RNA molecules isolated through chimeric SELEX. RNA. 1998;4(9):1165-75.

Calin GA, Dumitru CD, Shimizu M, Bichi R, Zupo S, Noch E, Aldler H, Rattan S, Keating M, Rai K, Rassenti L, Kipps T, Negrini M, Bullrich F, Croce CM. Frequent deletions and down-regulation of micro-RNA genes miR15 and miR16 at 13q14 in chronic lymphocytic leukemia. Proc Natl Acad Sci U S A. 2002;99(24):15524-9.

Calin GA, Ferracin M, Cimmino A, Di Leva G, Shimizu M, Wojcik SE, Iorio MV, Visone R, Sever NI, Fabbri M, Iuliano R, Palumbo T, Pichiorri F, Roldo C, Garzon R, Sevignani C, Rassenti L, Alder H, Volinia S, Liu CG, Kipps TJ, Negrini M, Croce CM. A MicroRNA signature associated with prognosis and progression in chronic lymphocytic leukemia. N Engl J Med. 2005;353(17):1793-801.

Cariati M, Purushotham AD. Stem cells and breast cancer. Histopathology 2008 ;52(1):99-107.

Cerchia L, Ducongé F, Pestourie C, Boulay J, Aissouni Y, Gombert K, Tavitian B, de Franciscis V, Libri D. Neutralizing aptamers from whole-cell SELEX inhibit the RET receptor tyrosine kinase. PLoS Biol. 2005;3(4):e123.

Cerchia L, De Franciscis V. Noncoding RNAs in cancer medicine. J Biomed Biotechnol. 2006;2006(4):73104.

Cerchia L, Esposito CL, Jacobs AH, Tavitian B, de Franciscis V. Differential SELEX in human glioma cell lines. *PLoS One* 2009;4(11):e7971.

Cerchia L, Esposito CL, Camorani S, Rienzo A, Stasio L, Insabato L, Affuso A, de Franciscis V. Targeting Axl with an high-affinity inhibitory aptamer. *Mol Ther*. 2012;20(12):2291-303.

Chaloin L, Lehmann MJ, Sczakiel G, Restle T. Endogenous expression of a high-affinity pseudoknot RNA aptamer suppresses replication of HIV-1. *Nucleic Acids Res*. 2002;30(18):4001-8.

Chang JC, Wooten EC, Tsimelzon A, Hilsenbeck SG, Gutierrez MC, Tham YL, Kalidas M, Elledge R, Mohsin S, Osborne CK, Chamness GC, Allred DC, Lewis MT, Wong H, O'Connell P. Patterns of resistance and incomplete response to docetaxel by gene expression profiling in breast cancer patients. *J Clin Oncol*. 2005;23(6):1169-77.

Charafe-Jauffret E, Monville F, Ginestier C, Dontu G, Birnbaum D, Wicha MS. Cancer stem cells in breast: current opinion and future challenges. *Pathobiology* 2008;75(2):75-84.

Chu TC, Twu KY, Ellington AD, Levy M. Aptamer mediated siRNA delivery. *Nucleic Acids Res* 2006;34:e73

Chung BI, Malkowicz SB, Nguyen TB, Libertino JA, McGarvey TW. Expression of the proto-oncogene Axl in renal cell carcinoma. *DNA Cell Biol*. 2003;22(8):533-40.

Cimmino A, Calin GA, Fabbri M, Iorio MV, Ferracin M, Shimizu M, Wojcik SE, Aqeilan RI, Zupo S, Dono M, Rassenti L, Alder H, Volinia S, Liu CG, Kipps TJ, Negrini M, Croce CM. miR-15 and miR-16 induce apoptosis by targeting BCL2. *Proc Natl Acad Sci USA*. 2005;102(39):13944-9.

Clayton H, Titley I, Vivanco Md. Growth and differentiation of progenitor/stem cells derived from the human mammary gland. *Exp Cell Res*. 2004;297(2):444-60.

Condorelli G, Vigliotta G, Iavarone C, Caruso M, Tocchetti CG, Andreozzi F, Cafieri A, Tecce MF, Formisano P, Beguinot L, Beguinot. PED/PEA-15 gene controls glucose transport and is overexpressed in type 2 diabetes mellitus. *EMBO J*. 1998;17(14):3858-66.

Creighton CJ, Li X, Landis M, Dixon JM, Neumeister VM, Sjolund A, Rimm DL, Wong H, Rodriguez A, Herschkowitz JI, Fan C, Zhang X, He X, Pavlick A, Gutierrez MC, Renshaw L, Larionov AA, Faratian D, Hilsenbeck SG, Perou CM, Lewis MT, Rosen JM, Chang JC. Residual breast cancers after conventional therapy display mesenchymal as well as tumor-initiating features. *Proc Natl Acad Sci U S A.* 2009;106(33):13820-5.

Daniel C, Young L, Medina D, Deome K. The influence of mammogenic hormones on serially transplanted mouse mammary gland. *Exp. Gerontol.* 1971; 6(1):95-101.

Dassie JP, Liu XY, Thomas GS, Whitaker RM, Thiel KW, Stockdale KR, Meyerholz DK, McCaffrey AP, McNamara JO, Giangrande PH. Systemic administration of optimized aptamer-siRNA chimeras promotes regression of PSMA-expressing tumors. *Nat Biotechnol* 2009;27:839-849.

Dontu G, Abdallah WM, Foley JM, Jackson KW, Clarke MF, Kawamura MJ, Wicha MS. In vitro propagation and transcriptional profiling of human mammary stem/progenitor cells. *Genes Dev.* 2003;17(10):1253-70.

Dontu G, Al-Hajj M, Abdallah WM, Clarke MF, Wicha MS. Stem cells in normal breast development and breast cancer. *Cell Prolif.* 2003;36 Suppl 1:59-72.

Dua P, Kim S, Lee DK. Nucleic acid aptamers targeting cell-surface proteins. *Methods* 2011;54(2):215-25.

Ellington AD, Szostak JW. In vitro selection of RNA molecules that bind specific ligands. *Nature* 1990;346:818–822.

Elmén J, Lindow M, Silahtaroglu A, Bak M, Christensen M, Lind-Thomsen A, Hedtjärn M, Hansen JB, Hansen HF, Straarup EM, McCullagh K, Kearney P, Kauppinen S. Antagonism of microRNA-122 in mice by systemically administered LNA-antimiR leads to up-regulation of a large set of predicted target mRNAs in the liver. *Nucleic Acids Res.* 2008;36(4):1153-62.

Farokhzad OC, Jon S, Khademhosseini A, Tran TN, Lavan DA, Langer R. Nanoparticle-aptamer bioconjugates: a new approach for targeting prostate cancer cells. *Cancer Res.* 2004;64(21):7668-72.

Fitzwater T, Polisky B. A SELEX primer. *Methods Enzymol.* 1996;267:275-301.

Ginestier C, Hur MH, Charafe-Jauffret E, Monville F, Dutcher J, Brown M, Jacquemier J, Viens P, Kleer CG, Liu S, Schott A, Hayes D, Birnbaum D, Wicha MS, Dontu G. ALDH1 is a marker of normal and malignant human mammary stem cells and a predictor of poor clinical outcome. *Cell Stem Cell*. 2007;1(5):555-67.

Good PD, Krikos AJ, Li SX, Bertrand E, Lee NS, Giver L, Ellington A, Zaia JA, Rossi JJ, Engelke DR. Expression of small, therapeutic RNAs in human cell nuclei. *Gene Ther*. 1997;4(1):45-54.

Gudjonsson T, Villadsen R, Nielsen HL, Rønnov-Jessen L, Bissell MJ, Petersen OW. Isolation, immortalization, and characterization of a human breast epithelial cell line with stem cell properties. *Genes Dev*. 2002;16(6):693-706.

Guo S, Tschammer N, Mohammed S, Guo P. Specific delivery of therapeutic RNAs to cancer cells via the dimerization mechanism of phi29 motor pRNA. *Hum Gene Ther* 2005;16:1097-1109

Gusterson BA, Warburton MJ, Mitchell D, Ellison M, Neville AM, Rudland PS. Distribution of myoepithelial cells and basement membrane proteins in the normal breast and in benign and malignant breast diseases. *Cancer Res*. 1982;42(11):4763-70.

Harada K, Frankel AD. Identification of two novel arginine binding DNAs. *EMBO J*. 1995;14(23):5798-811.

Hatakeyama H, Cheng H, Wirth P, Counsell A, Marcrom SR, Wood CB, Pohlmann PR, Gilbert J, Murphy B, Yarbrough WG, Wheeler DL, Harari PM, Guo Y, Shyr Y, Slebos RJ, Chung CH. Regulation of heparin-binding EGF-like growth factor by miR-212 and acquired cetuximab-resistance in head and neck squamous cell carcinoma. *PLoS One* 2010;5(9):e12702.

Hennighausen L, Robinson GW. Signaling pathways in mammary gland development. *Dev Cell*. 2001;1(4):467-75.

Hermann T, Patel DJ. Adaptive recognition by nucleic acid aptamers. *Science* 2000;287:820–825.

Hicke BJ, Stephens AW. Escort aptamers: a delivery service for diagnosis and therapy. *J Clin Invest*. 2000;106(8):923-8.

Hicke BJ, Stephens AW, Gould T, Chang YF, Lynott CK, Heil J, Borkowski S, Hilger CS, Cook G, Warren S, Schmidt PG. Tumor targeting by an aptamer. *J Nucl Med*. 2006;47(4):668-78.

Hutterer M, Knyazev P, Abate A, Reschke M, Maier H, Stefanova N, Knyazeva T, Barbieri V, Reindl M, Muigg A, Kostron H, Stockhammer G, Ullrich A. Axl and growth arrest-specific gene 6 are frequently overexpressed in human gliomas and predict poor prognosis in patients with glioblastoma multiforme. *Clin Cancer Res.* 2008;14(1):130-8.

Incoronato M, Garofalo M, Urso L, Romano G, Quintavalle C, Zanca C, Iaboni M, Nuovo G, Croce CM, Condorelli G. miR-212 increases tumor necrosis factor-related apoptosis-inducing ligand sensitivity in non-small cell lung cancer by targeting the antiapoptotic protein PED. *Cancer Res.* 2010;70(9):3638-46.

Incoronato M, Urso L, Portela A, Laukkanen MO, Soini Y, Quintavalle C, Keller S, Esteller M, Condorelli G. Epigenetic regulation of miR-212 expression in lung cancer. *PLoS One* 2011;6(11):e27722.

Katz B, Goldbaum M. Macugen (pegaptanib sodium), a novel ocular therapeutic that targets vascular endothelial growth factor (VEGF). *Int Ophthalmol Clin.* 2006;46(4):141-54.

Khati M, Schüman M, Ibrahim J, Sattentau Q, Gordon S, James W. Neutralization of infectivity of diverse R5 clinical isolates of human immunodeficiency virus type 1 by gp120-binding 2'F-RNA aptamers. *J Virol.* 2003;77(23):12692-8.

Kim DH, Behlke MA, Rose SD, Chang MS, Choi S, Rossi JJ. Synthetic dsRNA Dicer substrates enhance RNAi potency and efficacy. *Nat Biotechnol.* 2005;23(2):222-6.

Kim ND, Oberley TD, Yasukawa-Barnes J, Clifton KH. Stem cell characteristics of transplanted rat mammary clonogens. *Exp Cell Res.* 2000;260(1):146-59.

Kim AH, Reimers M, Maher B, Williamson V, McMichael O, McClay JL, van den Oord EJ, Riley BP, Kendler KS, Vladimirov VI. MicroRNA expression profiling in the prefrontal cortex of individuals affected with schizophrenia and bipolar disorders. *Schizophr. Res.* 2010;124:183–191.

Kolibaba KS, Druker BJ. Protein tyrosine kinases and cancer. *Biochim Biophys Acta.* 1997;1333(3):F217-48.

Koorstra JB, Karikari CA, Feldmann G, Bisht S, Rojas PL, Offerhaus GJ, Alvarez H, Maitra A. The Axl receptor tyrosine kinase confers an adverse prognostic influence in pancreatic cancer and represents a new therapeutic target. *Cancer Biol Ther.* 2009;8(7):618-26.

- Kordon EC, Smith GH. An entire functional mammary gland may comprise the progeny from a single cell. *Development* 1998;125(10):1921-30.
- Kumar MS, Erkeland SJ, Pester RE, Chen CY, Ebert MS, Sharp PA, Jacks T. Suppression of non-small cell lung tumor development by the let-7 microRNA family. *Proc Natl Acad Sci U S A*. 2008;105(10):3903-8.
- Kwak PB, Iwasaki S, Tomari Y. The microRNA pathway and cancer. *Cancer Sci*. 2010;101(11):2309-15.
- Lanford RE, Hildebrandt-Eriksen ES, Petri A, Persson R, Lindow M, Munk ME, Kauppinen S, Ørum H. Therapeutic silencing of microRNA-122 in primates with chronic hepatitis C virus infection. *Science*. 2010;327(5962):198-201.
- Lee RC, Feinbaum RL, Ambros V. The *C. elegans* heterochronic gene *lin-4* encodes small RNAs with antisense complementarity to *lin-14*. *Cell* 1993;75(5):843-54.
- Li X, Lewis MT, Huang J, Gutierrez C, Osborne CK, Wu MF, Hilsenbeck SG, Pavlick A, Zhang X, Chamness GC, Wong H, Rosen J, Chang JC. Intrinsic resistance of tumorigenic breast cancer cells to chemotherapy. *J Natl Cancer Inst*. 2008;100(9):672-9.
- Liu S, Dontu G, Wicha MS. Mammary stem cells, self-renewal pathways, and carcinogenesis. *Breast Cancer Res*. 2005;7(3):86-95.
- Livak KJ, Schmittgen TD. Analysis of relative gene expression data using real-time quantitative PCR and the 2(-Delta Delta C(T)) Method. *Methods* 2001;25(4):402-8.
- Lynam-Lennon N, Maher SG, Reynolds JV. The roles of microRNA in cancer and apoptosis. *Biol Rev Camb Philos Soc*. 2009;84(1):55-71.
- Lupold SE, Hicke BJ, Lin Y, Coffey DS. Identification and characterization of nuclease-stabilized RNA molecules that bind human prostate cancer cells via the prostate-specific membrane antigen. *Cancer Res* 2002;62:4029-4033.
- Mann MJ, Dzau VJ. Therapeutic applications of transcription factor decoy oligonucleotides. *J Clin Invest*. 2000;106(9):1071-5.
- McNamara JO, Andrechek ER, Wang Y, Viles KD, Rempel RE, Gilboa E, Sullenger BA, Giangrande PH. Cell type-specific delivery of siRNAs with aptamer-siRNA chimeras. *Nat Biotechnol* 2006;24:1005-1015.

Nana-Sinkam SP, Croce CM. Clinical applications for microRNAs in cancer. *Clin Pharmacol Ther.* 2013;93(1):98-104.

Nimjee SM, Rusconi CP, Sullenger BA. Aptamers: an emerging class of therapeutics. *Annu Rev Med.* 2005;56:555-83.

Mo YY. MicroRNA regulatory networks and human disease. *Cell Mol Life Sci.* 2012;69(21):3529-31.

Patil SD, Rhodes DG, Burgess DJ. DNA-based therapeutics and DNA delivery systems: a comprehensive review. *AAPS J.* 2005;7(1):E61-77.

Patrawala L, Calhoun T, Schneider-Broussard R, Li H, Bhatia B, Tang S, Reilly JG, Chandra D, Zhou J, Claypool K, Coghlan L, Tang DG. Highly purified CD44+ prostate cancer cells from xenograft human tumors are enriched in tumorigenic and metastatic progenitor cells. *Oncogene.* 2006;25(12):1696-708.

Perkins DO, Jeffries CD, Jarskog LF, Thomson JM, Woods K, Newman MA, Parker J S, Jin J, Hammond SM. microRNA expression in the prefrontal cortex of individuals with schizophrenia and schizoaffective disorder. *Genome Biol.* 2007;8: R27.

Pestourie C, Tavitian B, Duconge F. Aptamers against extracellular targets for in vivo applications. *Biochimie.* 2005;87(9-10):921-30.

Phillips TM, McBride WH, Pajonk F. The response of CD24(-/low)/CD44+ breast cancer-initiating cells to radiation. *J Natl Cancer Inst.* 2006;98(24):1777-85.

Ponti D, Costa A, Zaffaroni N, Pratesi G, Petrangolini G, Coradini D, Pilotti S, Pierotti MA, Daidone MG. Isolation and in vitro propagation of tumorigenic breast cancer cells with stem/progenitor cell properties. *Cancer Res.* 2005;65(13):5506-11.

Ponti D, Zaffaroni N, Capelli C, Daidone MG. Breast cancer stem cells: an overview. *Eur J Cancer* 2006;42(9):1219-24.

Potten CS, Watson RJ, Williams GT, Tickle S, Roberts SA, Harris M, Howell A. The effect of age and menstrual cycle upon proliferative activity of the normal human breast. *Br J Cancer* 1988;58(2):163-70.

Reya T, Morrison SJ, Clarke MF, Weissman IL. Stem cells, cancer, and cancer stem cells. *Nature* 2001;414(6859):105-11.

Reynolds BA, Weiss S. Clonal and population analyses demonstrate that an EGF-responsive mammalian embryonic CNS precursor is a stem cell. *Dev Biol.* 1996;175(1):1-13.

Rikova K, Guo A, Zeng Q, Possemato A, Yu J, Haack H, Nardone J, Lee K, Reeves C, Li Y, Hu Y, Tan Z, Stokes M, Sullivan L, Mitchell J, Wetzel R, Macneill J, Ren JM, Yuan J, Bakalarski CE, Villen J, Kornhauser JM, Smith B, Li D, Zhou X, Gygi SP, Gu TL, Polakiewicz RD, Rush J, Comb MJ. Global survey of phosphotyrosine signaling identifies oncogenic kinases in lung cancer. *Cell.* 2007;131(6):1190-203.

Rudland PS, Barraclough R, Fernig DG, Smith JA. Mammary stem cells in normal development and cancer. In: Potten CS. *Stem Cells* vol. 147.

Rusconi CP, Scardino E, Layzer J, Pitoc GA, Ortel TL, Monroe D, Sullenger BA. RNA aptamers as reversible antagonists of coagulation factor IXa. *Nature* 2002;419(6902):90-4.

Sainaghi PP, Castello L, Bergamasco L, Galletti M, Bellosta P, Avanzi GC. Gas6 induces proliferation in prostate carcinoma cell lines expressing the Axl receptor. *J Cell Physiol.* 2005;204(1):36-44.

Sgambato A, Casaluce F, Maione P, Rossi A, Rossi E, Napolitano A, Palazzolo G, Bareschino MA, Schettino C, Sacco PC, Ciardiello F, Gridelli C. The role of EGFR tyrosine kinase inhibitors in the first-line treatment of advanced non small cell lung cancer patients harboring EGFR mutation. *Curr Med Chem.* 2012;19(20):3337-52.

Shieh YS, Lai CY, Kao YR, Shiah SG, Chu YW, Lee HS, Wu CW. Expression of axl in lung adenocarcinoma and correlation with tumor progression. *Neoplasia.* 2005;7(12):1058-64.

Shigdar S, Lin J, Yu Y, Pastuovic M, Wei M, Duan W. RNA aptamer against a cancer stem cell marker epithelial cell adhesion molecule. *Cancer Sci.* 2011;102(5):991-8.

Shigdar S, Qiao L, Zhou SF, Xiang D, Wang T, Li Y, Lim LY, Kong L, Li L, Duan W. RNA aptamers targeting cancer stem cell marker CD133. *Cancer Lett.* 2013;330(1):84-95.

Sledz CA, Holko M, de Veer MJ, Silverman RH, Williams BR. Activation of the interferon system by short-interfering RNAs. *Nat Cell Biol.* 2003;5(9):834-9.

Soreq H, Wolf Y. NeurimmiRs: microRNAs in the neuroimmune interface. *Trends Mol. Med.* 2011;17:548–555.

Thompson JD, Gibson TJ, Plewniak F, Jeanmougin F, Higgins DG. The CLUSTAL_X windows interface: flexible strategies for multiple sequence alignment aided by quality analysis tools. *Nucleic Acids Res.* 1997;25(24):4876-82.

Tuerk C, Gold L. Systematic evolution of ligands by exponential enrichment: RNA ligands to bacteriophage T4 DNA polymerase. *Science* 1990;249:505–510.

Visvader JE. Cells of origin in cancer. *Nature* 2011;469(7330):314-22.

Vivanco Md. Biomarkers in breast cancer. *Methods Mol Biol.* 2010;593:137-56.

Wada R, Akiyama Y, Hashimoto Y, Fukamachi H, Yuasa Y. miR-212 is downregulated and suppresses methyl-CpG-binding protein MeCP2 in human gastric cancer. *Int. J. Cancer* 2009;127:1106–1114.

Wanet A, Tacheny A, Arnould T, Renard P. miR-212/132 expression and functions: within and beyond the neuronal compartment. *Nucleic Acids Res.* 2012;40(11):4742-53.

Wang WX, Huang Q, Hu Y, Stromberg AJ, Nelson PT. Patterns of microRNA expression in normal and early Alzheimer's disease human temporal cortex: white matter versus gray matter. *Acta Neuropathol.* 2011;121:193–205

Weiss S, Reynolds BA, Vescovi AL, Morshead C, Craig CG, van der Kooy D. Is there a neural stem cell in the mammalian forebrain? *Trends Neurosci.* 1996;19(9):387-93.

Wicha MS, Liu S, Dontu G. Cancer stem cells: an old idea. A paradigm shift. *Cancer Res.* 2006;66(4):1883-90.

Willis MC, Collins BD, Zhang T, Green LS, Sebesta DP, Bell C, Kellogg E, Gill SC, Magallanez A, Knauer S, Bendele RA, Gill PS, Janjić N. Liposome-anchored vascular endothelial growth factor aptamers. *Bioconjug Chem.* 1998;9(5):573-82.

Wu Y, Crawford M, Yu B, Mao Y, Nana-Sinkam SP, Lee LJ. MicroRNA delivery by cationic lipoplexes for lung cancer therapy. *Mol Pharm.* 2011;8(4):1381-9.

Wu CW, Li AF, Chi CW, Lai CH, Huang CL, Lo SS, Lui WY, Lin WC. Clinical significance of AXL kinase family in gastric cancer. *Anticancer Res.* 2002;22(2B):1071-8.

Wu J, Xie X. Comparative sequence analysis reveals an intricate network among REST, CREB and miRNA in mediating neuronal gene expression. *Genome Biol.* 2006;7(9):R85.

Wullner U, Neef I, Eller A, Kleines M, Tur MK, Barth S. Cell-specific induction of apoptosis by rationally designed bivalent aptamer-siRNA transcripts silencing eukaryotic elongation factor 2. *Curr Cancer Drug Targets* 2008;8:554-565.

Xiao Z, Shanguan D, Cao Z, Fang X, Tan W. Cell-specific internalization study of an aptamer from whole cell selection. *Chemistry* 2008;14(6):1769-75.

Zanca C, Garofalo M, Quintavalle C, Romano G, Acunzo M, Ragno P, Montuori N, Incoronato M, Tornillo L, Baumhoer D, Briguori C, Terracciano L, Condorelli G. PED is overexpressed and mediates TRAIL resistance in human non-small cell lung cancer. *J Cell Mol Med.* 2008;12(6A):2416-26.

Zhang Z, Chang H, Li Y, Zhang T, Zou J, Zheng X, Wu J. MicroRNAs: potential regulators involved in human anencephaly. *Int. J. Biochem. Cell Biol.* 2010;42, 367–374.

Zhang YX, Knyazev PG, Cheburkin YV, Sharma K, Knyazev YP, Orfi L, Szabadkai I, Daub H, Kéri G, Ullrich A. AXL is a potential target for therapeutic intervention in breast cancer progression. *Cancer Res.* 2008;68(6):1905-15.

Zhang B, Pan X, Cobb GP, Anderson TA. microRNAs as oncogenes and tumor suppressors. *Dev Biol.* 2007;302(1):1-12.

Zhou Q, Liu Y, Shin DS, Silangcruz J, Tuleuova N, Revzin A. Aptamer-containing surfaces for selective capture of CD4 expressing cells. *Langmuir* 2012;28(34):12544-9.

Zhou J, Rossi JJ. Aptamer-targeted cell-specific RNA interference. *Silence* 2010;1(1):4.

Zhou J, Swiderski P, Li H, Zhang J, Neff CP, Akkina R, Rossi JJ. Selection, characterization and application of new RNA HIV gp 120 aptamers for facile delivery of Dicer substrate siRNAs into HIV infected cells. *Nucleic Acids Res* 2009;37:3094-109.

Zuker M. Mfold web server for nucleic acid folding and hybridization prediction. *Nucleic Acids Res.* 2003;31(13):3406-15.



Cancer Research

miR-212 Increases Tumor Necrosis Factor–Related Apoptosis-Inducing Ligand Sensitivity in Non –Small Cell Lung Cancer by Targeting the Antiapoptotic Protein PED

Mariarosaria Inconorato, Michela Garofalo, Loredana Urso, et al.

Cancer Res 2010;70:3638-3646. Published OnlineFirst April 13, 2010.

Updated version Access the most recent version of this article at:
doi:[10.1158/0008-5472.CAN-09-3341](https://doi.org/10.1158/0008-5472.CAN-09-3341)

Supplementary Material Access the most recent supplemental material at:
<http://cancerres.aacrjournals.org/content/suppl/2010/04/13/0008-5472.CAN-09-3341.DC1.html>

Cited Articles This article cites by 30 articles, 14 of which you can access for free at:
<http://cancerres.aacrjournals.org/content/70/9/3638.full.html#ref-list-1>

Citing articles This article has been cited by 7 HighWire-hosted articles. Access the articles at:
<http://cancerres.aacrjournals.org/content/70/9/3638.full.html#related-urls>

E-mail alerts [Sign up to receive free email-alerts](#) related to this article or journal.

Reprints and Subscriptions To order reprints of this article or to subscribe to the journal, contact the AACR Publications Department at pubs@aacr.org.

Permissions To request permission to re-use all or part of this article, contact the AACR Publications Department at permissions@aacr.org.

miR-212 Increases Tumor Necrosis Factor–Related Apoptosis-Inducing Ligand Sensitivity in Non–Small Cell Lung Cancer by Targeting the Antiapoptotic Protein PED

Mariarosaria Incoronato¹, Michela Garofalo⁵, Loredana Urso¹, Giulia Romano¹, Cristina Quintavalle²,
Ciro Zanca², Margherita Iaboni², Gerald Nuovo⁵, Carlo Maria Croce⁵, and Gerolama Condorelli^{2,3,4}

Abstract

PED/PEA-15 (PED) is a death effector domain family member of 15 kDa with a broad antiapoptotic function found overexpressed in a number of different human tumors, including lung cancer. To date, the mechanisms that regulate PED expression are unknown. Therefore, we address this point by the identification of microRNAs that in non–small cell lung cancer (NSCLC) modulate PED levels. In this work, we identify miR-212 as a negative regulator of PED expression. We also show that ectopic expression of this miR increases tumor necrosis factor–related apoptosis-inducing ligand (TRAIL)–induced cell death in NSCLC cells. In contrast, inhibition of endogenous miR-212 by use of antago-miR results in increase of PED protein expression and resistance to TRAIL treatment. Besides, in NSCLC, we show both *in vitro* and *in vivo* that PED and miR-212 expressions are inversely correlated, that is, PED is upregulated and miR-212 is rarely expressed. In conclusion, these findings suggest that miR-212 should be considered as a tumor suppressor because it negatively regulates the antiapoptotic protein PED and regulates TRAIL sensitivity. *Cancer Res*; 70(9); 3638–46. ©2010 AACR.

Introduction

Lung cancer is one of the most common causes of cancer-related deaths worldwide. About 80% of all lung cancers are of the non–small cell lung carcinoma (NSCLC) type, which is divided in to three subtypes: squamous cell carcinoma (25–30%), adenocarcinoma (40%), and large-cell carcinoma (10–15%; ref. 1). Because of their resistance to therapeutic drugs, standard treatment of these tumors has only a 20% to 30% positive clinical response. Therefore, to develop new therapeutic strategies to improve therapy for NSCLC is important in understanding the molecular mechanisms involved in cell death resistance.

Apoptosis is the predominant mechanism by which cancer cells die in response to cytotoxic drugs. Resistance to drug treatment is due to deregulation of apoptosis-related proteins. Among these proteins is PED/PEA-15, a death effector domain

(DED) family member of 15 kDa having a variety of effects on cell growth and metabolism (2–4). PED/PEA-15 was found overexpressed in a number of different human tumors, including gliomas, squamous carcinoma, thyroid, breast, lung cancer, and B-cell chronic lymphocytic leukemia (5–9). PED/PEA-15 has a broad antiapoptotic action, being able to inhibit both the intrinsic and the extrinsic apoptotic pathways. Inhibition of the extrinsic pathway is accomplished through its DED, which likely acts as a competitive inhibitor for proapoptotic molecules during the assembly of the death-inducing signaling complex (3, 6). Recently, regulation of PED/PEA-15 phosphorylation by PTEN was shown to play a key role in determining whether a cell dies by type I or type II Fas-induced apoptosis (10). We recently showed that in NSCLC, PED/PEA-15 overexpression is responsible for a tumor necrosis factor–related apoptosis-inducing ligand (TRAIL)–resistant phenotype (9). Furthermore, PED is upregulated in breast cancer where it induces resistance to chemotherapeutic treatment (8, 9). To date, although PED/PEA-15 is overexpressed in a number of different cancer types, the mechanisms that regulate its expression are unknown.

An important mechanism of protein expression regulation involves microRNAs (miRNA). These molecules are evolutionarily conserved, endogenous noncoding RNAs of about 22 nucleotides (nt) in length that function at the posttranscriptional level (11). In animals, single-stranded miRNAs bind with specific mRNAs through sequences that are partially complementary to the 3' untranslated region (UTR) of the target mRNA (12). miRNAs are involved in numerous cellular processes including development, differentiation, proliferation, apoptosis, and response to stress (13, 14). To date, more than 600 human miRNAs have been experimentally identified and estimated to

Authors' Affiliations: ¹Fondazione IRCCS SDN, Naples, Italy; ²Dipartimento di Biologia e Patologia Cellulare e Molecolare and ³Facoltà di Scienze Biotechnologiche, "Federico II" University of Naples; ⁴Istituto di Endocrinologia e Oncologia Sperimentale, Consiglio Nazionale delle Ricerche, Naples, Italy; and ⁵Department of Molecular Virology, Immunology and Medical Genetics, Human Cancer Genetics Program, Comprehensive Cancer Center, The Ohio State University, Columbus, Ohio

Note: Supplementary data for this article are available at Cancer Research Online (<http://cancerres.aacrjournals.org/>).

M. Garofalo and L. Urso contributed equally to this work.

Corresponding Author: Gerolama Condorelli, Dipartimento di Biologia e Patologia Cellulare e Molecolare, Via Pansini, 5, 80131 Naples, Italy. Phone: 39-081-746-4416; Fax: 39-081-746-3308; E-mail: gecondor@unina.it.

doi: 10.1158/0008-5472.CAN-09-3341

©2010 American Association for Cancer Research.

regulate more than one third of cellular mRNAs. Interestingly, numerous oncogenes and tumor suppressor genes are regulated by miRNAs. With the advent of miRNA expression profiling, significant effort is being made to correlate miRNA expression with tumor prognosis (15, 16). To date, a number of downregulated miRNAs found in lung cancer correlate with patient survival (17, 18) and with therapeutic response (19).

In this article, we identify a miRNA that regulates PED/PEA-15 expression. Our data indicate that miR-212 negatively modulates PED/PEA-15 expression and sensitizes non-small cell lung cancer (NSCLC) cells to TRAIL-induced apoptosis. Moreover, we report that NSCLC-affected lung tissue overexpressing PED/PEA-15 protein has a concordant downregulation of miR-212.

Materials and Methods

Cell culture and transfection. Calu-1 (NSCLC) cells were grown in DMEM; H460 cells were grown in RPMI. Media were supplemented with 10% heat-inactivated fetal bovine serum (FBS), 2 mmol/L L-glutamine, and 100 units/mL penicillin/streptomycin. For transient transfection, cells at 50% confluency were transfected using Lipofectamine 2000 (Invitrogen) with 100 nmol/L (final) of pre-miR-212, pre-miR-34a, pre-miR-124a, scrambled, or antisense miR-212 (Applied Biosystems). Transfections were done with Lipofectamine 2000 according to the manufacturer's instructions (Invitrogen). Meg01 cells (human, chronic myelogenous leukemia cells) were grown in RPMI 1640 + 2 mmol/L glutamine + 10% FBS.

Lung cancer samples. A total of 18 snap-frozen normal and malignant lung tissues (12 men and 6 women; median age, 70.0 y; range, 55–82 y) were collected at the Ohio State University Medical Center (Columbus, OH).

Protein isolation and Western blotting. Cells were washed twice in ice-cold PBS and lysed in JS buffer [50 mmol/L HEPES (pH 7.5) containing 150 mmol/L NaCl, 1% glycerol, 1% Triton X100, 1.5 mmol/L MgCl₂, 5 mmol/L EGTA, 1 mmol/L Na₃VO₄, and 1× protease inhibitor cocktail]. Protein concentration was determined by the Bradford assay (Bio-Rad) using bovine serum albumin as the standard, and equal amounts of proteins were analyzed by SDS-PAGE (12.5% acrylamide). Gels were electroblotted onto polyvinylidene difluoride membranes (Millipore). For immunoblot experiments, membranes were blocked for 1 h with 5% nonfat dry milk in TBS containing 0.1% Tween 20 and incubated at 4°C overnight with primary antibody. Detection was done with peroxidase-conjugated secondary antibodies using the enhanced chemiluminescence system (Amersham-Pharmacia Biosciences). Primary antibodies used were anti-PED (3), anti-caspase-8 (Cell Signaling), and anti-β-actin (Sigma).

Cell death quantification. Calu-1 cells were transfected with pre-miR-212 or control for 48 h. Cells were then trypsinized, plated in 96-well plates in triplicate, and further incubated with 10 or 25 ng/mL superkiller TRAIL (Alexis Biochemicals) for 24 h. Cell viability was evaluated with the CellTiter 96 AQueous One Solution Cell Proliferation Assay (Promega) according to the manufacturer's protocol. Metabolically active cells were detected by adding 20 μL of MTS

to each well. After 2 h of incubation, the plates were analyzed in a Multilabel Counter (BioTek).

Cell death assessment by Annexin V staining. Calu1 cells were transfected with 100 nmol/L miR scrambled and with 100 nmol/L miR-212. After 48 h, cells were treated with 10 or 25 ng/mL of TRAIL for 24 h, harvested, washed twice with cold PBS, and stained with Annexin V-FITC Apoptosis Detection Kit 1 (BD Pharmingen). Briefly, cells were resuspended in 100 μL of 1× binding buffer and 5 μL of Annexin V and then incubated for 15 min at room temperature. Apoptotic cells were analyzed by flow cytometry.

RNA extraction and real-time PCR. Total RNAs (miRNA and mRNA) were extracted using miRNeasy Mini Kit (Qiagen) according to the manufacturer's protocol. Reverse transcription of total miRNA and mRNA was done starting from equal amounts of total RNA/sample (1 μg) using miScript Reverse Transcription Kit (Qiagen). For cultured cells, quantitative analyses of PED, glyceraldehyde-3-phosphate dehydrogenase (as an internal reference), miR-212, and RNU5A (as an internal reference) were done by real-time PCR using specific primers (Qiagen), miScript SYBR Green PCR Kit (Qiagen), and QuantiTect SYBR Green PCR Kit (Qiagen), respectively. The reaction for detection of mRNAs was done as follows: 95°C for 15 min, 40 cycles of 94°C for 15 s, 55°C for 30 s, and 72°C for 30 s. The reaction for detection of miRNAs was done as follows: 95°C for 15 min, 40 cycles of 94°C for 15 s, 55°C for 30 s, and 70°C for 30 s. To analyze PED and miR-212 expression in lung tissue specimens (neoplastic and normal tissue), real-time PCR was done using a standard TaqMan PCR Kit protocol on an Applied Biosystems 7900HT Sequence Detection System (Applied Biosystems). The reactions were incubated at 95°C for 10 min, followed by 40 cycles of 95°C for 15 s and 60°C for 1 min.

All reactions were run in triplicate. The threshold cycle (CT) is defined as the fractional cycle number at which the fluorescence passes the fixed threshold. For relative quantitation, the 2^(-ΔCT) method was used as previously described (20). Experiments were carried out in triplicate for each data point, and data analysis was done by using Bio-Rad IQ software.

Luciferase assay. The 3'UTR of the human *PED* gene was PCR amplified using the PED primers 5'-tctagaaggcaagagaccactcaacccca-3' (forward) and 5'-tctagaatgttctccaagagagagaggggaaggtt-3' (reverse) and cloned downstream of the Renilla luciferase stop codon in pGL3 control vector (Promega), giving rise to pcDNA/PED-clone1 (3). This construct was used to generate, by inverse PCR, the p3'-UTRmut-PED plasmid (primers: PED-mut1, FW 5'-tggttctactcctgtgctgctgag-taccagc-3', RW 5'-gctggtactcaggacagcacaggagtacaaca-3'; PED-mut2, FW 5'-agttgttctactcagcactctaaacctaggagg-3', RW 5'-cctccctaggttagagtgtgctgagtaggaacaac-3'). MeG01 cells were cotransfected with 1 μg of p3'-UTR-PED and with p3'-UTRmut-PED plasmid and 1 μg of the Renilla luciferase expression construct pRL-TK (Promega) with Lipofectamine 2000 (Invitrogen). Cells were harvested 24 h posttransfection and assayed with Dual Luciferase Assay (Promega) according to the manufacturer's instructions. Three independent experiments were done in triplicate.

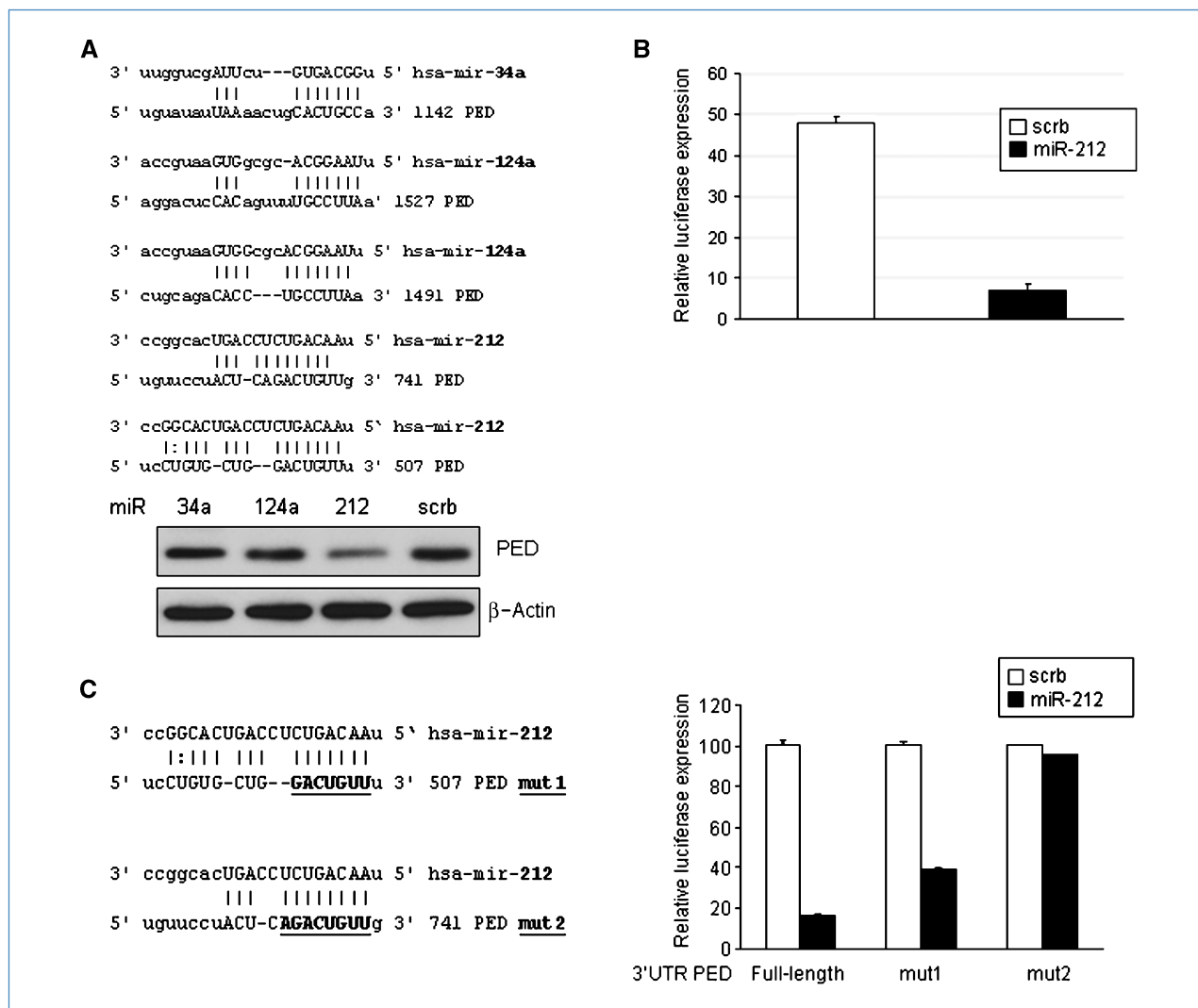


Figure 1. PED expression is regulated by miR-212. A, top, complementary sites on *PED* 3'UTR for miR-34a, miR-124a, and miR-212. The capital letters identify perfect base matches according to the Pictar, TargetScan, miRanda, and miRBase softwares (bottom). Western blot analysis of cellular extracts of Calu-1 cells transfected for 72 h with pre-miR-34a, pre-miR-124a, pre-miR-212, or a scrambled oligonucleotide (scr). Cell lysates were immunoblotted with anti-PED antibody. To confirm equal loading, the membrane was probed with anti- β -actin antibody as indicated. B, Meg01 cells were transiently cotransfected with the luciferase reporter containing *PED* 3'UTR and pre-miR-212 or scrambled oligonucleotide. C, left, complementary sites for miR-212 on *PED* 3'UTR. The bold letters identify the deletion regions of mutants (mut) 1 and 2, respectively. Right, Meg01 cells were transiently transfected with the luciferase reporter containing full-length *PED* 3'UTR, mut1, or mut2 in the presence of pre-miR-212 or scr. C and D, luciferase activity was evaluated 24 h after transfection as described in Materials and Methods. Representative of at least three independent experiments.

miRNA locked nucleic acid in situ hybridization of formalin-fixed, paraffin-embedded tissue section.

In situ hybridization was carried out on deparaffinized human lung and liver tissues using previously published protocol (21), which includes a digestion in pepsin (1.3 mg/mL) for 30 min. The sequence of the probes containing the six dispersed locked nucleic acid (LNA) modified bases with digoxigenin conjugated to the 5' end was miR-212-(5') UAACAGUCUCCA-GUCACGGCC. The probe cocktail and tissue miRNA were co-denatured at 60°C for 5 min, followed by hybridization at 37°C overnight and a low stringency wash in 0.2 \times SSC and 2% bovine serum albumin at 4°C for 10 min. The probe-target complex was seen due to the action of alkaline phosphatase

on the chromogen nitroblue tetrazolium and bromochlorodolyl phosphate. Negative controls included the use of a probe, which should yield a negative result in such tissues. No counterstain was used to facilitate colabeling for PED protein. After *in situ* hybridization for the miRNAs, as previously described (21), the slides were analyzed for immunohistochemistry using the optimal conditions for PED (1:800, cell conditioning for 30 min). For the immunohistochemistry, we used the Ultrasensitive Universal Fast Red system from Ventana Medical Systems. We used normal lung tissues as controls for these proteins. The percentage of tumor cells expressing PED and miR-212 was then analyzed with emphasis on colocalization of the respective targets (miR-212 and either PED).

Statistical analysis. Continuous variables are expressed as mean values \pm SD. One-tailed Student's *t* test was used to compare values of test and control samples. $P < 0.05$ was considered significant.

Results

Identification of miRNA involved in PED regulation. To identify miRNAs that specifically target PED (PED/PEA-15), we used bioinformatic analyses available on the web, including Pictar, TargetScan, miRanda, and miRBase. Comparing the results obtained from the different searches, we found that miR-34a, miR-124a, and miR-212 consistently showed the highest score of probability for targeting PED 3'UTR. PED 3'UTR contains two potential binding sites for miR-212 at nt 507 and nt 741, one for miR-34a at nt 1142, and two for miR-124a at nt 1491 and nt 1527 (Fig. 1A, top).

To assess whether exogenous expression of the selected miRNAs induced PED downregulation, we used Calu-1 cells,

which express high PED levels (9). To this end, Calu-1 cells were transiently transfected with 100 nmol/L of the indicated pre-miRNAs for 72 hours, and PED expression levels then identified by Western blot analysis (Fig. 1A, bottom). As shown, miR-212 induced the greatest decrease in PED protein.

The most widely used approach for experimentally validating miRNA targets is to clone the predicted miRNA-binding sequence downstream of a luciferase reporter construct and to cotransfect it with the miRNA of interest. To this end, we cloned the 3'UTR sequence of human PED into the luciferase expressing vector pGL3-control downstream of the luciferase stop codon; Meg01 cell lines were transiently transfected with this construct in the presence of pre-miR-212 or a scrambled oligonucleotide acting as a negative control. As reported in Fig. 1B, miR-212 significantly reduced luciferase activity compared with the scrambled oligonucleotide. This indicates that miR-212 binds to the 3'UTR of *Ped* and impairs PED mRNA translation.

As reported above, miR-212 targets two regions of the 3' UTR of PED mRNA (Fig. 1A). To determine which of the two regions is implicated in the binding with miR-212, we generated two deletion mutants (Fig. 1C, left): mut1, lacking the first binding site, GACTGTGTT (top); and mut2, lacking the second binding site, AGACTGTGTT (bottom). The two mutants were cloned into the 3'UTR of the luciferase gene and cotransfected with pre-miR-212 into the Meg01 cell line. As shown in Fig. 1C (right), miR-212 did not significantly reduce luciferase activity in the presence of the mut2 sequence. This result indicates that miR-212 targets PED mRNA at the AGACUGUU sequence.

miR-212 modulates PED mRNA levels. To assess whether PED upregulation in lung cancer cells was due to decreasing expression of miR-212, we analyzed in Calu-1 and H460 cells, expressing different amounts of PED protein (Fig. 2A), the levels of miR-212 and PED mRNA by real-time PCR. As shown in Fig. 2B and C, an inverse correlation between PED mRNA and miR-212 levels was found.

It is known that miRNAs regulate gene expression either by direct cleavage of the targeted mRNAs or by inhibiting translation (22). To determine whether the binding of miR-212 to PED 3'UTR results in mRNA degradation, Calu-1 cells were transfected for 48 or 72 hours with pre-miR-212, and PED expression was then evaluated by real-time PCR and Western blot. As shown in Fig. 3A, exogenous expression of miR-212 induced a marked reduction of PED mRNA (top) as well as PED protein (middle) levels. The efficiency of miR-212 transfection was evaluated by reverse transcription-PCR (RT-PCR; bottom). Next, to assess whether miR-212 plays a physiologic role in controlling PED expression, we treated H460 cells, which express high levels of miR-212, with a specific antago-miR-212. As shown in Fig. 3B, increased expression of PED mRNA (top) and PED protein (middle) was evident already at 48 hours of antago-miRNA transfection. The efficiency of antago-miR-212 transfection was evaluated by RT-PCR of the endogenous miRNA (bottom). Taken together, the results show that in lung cancer cells, PED and miR-212 expressions are inversely correlated and that miR-212 regulates PED expression.

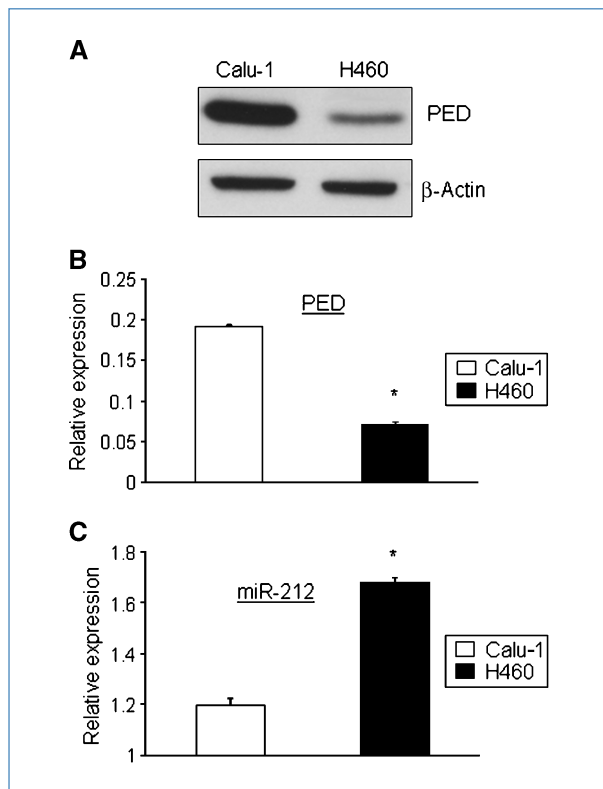


Figure 2. PED and miR-212 expression levels are inversely correlated in NSCLC. A, cell lysates from Calu-1 and H460 cells were immunoblotted with anti-PED antibody. To confirm equal loading, the membrane was immunoblotted with anti- β -actin antibody. Blots are representative of at least four independent experiments. B and C, total RNA (mRNAs and miRNAs) was extracted from Calu-1 and H460 cells and 1 μ g was reverse transcribed and amplified as described in Materials and Methods. Relative expressions of PED mRNA (B) and miR-212 (C) were calculated using the comparative CT methods. Columns, mean of four different experiments; bars, SD. *, $P < 0.05$, Student's *t* test. There is an inverse correlation between PED and miR-212 expressions in NSCLC.

miR-212 and PED mRNA levels in NSCLC tissue. To evaluate whether PED upregulation in lung cancer is related to decreased miR-212 levels also *in vivo*, we analyzed PED and miR-212 expression levels in tissue specimens collected from 18 patients (14 NSCLC-affected individuals and 4 with normal lung tissue). As shown in Fig. 4, in normal lung samples, the levels of miR-212 were high whereas PED was expressed at low levels. On the contrary, in the majority of lung cancer samples, miR-212 was expressed at low levels and PED was overexpressed.

To corroborate these findings, *in situ* hybridization analysis was done, using 5'-dig-labeled LNA probes, on NSCLC and normal lung tissues, followed by immunohistochemistry for PED (Fig. 5). MiR-212 and PED expressions were inversely related in NSCLC and the adjacent normal lung tissues. Lung cancer cells showed high expression of PED and rarely expressed miR-212 (Fig. 5A-C), whereas the adjacent nonmalignant lung expressed miR-212 abundantly and rarely showed detectable PED signal (Fig. 5A-C). Costaining of PED and miR-212 showed that the two labelings did not overlap

(Fig. 5C-c), showing that PED and miR-212 were not expressed in the same cell. *In situ* hybridization was done for 110 samples. The majority of cancer cells were positive for PED (84%). Seventy-three percent of the samples were negative for miR-212. When we analyzed for double staining, we found that 60% (65 of 110 patients) of the cells were PED positive/miR-212 negative (PED⁺/miR⁻), 24% (26 of 110 patients) were PED⁺/miR⁺, 3.6% (4 of 110 patients) were PED⁻/miR⁺, and 13% (15 of 110 patients) were PED⁻/miR⁻. These results further support our above finding that the upregulation of PED in lung cancer is dependent on decreased miR-212 levels.

MiR-212 increases TRAIL-induced cell death in NSCLC cells. We have previously shown that a TRAIL-resistant phenotype in NSCLC is related to overexpression of PED (9). The observation that miR-212 targets PED suggests that ectopic expression of this miRNA should increase sensitivity to TRAIL. To this aim, we transfected Calu-1 cells with pre-miR-212, and caspase-8 activation was then evaluated following treatment with TRAIL (Fig. 6A). As shown, PED expression decreased in the presence of exogenous miR-212, and caspase-8 activation

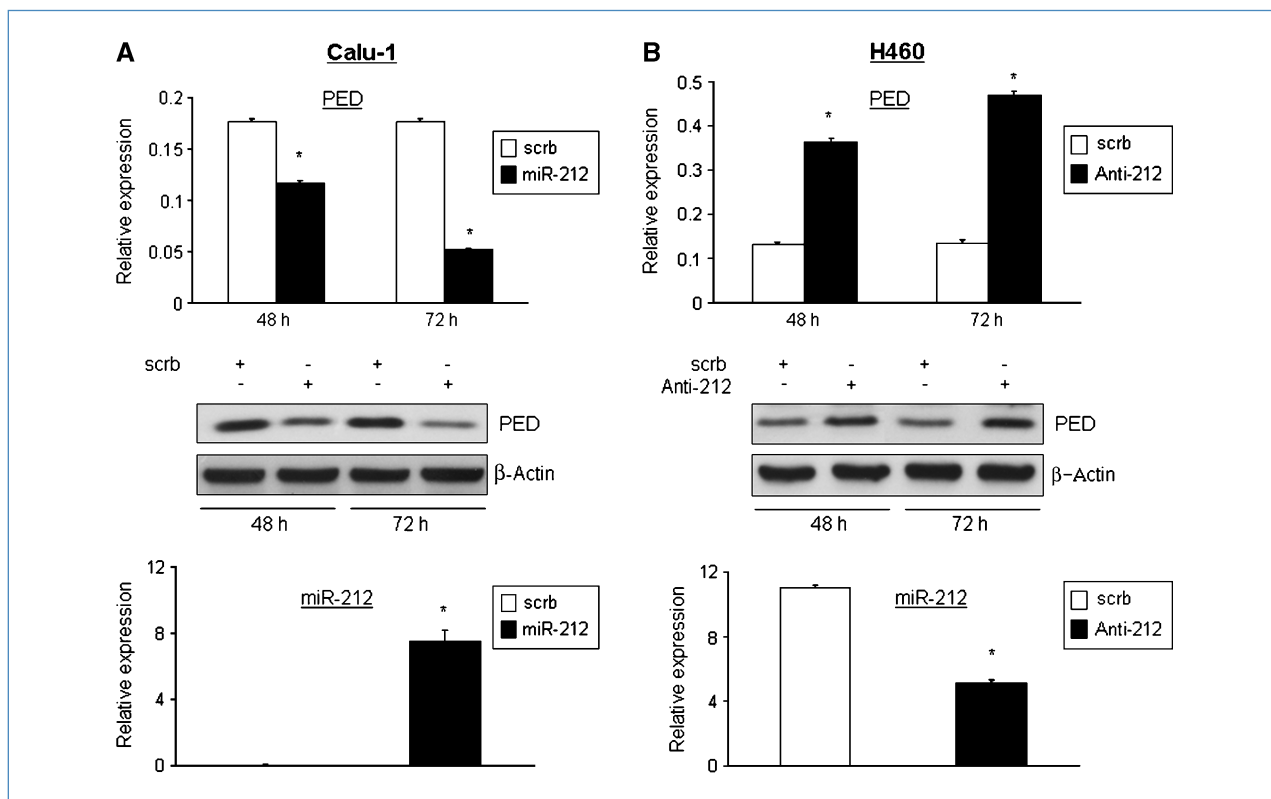


Figure 3. miR-212 regulates PED expression levels. A, top, Calu-1 cells were transfected for 48 and 72 h with pre-miR-212 or scrb. After transfection, total RNA was extracted and 1 μ g was reverse transcribed and amplified as described in Materials and Methods. As shown, PED mRNA was downregulated by miR-212 transfection. Middle, cell lysates from Calu-1 cells were collected after 48 and 72 h from pre-miR-212 or scrb transfections and immunoblotted with anti-PED antibody. To confirm equal loading, the membrane was immunoblotted with anti- β -actin antibody. As shown, decreasing amount of PED protein was evident in the presence of exogenous pre-miR-212 (bottom). Relative expression of ectopic miR-212 after the transfection was evaluated. B, top, H460 cells were transfected for 48 and 72 h with antago-miR-212 (anti-212) or scrb. After transfection, total RNA was extracted and 1 μ g was reverse transcribed and amplified as described in Materials and Methods. As shown, an increasing amount of PED mRNA was evident in the presence of exogenous anti-212 (middle). Cell lysates from H460 cells were collected after 48 and 72 h from anti-212 or scrb transfections and immunoblotted with anti-PED antibody. To confirm equal loading, the membrane was immunoblotted with anti- β -actin antibody. As shown, an increasing amount of PED protein was evident in the presence of exogenous anti-212 (bottom). Relative expression of endogenous miR-212 after the antago-miR-212 transfection was evaluated. Blots are representative of at least four independent experiments. Columns, mean of four different experiments; bars, SD. *, $P < 0.05$, Student's t test.

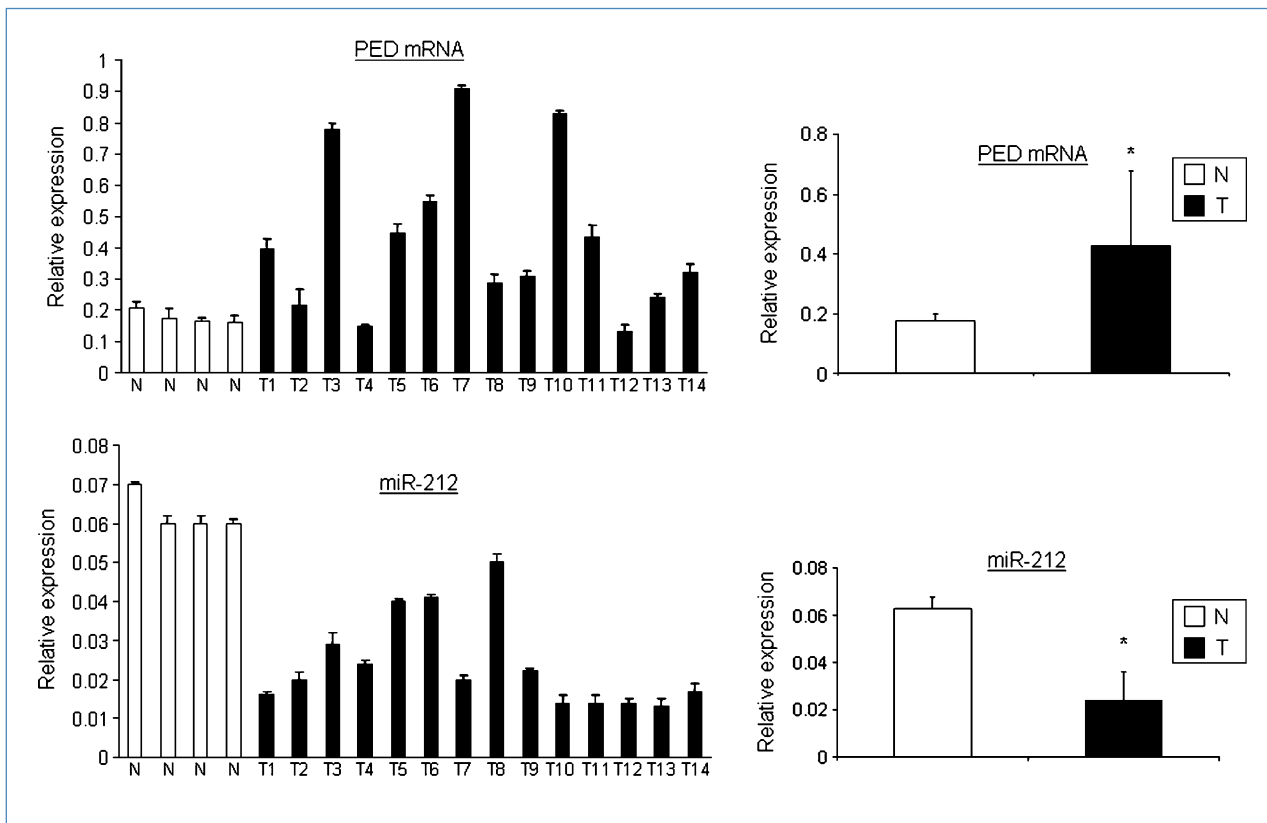


Figure 4. Correlation of endogenous miR-212 and PED mRNA expression levels in human lung cancer. Left, total RNA extracted from tissue specimens collected from 14 NSCLC-affected individuals and 4 control individuals was used to analyze miR-212 and PED mRNA expression by real-time PCR (right). Average of control versus tumor samples. Columns, mean PED or miR-212 expression of all the tumor samples (T) and normal tissue (N); bars, SD. *, $P < 0.05$, t test. As shown, there is an inverse correlation between miR-212 and PED mRNA expression levels. The normal lung RNA expressed high miR-212 and low PED mRNA levels; all the tumors analyzed expressed high PED mRNA and very low miR-212 levels.

was evident 2 hours after TRAIL treatment (compare lane 5 with lane 6 and lane 7 with lane 8). To further confirm this result, we analyzed TRAIL-induced cell death in the presence of exogenous pre-miR-212 with a cell viability assay (Supplementary Fig. S1A) and Annexin V apoptosis assay (Fig. 6B and Supplementary Fig. S1B for representative dot blot). By time course and dose/response analysis (data not shown), we found that to better appreciate a difference in cell viability, low concentrations of TRAIL were needed. To this end, Calu-1 cells were transfected for 48 hours with pre-miR-212, then stimulated with 10 and 25 ng/mL of TRAIL for 24 hours, and cell death was evaluated. As shown in Fig. 6B, transfection of miR-212 increased TRAIL-induced cell death up to 3-fold that of Calu-1 cells. Thus, PED downregulation induced by miR-212 increases sensitivity to TRAIL in lung cancer cells.

To further evaluate the role of miR-212 in apoptosis sensitivity, TRAIL-sensitive H460 cells were transfected with antagomiR-212 to decrease endogenous miR-212 and then analyzed for their susceptibility to TRAIL-induced cell death. As shown in Fig. 6C, antago-miR treatment increased PED protein and rendered H460 cells more resistant to TRAIL. To confirm that PED is an important target of miR-212 for regulation of apoptosis, Calu-1 cells were transfected with pre-miR-212 in the presence or in the absence of PED-myc

cDNA that lacks 3'UTR. As shown in Fig. 6D, ectopic expression of miR-212 and PED-myc cDNA restores the apoptotic resistance, assessed as caspase-8 activation. To confirm this result, we analyzed TRAIL-induced cell death in the presence of exogenous pre-miR-212 and PED-myc with a cell viability assay, obtaining the same results (Supplementary Fig. S1C). Taken together, these results indicate that miR-212 increases TRAIL sensitivity by targeting the antiapoptotic protein PED.

Discussion

The resistance of tumors to current chemotherapeutic protocols remains a major problem in cancer therapy. Defects in the apoptotic program may contribute to treatment resistance and tumor progression and may be caused by deregulated expression of antiapoptotic molecules. Better knowledge of tumor biology is providing the opportunity to treat lung cancer with a new class of anticancer drugs. PED is overexpressed in lung cancer, as well as in other human tumors including gliomas, squamous carcinoma, breast cancer, and thyroid cancer, and its overexpression is related to resistance to chemotherapy and TRAIL-induced cell death (4–9). Furthermore, we recently showed that PED is upregulated and induces resistance to TRAIL in NSCLC (9). Even so, the

molecular mechanisms of deregulation of PED expression in cancer cells are still unknown. We therefore have set out to identify possible miRNAs able to regulate PED expression in human lung cancer.

Here, we found that in lung cancer cells, miR-212 was able to target PED 3'UTR and decrease its levels, thus suggesting that by maintaining PED levels low, miR-212 action may contribute to tumor suppression.

Over the past few years, several miRNAs have been implicated in various human cancers. Both losses and gains of miR function have been shown to contribute to cancer development through a range of mechanisms (23, 24).

More often in various human tumors has been observed an overexpression of miRNAs, and several of these miRNAs function as oncogenes. When downregulated, miRNAs are considered tumor suppressor because they usually prevent tumor development by negatively inhibiting molecules involved in apoptosis resistance.

Different studies show that lung adenocarcinoma has a miR expression signature that greatly adapts to the use of clinical data in predicting an individual's survival. Low expression of let-7a and high expression of miR-155 are linked to unfavorable clinical outcome in lung cancer (17). The miR-34 cluster (miR-34a, miR-34b, miR-34c) is repressed in cancers and miR-34c is involved in p53 tumor suppression in many cancers, including lung cancer (25, 26). Bandi et al. (27) identified miR-15a and miR-16 as frequently deleted in

NSCLC, implying an increase of cell cycle. Furthermore, Nasser et al. (28) showed that miR-1 was downregulated in lung cancer and was related to increased migration and motility of lung cancer cells.

Using real-time RT-PCR, Yu et al. (29) analyzed miR expression in 112 different NSCLC patients. They found that two miRNAs acted as antitumoral genes (miR-221 and let-7a) and three miRNAs were risky for NSCLC (miR-137, miR-372, and miR-182). Liu et al. (30) found that miR-34c, miR-145, and miR-142-5p were suppressed in transgenic lung cancers as well as human normal versus malignant lung tissues.

MiR-212 expression levels in human cancer have not been extensively investigated thus far. Recently, miR-212 downregulation has been found to be involved in lung cancer response to chemotherapy, in particular to docetaxel (31). The molecular targets responsible to this resistance have not been identified thus far, but it would be interesting to speculate that PED may participate in this process.

Our data show that in sample specimens from lung cancer, miR-212 expression is low compared with normal samples. Interestingly, miR-212 expression inversely correlates with PED expression and with response to TRAIL treatment. Therefore, miR-212 expression could predict therapeutic response to TRAIL in lung cancer.

The mechanisms of miR-212 downregulation in human cancer are not clear at the moment. miR-212 is located on human chromosome 17, in a region that is frequently lost

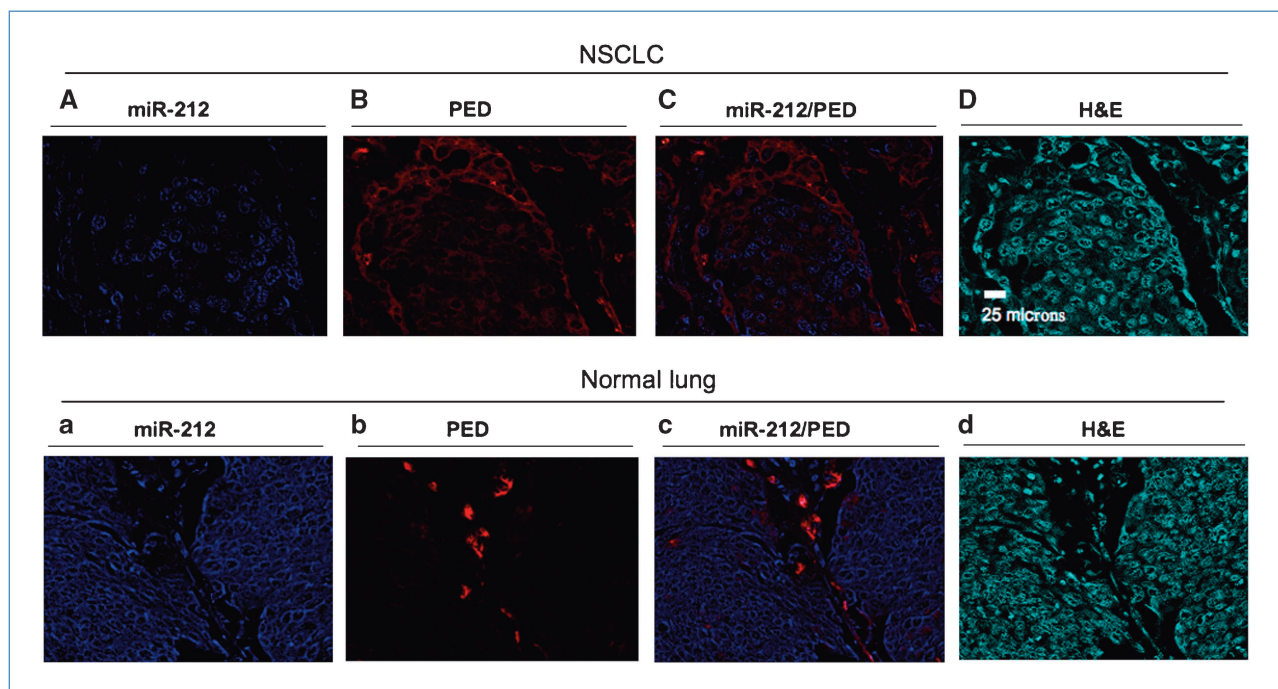


Figure 5. Immunohistochemistry and *in situ* hybridization of lung carcinoma and normal tissue samples. MiR-212 (blue; A-a) and PED (red; B-b) expressions were inversely related in lung cancer and the adjacent normal lung tissues (C-c shows colocalization expression of PED and miR-212). Top, PED (B) and miR-212 (A) expressions were confined mostly to cancer cells. However, note that cancer cells express PED and do not express miR-212 and vice versa (C). Bottom, a nest of cancer cells expressing only miR-212 (a). Note that PED expression (b) is confined to the benign stromal cells that are found in the desmoplastic tissue surrounding the cancer cells nest. Bar, 25 μ m. The magnification is the same for all images. D-d, H&E. One hundred ten lung carcinoma and normal samples were analyzed. As described in the text, the majority of cancer cells were positive for PED and negative for miR-212. In the cases of lung carcinoma where both miR-212 and PED expressions were noted, cancer cells expressing PED were distinct from those expressing miR-212.

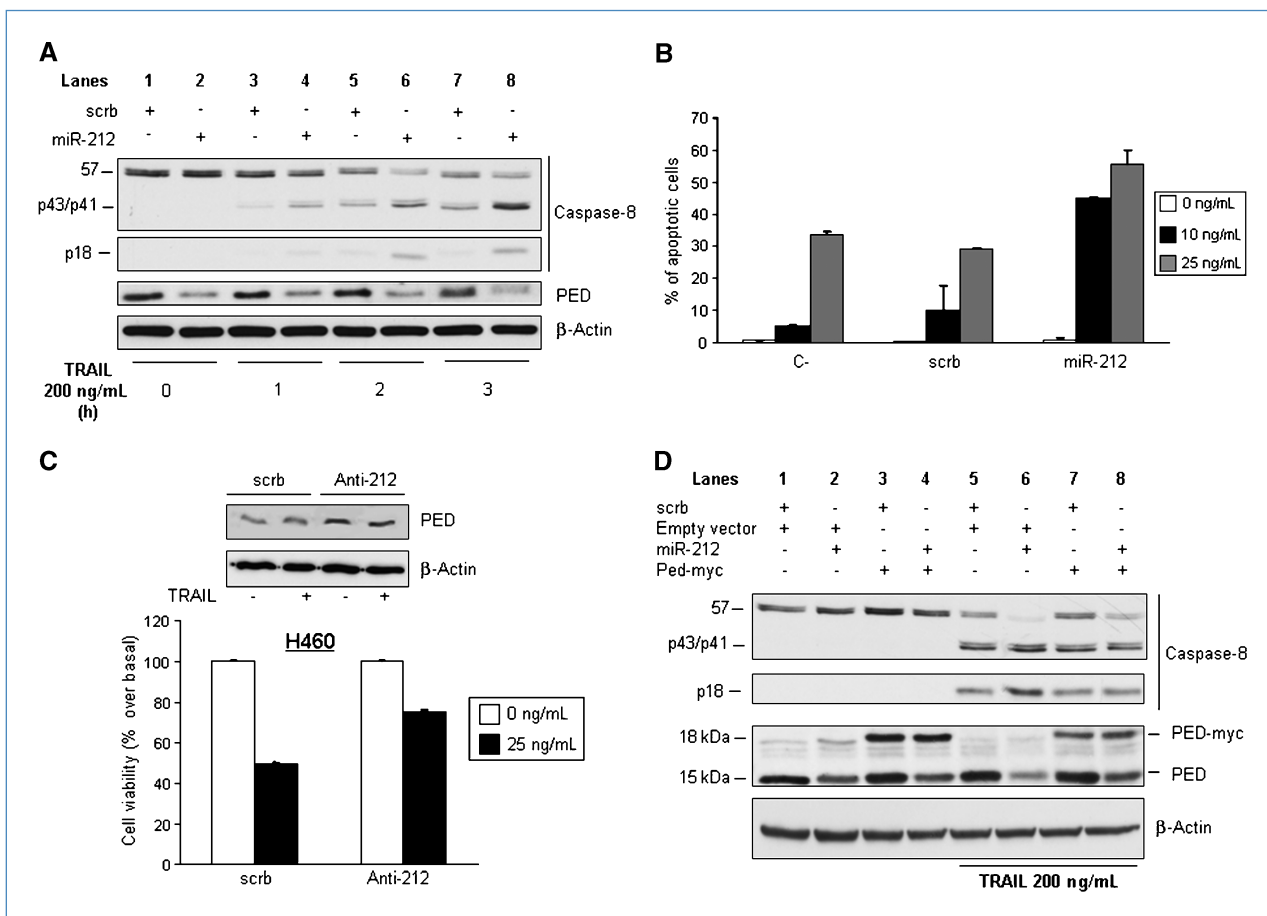


Figure 6. miR-212 transfection induces TRAIL sensitivity. **A**, Calu-1 cells were transfected either with pre-miR-212 or with scrb. After 72 h, cells were treated with 200 ng/mL Super-Killer TRAIL for the indicated times. Lysates were analyzed by Western blotting with anti-caspase-8 and anti-PED antibodies. Cleavage of caspase-8 was more evident in Calu-1 cells transfected with miR-212 compared with scrb. β -Actin antibody was used as loading control. **B**, Calu-1 cells were transfected either with pre-miR-212 or with scrb for 48 h. Then, the cells were incubated with 10 or 25 ng/mL of Super-Killer TRAIL for 24 h. Apoptosis was evaluated with Annexin V staining. Columns, mean of four independent experiments in triplicate; bars, SD. Downregulation of PED by miR-212 was responsible for increased sensitivity of Calu-1 cells to TRAIL-mediated cell death. **C**, H460 cells were transfected either with anti-212 or with scrb for 48 h, then the cells were incubated with 25 ng/mL Super-Killer TRAIL for 24 h. Top, upregulation of PED expression after antago-miR transfection was evaluated by Western blotting using anti-PED antibody. β -Actin antibody was used as loading control. Bottom, cell viability was evaluated by CellTiter Assay. Columns, mean of four independent experiments in triplicate; bars, SD. **D**, Calu-1 cells were transfected with miR-212 in the presence or absence of PED-myc recombinant protein. After 72 h, cells were treated with 200 ng/mL Super-Killer TRAIL for 3 h and caspase-8 activation was analyzed by Western blotting with anti-caspase-8 antibodies. Cleavage of caspase-8 was more evident in Calu-1 cells transfected with miR-212 in the absence of PED-myc recombinant protein. Expressions of PED-myc (18 kDa) and endogenous PED (15 kDa) were evaluated with anti-PED antibody. β -Actin antibody was used as loading control.

in different human cancers (32), and this may represent a mechanism to explain its low expression.

The silencing of miR in cancer can be caused not only by deletions and mutations but also by epigenetic changes. Altered patterns of epigenetic modifications, in particular the methylation of CpG islands in the promoter regions of some miRs, have been described (33). The miR-212 promoter region is possibly rich in CpG islands. Experiments are under way in our lab to clarify whether methylation may be a mechanism involved in the regulation of miR-212 expression levels.

In summary, miRs are potential antineoplastic agents. Perhaps combination therapy with different miRs will be needed to confer desired antitumorigenic effects. It will be critical to

discern which miRs are overexpressed in lung cancer and which need to be inactivated to inhibit lung carcinogenesis. Conceivably, these miRs or their derivatives would become agents to treat or chemoprevent lung cancer.

Disclosure of Potential Conflicts of Interest

No potential conflicts of interest were disclosed.

Acknowledgments

We thank Dr. Vittorio de Franciscis and Michael Latronico for paper revision, and Maria Fiammetta Romano and Simona Romano for their help with FACS experiments.

Grant Support

Associazione Italiana Ricerca sul Cancro (G. Condorelli), Ministero dell'Istruzione, dell'Università e della Ricerca-Fondo per gli Investimenti della Ricerca di Base grant RBIN04J4J7, EU grant EML (European Molecular Imaging Laboratories Network) contract no. 503569, and Fondazione SDN.

The costs of publication of this article were defrayed in part by the payment of page charges. This article must therefore be hereby marked *advertisement* in accordance with 18 U.S.C. Section 1734 solely to indicate this fact.

Received 09/10/2009; revised 01/12/2010; accepted 02/02/2010; published OnlineFirst 04/13/2010.

References

- Travis WD. Pathology of lung cancer. *Clin Chest Med* 2002;23:65–81.
- Condorelli G, Vigliotta G, Cafieri A, et al. PED/PEA-15: an anti-apoptotic molecule that regulates FAS/TNFR1-induced apoptosis. *Oncogene* 1999;18:4409–15.
- Condorelli G, Vigliotta G, Iavarone C, et al. PED/PEA-15 gene controls glucose transport and is overexpressed in type 2 diabetes mellitus. *EMBO J* 1998;17:3858–66.
- Renault F, Formstecher E, Callebaut I, Junier MP, Chneiweiss H. The multifunctional protein PEA-15 is involved in the control of apoptosis and cell cycle in astrocytes. *Biochem Pharmacol* 2003;66:1581–8.
- Xiao C, Yang BF, Asadi N, Beguinot F, Hao C. Tumor necrosis factor-related apoptosis-inducing ligand-induced death-inducing signaling complex and its modulation by c-FLIP and PED/PEA-15 in glioma cells. *J Biol Chem* 2002;277:25020–5.
- Kitsberg D, Formstecher E, Fauquet M, et al. Knock-out of the neural death effector domain protein PEA-15 demonstrates that its expression protects astrocytes from TNF α -induced apoptosis. *J Neurosci* 1999;19:8244–51.
- Garofalo M, Romano G, Quintavalle C, et al. Selective inhibition of PED protein expression sensitizes B-cell chronic lymphocytic leukaemia cells to TRAIL-induced apoptosis. *Int J Cancer* 2007;120:1215–22.
- Stassi G, Garofalo M, Zerilli M, et al. PED mediates AKT-dependent chemoresistance in human breast cancer cells. *Cancer Res* 2005;65:6668–75.
- Zanca C, Garofalo M, Quintavalle C, et al. PED mediates TRAIL resistance in human non small cell lung cancer. *J Cell Mol Med* 2008;12:2416–26.
- He L, Hannon GJ. MicroRNAs: small RNAs with a big role in gene regulation. *Nat Rev Genet* 2004;5:522–31.
- Lagos-Quintana M, Rauhut R, Lendeckel W, Tuschl T. Identification of novel genes coding for small expressed RNAs. *Science* 2001;294:853–8.
- Lim LP, Lau NC, Garrett-Engele P, et al. Microarray analysis shows that some microRNAs down-regulate large numbers of target mRNAs. *Nature* 2005;433:769–73.
- Chen CZ, Li L, Lodish HF, Bartel DP. MicroRNAs modulate hematopoietic lineage differentiation. *Science* 2004;303:83–6.
- Cheng AM, Byrom MW, Shelton J, Ford LP. Antisense inhibition of human miRNAs and indications for an involvement of miRNA in cell growth and apoptosis. *Nucleic Acids Res* 2005;33:1290–7.
- Calin GA, Croce CM. MicroRNA-cancer connection: the beginning of a new tale. *Cancer Res* 2006;66:7390–4.
- Calin GA, Croce CM. MicroRNA signatures in human cancers. *Nat Rev Cancer* 2006;6:857–66.
- Yanaihara N, Caplen N, Bowman E, et al. Unique microRNA molecular profiles in lung cancer diagnosis and prognosis. *Cancer Cell* 2006;9:189–98.
- Takamizawa J, Konishi H, Yanagisawa K, et al. Reduced expression of the let-7 microRNAs in human lung cancers in association with shortened postoperative survival. *Cancer Res* 2004;64:3753–6.
- Garofalo M, Quintavalle C, Di Leva G, et al. MicroRNA signatures of TRAIL resistance in human non-small cell lung cancer. *Oncogene* 2008;27:3845–55.
- Livak KJ, Schmittgen TD. Analysis of relative gene expression data using real-time quantitative PCR and the 2^(- $\Delta\Delta C_T$) method. *Methods* 2001;25:402–8.
- Nuovo G, Lee EJ, Lawler S, Godlewski J, Schmittgen T. *In situ* detection of mature microRNAs by labeled extension on ultramer templates. *Biotechniques* 2009;46:115–26.
- Robins H, Press WH. Human microRNAs target a functionally distinct population of genes with AT-rich 3' UTRs. *Proc Natl Acad Sci U S A* 2005;102:15557–62.
- Croce CM. Causes and consequences of microRNA dysregulation in cancer. *Nat Rev Cancer* 2009;10:704–14.
- Garofalo M, Condorelli GL, Croce CM, Condorelli G. MicroRNAs as regulators of death receptors signaling. *Cell Death Differ* 2009, Epub ahead of print.
- He H, Jazdzewski K, Li W, et al. The role of microRNA genes in papillary thyroid carcinoma. *Proc Natl Acad Sci U S A* 2005;102:19075–80.
- Bommer GT, Gerin I, Feng Y, et al. p53-mediated activation of miRNA34 candidate tumor-suppressor genes. *Curr Biol* 2007;17:1298–307.
- Bandi N, Zbinden S, Gugger M, et al. miR-15a and miR-16 are implicated in cell cycle regulation in a Rb-dependent manner and are frequently deleted or downregulated in non-small cell lung cancer. *Cancer Res* 2009;69:5553–9.
- Nasser MW, Datta J, Nuovo G, et al. Down-regulation of micro-RNA-1 (miR-1) in lung cancer. Suppression of tumorigenic property of lung cancer cells and their sensitization to doxorubicin-induced apoptosis by miR-1. *J Biol Chem* 2008;283:33394–405.
- Yu SL, Chen HY, Chang GC, et al. MicroRNA signature predicts survival and relapse in lung cancer. *Cancer Cell* 2008;13:48–57.
- Liu X, Sempere LF, Galimberti F, et al. Uncovering growth-suppressive MicroRNAs in lung cancer. *Clin Cancer Res* 2009;15:1177–83.
- Rui W, Bing F, Hai-Zhu S, Wei D, Long-Bang C. Identification of microRNA profiles in docetaxel-resistant human non-small cell lung carcinoma cells (SPC-A1). *J Cell Mol Med* 2009, Epub ahead of print.
- Konishi H, Sugiyama M, Mizuno K, et al. Detailed characterization of a homozygously deleted region corresponding to a candidate tumor suppressor locus at distal 17p13.3 in human lung cancer. *Oncogene* 2003;22:1892–905.
- Peacock JW, Palmer J, Fink D, et al. PTEN loss promotes mitochondrially dependent type II Fas-induced apoptosis via PEA-15. *Mol Cell Biol* 2009;29:1222–34.

Correction

**Correction: Online Publication Dates for
Cancer Research April 15, 2010 Articles**

The following articles in the April 15, 2010 issue of *Cancer Research* were published with an online publication date of April 6, 2010 listed, but were actually published online on April 13, 2010:

Garmy-Susini B, Avraamides CJ, Schmid MC, Foubert P, Ellies LG, Barnes L, Feral C, Papayannopoulou T, Lowy A, Blair SL, Cheresh D, Ginsberg M, Varner JA. Integrin $\alpha 4 \beta 1$ signaling is required for lymphangiogenesis and tumor metastasis. *Cancer Res* 2010;70:3042–51. Published OnlineFirst April 13, 2010. doi:10.1158/0008-5472.CAN-09-3761.

Vincent J, Mignot G, Chalmin F, Ladoire S, Bruchard M, Chevriaux A, Martin F, Apetoh L, Rébé C, Ghiringhelli F. 5-Fluorouracil selectively kills tumor-associated myeloid-derived suppressor cells resulting in enhanced T cell-dependent antitumor immunity. *Cancer Res* 2010;70:3052–61. Published OnlineFirst April 13, 2010. doi:10.1158/0008-5472.CAN-09-3690.

Nagasaka T, Rhee J, Kloor M, Gebert J, Naomoto Y, Boland CR, Goel A. Somatic hypermethylation of *MSH2* is a frequent event in Lynch syndrome colorectal cancers. *Cancer Res* 2010;70:3098–108. Published OnlineFirst April 13, 2010. doi:10.1158/0008-5472.CAN-09-3290.

He X, Ota T, Liu P, Su C, Chien J, Shridhar V. Downregulation of HtrA1 promotes resistance to anoikis and peritoneal dissemination of ovarian cancer cells. *Cancer Res* 2010;70:3109–18. Published OnlineFirst April 13, 2010. doi:10.1158/0008-5472.CAN-09-3557.

Fiorentino M, Judson G, Penney K, Flavin R, Stark J, Fiore C, Fall K, Martin N, Ma J, Sinnott J, Giovannucci E, Stampfer M, Sesso HD, Kantoff PW, Finn S, Loda M, Mucci L. Immunohistochemical expression of BRCA1 and lethal prostate cancer. *Cancer Res* 2010;70:3136–9. Published OnlineFirst April 13, 2010. doi:10.1158/0008-5472.CAN-09-4100.

Veronese A, Lupini L, Consiglio J, Visone R, Ferracin M, Fornari F, Zanesi N, Alder H, D'Elia G, Gramantieri L, Bolondi L, Lanza G, Querzoli P, Angioni A, Croce CM, Negrini M. Oncogenic role of *miR-483-3p* at the *IGF2/483* locus. *Cancer Res* 2010;70:3140–9. Published OnlineFirst April 13, 2010. doi:10.1158/0008-5472.CAN-09-4456.

Lu W, Zhang G, Zhang R, Flores LG II, Huang Q, Gelovani JG, Li C. Tumor site-specific silencing of *NF- κ B p65* by targeted hollow gold nanosphere-mediated photothermal transfection. *Cancer Res* 2010;70:3177–88. Published OnlineFirst April 13, 2010. doi:10.1158/0008-5472.CAN-09-3379.

Geng H, Rademacher BL, Pittsenbarger J, Huang C-Y, Harvey CT, Lafortune MC, Myrthue A, Garzotto M, Nelson PS, Beer TM, Qian DZ. ID1 enhances docetaxel cytotoxicity in prostate cancer cells through inhibition of p21. *Cancer Res* 2010;70:3239–48. Published OnlineFirst April 13, 2010. doi:10.1158/0008-5472.CAN-09-3186.

Yoo BK, Chen D, Su Z-z, Gredler R, Yoo J, Shah K, Fisher PB, Sarkar D. Molecular mechanism of chemoresistance by astrocyte elevated gene-1. *Cancer Res* 2010;70:3249–58. Published OnlineFirst April 13, 2010. doi:10.1158/0008-5472.CAN-09-4009.

Lu ZH, Shvartsman MB, Lee AY, Shao JM, Murray MM, Kladney RD, Fan D, Krajewski S, Chiang GG, Mills GB, Arbeit JM. Mammalian target of rapamycin activator RHEB is frequently overexpressed in human carcinomas and is critical and sufficient for skin epithelial carcinogenesis. *Cancer Res* 2010;70:3287–98. Published OnlineFirst April 13, 2010. doi:10.1158/0008-5472.CAN-09-3467.

Hattermann K, Held-Feindt J, Lucius R, Mürköster SS, Penfold MET, Schall TJ, Mentlein R. The chemokine receptor CXCR7 is highly expressed in human glioma cells and mediates antiapoptotic effects. *Cancer Res* 2010;70:3299–308. Published OnlineFirst April 13, 2010. doi:10.1158/0008-5472.CAN-09-3642.

Nadiminty N, Lou W, Sun M, Chen J, Yue J, Kung H-J, Evans CP, Zhou Q, Gao AC. Aberrant activation of the androgen receptor by NF- κ B2/p52 in prostate cancer cells. *Cancer Res* 2010;70:3309–19. Published OnlineFirst April 13, 2010. doi:10.1158/0008-5472.CAN-09-3703.

Acu ID, Liu T, Suino-Powell K, Mooney SM, D'Assoro AB, Rowland N, Muotri AR, Correa RG, Niu Y, Kumar R, Salisbury JL. Coordination of centrosome homeostasis and DNA repair is intact in MCF-7 and disrupted in MDA-MB 231 breast cancer cells. *Cancer Res* 2010;70:3320–8. Published OnlineFirst April 13, 2010. doi:10.1158/0008-5472.CAN-09-3800.

McFarlane C, Kelvin AA, de la Vega M, Govender U, Scott CJ, Burrows JF, Johnston JA. The deubiquitinating enzyme USP17 is highly expressed in tumor biopsies, is cell cycle regulated, and is required for G₁-S progression. *Cancer Res* 2010;70:3329–39. Published OnlineFirst April 13, 2010. doi:10.1158/0008-5472.CAN-09-4152.

Dudka AA, Sweet SMM, Heath JK. Signal transducers and activators of transcription-3 binding to the fibroblast growth factor receptor is activated by receptor amplification. *Cancer Res* 2010;70:3391–401. Published OnlineFirst April 13, 2010. doi:10.1158/0008-5472.CAN-09-3033.

Cho SY, Xu M, Roboz J, Lu M, Mascarenhas J, Hoffman R. The effect of CXCL12 processing on CD34⁺ cell migration in myeloproliferative neoplasms. *Cancer Res* 2010;70:3402–10. Published OnlineFirst April 13, 2010. doi:10.1158/0008-5472.CAN-09-3977.

Published OnlineFirst 05/11/2010.

©2010 American Association for Cancer Research.
doi: 10.1158/0008-5472.CAN-10-1347

c-FLIP_L enhances anti-apoptotic Akt functions by modulation of Gsk3 β activity

C Quintavalle¹, M Inconato², L Puca¹, M Acunzo¹, C Zanca¹, G Romano², M Garofalo^{1,3}, M Iaboni¹, CM Croce³ and G Condorelli^{*,1,4,5}

Akt is a serine–threonine kinase that has an important role in transducing survival signals. Akt also regulates a number of proteins involved in the apoptotic process. To find new Akt interactors, we performed a two-hybrid screening in yeast using full-length Akt cDNA as bait and a human cDNA heart library as prey. Among 200 clones obtained, two of them were identified as coding for the c-FLIP_L protein. c-FLIP_L is an endogenous inhibitor of death receptor-induced apoptosis through the caspase-8 pathway. Using co-immunoprecipitation experiments of either transfected or endogenous proteins, we confirmed the interaction between Akt and c-FLIP_L. Furthermore, we observed that c-FLIP_L overexpression interferes with Gsk3- β phosphorylation levels. Moreover, through its effects on Gsk3 β , c-FLIP_L overexpression in cancer cells induced resistance to tumor necrosis factor-related apoptosis-inducing ligand (TRAIL). This effect was mediated by the regulation of p27^{Kip1} and caspase-3 expression. These results indicate the existence of a new mechanism of resistance to TRAIL in cancer cells, and unexpected functions of c-FLIP_L.

Cell Death and Differentiation (2010) 17, 1908–1916; doi:10.1038/cdd.2010.65; published online 28 May 2010

Apoptosis, or programmed cell death, is an evolutionarily conserved mechanism of elimination of unwanted cells. This endogenous death machinery is triggered via two principal signaling pathways.¹ The extrinsic pathway is activated by the engagement of death receptors on the cell surface. The binding of ligands, such as Fas, tumor necrosis factor (TNF), or TNF-related apoptosis-inducing ligand (TRAIL) to cognate death receptors (DRs) induces the formation of the death-induced signaling complex (DISC). This DISC complex in turn recruits caspase-8 and promotes the cascade of procaspase activation.² The intrinsic pathway is triggered by various intracellular and extracellular stresses, signals of which converge mainly to the mitochondria.^{2,3} The balance between pro- and anti-apoptotic members of apoptosis is crucial for the regulation of survival and cell death. Aberrant resistance to apoptosis may lead to the development of cancer.

Cellular FLICE-inhibitory protein (c-FLIP) is a death effector domain (DED)-containing family member that inhibits one of the most proximal steps of DR-mediated apoptosis. Two isoforms of c-FLIP are commonly detected in human cells: a long form (c-FLIP_L) and a short form (c-FLIP_S). c-FLIP_L, a 55-kDa protein, contains two DEDs and a caspase-like domain, whereas c-FLIP_S, a 26-kDa protein consists only of two DEDs.⁴ Both isoforms are recruited to the DISC, prevent procaspase-8 activation and block DR-mediated apoptosis, although through different mechanisms.^{5,6} c-FLIP_L is overexpressed in a number of different tumors and its overexpression is related to TRAIL resistance.^{7,8} Beside cell

death, c-FLIP_L might also regulate other DR-mediated signals that may be important for tumor-promoting functions, such as proliferation, migration, inflammation or metastasis.^{9–11} The activation of the transcription factor NF- κ B, the PKB/Akt pathway and mitogen-activated protein kinases (MAPKs), such as c-Jun N-terminal kinase (JNK), extracellular signal-regulated kinase (ERK) and p38, has been demonstrated to be a consequence of DR triggering.⁹ Akt is a serine–threonine kinase that regulates the expression and the function of a number of proteins involved in the apoptotic process.¹² Akt interaction or phosphorylation of different signaling molecules may regulate their function by different mechanisms, including increased protein stability, cellular localization or binding to a different cellular partner. Akt interacts with a number of proteins involved in apoptotic signaling cascades, including BAD,¹³ caspase-9,¹⁴ the Forkhead transcription factor FOXO3¹⁵ and Bcl-w.¹⁶ The interaction of Akt with one of these proteins prevents apoptosis through several different mechanisms.¹³ One major Akt substrate is the serine–threonine kinase Gsk3.¹⁷ Originally studied for its role in glycogen metabolism and insulin action, Gsk3, present in the cells in two isoforms, Gsk3 α and Gsk3 β , has subsequently been shown to have central functions in many cellular processes, including transcription, cell cycle division, cell fate determination and stem cell maintenance, as well as in apoptosis.^{17,18} Gsk3 is constitutively active in resting cells, and is functionally inactivated after phosphorylation in response to different stimuli.

¹Department of Cellular and Molecular Biology and Pathology, 'Federico II' University of Naples, Naples, Italy; ²Fondazione SDN, Naples, Italy; ³Department of Molecular Virology, Immunology and Medical Genetics, Human Cancer Genetics Program, Comprehensive Cancer Centre, The Ohio State University, Columbus, OH, USA; ⁴IEOS, CNR, Naples, Italy and ⁵Facoltà di Scienze Biotechnologiche, 'Federico II' University of Naples, Naples, Italy

*Corresponding author: G Condorelli, Dipartimento di Biologia e Patologia Cellulare e Molecolare & Facoltà di Scienze Biotechnologiche, Università degli Studi di Napoli "Federico II", Via Pansini, 5. 80131 Naples, Italy. Tel: +39 081 7464416; Fax: +39 081 7463308; E-mail: gecondor@unina.it

Keywords: apoptosis; AKT; Bcl-2 family

Abbreviations: TRAIL, TNF-Related Apoptosis Inducing Ligand; DISC, Death-induced signaling complex; TNF, Tumor necrosis factor; DR, Death receptors; c-FLIP, Cellular FLICE-inhibitory protein; DED, Death Effector Domain; MAPK, mitogen-activated protein kinases; JNK, cJun N-terminal kinase; Akt D-, kinase-dead Akt; Akt D+, constitutively active Akt; ERK, extracellular signal-regulated kinase; cIAP-1, cellular inhibitor of apoptosis protein-1; NSCLC, non small cell lung cancer

Received 28.4.09; revised 15.3.10; accepted 15.4.10; Edited by M Piacentini; published online 28.5.10

In this study, we set out to find and investigate new possible partners of Akt that may participate in the regulation of the apoptosis pathway. In this study, we provide evidence that Akt directly interacts with c-FLIP_L. Furthermore, we demonstrate that c-FLIP_L modulates the activation of Gsk3β. We also provide evidence that this interaction is important for the regulation of TRAIL sensitivity, through the regulation of p27 and caspase-3 levels.

Results

Akt interacts with c-FLIP_L. To find new Akt interactors, we performed a yeast two-hybrid screening. We used the

full-length human Akt cDNA sequence as bait and a human cDNA heart library as prey. Among the 200 clones obtained, two were identified to code for the anti-apoptotic protein, c-FLIP_L. To prove the interaction between Akt and c-FLIP_L, we performed immunoprecipitation experiments on endogenous proteins and on protein extracts from cells transfected with Akt and c-FLIP_L cDNAs. We were able to confirm the Akt-c-FLIP_L interaction in extracts from transfected cells (Figure 1a), and in endogenous proteins from different cell lines (Figure 1b). To verify whether Akt activity has a role in Akt-c-FLIP_L interaction, HeLa cells were transfected with either wild-type Akt cDNA or with two different Akt mutants: kinase-dead Akt (Akt D) and constitutively active Akt (Akt D+). Protein extracts were

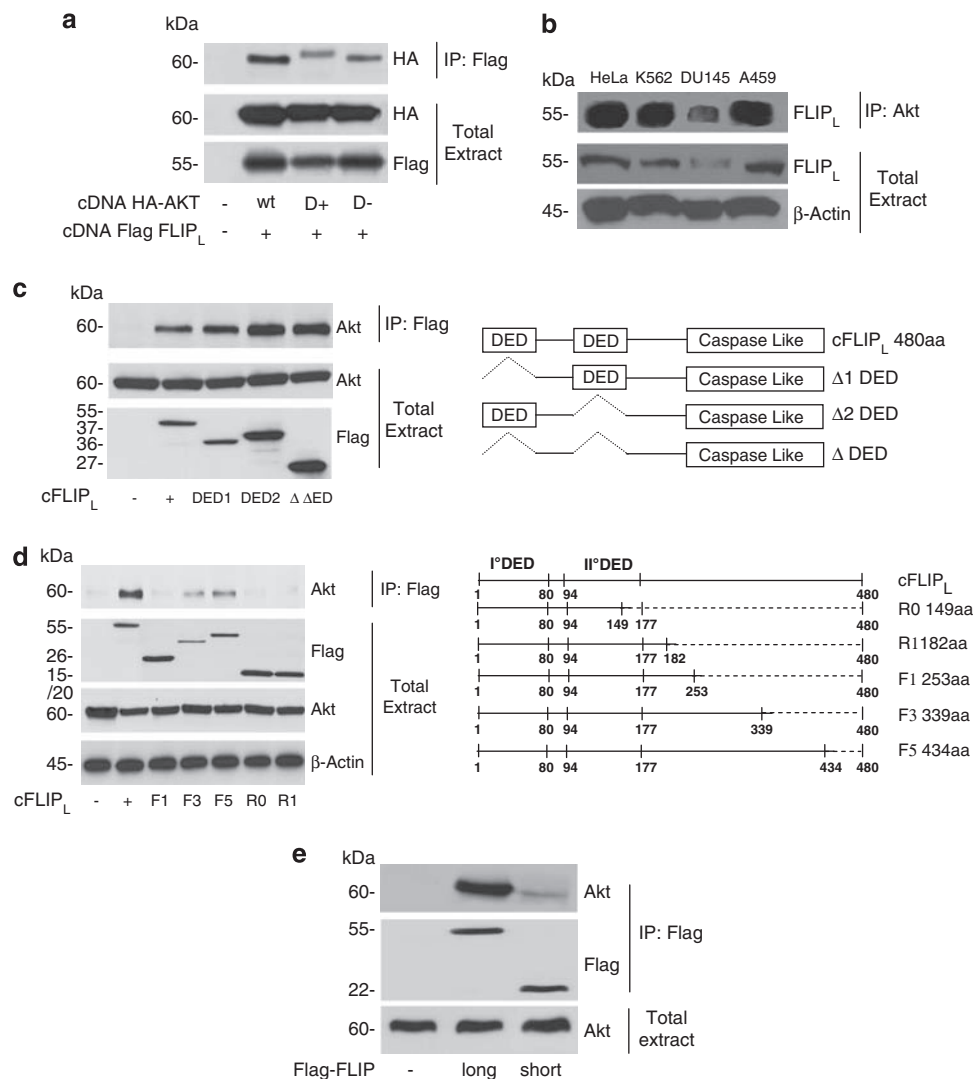


Figure 1 Akt interacts with c-FLIP_L. (a) HeLa cells were co-transfected with HA-Akt WT, Akt D+ or Akt D- cDNAs and c-FLIP_L for 48 h, as indicated. Protein extracts were immunoprecipitated (IP) with anti-Flag antibody and blotted with an anti-HA antibody. As negative control, proteins were incubated with beads without antibody. Total lysates were immunoblotted with the indicated antibody. (b) Co-immunoprecipitation of endogenous proteins. Equal amounts of total cell proteins from HeLa, K562, DU145 and A459 cell lines were immunoprecipitated with anti-Akt antibody and blotted with anti-c-FLIP_L or anti-β-actin antibodies. (c and d) Identification of FLIP-Akt interaction site. HEK-293 cells were transfected with 2 μg of either wt c-FLIP_L cDNA or the N-terminal deletion mutants, c-FLIP_L I-DED, c-FLIP_L II-DED, c-FLIP_L Δ-DED (c), or the C-terminal deletion mutants c-FLIP_L-F1, c-FLIP_L-F3, c-FLIP_L-F5, c-FLIP_L-R0 and c-FLIP_L-R1 (d), as indicated. Protein extracts were immunoprecipitated with anti-Flag antibody and blotted with anti-Akt antibody. Total extracts were loaded as control, and blotted with anti-Akt or anti-Flag antibodies. Akt was not able to interact with F1, R0 and R1 mutants, indicating that Akt-c-FLIP interacting region is included from a.a. 253 to a.a. 339. (e) HEK-293T cells were transfected with c-FLIP_L or c-FLIP_S cDNA. Total lysates were immunoprecipitated with an anti-Flag antibody and then blotted with an anti-Akt antibody

immunoprecipitated using a monoclonal anti-Flag antibody and subsequently blotted using an anti-HA antibody. As shown in Figure 1a, c-FLIPL interacted at comparable levels with both the activated kinase and the kinase-dead Akt.

c-FLIP_L is characterized by two death effector domains (DEDs), which are important for interaction with members of the apoptosis cascade. We examined whether these DED domains were important for the interaction with Akt. For this purpose, we generated three different mutants: cFLIP_L I-DED, missing the first DED; cFLIP_L II-DED, missing the second DED; and cFLIP_L Δ-DED, missing both DEDs. The three mutants were transfected together with HA-Akt cDNA into HeLa cells. Extracts were immunoprecipitated using anti-Flag antibody and blotted with an anti-HA antibody. As shown in Figure 1c, all the c-FLIP_L deletion mutants interacted with Akt, indicating that neither DED domain is necessary for the interaction with Akt.

We next investigated whether the carboxy terminal of c-FLIP_L was the region of interaction with Akt. For this purpose, we generated different carboxy-terminal c-FLIP_L mutants named: c-FLIP_L F1 (a.a. 1–253), c-FLIP_L F3 (a.a. 1–339), c-FLIP_L F5 (a.a. 1–434), c-FLIP_L R0 (a.a. 1–149) and c-FLIP_L R1 (a.a. 1–182). Each mutant was transfected together with HA-Akt cDNA in HEK-293 cells. Extracts were immunoprecipitated after 48 h with anti-Flag antibody and blotted with anti-HA antibody. Akt interacted with F3 and F5 mutants but not with F1, R0 or R1 mutants (Figure 1d). The interaction of Akt with the short c-FLIP isoform (FLIPs) was barely detectable (Figure 1e). This suggests that the Akt-c-FLIP-interacting region is located between a.a. 253 and a.a. 339, within the caspase-like domain.

Role of c-FLIP_L on growth factor-mediated Akt signaling. Beside cell death, c-FLIP_L also regulates other DR-mediated signals. Thus, we set out to verify whether Akt-c-FLIP_L interaction might modulate Akt activation. For this purpose, we first transfected increasing amounts of c-FLIP_L cDNA and assessed the levels of the activated Akt using specific phospho-Akt antibodies. The overexpression of c-FLIP_L did not induce significant differences in insulin-induced Akt phosphorylation (Figure 2a), even though it modified the phosphorylation of Gsk3β. As shown in Figure 2b, c-FLIP expression induced a reduction in endogenous Gsk3β basal phosphorylation level, in a dose-dependent manner. A similar inhibition of Gsk3β phosphorylation, both basal and upon insulin stimulation, was observed on co-transfecting the HA-Gsk3β together with c-FLIP (Figure 2c). Such inhibition was not observed in the presence of c-FLIP_S (Figure 2f).

This inhibition was not observed in HeLa cells transfected with c-FLIP_L mutants that do not interact with Akt, suggesting that Akt-c-FLIP interaction is necessary for this effect (Figure 2d and e).

Role of c-FLIP modulation of Gsk3β pathway on TRAIL-induced cell death. Although it has been clearly shown that c-FLIP_L overexpression may cause resistance to TRAIL, the effects of Gsk3β on cell death are more controversial.¹⁹ However, recently it was described that Gsk3β is involved in the resistance to TRAIL-induced apoptosis. Therefore, we

investigated whether c-FLIP_L-induced apoptosis resistance upon extrinsic pathway activation was at least in part mediated by its effects on Gsk3β activation.

For this purpose, HeLa cells were transfected with Flag c-FLIP_L cDNAs alone or in the presence of lithium chloride, an inhibitor of Gsk3 activity.²⁰ The cells were subsequently incubated with TRAIL, and cell death was assessed using a cell viability assay or with propidium iodide staining followed by FACS analysis. As shown in Figure 3a and b, c-FLIPL overexpression decreased the sensitivity of HeLa to TRAIL-induced apoptosis. However, treatment with LiCl completely counteracted the protective effect of c-FLIP on cell death (Figure 3a and b). To exclude unspecific effects of LiCl on cell death, the role of the Gsk3β pathway in the anti-apoptotic effect of c-FLIP was further evaluated using a specific Gsk3β kinase-inactive cDNA (Gsk3β-KI) and measuring caspase-8 activation. As shown in Figure 3c and d, c-FLIP_L overexpression reduced TRAIL-induced caspase-8 activation, and this effect was counteracted by both LiCl and Gsk3β-KI cDNA. LiCl and Gsk3β-KI or Gsk3β WT cDNA did not produce any effects on endogenous c-FLIP_L levels (Supplementary Figure 1a).

Effects of c-FLIP_L on p27^{Kip1} expression. Recently, Gsk3β inhibition has been suggested to regulate the cell cycle through regulation of p27^{Kip1} levels.²¹ In addition, we have recently shown that miRNAs regulate p27^{Kip1} expression and TRAIL sensitivity.²² Therefore, we addressed the question of whether the effect of c-FLIP_L on TRAIL resistance was mediated through Gsk3β activity and thus on p27 expression levels.

As shown in Figure 4a, we observed that the levels of p27^{Kip1} were drastically reduced in HEK-293 cells stably overexpressing c-FLIP_L. A similar result was observed also in HeLa cells stably (HeLa Tween FLIP) or transiently overexpressing c-FLIP_L (Flag FLIP; Figure 4b). However, overexpression of c-FLIP_L deletion mutants of the Akt interaction site did not induce reduction in p27^{Kip1} levels (Figure 4c). Moreover, this effect was not observed in the presence of c-FLIP_S (Figure 4f).

The downregulation of Gsk3β, by a specific siRNA or inactivation with LiCl, induced an increase in p27^{Kip1} levels in HeLa Tween FLIP_L compared to cells transfected with a scrambled siRNA (Figure 4d). Taken together these results indicate that the effect of c-FLIP on p27^{Kip1} is mediated by Gsk3β activity. We next investigated whether c-FLIP_L-Gsk3 regulate p27^{Kip1} at mRNA levels. To assess this point, HeLa cells were transfected with 5 μg of Flag c-FLIP_L cDNA or a control vector for 48 h, and p27^{Kip1} cDNA levels were evaluated by real-time PCR. Interestingly, we observed a significant reduction of p27^{Kip1} mRNA levels in HeLa cells transfected with c-FLIP_L but not with its mutant (Figure 4e), suggesting that the c-FLIP_L-Gsk3 pathway regulates p27^{Kip1} expression levels through a transcriptional mechanism.

The effect of p27^{Kip1} on TRAIL-mediated apoptotic signaling. We recently provided evidence that p27^{Kip1} is involved in TRAIL resistance in non-small cell lung cancer (NSCLC).²² We demonstrated that in TRAIL-resistant CALU-1 cells, miR-222 and miR-221 are overexpressed and target

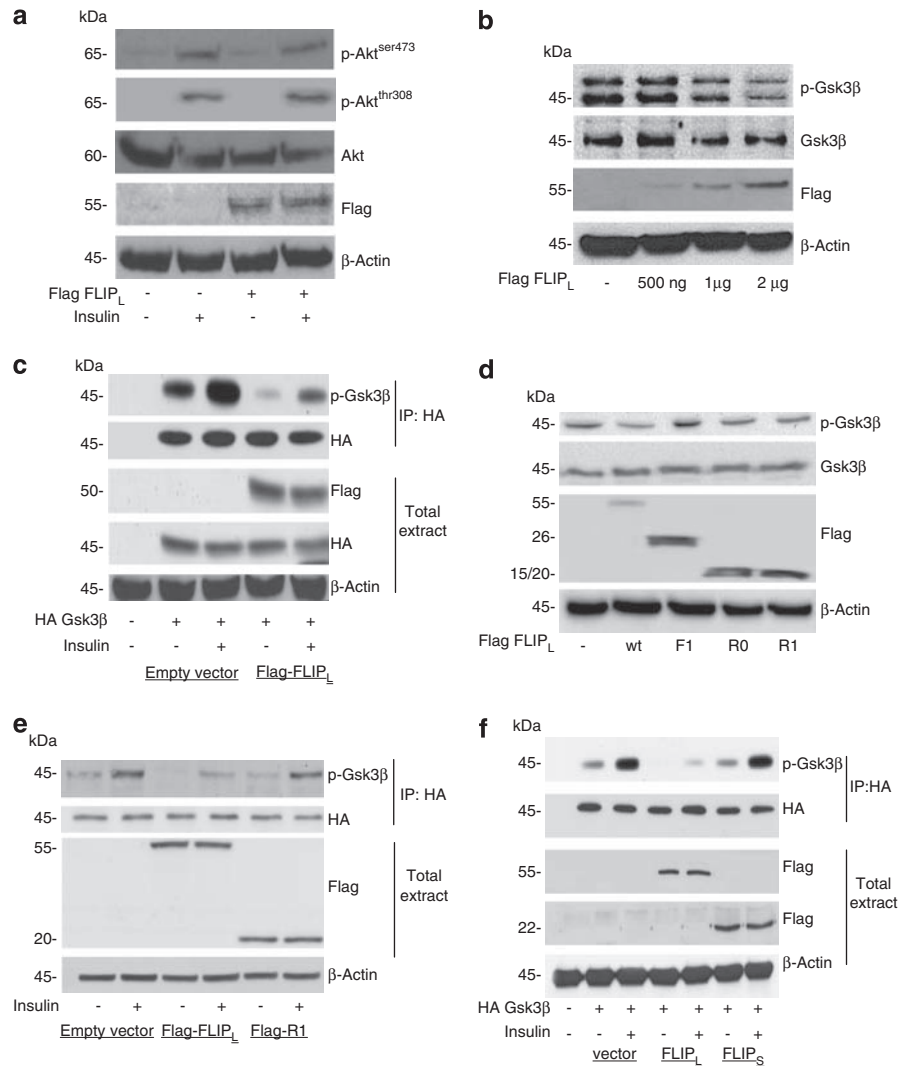


Figure 2 Role of c-FLIP_L on Akt-Gsk3β signaling pathway. **(a)** c-FLIP effects on Akt activation. HeLa cells were transfected with c-FLIP_L cDNA for 24 h, serum-starved for 12 h and then treated with insulin (100 nM) for 15 min. Total cellular extracts were resolved by western blot and analyzed with the indicated antibodies. FLIP overexpression does not affect Akt phosphorylation. **(b)** Western blot analysis of p-Gsk3β and Gsk3β expression in HeLa WT or transfected with different concentrations of c-FLIP_L cDNA (500 ng, 1 μg and 2 μg) for 48 h. We observed a strong reduction of Gsk3β phosphorylation. **(c)** HeLa cells were transfected with HA-Gsk3β cDNA, and c-FLIP_L cDNA or control vector, as indicated for 24 h. Cells were starved for 12 h and then treated with insulin (100 nM) for 15 min. Cell lysates were immunoprecipitated with anti-HA antibody and blotted with phospho-Gsk3β antibody. **(d)** Western blot analysis of HeLa cells transfected with c-FLIP-WT, c-FLIP-F1, c-FLIP-R0 or c-FLIP-R1 cDNA. Total lysates were analyzed with anti-phospho-Gsk3β, Gsk3, Flag and β-actin antibodies. c-FLIP mutants were not able to decrease phospho Gsk3β levels. **(e)** HeLa cells were transfected with HA-Gsk3β and c-FLIP-R1 cDNA or with a control vector, treated with insulin (100 nM) for 15 min, immunoprecipitated with anti-HA antibodies, and blotted with p-Gsk3β antibodies. Total lysates were analyzed with the indicated antibodies. c-FLIP mutant overexpression did not reduce Gsk3β phosphorylation. **(f)** HeLa cells were transfected with HA-Gsk3β cDNA, and c-FLIP_L cDNA, c-FLIP_S cDNA or control vector, as indicated for 24 h. Cells were serum starved for 12 h and then treated with insulin (100 nM) for 15 min. Cell lysates were immunoprecipitated with anti-HA antibody and blotted with anti-phospho-Gsk3β antibody

p27^{Kip1}, inducing its downregulation. However, TRAIL-sensitive H460 cells exhibited reduced levels of miR-222 and miR-221 and increased p27^{Kip1} expression. We therefore investigated whether p27^{Kip1} modulated sensitivity to TRAIL-mediated cell death through the regulation of the apoptotic machinery molecules. To this aim, HeLa TWEEN FLIP cells, which express p27^{Kip1} at very low levels, were transfected with HA-p27 cDNA, and caspase-3 levels were investigated by western blot analysis. We observed a significant increase in caspase-3 levels (Figure 5a). Furthermore, silencing of p27^{Kip1} using a specific siRNA in

H460 cells, which express p27^{Kip1} at high levels, resulted in reduction in caspase-3 level (Figure 5b).

To further confirm the role of the FLIP-Gsk3 pathway on TRAIL apoptotic machinery, we evaluated caspase-3 levels in HeLa TWEEN c-FLIP-overexpressing cells, Gsk3 pathway of which was inhibited either by Gsk3 siRNA or by LiCl treatment. Both inhibitions resulted in an increase in caspase-3 expression levels, whereas no differences were observed in FADD levels (Figure 5c).

We investigated whether c-FLIP_L modulated caspase-3 transcript levels through a transcriptional mechanism by

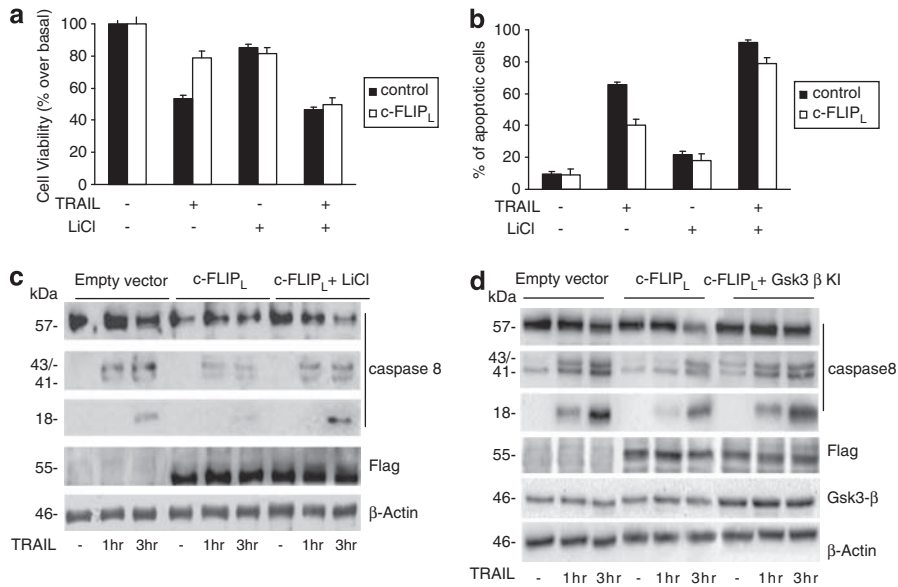


Figure 3 Role of c-FLIP_L and Gsk3 β signaling pathway on TRAIL-induced cell death. Cell death quantification – HeLa cells were transfected with 2 μ g of c-FLIP_L cDNA for 24 h, plated in 96-well plates in triplicate and then treated with SuperKiller TRAIL (500 ng/ml) and lithium chloride (20 mmol) for 48 h, as indicated. Cell viability was assessed by Cell Vitality assay (a) or by propidium iodide staining and FACS analysis (b). (c and d) Western blot analysis of caspase-8 activation. The inhibition of Gsk3 β was obtained by transfection of HeLa cells with kinase-inactive Gsk3 β cDNA or by treatment with 20 mmol lithium chloride for 24 h. Cells were incubated with 500 ng/ml TRAIL for 1 or 3 h. The inhibition of Gsk3 β induced an increase of caspase-8 activation in c-FLIP-overexpressing cells

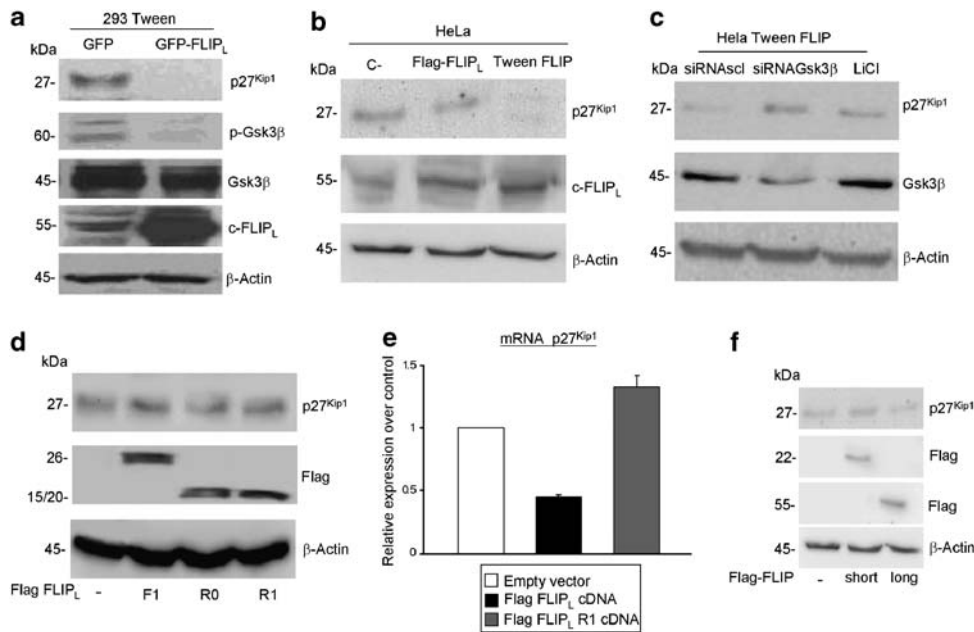


Figure 4 c-FLIP overexpression regulates p27^{Kip1} levels through Gsk3 β . Western blot analysis of Gsk3 β , p-Gsk3 β and p27^{Kip1} levels in different cell lines. (a) HEK-293-Tween GFP and tween-GFP c-FLIP_L; (b) HeLa cells transfected with c-FLIP_L cDNA and HeLa Tween c-FLIP_L. There is an inverse correlation between FLIP and p-Gsk3 levels. (c) Western blot analysis of p27^{Kip1} levels in HeLa cells transfected with c-FLIP_L mutants F1, R0 and R1 cDNA. (d) Effects of inhibition of Gsk3 β on p27^{Kip1} expression. HeLa Tween FLIP cells were transfected with Gsk3 β siRNA or scrambled siRNA or treated with 20 mmol lithium chloride for 24 h. Levels of p27^{Kip1} and Gsk3 β were analyzed by immunoblotting. (e) Real time PCR analysis of p27^{Kip1} mRNA with transfection of FLIP_L cDNA in HeLa cells. c-FLIP reduces p27^{Kip1} levels through Gsk3 β . c-FLIP deletion mutants were not able to reduce p27^{Kip1} levels. (f) Total lysates of HeLa cells transfected with c-FLIP_L, c-FLIP_s or control vector were analyzed for p27 expression

real-time PCR. Interestingly, we observed a significant reduction in *caspase-3* mRNA levels in HeLa cells transfected with c-FLIP_L compared with controls, whereas this effect was not observed in FLIP R1 mutant (Figure 5d).

Finally, we also examined the activity of caspase-3 by the colorimetric CaspACE assay in HeLa cells transfected with an empty vector or with c-FLIP_L cDNA. The expression of c-FLIP_L induced a reduction of caspase-3 activity

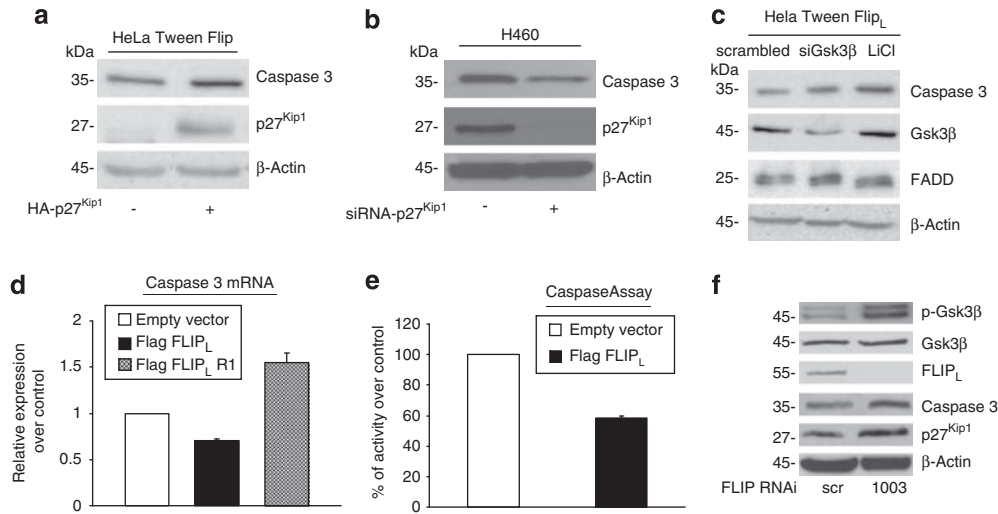


Figure 5 Role of p27^{Kip1} on caspase-3 expression. **(a)** HeLa Tween FLIP cells transfected with HA-p27^{Kip1} cDNA were analyzed by western blotting for caspase-3. Loading and transfection control were analyzed with anti-p27^{Kip1} and anti-β-actin antibodies. p27 overexpression induced an increase in caspase-3 expression levels. **(b)** Western blot analysis of caspase-3 and -8 in H460 cells on transfection of p27^{Kip1} siRNA. The inhibition of p27 decreases caspase-3 levels. **(c)** Immunoblotting of HeLa Tween FLIP cells upon transfection of scrambled siRNA (sc-si), Gsk3β siRNA or treatment with 20 mM lithium chloride for 24 h with caspase-3, FADD or Gsk3β antibodies. The inhibition of Gsk3 pathway resulted in an increase in expression levels of caspase-3, whereas no differences were observed in FADD and caspase-8 expression. **(d)** Real-time PCR of *caspase-3* mRNA on transfection in HeLa cells with Flag-FLIP_L cDNA. FLIP overexpression induced a significant reduction of *caspase-3* mRNA levels. **(e)** Quantification of caspase-3 activity by Colorimetric CaspACE Assay System in HeLa cells transfected with an empty vector or Flag-FLIP_L cDNA. **(f)** Total lysate of HeLa cells expressing RNAi constructs for c-FLIP (FLIP 1003) or with a scrambled control. A total of 40 μg of proteins were loaded and blotted with the indicated antibodies. β-Actin was used as the loading control. FLIP downregulation induced an increase of GSK3β phosphorylation, p27 and caspase-3 levels. Representative experiment was performed in triplicates

(Figure 5e). All these effects were reverted when c-FLIP_L endogenous levels were downregulated by a specific c-FLIP_L siRNA (Figure 5f). The effects of specific RNAi constructs for c-FLIP on FLIP expression levels are shown in Supplementary Figure 1b.

Discussion

In this study, we provide evidence for a new role of c-FLIP_L. c-FLIP_L has been identified as an inhibitor of apoptosis triggered by the engagement of death receptors, such as Fas or TRAIL.^{23,24} c-FLIP_L has also been implicated in other cellular functions, such as control of gene expression by ERK and NF-κB.^{9,25}

We demonstrate, to the best of our knowledge, for the first time that Akt interacts with c-FLIP_L, and that this interaction functionally regulates Gsk3β activation and apoptosis. Recently, Giampietri *et al.*²⁶ described that in c-FLIP transgenic mice, the phosphorylation of Akt and Gsk3β were reduced compared with control animals, even though caspase-3 activity was unchanged, highlighting an apoptosis-independent role of c-FLIP on pressure overload-mediated cardiac hypertrophy. The role of c-FLIP in heart development has been previously described in c-FLIP ko mice that, similar to FADD ko mice, developed severe defects of heart development.^{27,28} These studies identify c-FLIP as a new regulator of heart development and the hypertrophic response, possibly through Gsk3 signaling.

In this study, by genetic and biochemical methodologies, we have demonstrated that Akt is able to interact with c-FLIP_L in the region stretching from a.a. 253 to a.a. 339 of the c-FLIP_L

protein. We observed that overexpression of c-FLIP_L, although does not interfere with insulin-induced Akt activation, almost abolishes Gsk3β phosphorylation. The effects on Gsk3β were abrogated when we overexpressed c-FLIP_L mutants that do not bind Akt. This may mean that, by binding to Akt, c-FLIP_L relegates the kinase in a different cellular compartment, and abolishes its ability to bind and phosphorylate its substrates. It is interesting that the phosphorylation of other Akt substrates besides Gsk3β, such as BAD, was reduced in c-FLIP_L-overexpressing cells (data not shown).

It has been reported that Gsk3β contributes both to cell death and cell survival, depending on the cellular system and the appropriate stimuli.¹⁹ Several studies indicated that inhibition of Gsk3β activity in cancer cells potentiates apoptosis stimulated by death receptor.^{29–32} Furthermore, knocking out Gsk3β or inhibiting Gsk3β using lithium chloride, potentiates TNF-induced apoptosis, indicating an anti-apoptotic role for Gsk3β.³⁰

Therefore, we asked whether c-FLIP_L-mediated reduction of Gsk3β phosphorylation, and thus increase in its kinase activity, might be necessary for the anti-apoptotic function of c-FLIP_L. Interestingly, when we interfered with Gsk3β activity, either using LiCl or with overexpression of a kinase-inactive form of Gsk3, anti-apoptotic c-FLIP_L effects were significantly reduced. Thus, Gsk3β may act as an important mediator that participates in FLIP's anti-apoptotic function in human cancer.

We have recently demonstrated that p27 expression is linked to TRAIL resistance in NSCLC cells overexpressing miR-222.²² We therefore investigated the level of p27 in different cells overexpressing c-FLIP_L. Interestingly, we observed an inverse correlation between the c-FLIP_L and

p27 expression levels, as well as Gsk3 β phosphorylation. This was also true in forced c-FLIP_L-expressing cells (HEK-293 and HeLa). We then investigated whether c-FLIP could affect p27 levels through the activation of Gsk3 β . For this purpose, we interfered with Gsk3 β expression levels or activity in c-FLIP_L-overexpressing cells and evaluated p27 levels. We observed that Gsk3 β inhibition increased protein and mRNA levels of p27. The effects of FLIP_L on p27 depend on its interaction with Akt, as c-FLIP_L WT overexpression, but not its Akt-binding-site deletion mutants, was able to reduce p27 mRNA level. Recently, Wang *et al.*²¹ described that Gsk3 β negatively regulates p27 protein in MLL leukemia cells, thus being critical for the maintenance of MLL leukemia, and prospecting Gsk3 as an interesting target for this form of cancer. In the MLL cellular system, the effects were mainly at the protein level because the inhibition of Gsk3 β did not affect mRNA levels. Therefore, although the final effect is similar, the functional relationships of Gsk3 β with p27 seem to be cell type dependent. Gsk3 β is a negative regulator of heart hypertrophy.³³ Interestingly, Hauck³⁴ recently described that silencing p27 induced cardiomyocyte hypertrophic growth in the absence of growth-factor stimulation. It is interesting to speculate that Gsk3 β mediates negative regulation of hypertrophic growth through its effects on p27 expression levels.

Finally, we investigated the mechanisms of c-FLIP-Gsk3 β -p27-mediated inhibition of cell death, by the evaluation of protein and mRNA levels of apoptosis-signaling molecules.

We showed that the absence of p27 induces a reduction in caspase-3 levels. This effect was mediated by Gsk3 β because its inactivation induced an increase in caspase-3 level. The effect was specific on caspase-3 because other apoptosis-signaling molecules, such as FADD, were not affected. This effect occurred at the transcriptional level because c-FLIP_L overexpression, but not its mutants, was able to reduce *caspase-3* mRNA level, as assessed by RT-PCR. The overexpression of c-FLIP_L also induces a significant reduction in the amount of the active caspase in untreated cells. Thus, taken together these data depict a model in which in c-FLIP-overexpressing cells, the activation of Gsk3 β induces a reduction in p27^{Kip1} and caspase-3 expression and activity levels, and thus a reduction in TRAIL-induced cell death (Figure 6).

Recently, Gsk3 β has been described as a protein complex associated with death receptors, DDX3, and cellular inhibitor of apoptosis protein-1 (cIAP-1).²⁹ In that study, Gsk3 β inhibited apoptosis by interfering with DISC formation and caspase-8 activation. Our data reveal other possible mechanisms through which Gsk3 might inhibit apoptosis, that is, through regulation of p27 expression and that of downstream caspase-3 (Figure 6).

Our data show that c-FLIP overexpression strongly reduces Akt-mediated Gsk3 β phosphorylation. Furthermore, its down-regulation by a specific c-FLIP siRNA resulted in an increase in Gsk3 β phosphorylation, as well as in p27 and caspase-3 levels.

In conclusion, this study demonstrates that anti-apoptotic functions of c-FLIP_L are mediated by its effects on Gsk3 β activity, and p27 and caspase-3 levels. These findings may be of importance in optimizing a strategy for the treatment of TRAIL-resistant human cancer.

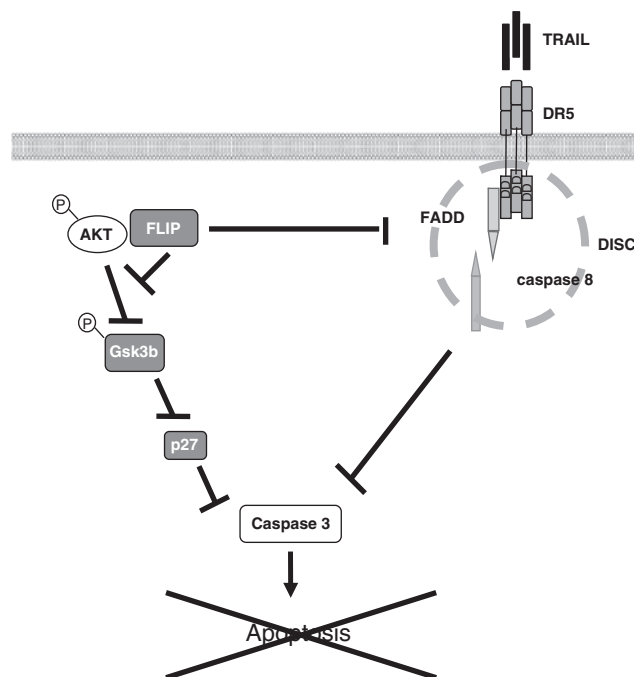


Figure 6 Role of cFLIP-Gsk3 signaling pathway in the regulation of cell death. In FLIP-overexpressing cells, activation of Gsk3 β induces a reduction in p27^{Kip1} and caspase-3 expression levels and a reduction in TRAIL-induced cell death

Materials and Methods

Materials. Media, sera and antibiotics for cell culture were purchased from Life Technologies (Grand Island, NY, USA). Protein electrophoresis reagents were obtained from Bio-Rad (Richmond, VA, USA). Western blotting and ECL reagents were procured from GE Healthcare (Piscataway, NJ, USA). All other chemicals were from Sigma (St. Louis, MO, USA). The antibodies: anti-caspase-8 antibody (1C12), anti-Akt, anti-P-Akt, anti-P-Gsk3 β , anti-Gsk3 β and anti-p27^{Kip1} were purchased from Cell Signaling Technology (Danvers, MA, USA); anti-caspase-3 antibody was obtained from Abcam (Cambridge, MA, USA); anti-c-FLIP (NF6) antibody was purchased from Alexis (Lausen, Switzerland); anti-Flag M2 and anti- β -actin antibodies were obtained from Sigma; anti-HA antibody was obtained from Covance (Berkeley, CA, USA). SuperKiller TRAIL was purchased from Alexis.

Plasmids. The plasmids pcDNA3 Flag(hs)FLIP_L and FLIP_S were kindly provided by Professor Pasquale Vito and Henning Walczak, respectively. Akt WT, Akt E40K (constitutively active, HA-Akt D +) and Akt K179M (dominant-negative HA-Akt D) with an HA tag were a kind gift of Professor Gianluigi Condorelli. Gsk3 β WT and Gsk3 β kinase inactive (KI) cDNAs were kindly provided by Professor Junichi Sadoshima. p27 cDNA was kindly provided by Professor Alfredo Fusco. pRetroSuper vectors expressing RNAi for c-FLIP were obtained from Professor Simone Fulda.

Cell culture. Human HeLa, HEK-293, K562 and A459 cell lines were grown in DMEM containing 10% heat-inactivated FBS with 2 mM L-glutamine and 100 U/ml penicillin-streptomycin. DU145 and H460 cell lines were grown in RPMI containing 10% heat-inactivated FBS with 2 mM L-glutamine and 100 U/ml penicillin-streptomycin.

Yeast two-hybrid system. All experiments were performed in the yeast reporter MaV203. The human heart cDNA library was obtained from Invitrogen (Carlsbad, CA, USA). Screening of the library was performed essentially following instructions for the ProQuest two-hybrid system (Life Technologies) and has been previously described.³⁵ The GAL4 DNA-binding domain/human Akt fusion was obtained from Dr. Alfonso Bellacosa (Fox Chase Cancer Center, Philadelphia, PA, USA). Subsequently, yeast pLEx4-Akt plasmid was transformed with the pPC86AD cDNA library and plated onto plates lacking histidine in the presence of 3AT

Acknowledgements. We thank Dr. V de Franciscis and M Latronico for paper revision; and LR Vitiani for preparation of c-FLIP-overexpressing cells. This study was partially supported by funds from: Associazione Italiana Ricerca sul Cancro (AIRC) (to GC), MIUR-FIRB (RBIN04J4J7) and EU grant EMIL (European Molecular Imaging Laboratories Network) contract number 503569.

- Hengartner MO. The biochemistry of apoptosis. *Nature* 2000; **407**: 770–776.
- Okada H, Mak TW. Pathways of apoptotic and non-apoptotic death in tumour cells. *Nat Rev Cancer* 2004; **4**: 592–603.
- Ghobrial IM, Witzig TE, Adjei AA. Targeting apoptosis pathways in cancer therapy. *CA Cancer J Clin* 2005; **55**: 178–194.
- Peter ME. The flip side of FLIP. *Biochem J* 2004; **382** (Part2): e1–e3.
- Scaffidi C, Schmitz I, Krammer PH, Peter ME. The role of c-FLIP in modulation of CD95-induced apoptosis. *J Biol Chem* 1999; **274**: 1541–1548.
- Irmeler M, Thome M, Hahne M, Schneider P, Hofmann K, Steiner V *et al*. Inhibition of death receptor signals by cellular FLIP. *Nature* 1997; **388**: 190–195.
- Safa AR, Day TW, Wu CH. Cellular FLICE-like inhibitory protein (c-FLIP): a novel target for cancer therapy. *Curr Cancer Drug Targets* 2008; **8**: 37–46.
- Lin Y, Liu X, Yue P, Benbrook DM, Berlin KD, Khuri FR *et al*. Involvement of c-FLIP and survivin down-regulation in flexible heteroarotinoid-induced apoptosis and enhancement of TRAIL-initiated apoptosis in lung cancer cells. *Mol Cancer Ther* 2008; **7**: 3556–3565.
- Kataoka T, Budd RC, Holler N, Thome M, Martinon F, Irmeler M *et al*. The caspase-8 inhibitor FLIP promotes activation of NF-kappaB and Erk signaling pathways. *Curr Biol* 2000; **10**: 640–648.
- Maedler K, Fontana A, Ris F, Sergeev P, Toso C, Oberholzer J *et al*. FLIP switches Fas-mediated glucose signaling in human pancreatic beta cells from apoptosis to cell replication. *Proc Natl Acad Sci USA* 2002; **99**: 8236–8241.
- Fang LW, Tai TS, Yu WN, Liao F, Lai MZ. Phosphatidylinositol 3-kinase priming couples c-FLIP to T cell activation. *J Biol Chem* 2004; **279**: 13–18.
- Franke TF, Hornik CP, Segev L, Shostak GA, Sugimoto C. PI3K/Akt and apoptosis: size matters. *Oncogene* 2003; **22**: 8983–8998.
- Datta SR, Dudek H, Tao X, Masters S, Fu H, Gotoh Y *et al*. Akt phosphorylation of BAD couples survival signals to the cell-intrinsic death machinery. *Cell* 1997; **91**: 231–241.
- Cardone MH, Roy N, Stennicke HR, Salvesen GS, Franke TF, Stanbridge E *et al*. Regulation of cell death protease caspase-9 by phosphorylation. *Science* 1998; **282**: 1318–1321.
- Brunet A, Bonni A, Zigmond MJ, Lin MZ, Juo P, Hu LS *et al*. Akt promotes cell survival by phosphorylating and inhibiting a Forkhead transcription factor. *Cell* 1999; **96**: 857–868.
- Garofalo M, Quintavalle C, Zanca C, De Rienzo A, Romano G, Acunzo M *et al*. Akt regulates drug-induced cell death through Bcl-w downregulation. *PLoS ONE* 2008; **3**: e4070.
- Doble B, Woodgett J. GSK-3: tricks of the trade for a multi-tasking kinase. *J Cell Sci* 2003; **116** (Part 7): 1175–1186.
- Cohen P, Frame S. The renaissance of GSK3. *Nat Rev Mol Cell Biol* 2001; **2**: 769–776.
- Beurel E, Jope RS. The paradoxical pro- and anti-apoptotic actions of GSK3 in the intrinsic and extrinsic apoptosis signaling pathways. *Prog Neurobiol* 2006; **79**: 173–189.
- Jope RS. Lithium and GSK-3: one inhibitor, two inhibitory actions, multiple outcomes. *Trends Pharmacol Sci* 2003; **24**: 441–443.
- Wang Z, Smith KS, Murphy M, Piloto O, Somerville TC, Cleary ML. Glycogen synthase kinase 3 in MLL leukaemia maintenance and targeted therapy. *Nature* 2008; **455**: 1205–1209.
- Garofalo M, Quintavalle C, Di Leva G, Zanca C, Romano G, Taccioli C *et al*. MicroRNA signatures of TRAIL resistance in human non-small cell lung cancer. *Oncogene* 2008; **27**: 3845–3855.
- Bélanger C, Gravel A, Tomoiu A, Janelle ME, Gosselin J, Tremblay MJ *et al*. Human herpesvirus 8 viral FLICE-inhibitory protein inhibits Fas-mediated apoptosis through binding and prevention of procaspase-8 maturation. *J Hum Virol* 2001; **4**: 62–73.
- Djerbi M, Screpanti V, Catrina AI, Bogen B, Biberfeld P, Grandien A. The inhibitor of death receptor signaling, FLICE-inhibitory protein defines a new class of tumor progression factors. *J Exp Med* 1999; **190**: 1025–1032.
- Lens SM, Kataoka T, Fortner KA, Tinel A, Ferrero I, MacDonald RH *et al*. The caspase 8 inhibitor c-FLIP(L) modulates T-cell receptor-induced proliferation but not activation-induced cell death of lymphocytes. *Mol Cell Biol* 2002; **22**: 5419–5433.
- Giampietri C, Petrunaro S, Musumeci M, Coluccia P, Antonangeli F, De Cesaris P *et al*. c-Flip overexpression reduces cardiac hypertrophy in response to pressure overload. *J Hypertens* 2008; **26**: 1008–1016.
- Yeh WC, Irie A, Elia AJ, Ng M, Shu HB, Wakeham A *et al*. Requirement for Casper (c-FLIP) in regulation of death receptor-induced apoptosis and embryonic development. *Immunity* 2000; **12**: 633–642.
- Yeh WC, Pompa JL, McCurrach ME, Shu HB, Elia AJ, Shahinian A *et al*. FADD: essential for embryo development and signaling from some, but not all, inducers of apoptosis. *Science* 1998; **279**: 1954–1958.
- Sun M, Song L, Li Y, Zhou T, Jope RS. Identification of an antiapoptotic protein complex at death receptors. *Cell Death Differ* 2008; **15**: 1887–1900.
- Hoeflich KP, Luo J, Rubie EA, Tsao MS, Jin O, Woodgett JR. Requirement for glycogen synthase kinase-3beta in cell survival and NF-kappaB activation. *Nature* 2000; **406**: 86–90.
- Liao X, Zhang L, Thrasher JB, Du J, Li B. Glycogen synthase kinase-3beta suppression eliminates tumor necrosis factor-related apoptosis-inducing ligand resistance in prostate cancer. *Mol Cancer Ther* 2003; **2**: 1215–1222.
- Rottmann S, Wang Y, Nasoff M, Deveraux QL, Quon KC. A TRAIL receptor-dependent synthetic lethal relationship between MYC activation and GSK3beta/FBW7 loss of function. *Proc Natl Acad Sci USA* 2005; **102**: 15195–15200.
- Markou T, Cullingford TE, Giraldo A, Weiss SC, Alsafi A, Fuller SJ *et al*. Glycogen synthase kinases 3alpha and 3beta in cardiac myocytes: regulation and consequences of their inhibition. *Cell Signal* 2008; **20**: 206–218.
- Hauck L, Harms C, An J, Rohne J, Gertz K, Dietz R *et al*. Protein kinase CK2 links extracellular growth factor signaling with the control of p27(Kip1) stability in the heart. *Nat Med* 2008; **14**: 315–324.
- Missero C, Pirro MT, Simeone S, Pischetola M, Di Lauro R. The DNA glycosylase T:G mismatch-specific thymine DNA glycosylase represses thyroid transcription factor-1-activated transcription. *J Biol Chem* 2001; **276**: 33569–33575.
- Todaro M, Zerilli M, Ricci-Vitiani L, Bini M, Perez Alea M, Maria Florena A *et al*. Autocrine production of interleukin-4 and interleukin-10 is required for survival and growth of thyroid cancer cells. *Cancer Res* 2006; **66**: 1491–1499.
- Brummelkamp TR, Bernards R, Agami R. Stable suppression of tumorigenicity by virus-mediated RNA interference. *Cancer Cell* 2002; **2**: 243–247.

Supplementary Information accompanies the paper on Cell Death and Differentiation website (<http://www.nature.com/cdd>)

ORIGINAL ARTICLE

miR-221/222 overexpression in human glioblastoma increases invasiveness by targeting the protein phosphatase PTP μ C Quintavalle¹, M Garofalo², C Zanca¹, G Romano³, M Iaboni¹, M del Basso De Caro⁴, JC Martinez-Montero⁵, M Incoronato³, G Nuovo², CM Croce² and G Condorelli^{1,6,7}

¹Department of Cellular and Molecular Biology and Pathology, 'Federico II' University of Naples, Naples, Italy; ²Department of Molecular Virology, Immunology and Medical Genetics, Human Cancer Genetics Program, Comprehensive Cancer Center, The Ohio State University, Columbus, OH, USA; ³Fondazione IRCCS SDN, Naples, Italy; ⁴Dipartimento di Scienze Biomorfologiche e Funzionali, Sezione di Anatomia Patologica e Fitopatologia; ⁵Instituto Oftalmico Hospital Universitario Gregorio Marañon, Madrid, Spain; ⁶IEOS, CNR, Naples, Italy and ⁷Facoltà di Scienze Biotechnologiche, 'Federico II' University of Naples, Naples, Italy

Glioblastoma is the most frequent brain tumor in adults and is the most lethal form of human cancer. Despite the improvements in treatments, survival of patients remains poor. In order to identify microRNAs (miRs) involved in glioma tumorigenesis, we evaluated, by a miRarray, differential expression of miRs in the tumorigenic glioma LN-18, LN-229 and U87MG cells compared with the non-tumorigenic T98G cells. Among different miRs we focused our attention on miR-221 and -222. We demonstrated the presence of a binding site for these two miRs in the 3' untranslated region of the protein tyrosine phosphatase μ (PTP μ). Previous studies indicated that PTP μ suppresses cell migration and is downregulated in glioblastoma. Significantly, we found that miR-221 and -222 overexpression induced a downregulation of PTP μ as analyzed by both western blot and real-time PCR. Furthermore, miR-222 and -221 induced an increase in cell migration and growth in soft agar in glioma cells. Interestingly, the re-expression of PTP μ gene was able to revert the miR-222 and -221 effects on cell migration. Furthermore, we found an inverse correlation between miR-221 and -222 and PTP μ in human glioma cancer samples. In conclusion, our results suggest that miR-221 and -222 regulate glioma tumorigenesis at least in part through the control of PTP μ protein expression.

Oncogene advance online publication, 11 July 2011; doi:10.1038/onc.2011.280

Keywords: Glioma; microRNA; tumorigenesis; apoptosis

Introduction

Gliomas are the most common primary tumors in the brain and are divided into four clinical grades on the basis of their histology and prognosis (Tran and

Rosenthal, 2010). Among them, glioblastoma (GB, grade IV) are highly invasive, very aggressive and are one of the most incurable forms of cancer in humans (Purov and Schiff, 2009). In spite of recent improvements of surgical and radiotherapeutic techniques, the prognosis for glioblastoma patients is still very poor with a mean survival time after diagnosis ranging from 9 to 12 months. The treatment strategies for this disease have not changed appreciably for many years, and most are based on a limited understanding of the biology of the disease. In fact, although a number of genetic and molecular lesions have been correlated to glioblastoma progression, the deep understanding of the molecular markers is fundamental to develop targets for glioblastoma treatment. Small non-coding RNAs named microRNAs (miRs) are a class of endogenous non-coding, highly conserved RNAs of ~22 nucleotides in length that are encoded in plant and animal genomes. miRs are involved in the pathogenesis of most cancers (Calin and Croce, 2006). They negatively regulate mRNA expression by repressing translation or directly cleaving the targeted mRNA. In the last few years, our understanding of the role of miRNA has expanded from the initially identified functions in the development of round worms to a highly expressed and ubiquitous regulators implicated in a wide array of critical processes, including proliferation, cell death, differentiation, metabolism and, importantly, tumorigenesis (Croce, 2009). miRs profiling achieved by various methods has allowed the identification of signatures associated with diagnosis, staging, progression, prognosis and response to treatment of human tumors. Therefore, miRNA 'fingerprinting' represents a new addition to the diagnostic and prognostic tools to be used in medical oncology. In this study we evaluated by a miR array differential expression of miRs in tumorigenic glioma LN18, LN229 and U87MG cells compared with the non-tumorigenic T98G cells. Among different miRs we focused our attention on miRs -221 and -222. Our results show that miRs -221 and -222 target the protein tyrosine phosphatase μ (PTP μ). PTP μ regulates cell invasiveness and adhesion (Burgoyne *et al.*, 2009a), and has been found downregulated in human GB (Burgoyne *et al.*, 2009b). The present study describes

Correspondence: Professor G Condorelli, Dipartimento di Biologia e Patologia Cellulare e Molecolare, Università degli Studi di Napoli 'Federico II', Facoltà di Scienze Biotechnologiche, Ed 19 A, II floor, Via Pansini, 5, Naples, NA 80131, Italy.

E-mail: gecondor@unina.it

Received 21 December 2010; revised and accepted 31 May 2011

for the first time PTP μ as a miR-222 and -221 target and explores the role of those miRs, through this target, in GB tumorigenesis and invasiveness.

Results

miRs expression in glioma cell lines

T98G, U87MG, LN-18 and LN-229 glioma cells have been described as having a different tumorigenic behavior (Cerchia *et al.*, 2009). In fact, while T98G are not able to grow in nude mice and to form colonies, U87MG, LN-18 and LN-229 cells are able to form tumors when injected in nude mice and to form colonies in soft agar, even in the absence of serum. We confirmed these data using soft agar and xenograft growth in nude mice (Supplementary Figure 1). In order to investigate

Table 1 Upregulated miRs in tumorigenic glioma cells

MiR	Intensities of U87MG	Intensities of T98G	Fold change
hsa-miR-221	11150.1	1763.5	6.323
hsa-miR-125b	4697.4	1020.4	4.603
hsa-miR-21	6236.3	1662.4	3.751
hsa-miR-222	16685.8	6014	2.774
hsa-miR-34a	319.1	26.7	11.951

All differentially expressed miRs have $Q < 0.01$ (false positive rate), t -test $P < 0.05$.

These miRs were identified by PAM as predictor of glioma cells with the lowest misclassification error.

the involvement of miR in glioma tumorigenesis, we analyzed miR expression profile in the tumorigenic glioma LN-18 and LN-229 and U87MG cells versus non-tumorigenic T98G cells. The analysis was performed with a microarray chip containing 1150 miR probes, including 326 human and 249 mouse miRs, spotted in duplicates (Liu *et al.*, 2004). Pairwise significance analysis (PAM) of the microarray indicated that five miR genes were significantly overexpressed in tumorigenic cells with a > 2.5 -fold change (Table 1). We focus our attention on miR-221 and miR-222, as we and others have already demonstrated that those miRs are frequently overexpressed in a number of human tumors (Pallante *et al.*, 2006; Pineau *et al.*, 2010; Sredni *et al.*, 2010). In order to confirm the array results, we analyzed the levels of miR-222 and -221 with real-time PCR (RT-PCR). Accordingly with microarray data, we found an upregulation of these two miRs in tumorigenic cells (U87MG, LN-18 and LN-229) compared with non-tumorigenic one (T98G) (Figure 1a). We confirmed those data in a larger number of glioma cell lines, with a different tumorigenic phenotype (Supplementary Figure 3A). As shown in Supplementary Figure 3B also the non-tumorigenic cell lines LN-308, A172 and LN-428 express low levels of miR-221 and -222 if compared with the tumorigenic lines LN-319, LN-18 and LN-229. As expected, the predicted miR-221 and -222 targets, p27^{kip1}, and PTEN were expressed at decreased levels in the non-tumorigenic U87MG cells (Figure 1b) as compared with T98G cells. Similar results were obtained in the other non-tumorigenic cells (data not shown).

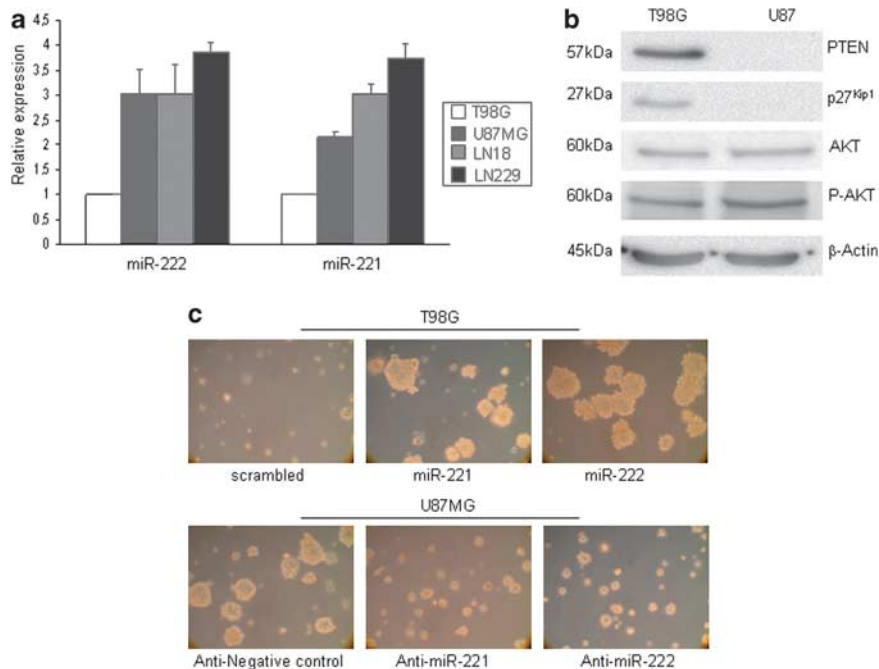


Figure 1 Expression of miR-222 and -221 and their targets in T98G and U87MG glioma cells. (a) Real-time PCR of miR-221 and -222 in glioma cells. Representative of at least three independent experiments. (b) Western blot analysis of the known miR-221 and -222 targets, PTEN and p27^{kip1}. As a consequence of decreased PTEN protein levels, p-AKT levels were increased, although total AKT levels were comparable. β -Actin was used as the loading control. (c) Soft agar growth of T98G cells transiently transfected with miR-221, -222 or a scrambled sequence and of U87MG cells transfected with anti-miR-221, anti-miR-222 or a scrambled sequence.

In order to verify the involvement of these miRs in glioma tumorigenesis we transfected the T98G cells with pre-miR-221 and pre-miR-222 or with a scrambled sequence, and U87MG cells with and anti-miR-221 and -222 or with anti-miR negative control. As shown in Figure 1c by soft agar assay, miR-221 and -222 overexpression resulted in a phenotypic change of T98G cells that become able to form colonies. Similar results were obtained in LN-18, LN-229 cells transfected with miR-222 or -221 (data not shown). Furthermore, the tumorigenic U87MG overexpressing anti-miR-221 and -222 exhibited a much weaker capacity to form colonies in soft agar. Similar results were obtained when T98G stably overexpressing miRs with a tween vector were plated in soft agar. Cells expressing the control tween vector did not produce colonies in soft agar (Supplementary Figure 3D), meanwhile T98G-tween-miR-221 formed a large number of colonies indicating a greater tumorigenic behavior of cells overexpressing miR-221/222.

Identification of PTP μ as a new target of miR-221 and -222

To find new miR-221 and -222 targets, we used bioinformatics analysis. Comparing the results obtained from the different searches, we found that the protein phosphatase PTP μ was predicted as a target of miR-222 by the miRanda algorithm (www.microrna.org/microrna/home.do). RNAhybrid also predicted a possible binding region of miR-221 and -222 in the 3' untranslated region (UTR) of PTP μ (Figure 2a). The most widely used approach for experimentally validating miRNA targets is to clone the predicted miRNA-binding sequence downstream of a luciferase reporter construct, and to co-

transfect it with the miRNA of interest for luciferase assays. To this end, we cloned the 3'UTR sequence of human PTP μ into the luciferase-expressing vector pGL3-control downstream of the luciferase stop codon; Meg01 cells were transiently transfected with this construct in the presence of pre-miR-221 and pre-miR222 or in the presence of a scrambled oligonucleotide acting as a negative control. As reported in Figure 2c, miR-221 and miR-222 significantly reduced luciferase activity compared with the scrambled oligonucleotide. This indicates that miR-221 and -222 bind to the 3'UTR of *ptpm* and impair its mRNA translation. We observed a similar effect in the presence of both miRs added at the same time, indicating that the target site of the miRs in the 3'UTR of PTP μ is the same. In order to further confirm that the region was specific for the binding with miR-222 and -221, we generated a deletion mutant (Figure 2b) lacking the binding site, ATGTAGC. The mutant was cloned into the 3'UTR of the luciferase gene and co-transfected with pre-miR-221 and -222 in Meg01 cells. As shown in Figure 2d, miR-221 and -222 added singularly or at the same time, did not significantly reduce luciferase activity in the presence of the 3'UTR PTP μ mut sequence. This result indicates that miR-221 and -222 target PTP μ mRNA at the ATGTAGC sequence.

Expression of PTP μ and miR-222 and -221 in glioma

To assess whether the expression of PTP μ was inversely correlated with miR-221 and -222 in glioma cells, we analyzed the levels of the protein phosphatase in the different glioma cells. We found reduced PTP μ protein (Figure 3a) and mRNA levels (Figure 3b) in U87MG, LN-18 and LN-229 cells overexpressing miR-221 and -222 compared with T98G.

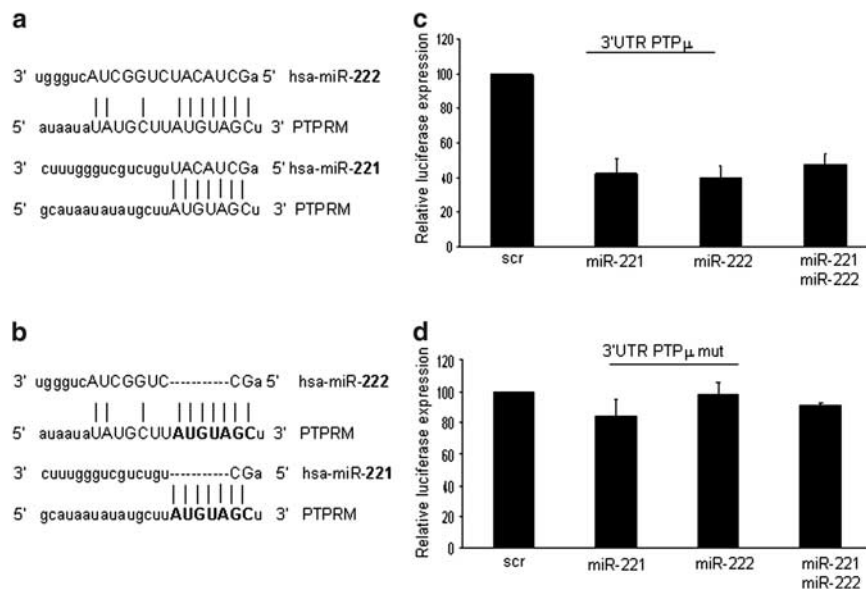


Figure 2 Identification of target sites in the 3'-UTR of PTP μ . Complementary sites for miR-222 and -221 on wild-type (a) or mutated (b) PTP μ 3'UTR. The capital letters identify perfect base matches according to miRanda software (www.microrna.org/microrna/home.do). The bold letters identify the deleted regions. For luciferase activity, Meg01 cells were transiently co-transfected with the luciferase reporter containing wild-type PTP μ -3'UTR (c) or PTP μ -3'UTR mutant (d) in the presence of pre-miR-222, miR-221, pre-miR-221 and miR-222 together or scrambled oligonucleotide. Luciferase activity was evaluated 24h after transfection as described in Materials and methods. Representative of at least three independent experiments.

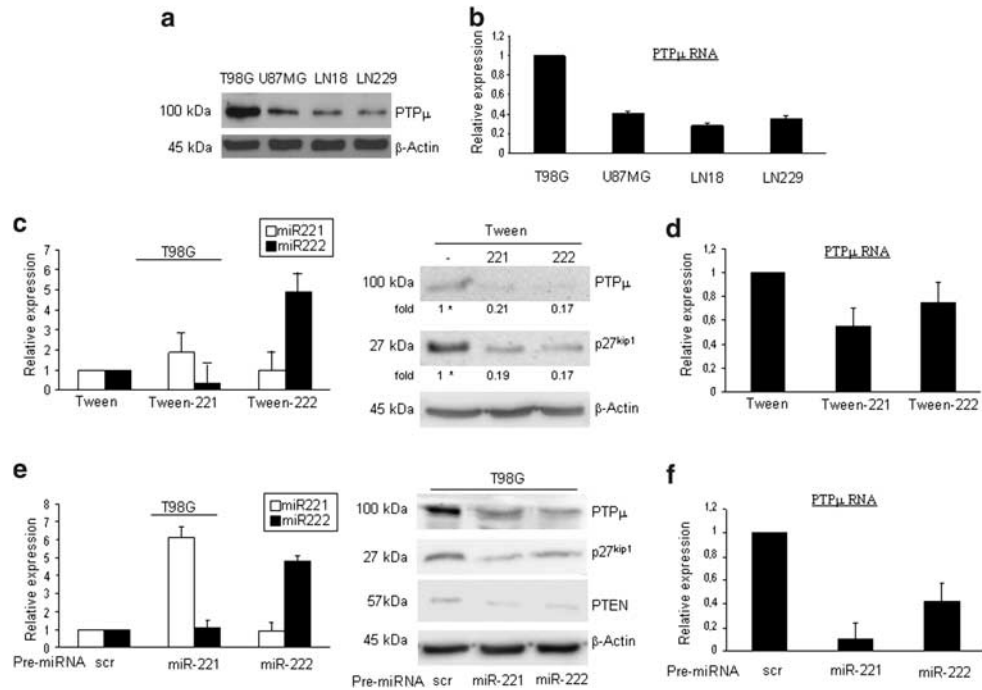


Figure 3 PTP μ and miR-222/221 expression levels are inversely correlated in glioma. PTP μ protein (a) and RNA (b) expression levels in T98G, U87MG LN18 and LN229 cells. Cell lysates were immunoblotted with anti-PTP μ antibody. To confirm equal loading, the membrane was immunoblotted with anti- β -Actin antibody. Effect of miR transfection on PTP μ expression: miR-222 and -221 constitutive (c) or transient (e) expression in glioma cells induced a decrease of PTP μ protein (c, e) and RNA (d, f) expression levels. Relative expressions of mRNA and miR-221 were calculated using the comparative threshold cycle methods. Columns, mean of four different experiments; bars, s.d.. Fold values are expressed relative to the reference points indicated by * symbol.

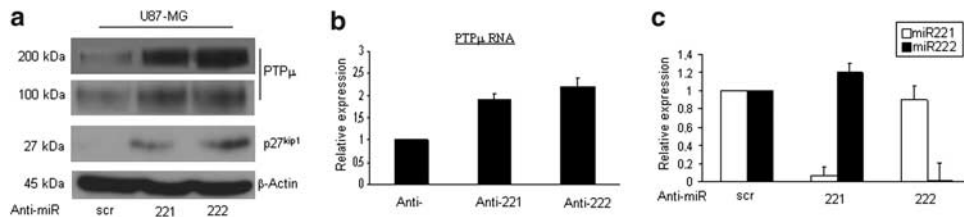


Figure 4 Effects of anti miR-222 and -221 on PTP μ expression levels in glioma. PTP μ protein (a) and RNA (b) expression levels in U87MG cells transfected with anti miR-222, -221 or control scrambled (scr). The anti-miRs were able to increase PTP μ expression levels. (c) Anti-miR transfection reduced miR levels as analyzed by real-time PCR. Columns, mean of four different experiments; bars, s.d.

To confirm these data, we extended our analysis to different tumorigenic and non-tumorigenic cell lines. As shown in Supplementary Figure 3B, LN-308 and LN-428 cells that express high levels of PTP μ protein express low level of miR-221 if compared with LN-319, LN-18 and LN-229 which overexpress miR-221 and have low levels of PTP μ . The only exception was represented by A172. These cells have been already reported to be non-tumorigenic (Ridder *et al.*, 1987; Liang *et al.*, 2002; Cerchia *et al.*, 2009). Our data show that in A172 cells PTP μ expression is low even in the presence of low miR-221 levels. However, A172 cells have been reported to be strongly invasive even if they are not tumorigenic (Ridder *et al.*, 1987). It is then possible that in this cell line other mechanisms are involved in the regulation of PTP μ expression and tumorigenic phenotype.

In order to establish a causative link with miRs-222 and -221 and PTP μ , we stably infected T98G cells with a Tween

lentiviral construct expressing miR-221 and -222, and then analyzed PTP μ protein and mRNA levels. miR expression in infected cells was evaluated by RT-PCR (Figure 3c). We observed decreased PTP μ protein (Figure 3c) and mRNA expression levels (Figure 3d) in miR-222 and -221 stably expressing cells. The same effect was observed in T98G cells transiently transfected with a synthetic pre-miR-222 and miR-221. We also observed a decrease of known miR-221/222 targets, the proteins PTEN and p27^{Kip1} (Figure 3e and f). The efficiency of miR expression upon transfection was monitored by RT-PCR (Figure 3e). Consistently with these data, U87-MG cells transfected with the anti-miR-222 and -221 showed an increase of PTP μ protein (Figure 4a) and RNA levels (Figure 4b). The efficiency of miR downregulation upon anti-miR transfection was monitored by RT-PCR (Figure 4c). Similar results were obtained by transfecting anti-miR-222 in LN-229 and LN-18 (data not shown).

miR-221 and -222 regulates cell motility in glioma cells

We hypothesized that miR-221 and -222 promote cell migration by regulating PTP μ expression. To this end, we analyzed cell motility through a transwell assay in U87MG, LN-229, LN-18 and T98G parental cells, and T98G transduced with control vector (T98G-tween), or lenti-miR221 and -222 vector (T98G miR-221 and T98G miR-222). As shown in Figure 5a, U87MG, LN-18 and LN-229 cells have a higher migration rate than T98G cells. The upregulation of miR-221 and -222 in T98G cells induced an increase of cell motility. The same result was obtained in T98G cells transiently transfected with miR-221 and -222. Conversely, expression of anti-miR-222 was able to reduce cell migration of U87MG (Figure 5b). We also tested the effects of miRs or anti-miR expression on cell adhesion, obtaining the same results (data not shown). In agreement with the existing data (Burgoyne *et al.*, 2009a), we demonstrate that

transfection of T98G cells with two different PTP short hairpin RNA interference (shRNAi) (#1, #2) induced a strong reduction of PTP expression levels (Supplementary Figure 2B) and at the same time an increase of cell motility (Figure 5c). The same effect was not observed in T98G transfected with p27^{kip1} and PTEN siRNAs (Supplementary Figure 4B). In addition, we also show that the overexpression of PTP μ complementary DNA in U87MG cells (Supplementary Figure 2A) induced a decrease of cell motility (Figure 5c). This result suggests that PTP μ protein is able to control cell motility in glioma cells. miRs may target different proteins. In order to demonstrate that migration/adhesion effects observed were carried out by PTP μ , we transfected T98G tween, tween-221 and tween-222 with ectopic PTP μ complementary DNA lacking the miRNA-binding site in its 3'UTR, before assaying migration and adhesion. Levels of transfected PTP μ were analyzed by

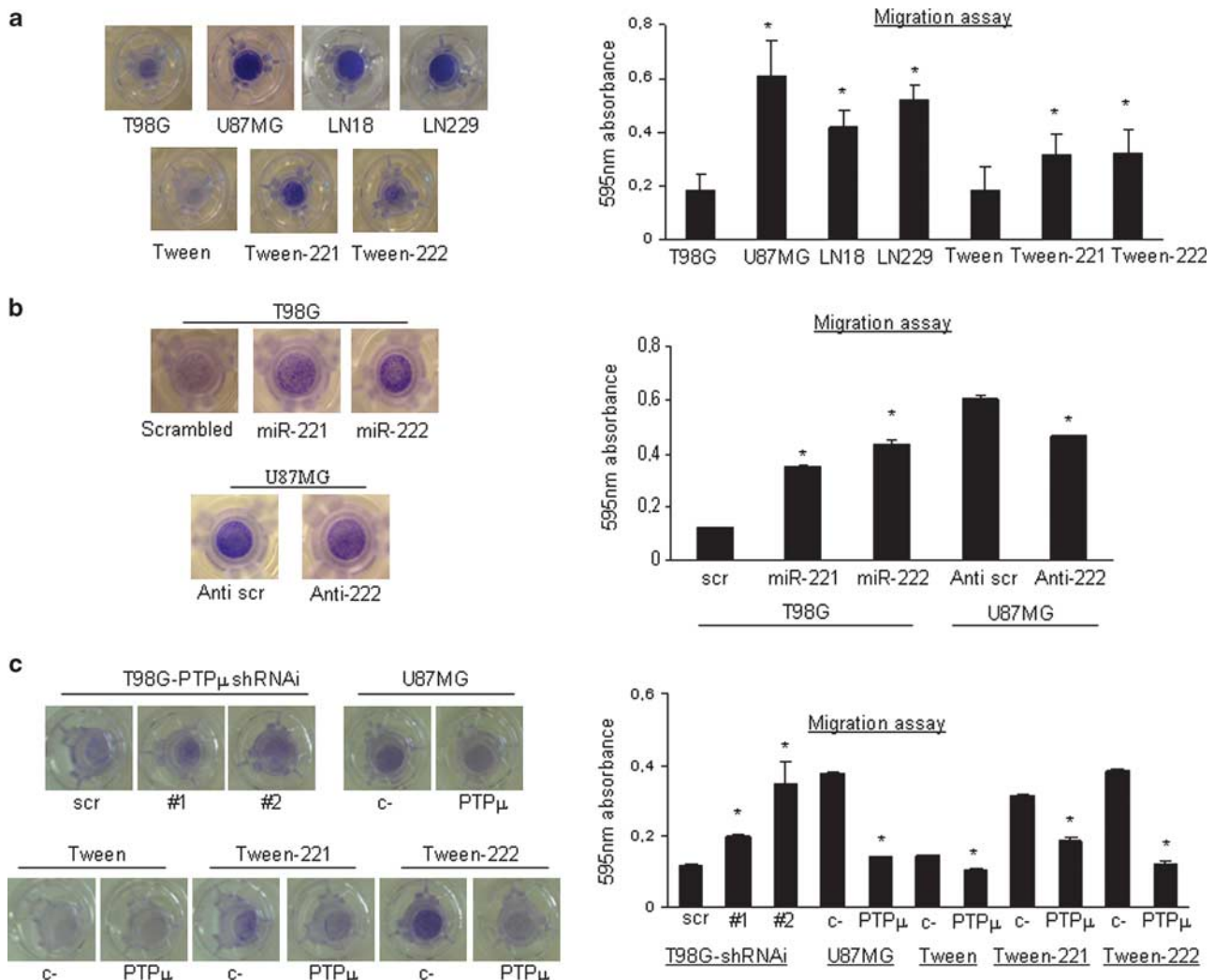


Figure 5 Effects of miR-222 and -221 on cell migration and adhesion. T98G glioma cells showed lower migration compared with U87MG, LN18 and LN229 cells (a), whereas T98G cells stably (a) or transiently (b) transfected with miR-222 and -221 exhibited increased migration levels. Transfection of PTP μ complementary DNA in miR-222 and -221 overexpressing cells was able to rescue the effect of both miRs on invasion (c), whereas T98G transfected with two different PTPshRNAi (#1, #2) exhibited higher migration compared with control scrambled small hairpin RNA (scr) (c). Each assay was performed three times in independent experiments (n = 3). Error bars indicate standard deviation. *P < 0.05

western blot (Supplementary Figure 2A). Interestingly, transfection of PTP μ in miR-221- and -222-overexpressing U87MG cells, was able to overcome the effects of both miRs (Figure 5c). These rescue experiments proved the causative connection between miR-222, PTP μ and glioma cell motility.

Effect of PTP μ expression on other miR-221/222 targets
As it has been recently described that miRs targeting multiple proteins may differently affect cellular behavior (Poliseno *et al.*, 2010), we investigated whether inhibiting the expression of one target may affect the expression of the others. Therefore, to exclude that the effects of PTP μ knockdown were mediated in a large part by changes in PTEN and p27^{Kip1} protein expression, we specifically silenced PTP μ and then evaluated expression levels of PTEN and p27^{Kip1}. As shown in supplementary Figure 2B, the knock down of PTP μ did not produce changes in expression of either PTEN or p27^{Kip1}. Moreover, silencing of PTEN or p27^{Kip1} in T98G did not produce any changes in PTP μ protein expression (Supplementary Figure 4A) or in tumorigenicity, as the number of colonies grown in soft agar were comparable to that observed in cells transfected with a control siRNA (Supplementary Figure 4C).

miR-222 and PTP μ mRNA levels in glioma

To evaluate whether PTP μ downregulation in GB was related to increased miR-222 and -221 levels also *in vivo*, we analyzed PTP μ protein and miR-222 and -221 expression levels in tumor tissue specimens collected from 18 glioblastoma grade IV patients. miR-221 and -222 increased expression was not observed in all patient analyzed. We divided samples in two groups: high-expressing miR-221 and -222, low-expressing PTP μ (A) (12/18, 67%) and low-expressing miR-221 and -222 and high-expressing PTP μ (B) (6/18, 33%). In both group we observed an inverse correlation between miR-221 and -222 with PTP μ (Figure 6).

To corroborate the inverse relation between miR-221/222 and PTP μ *in vivo*, *in situ* hybridization analysis was performed using 5'-digoxigenin-labeled locked nucleic acid probes on 66 glioma cancers (Table 2), followed by immunohistochemical detection of co-expression of PTP μ protein. As shown in Figure 7A, miR-222 was

abundantly expressed in high-grade glioma and rarely found in normal cells. No co-expression was found with PTP μ . Same result was obtained for miR-221 (data not shown). Importantly, it was evident that miR-221/222 was abundantly expressed in grade III and IV aggressive cases glioblastoma as shown by comparing grade IV GB with oligodendroglioma, a slowly growing glioma (Figure 7). Conversely, PTP μ was highly expressed in oligodendroglioma and normal brain compared with grade IV glioblastoma.

Discussion

GB are among the most deadly types of cancer (Tran and Rosenthal, 2010). Advances in standard treatments for this tumor, such as surgery, radiotherapy and chemotherapy, have not significantly increased patient survival (Huse and Holland, 2010). The lethality of GB can be attributed to the capacity of the cells to migrate and develop foci throughout the brain (Demuth and Berens, 2004). It is thought that the invasive behavior of glioblastoma cells is one of the most important causes of poor clinical outcome, enabling tumor cells to actively egress from the main mass and invade the surrounding normal brain where they are out of reach of surgical resection, radiation and chemotherapy (Giese *et al.*, 2003).

The mechanisms of the spreading phenotype are not well understood so far. It was recently demonstrated that the receptor PTP μ negatively regulates GB cell migration (Burgoyne *et al.*, 2009a). PTP μ is the prototype of the type IIb subfamily of receptor PTPs (RPTP). This phosphatase is able to sense an extracellular signal via its extracellular segment and to

Table 2 PTP μ and miR-222 staining on glioma tumors

	Grade I and II astrocytomas (N = 26)	Grade III and IV glioblastomas (N = 40)	Total gliomas (N = 66)
miR-222 + /PTP μ -	7 (27%)	13 (32%)	20 (31%)
miR-222 - /PTP μ +	3 (11%)	2 (6%)	5 (7%)

Abbreviations: PTP μ , protein tyrosine phosphatase μ . Results of miR-222 *in situ* hybridization and PTP μ immunohistochemistry on 66 gliomas (26 Grade I and II, 40 Grade III and IV). N, indicates the number of sample analyzed.

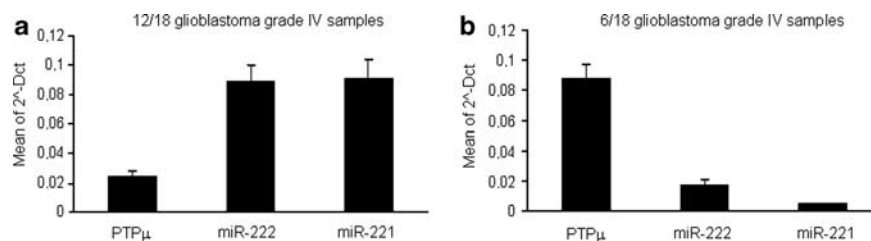


Figure 6 Correlation of endogenous miR-222 and PTP μ mRNA expression levels in human glioma. Total RNA extracted from tissue specimens collected from 18 GB individuals was used to analyze miR-222/221 and PTP μ mRNA expression by RT-PCR. We divided samples in two groups: high-expressing miR-221 and -222 and low-expressing PTP μ (a) (12/18, 67%) and low-expressing miR-221 and -222 and high-expressing PTP μ (b) (6/18, 33%). In each group we observed an inverse correlation between miR-221 and -222 with PTP μ was observed.

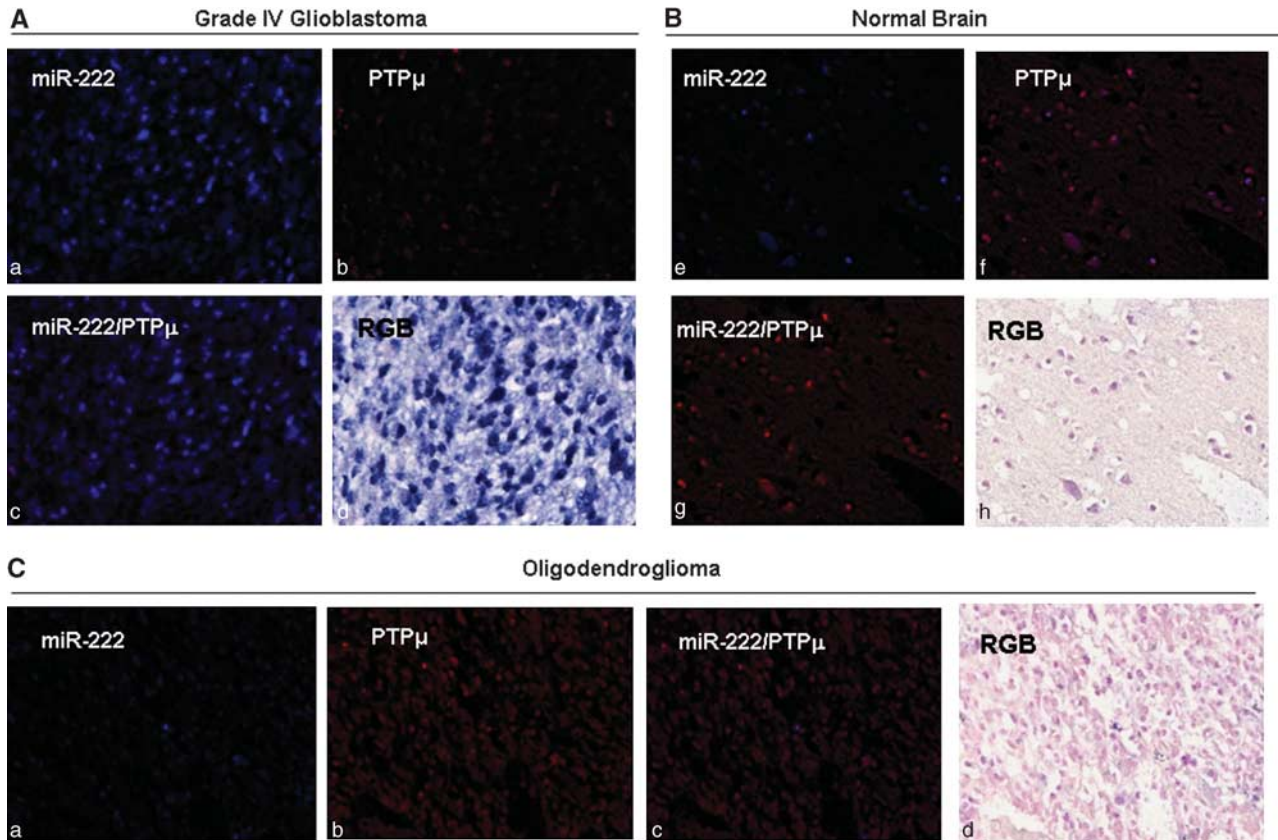


Figure 7 Correlation of the *in situ* co-detection miR-221 and PTP expression in benign and malignant brain tissue. (A) A total of 66 low- and high- grade glioma on a TMA were analyzed for miR-222 expression by *in situ* hybridization and then for PTP μ , respectively, by immunohistochemistry. Panel A shows miR-222 signal (fluorescent blue) and panel B shows the PTP μ signal (fluorescent red) in a grade IV glioblastoma. Panel C shows the mixed signal in which fluorescent yellow is indicative of miR-222 and protein co-expression; note the lack of miR-222 and PTP μ co-expression. Panel D shows the RGB image of the *in situ* hybridization/immunohistochemical reaction shown in panels b–d. (B) In the normal brain one sees the miR-222 signal (fluorescent blue) in panel e and the PTP μ image as fluorescent red (panel f). As described in the text, the majority of normal brain was negative for miR-222 (panel e) and positive for PTP μ (panel f). Panel g shows the mixed signal in which fluorescent yellow is indicative of miR and protein co-expression. Panel h shows the RGB image of the *in situ* hybridization/immunohistochemical reaction shown in panels e–g. (C) Finally, on four oligodendrogliomas, only 1/4 was miR-222+ and 4/4 were PTP μ positive. Panel a shows miR-222 signal (fluorescent blue) and panel b is the PTP μ signal (fluorescent red). Panel c shows the mixed signal in which fluorescent yellow is indicative of miR and protein co-expression; note the lack of miR-222 and PTP μ co-expression. Panel d shows the RGB image of the *in situ* hybridization/immunohistochemical reaction shown in panels b–d.

transduce this signal intracellularly via its phosphatase activity (Brady-Kalnay *et al.*, 1995). In a xenograft mouse model of intracranially injected U87MG cells, PTP μ small hairpin RNA was able to induce cell migration and dispersal (Burgoyne *et al.*, 2009a). PTP μ may be considered as a ‘migration suppressor’ with regard to the diffuse infiltrative growth pattern observed in human gliomas. It was previously shown that PTP μ protein is downregulated in glioblastoma and that its levels correlated to tumor stage (Burgoyne *et al.*, 2009b). In particular, a striking loss of PTP μ protein was observed in highly dispersive GB compared with less dispersive low-grade astrocytomas and normal brain (Burgoyne *et al.*, 2009a). It was recently demonstrated that one mechanism of PTP μ downregulation in GB is proteolytic breakdown (Burgoyne *et al.*, 2009b).

In this work, we identified a new molecular mechanism of PTP μ downregulation in human glioma, by identifying two related miRs that target this phosphatase.

In order to identify new signatures of GB invasiveness, we investigated the microRNA expression profile of tumorigenic glioma cells compared with non-tumorigenic cells. We identified five miR genes significantly overexpressed in tumorigenic cells with a >2.5-fold change. Among the different miRs we focused our attention on two highly related miRs, miR-221 and -222. MiR-222 and -221 expression levels in human cancer have been extensively investigated (Garofalo *et al.*, 2008, 2009) and have been frequently found overexpressed in a number of human tumors (Pallante *et al.*, 2006; Garofalo *et al.*, 2008, 2009, 2010; Conti *et al.*, 2009; Pineau *et al.*, 2010). In previous works we demonstrated that miR-221 and miR-222 regulate death receptor signaling and TRAIL apoptosis sensitivity in non-small cell lung cancer and in hepatocarcinoma by modulating p27kip1, PTEN and TIMP3 expression (Garofalo *et al.*, 2008, 2009). In GB tissues and cell lines miR-222 and -221 were found overexpressed

(Ciafrè *et al.*, 2005; Conti *et al.*, 2009) and correlated to the stage of the disease. However, the molecular targets of those miRs potentially involved in GB's invasive behavior had not been clarified. In this manuscript we provide evidence for the first time that miR-222 and -221 bind to the 3'UTR region of PTP μ and are able to downregulate PTP μ at RNA and protein levels. By luciferase assay, we also identified the 3'UTR region of the *PTP* gene that represents the miR-binding site.

As PTP μ has been described to be able to suppress glioma cell migration (Burgoyne *et al.*, 2009a), we hypothesized that miR-221 and -222 promote cell migration by downregulating PTP μ expression. In fact, the analysis of cell motility in T98G cells transduced with miR-221 or -222 demonstrated that upregulation of those miRs induced an increase of cell motility. The same result was obtained in T98G cells transiently transfected with either miR-221 or -222. Conversely the expression of anti-miR -222 was able to reduce cell migration. Comparable results were obtained when we analyzed cell adhesion phenotype of glioma cells. As miRNAs can affect many different proteins, we validated the migration/adhesion effects by co-transfection of miR-222 and ectopic PTP μ lacking the miRNA binding site in its 3'UTR. These rescue experiments proved the causative connection between miR-222/221 PTP μ and migration/invasion.

Moreover, our data show that in specimens of glioma, miR-222 and -221 expression inversely correlates with that of PTP μ . Therefore, miR-222 and -221 expression levels could predict the aggressive behavior of glioma. Over the past few years, several miRs have been implicated in various human cancers. Both losses and gains of miR function have been shown to contribute to cancer development through a range of mechanisms (Croce, 2009). Several miRs have been implicated in glioma formation, including miR-21, -7, -124a, -137, -221, -222, -34a, -125b, 146b and -181 family (Huse and Holland, 2010). Interestingly, in our model we found almost the same set of de-regulated miRs, indicating that they may be a molecular signature of glioblastoma cells.

Some of those miRs have been specifically described to be involved in the invasive glioma phenotype. In particular, inhibition of miR-21 reduces motility and invasiveness of glioma cells through the regulation of RECK, a membrane-anchored matrix metalloproteinase inhibitor important for extracellular matrix (ECM) remodeling (Gabriely *et al.*, 2008). Similarly, Xia *et al.*, 2009 described that miR-146b significantly reduced the migration and invasion of glioma cells by targeting one matrix metalloproteinase family member, matrix metalloproteinase16. miR-7, through targeting of EGFR and AKT activity, has also been implicated in GBM invasiveness (Kefas *et al.*, 2008). Our data provide evidence for the role of miR-222 and -221 in glioma cell migration/invasion through PTP regulation.

In conclusion, this study has identified a new mechanism of oncogenic action by miRs-222/-221 overexpression, leading to dissemination and invasion of GB

cells, causing a very aggressive behavior. Our results suggest that miR-221 and -222 regulate glioma tumorigenesis at least in part through the control of PTP μ protein expression.

Materials and methods

Cell culture and transfection

U87MG, T98G, LN-308, LN-319, A172 and LN-428 cells were grown in Dulbecco's modified Eagle's medium. LN-18 and LN-229 were grown in Advanced Dulbecco's modified Eagle's medium (Gibco, Invitrogen, Milan, Italy), Meg01 cells (human, chronic myelogenous leukemia cells) were grown in RPMI 1640 + 2 mM glutamine + 10% fetal bovine serum. Media were supplemented with 10% heat-inactivated fetal bovine serum, 2 mM L-glutamine and 100 U/ml penicillin/streptomycin. For miRs transient transfection, cells at 50% confluency were transfected using Oligofectamine (Invitrogen) with 100 nM (final) of pre-miR-221 and 222, scrambled or Anti miR-222 and Anti miR-221 (Applied Biosystems, Milan, Italy). For PTP μ transient transfection, cells were transfected using Lipofectamine and Plus Reagent with 5 μ g of PTP μ complementary DNA (Origene, Rockville, MD, USA) for 24 h. To knock-down *PTP μ* gene, specific small hairpin RNA were obtained by Open Biosystems (Huntsville, AL, USA) and were transfected using lipofectamine 2000. After 24 h the cells were treated for 24 h with 500 ng/ml of puromycin for selection of transfected cells. Two clones stably expressing small hairpin RNAi-PTP μ were obtained. To knock-down p27^{kip1} and PTEN, cells were transfected with p27^{kip1}- and PTEN-specific siRNAs from SantaCruz Biotechnology (Heidelberg, Germany) using lipofectamine 2000. TWEEN empty vector, TWEEN miR-221 or TWEEN miR-222 vectors, were obtained from Dr Ruggero De Maria (Rome).

Virus production

We produced vector stocks by calcium phosphate transient transfection, co-transfecting three plasmids in 293T human embryonic kidney cells, as these cells are good DNA recipients. The three plasmid are: the packaging plasmid, pCMVDR8.74 designed to provide the HIV proteins needed to produce the virus particle; the envelope-coding 57 plasmid, pMD.G, for pseudotyping the virion with VSV-G and TWEEN miR-221 or miR-222 vector, the transgene coding plasmids. The calcium phosphate-DNA precipitate was allowed to stay on the cells for 14–16 h, after which the medium was replaced, collected 48 h later, centrifuged at 1000 r.p.m. for 5 min at room temperature and filtered through 0.22 mm pore nitrocellulose filters. On the day of infection, the medium was removed and replaced with viral supernatant to which 4 mg/ml of polybrene had been added. Cells were then centrifuged in their plate for 45 min in a Beckman GS-6KR centrifuge (Beckman, Milan, Italy), at 1800 r.p.m. and 32 °C. After centrifugation, cells were kept for either 1 h 15 min or ON in a 5% CO₂ incubator at 32 or 37 °C, respectively. After exposure, cells were washed twice with cold phosphate-buffered saline and fresh medium added. At either 12 or 48 h after the infection, cells were washed with phosphate-buffered saline, harvested with trypsin/EDTA and analyzed by FACS for GFP expression. The GFP positive were sorted by a FACSScan.

Soft agar assay

In all, 10³ cells were plated in 60 mm dishes in a solution containing Dulbecco's modified Eagle's medium 2 \times (Sigma,

St Louis, MO, USA), TPB Buffer (Difco, BD, Franklin Lakes, NJ, USA), and 1.25% of Noble Agar (Difco). Briefly, cells were harvested and counted then a layer of 7 ml with the solution containing Noble Agar were left to polymerize on the bottom of the dishes. Then cells were resuspended in 2 ml of same solution and plated. Cells were left grown for 2 weeks in the incubator.

Injection of glioma cells in nude mice

Nude mice were provided by Charles River. A total of 10^5 cells of T98G, LN-18, LN-229 and U87MG were subcutaneously injected in one flank of the mice. Five mice for each cell type were injected. Mice were followed for 4 weeks and the tumors were measured and photographed.

Protein isolation and western blotting

Cells were washed twice in ice-cold phosphate-buffered saline, and lysed in JS buffer (50 mM HEPES pH 7.5 containing 150 mM NaCl, 1% glycerol, 1% Triton \times 100, 1.5 mM MgCl₂, 5 mM EGTA, 1 mM Na₃VO₄, and 1 \times protease inhibitor cocktail). Protein concentration was determined by the Bradford assay (BioRad, Milan, Italy) using bovine serum albumin as the standard, and equal amounts of proteins were analyzed by SDS-polyacrylamide gel electrophoresis (12.5% acrylamide). Gels were electroblotted onto nitrocellulose membranes (Millipore, Bedford, MA, USA). For immunoblot experiments, membranes were blocked for 1 h with 5% non-fat dry milk in tris buffered saline containing 0.1% Tween-20, and incubated at 4 °C over night with primary antibody. Detection was performed by peroxidase-conjugated secondary antibodies using the enhanced chemiluminescence system (Amersham-Pharmacia Biosciences, GE Healthcare, Milan, Italy). Primary antibodies used were: anti-PTP μ (SantaCruz), anti- β Actin (Sigma), P-Ser-AKT (Promega, Milan, Italy) and anti-p27, -AKT, -PTEN (Cell Signaling, Danvers, MA, USA).

miRNA microarray experiments

In all, 5 μ g of total RNA from each sample was reverse transcribed using biotin-end-labeled random-octamer oligonucleotide primer. Hybridization of biotin-labeled complementary DNA was performed on a new Ohio State University custom miRNA microarray chip (OSU_CCC version 3.0, NCBI accession GPL5106), which contains 1150 miRNA probes, including 326 human and 249 mouse *miRNA* genes, spotted in duplicates. The hybridized chips were washed and processed to detect biotin-containing transcripts by streptavidin-Alexa647 conjugate and scanned on an Axon 4000B microarray scanner (Axon Instruments, Sunnyvale, CA, USA).

Raw data were normalized and analyzed with GENESPRING 7.2 software (zcomSilicon Genetics, Redwood City, CA, USA). Expression data were median-centered by using both the GENESPRING normalization option and the global median normalization of the BIOCONDUCTOR package (<http://www.bioconductor.org>) with similar results. Statistical comparisons were done by using the GENESPRING analysis of variance tool, predictive analysis of microarray (PAM) and the significance analysis of microarray (SAM) software (<http://www-stat.stanford.edu/~tibs/SAM/index.html>).

Glioma cancer samples

A total of 18 paraffined high-grade glioma samples were collected at the Federico II University of Naples, Italy and tumor bank Unit of the Spanish National Cancer Research (CNIO) Madrid, Spain. RNA was isolated with RecoverALL

Total Nucleic Acid Isolation kit from Ambion (Ambion Inc., Austin TX, USA). The samples were stored at -80 °C.

RNA extraction and RT-PCR

Total RNAs (miRNA and mRNA) were extracted using Trizol (Invitrogen) according to the manufacturer's protocol. Reverse transcription of total miRNA was performed starting from equal amounts of total RNA/sample (1 μ g) using miScript reverse Transcription Kit (Qiagen, Milan, Italy), for mRNA was used SuperScript III Reverse Transcriptase (Invitrogen). For cultured cells, quantitative analysis of PTP μ , β -Actin (as an internal reference), miR-221/222 and RNU5A (as an internal reference) were performed by RT-PCR using specific primers (Qiagen), miScript SYBR Green PCR Kit (Qiagen) and iQ SYBR Green Supermix (BioRad), respectively. The reaction for detection of mRNAs was performed as follow: 95 °C for 15', 40 cycles of 94 °C for 15", 60 °C for 30" and 72 °C for 30". The reaction for detection of miRNAs was performed as follow: 95 °C for 15', 40 cycles of 94 °C for 15", 55 °C for 30" and 70 °C for 30". All reactions were run in triplicate. The threshold cycle is defined as the fractional cycle number at which the fluorescence passes the fixed threshold. For relative quantization the $2^{(-\Delta\Delta CT)}$ method was used as previously described (Livak and Schmittgen, 2001). Experiments were carried out in triplicate for each data point, and data analysis was performed by using software (BioRad).

Luciferase assay

The 3' UTR of the human *PTP μ* gene was PCR amplified using the following primers: PTP μ Fw: 5'-TCTAGACGAGGTGGC CCTGGAATACTTGAATTCT-3' and PTP μ Rw 5'-TCTAG AGCATTTTGTGAATGAGTCCTCCCCCAA-3', and cloned downstream of the Renilla luciferase stop codon in pGL3 control vector (Promega). This construct was used to generate, by inverse PCR, the UTRmut-PTP μ plasmid (primers: PTP μ -mut: Fw 5'-GCATAATATATGCTTGCTTTCCAGGACTA ACAGATAAATGTG-3'; Rw 5'-CACATTTATCTGTTAGT CCTGGAAAGCAAGCATATATTATGC-3'. MeG01 cells were co-transfected with 1 μ g of UTR- PTP μ plasmid and with UTRmut- PTP μ plasmid and 1 μ g of a Renilla luciferase expression construct pRL-TK (Promega) with Lipofectamine 2000 (Invitrogen). Cells were harvested 24 h post-transfection and assayed with Dual Luciferase Assay (Promega) according to the manufacturer's instructions. We used MEG01 cell lines as they express low levels of miR-221 and -222 and also because they are easily transfectable (Incoronato et al., 2010). Three independent experiments were performed in triplicate.

MiRNA locked nucleic acid in situ hybridization of formalin-fixed, paraffin-embedded tissue section

In situ hybridization was carried out on deparaffinized human glioma tissues sections using previously published protocol (Nuovo et al., 2009), which includes a digestion in pepsin (1.3 mg/ml) for 30 min. The sequences of the probes containing the six dispersed locked nucleic acid locked nucleic acid-modified bases with digoxigenin conjugated to the 5' end were: miR-221(5') GAAACCCAGCAGACAATGTAGCT; miR-222(5') ACCC AGTAGCCAGATGTAGCT. The probe cocktail and tissue miRNA were co-denatured at 60 °C for 5 min, followed by hybridization at 37 °C overnight and a low-stringency wash in 0.2 \times SSC and 2% bovine serum albumin at 4 °C for 10 min. The probe-target complex was seen due to the action of alkaline phosphatase on the chromogen nitroblue tetrazolium and bromochloroindolyl phosphate (NBT/BCIP). Negative controls included the use of a probe, which should yield a negative result in such tissues. No counterstain was used, to facilitate co-labelling for

PTP μ protein. After *in situ* hybridization for the miRNAs, as previously described (Nuovo *et al.*, 2009; Inconato *et al.*, 2010), the slides were immunostained to identify PTP μ protein expression. The anti-PTP μ antibody (Santacruz) was incubated at 1:200 for 30 min. For the immunodetection, we used the Ultrasensitive Universal Fast Red system from Ventana Medical Systems. We used low-grade glioma tissues known to express PTP μ (Burgoyne *et al.*, 2009a) as positive control of PTP protein expression. The percentage of tumor cells expressing PTP μ and miR-221&222 was then analyzed with emphasis on co-localization of the respective targets.

Migration assay

Transwells Permeable Supports, 6.5 mm diameter inserts, 8.0 μ m pore size, polycarbonate membrane (Corning Incorporate, Corning, NY, USA) were used to perform migration assay. T98G and U87MG cells were grown as indicated above, then harvested by TrypLE Express (Invitrogen, Carlsbad, CA, USA), and 10^5 cells were washed three times and then resuspended in 1% fetal bovine serum containing Dulbecco's modified Eagle's medium medium and seeded in the upper chamber. The lower chamber of the transwell was filled with 600 μ l of culture medium containing 10% fetal bovine serum, 5 μ g/ml fibronectin, as an adhesive substrate. Cells were incubated at 37 °C for 24 h. The transwells were then removed from the 24-well plates and stained with 0.1% Crystal Violet in 25% methanol. Non-migrated cells

were scraped off the top of the transwell with a cotton swab. Percentage of migrated cells was evaluated by eluting crystal violet with 1% SDS and reading the absorbance at λ 570 nm.

Statistical analysis

Continuous variables are expressed as mean values \pm s.d. One-tailed Student's *t*-test was used to compare values of test and control samples. $P < 0.05$ was considered significant. Fold increase of the bands was calculated using ImageJ program available on web.

Conflict of interest

The authors declare no conflict of interest.

Acknowledgements

This work was partially supported by funds from Associazione Italiana Ricerca sul Cancro, AIRC to GC (Grant n.ro 10620) and MERIT (RBNE08E8CZ_002) to GC. CQ is supported by a Federazione Italiana Ricerca sul Cancro (FIRC) Post-Doctoral Research Fellowship. CZ is supported by an American-Italian Cancer Foundation Post-Doctoral Research Fellowship.

References

- Brady-Kalnay SM, Rimm DL, Tonks NK. (1995). Receptor protein tyrosine phosphatase PTP μ associates with cadherins and catenins *in vivo*. *J Cell Biol* **130**: 977–986.
- Burgoyne AM, Palomo JM, Phillips-Mason PJ, Burden-Gulley SM, Major DL, Zaremba A *et al.* (2009a). PTP μ suppresses glioma cell migration and dispersal. *Neuro Oncol* **11**: 767–778.
- Burgoyne AM, Phillips-Mason PJ, Burden-Gulley SM, Robinson S, Sloan AE, Miller RH *et al.* (2009b). Proteolytic cleavage of protein tyrosine phosphatase μ regulates glioblastoma cell migration. *Cancer Res* **69**: 6960–6968.
- Calin GA, Croce CM. (2006). MicroRNA signatures in human cancers. *Nat Rev Cancer* **6**: 857–866.
- Cerchia L, Esposito CL, Jacobs AH, Tavittian B, de Francisic V. (2009). Differential SELEX in human glioma cell lines. *PLoS ONE* **4**: e7971.
- Ciafrè SA, Galardi S, Mangiola A, Ferracin M, Liu CG, Sabatino G *et al.* (2005). Extensive modulation of a set of microRNAs in primary glioblastoma. *Biochem Biophys Res Commun* **334**: 1351–1358.
- Conti A, Aguenouz M, La Torre D, Tomasello C, Cardali S, Angileri FF *et al.* (2009). miR-21 and 221 upregulation and miR-181b downregulation in human grade II-IV astrocytic tumors. *J Neurooncol* **93**: 325–332.
- Croce CM. (2009). Causes and consequences of microRNA dysregulation in cancer. *Nat Rev Genet* **10**: 704–714.
- Demuth T, Berens ME. (2004). Molecular mechanisms of glioma cell migration and invasion. *J Neurooncol* **70**: 217–228.
- Gabriely G, Wurdinger T, Kesari S, Esau CC, Burchard J, Linsley PS *et al.* (2008). MicroRNA 21 promotes glioma invasion by targeting matrix metalloproteinase regulators. *Mol Cell Biol* **28**: 5369–5380.
- Garofalo M, Condorelli GL, Croce CM, Condorelli G. (2010). MicroRNAs as regulators of death receptors signaling. *Cell Death Differ* **2010**: 2.
- Garofalo M, Di Leva G, Romano G, Nuovo G, Suh SS, Ngankou A *et al.* (2009). miR-221&222 regulate TRAIL resistance and enhance tumorigenicity through PTEN and TIMP3 downregulation. *Cancer Cell* **16**: 498–509.
- Garofalo M, Quintavalle C, Di Leva G, Zanca C, Romano G, Taccioli C *et al.* (2008). MicroRNA signatures of TRAIL resistance in human non-small cell lung cancer. *Oncogene* **27**: 3845–3855.
- Giese A, Bjerkvig R, Berens ME, Westphal M. (2003). Cost of migration: invasion of malignant gliomas and implications for treatment. *J Clin Oncol* **21**: 1624–1636.
- Huse JT, Holland EC. (2010). Targeting brain cancer: advances in the molecular pathology of malignant glioma and medulloblastoma. *Nat Rev Cancer* **10**: 319–331.
- Inconato M, Garofalo M, Urso L, Romano G, Quintavalle C, Zanca C *et al.* (2010). miR-212 increases tumor necrosis factor-related apoptosis-inducing ligand sensitivity in non-small cell lung cancer by targeting the antiapoptotic protein PED. *Cancer Res* **70**: 3638–3646.
- Kefas B, Godlewski J, Comeau L, Li Y, Abounader R, Hawkinson M *et al.* (2008). microRNA-7 inhibits the epidermal growth factor receptor and the Akt pathway and is down-regulated in glioblastoma. *Cancer Res* **68**: 3566–3572.
- Liang Y, Li X-Y, Rebar EJ, Li P, Zhou Y, Chen B *et al.* (2002). Activation of vascular endothelial growth factor A transcription in tumorigenic glioblastoma cell lines by an enhancer with cell type-specific DNase I accessibility. *J Biol Chem* **vol277**: pp. 20087–20094.
- Liu CG, Calin GA, Meloon B, Gamliel N, Sevignani C, Ferracin M *et al.* (2004). An oligonucleotide microchip for genome-wide microRNA profiling in human and mouse tissues. *Proc Natl Acad Sci USA* **101**: 9740–9744.
- Livak KJ, Schmittgen TD. (2001). Analysis of relative gene expression data using real-time quantitative PCR and the 2(-Delta Delta C(T)) Method. *Methods* **25**: 402–408.
- Nuovo G, Lee EJ, Lawler S, Godlewski J, Schmittgen T. (2009). In situ detection of mature microRNAs by labeled extension on ultramer templates. *Biotechniques* **46**: 115–126.
- Pallante P, Visone R, Ferracin M, Ferraro A, Berlingieri MT, Troncone G *et al.* (2006). MicroRNA deregulation in human thyroid papillary carcinomas. *Endocr Relat Cancer* **13**: 497–508.
- Pineau P, Volinia S, McJunkin K, Marchio A, Battiston C, Terris B *et al.* (2010). miR-221 overexpression contributes

- to liver tumorigenesis. *Proc Natl Acad Sci USA* **107**: 264–269.
- Poliseno L, Salmena L, Zhang J, Carver B, Haveman WJ, Pandolfi PP. (2010). A coding-independent function of gene and pseudogene mRNAs regulates tumour biology. *Nature* **465**: 1033–1038.
- Purow B, Schiff D. (2009). Advances in the genetics of glioblastoma: are we reaching critical mass? *Nat Rev Neurol* **5**: 419–426.
- Ridder LI, Laerum OD, Mørk SJ, Bigner DD. (1987). Invasiveness of human glioma cell lines in vitro: relation to tumorigenicity in athymic mice. *Acta Neuropathologica* **72**: 207–213.
- Sredni ST, Bonaldo Mde F, Costa FF, Huang CC, Hamm CA, Rajaram V *et al*. (2010). Upregulation of mir-221 and mir-222 in atypical teratoid/rhabdoid tumors: potential therapeutic targets. *Childs Nerv Syst* **26**: 279–283.
- Tran B, Rosenthal MA. (2010). Survival comparison between glioblastoma multiforme and other incurable cancers. *J Clin Neurosci* **17**: 417–421.
- Xia H, Qi Y, Ng SS, Chen X, Li D, Chen S *et al*. (2009). microRNA-146b inhibits glioma cell migration and invasion by targeting MMPs. *Brain Res* **1269**: 158–165.

Supplementary Information accompanies the paper on the Oncogene website (<http://www.nature.com/onc>)

ORIGINAL ARTICLE

Effect of miR-21 and miR-30b/c on TRAIL-induced apoptosis in glioma cells

C Quintavalle^{1,2,7}, E Donnarumma^{3,7}, M Iaboni^{1,2}, G Roscigno^{1,2}, M Garofalo⁴, G Romano³, D Fiore¹, P De Marinis⁵, CM Croce⁴ and G Condorelli^{1,2,6}

Glioblastoma is the most frequent brain tumor in adults and is the most lethal form of human cancer. Despite the improvements in treatments, survival of patients remains poor. To define novel pathways that regulate susceptibility to tumor necrosis factor-related apoptosis-inducing ligand (TRAIL) in glioma, we have performed genome-wide expression profiling of microRNAs (miRs). We show that in TRAIL-resistant glioma cells, levels of different miRs are increased, and in particular, miR-30b/c and -21. We demonstrate that these miRs impair TRAIL-dependent apoptosis by inhibiting the expression of key functional proteins. T98G-sensitive cells treated with miR-21 or -30b/c become resistant to TRAIL. Furthermore, we demonstrate that miR-30b/c and miR-21 target respectively the 3' untranslated region of caspase-3 and TAp63 mRNAs, and that those proteins mediate some of the effects of miR-30 and -21 on TRAIL resistance, even in human glioblastoma primary cells and in lung cancer cells. In conclusion, we show that high expression levels of miR-21 and -30b/c are needed to maintain the TRAIL-resistant phenotype, thus making these miRs as promising therapeutic targets for TRAIL resistance in glioma.

Oncogene advance online publication, 10 September 2012; doi:10.1038/onc.2012.410

Keywords: glioblastoma; TRAIL; therapy; microRNA; treatment; apoptosis

INTRODUCTION

Glioblastomas are the most common primary tumors of the brain and are divided into four clinical grades on the basis of their histology and prognosis.¹ These tumors are highly invasive, very aggressive and are one of the most incurable forms of cancer in humans.² The treatment strategies for this disease have not changed appreciably for many years, and failure of treatment occurs in the majority of patients owing to the strong resistant phenotype. Therefore, the development of new therapeutic strategies is necessary for this type of cancer.

A novel interesting therapeutic approach is the reactivation of apoptosis using member of TNF (tumor necrosis factor)-family, of which the tumor necrosis factor-related apoptosis-inducing ligand (TRAIL) holds the greatest interest. Apoptosis is a particularly desirable treatment outcome, as it eradicates cancer cells without causing a major inflammatory response, which could provide unwanted survival signals. However, many cancers develop functional defects in the drug-induced apoptosis pathway, which may lead to constitutive or acquired resistance. To this end, alternative pathways, such as the one activated by death receptors including Fas/Apo-1, or DR4 (TRAIL-R1) and DR5 (TRAIL-R2), are being explored for cancer treatment. TRAIL is a relatively new member of the TNF family, known to induce apoptosis in a variety of cancers.³ Treatment with TRAIL induces programmed cell death in a wide range of transformed cells, both *in vivo* and *in vitro*, without producing significant effects in normal cells.^{3,4} Therefore, recombinant TRAIL or monoclonal antibodies against its receptors (TRAIL-R1 and TRAIL-R2) are in phase II/III

clinical trials for different kinds of tumors, either as a single agent or in combination with chemotherapy.^{5,6}

However, a significant proportion of human cancer cells are resistant to TRAIL-induced apoptosis, and the mechanisms of sensitization seem to differ among cell types. Different studies relate resistance to TRAIL-induced cell death to downstream factors. It has been shown that downregulation of two anti-apoptotic proteins such as PED (Phosphoprotein enriched in diabetes) or cellular-FLICE such as inhibitory protein (c-FLIP) can sensitize cells to TRAIL-induced apoptosis.^{7–9} However the mechanism of TRAIL resistance is still largely unknown.

miRs are a class of endogenous non-coding RNA of 19–24 nucleotides in length that has an important role in the negative regulation of gene expression blocking translation or directly cleaving the targeted mRNA.¹⁰ miRs are involved in the pathogenesis of most cancers.¹⁰ In the last few years, our understanding of the role of miRNA has expanded from the initially identified functions in the development of round worms to a highly expressed and ubiquitous regulators implicated in a wide array of critical processes, including proliferation, cell death and differentiation, metabolism and, importantly, tumorigenesis.¹¹ We have recently showed an important role of microRNAs in TRAIL sensitivity in non-small cell lung cancer (NSCLC).^{12–14}

In this study, to identify novel mechanisms implicated in TRAIL resistance in human glioma, we performed a genome-wide expression profiling of miRs in different cell lines. We found that miR-30b/c and -21 are markedly upregulated in TRAIL-resistant, and downregulated in TRAIL-sensitive glioma cells.

¹Department of Cellular and Molecular Biology and Pathology, 'Federico II' University of Naples, Naples, Italy; ²IEOS, CNR, Naples, Italy; ³Fondazione IRCCS SDN, Naples, Italy; ⁴Department of Molecular Virology, Immunology and Medical Genetics, Human Cancer Genetics Program, Comprehensive Cancer Center, The Ohio State University, Columbus, OH, USA; ⁵Neurosurgery Unit, Ospedale A. Cardarelli, Napoli, Italy and ⁶Facoltà di Scienze Biotechnologiche, 'Federico II' University of Naples, Naples, Italy. Correspondence: Professor G Condorelli, Department of Cellular and Molecular Biology and Pathology, 'Federico II' University of Naples, Via Pansini, 5, Ed 19 A, II floor, Naples 80131, Italy. E-mail: gecondor@unina.it

⁷These authors contributed equally to this work.

Received 28 February 2012; revised 13 June 2012; accepted 23 July 2012

Our experiments indicate that miR-30b/c and -21 modulate TRAIL sensitivity in glioma cells mainly by modulating caspase-3 and *TAp63* expression and TRAIL-induced caspase machinery.

RESULTS

Selection of TRAIL-sensitive vs TRAIL-resistant glioma cell lines

We analyzed TRAIL sensitivity of different human glioma cell lines. Cells were exposed to TRAIL at two different concentrations for 24 h and cell death was assessed using the MTT assay (Figure 1a) or propidium iodide staining (Figure 1b). As shown in Figure 1, we can distinguish two sets of cells: TB10, LN229, U251 and U87MG cells exhibited total or partial TRAIL resistance, whereas T98G and LN18 cells underwent TRAIL-induced cell death.

miRs expression screening in TRAIL-resistant vs TRAIL-sensitive glioma cell lines

To investigate the involvement of miRs in TRAIL resistance in glioblastoma cell lines, we analyzed the miRs expression profile in the most TRAIL-resistant glioma cells (TB10 and LN229) vs the TRAIL-sensitive cells (T98G and LN18). The analysis was performed with a microarray chip containing 1150 miR probes, including 326 human and 249 mouse miRs, spotted in duplicates. Data obtained indicated that seven miRs (miR-21, -30b, -30c, -181a, -181d, -146 and -125b) were significantly overexpressed in resistant glioma cells with at least > 1.9-fold change (Table 1). Quantitative real-time-polymerase chain reaction (qRT-PCR) validated the microarray analysis (data not shown).

Role of miRs in TRAIL resistance in glioma

To test the role of these overexpressed miRs in TRAIL sensitivity in glioma, we transfected T98G TRAIL-sensitive cells with miR-21, -30b, -30c, -181a, -146 and -125b. TRAIL sensitivity was evaluated by MTT assay, propidium iodide staining and colony assay. We obtained significant results only for miR-30b/c and miR-21 that

were then extensively investigated. In fact, data obtained with MTT assay and FACS analysis showed that the overexpression of miR-30b/c and -21 was able to revert TRAIL sensitivity in T98G (Figures 2a and b). Similar results were obtained in LN18 cells (Figures 2c and d). This effect was not restricted to glioma, as miR-30 and miR-21 were able to exert an anti-apoptotic action also in non small cell lung cancer (NSCLC) (Supplementary Figure 3B). We further evaluated TRAIL sensitivity by colony assay. T98G and LN18 cells were transfected with miR-scrambled, miR-30b/c and miR-21 for 48 h and then were treated with 50 or 100 ng/ml of superKiller TRAIL for 24 h. Cells were grown for 6 days and then coloured with crystal violet-methanol solution (Supplementary Figures 1A and B). The results indicated that both miRs induced an increase of TRAIL resistance.

To further explore the role of miR-21 and -30b/c on TRAIL sensitivity, we transfected U251 (Figure 3a) or LN229 (Figure 3b) TRAIL-resistant cells with anti-miR-21, -30b, 30c, or with a scrambled sequence. As shown in Figures 3a and b, transfection of the anti-miR sequences was able to sensitize U251 and LN229 cells to TRAIL. Anti-miR-21 and -30c were also able to sensitize to TRAIL the CALU-1-resistant non-small cell lung cancer (NSCLC) TRAIL-resistant cell lines (Supplementary Figure 3C), indicating that this effect was not restricted to glioma.

Identification of cellular targets of miR-30b/c and miR-21 in glioma cells

To identify cellular targets of miR-30b/c and -21, we used as first attempt a bioinformatic search, using programs available on the web including Pictar, TargetScan, miRanda and Microcosm target.

miR-21 targets different tumor suppressor genes and proteins potentially involved in TRAIL resistance in glioblastoma cells, such as PTEN (phosphatase and tensin homologue), PDCD4 (programmed cell death 4), TPM1 (Tropomyosin 1) and p53.^{15–17} Computer-assisted analysis identified the presence of evolutionary-conserved binding sites for miR-21 in *TAp63* gene. We focused our attention on this p53 family member, as it regulates the expression of TRAIL receptors and molecules involved in TRAIL signaling.¹⁸ We also searched for miR-30 targets and among them we focused on caspase-3.

TRAIL-resistant and TRAIL-sensitive glioma or NSCLC cells exhibited different levels of miR-21 and -30c assessed by either qRT-PCR (Figure 4a and Supplementary Figure 3A) or by northern blot analysis (Supplementary Figure 4). Interestingly, we observed a reduction of protein (Figure 4b and Supplementary Figure 3D) and mRNA (Figure 4c) levels of *TAp63* and caspase-3 upon, respectively, miR-21 or miR-30c and miR-30b (data not shown) transfection in TRAIL-sensitive cell lines. We didn't observe a

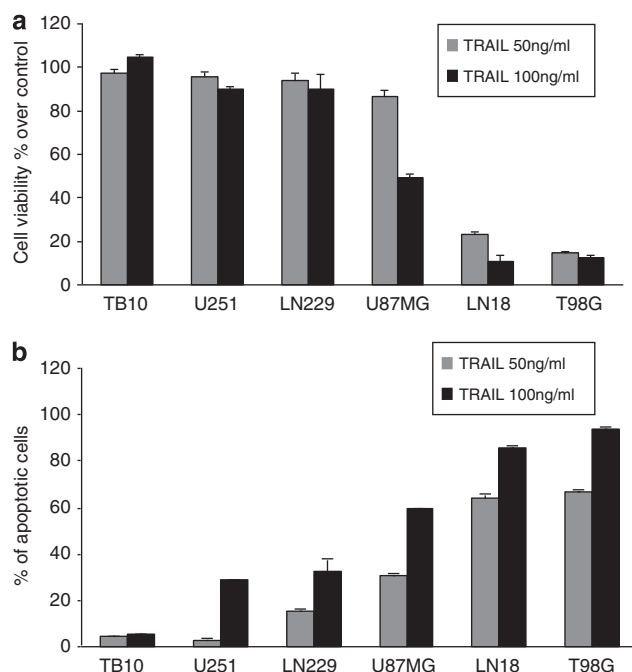


Figure 1. TRAIL sensitivity of glioblastoma cells. Glioblastoma cell lines (10^4 cell) were treated with superKiller TRAIL. After 24 h of treatment, the effect on cell death was assessed with MTT assay (a) or by propidium iodide staining and FACS analysis (b).

Table 1. microRNA identified in TRAIL-resistant glioma (LN229 and TB10) compared with TRAIL-sensitive (T98G, LN18) cells

miR	P-value	Fold difference
hsa-miR-125b1-A	6.09e – 05	3.033
hsa-miR-30b-A	9.14e – 05	2.041
hsa-miR-30c-A	0.0001199	2.337
hsa-miR-146b-A	0.0001556	5.972
hsa-miR-181a-5p-A	0.0004698	2.66
hsa-miR-181d-A	0.0004817	3.035
hsa-miR-21-A	0.0032482	1.949

miRNA expression profiles in TRAIL-sensitive vs TRAIL-resistant cells. miRNA screening was performed in triplicate for TRAIL-sensitive and TRAIL-resistant cell lines by a microarray as described in Materials and methods. A two-tailed, two-sample *t*-test was used ($P < 0.05$). Seven miRNAs were found to be significantly deregulated in TRAIL-resistant cells compared with the TRAIL sensitive.

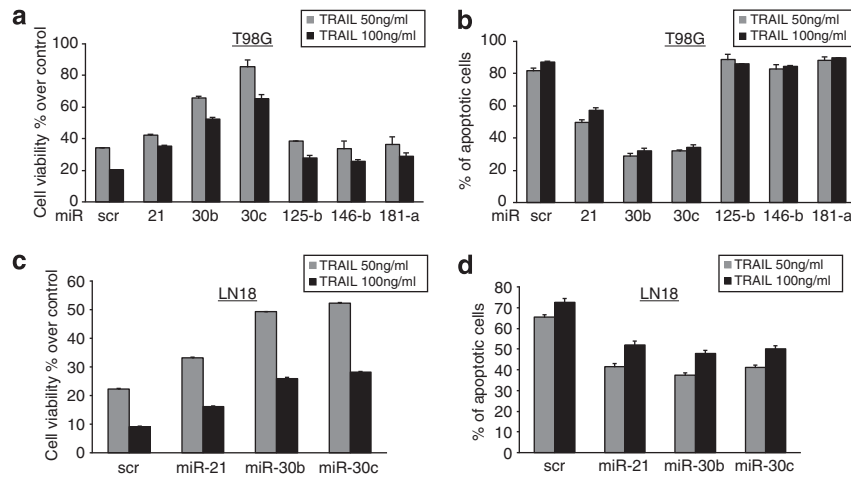


Figure 2. Effect of miR-21 and miR-30c overexpression on TRAIL-sensitive glioblastoma cells. T98G (**a, b**) cells were transfected with miR-21, miR-30b, miR-30c, miR-125b, miR-146b and miR-181a. LN18 (**c, d**) were transfected with miR-21, miR-30b and miR-30c. 10^4 cells were then treated with two different concentrations of superkiller TRAIL. After 24 h of treatment, cell viability was assessed with MTT assay (**a, c**) or with propidium iodide staining and FACS analysis (**b, d**). Both miR-21 and miR-30 induce TRAIL resistance in glioma cells.

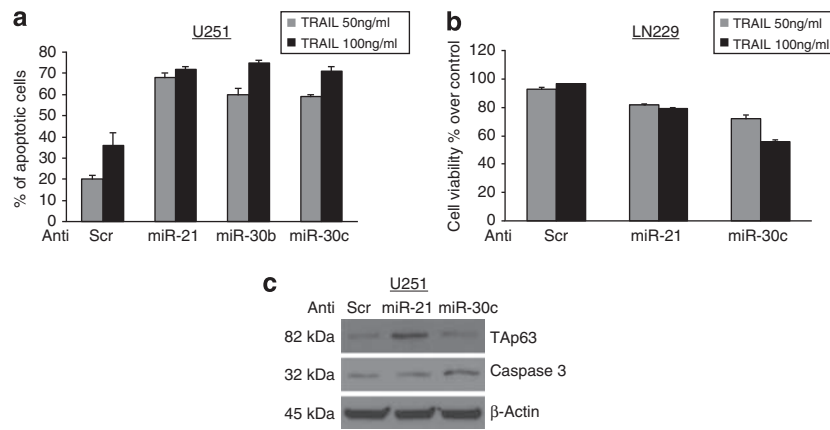


Figure 3. Effects of anti-miR-21 and anti-miR-30b/c on TRAIL sensitivity. Knock down of miR-21 and anti-miR-30b/c increases the percentage of apoptotic cells as assessed by propidium iodide staining in U251 cells (**a**) and decreases the cell viability of LN229 (**b**). (**c**) Tap63 and caspase-3 western blot analysis of U251 cells transfected with a scrambled sequence as negative control and with anti-miR-21 or anti-miR-30c, as indicated.

decrease in the levels of other caspases upon miR-30c transfection (Figure 4b). On the contrary, Tap63 and caspase-3 protein levels increased upon anti-miR-21 and anti-miR-30c transfection (Figure 3c and Supplementary Figure 3D) in TRAIL-resistant cell lines. To verify a direct link between the miR-21/Tap63 and miR-30b/c and caspase-3, we performed luciferase assay by co-transfecting pGL3-3' untranslated region (UTR) vectors along with miR-21 or miR-30c. The results obtained indicated a direct interaction of miR-21 with Tap63 and miR-30c with caspase-3 (Figure 4d). As indicated in Figure 4d, miR-30b and -30c have the same seed sequence that recognizes caspase-3, differing only at the latest four nucleotides of the 5'. Therefore, miR-30b down-regulates caspase-3 at the same extent than miR-30c (data not shown). Deletions in seed complementary sites rescued the repression of miR-21 and miR-30c on their identified targets (Figure 4d).

Validation of miR-21 and miR-30b/c mechanisms of action

To demonstrate that miR-21 and miR-30b/c, by downregulating Tap63 and caspase-3, are responsible for the TRAIL resistance observed in T98G and LN18 cells, we transfected T98G with

caspase-3 or Tap63 complementary DNAs lacking the miRNA-binding site in their 3'UTR or with a control vector and miR-30c (Figure 5a) or miR-21 (Figure 5b). Interestingly, transfection of Tap63 and caspase-3 was able to overcome the effects of miR-21 and miR-30c, decreasing cell viability and increasing apoptosis (Figures 5a and b). The data were confirmed by colony assay in T98G cells (Supplementary Figures 2A and B). Similar results were obtained when we analyzed miR-30b (data not shown). These rescue experiments proved the causative link between miR-21/Tap63 and caspase-3/miR-30b/c and TRAIL sensitivity.

Effect of miR-21 and miR-30c expression on TRAIL sensitivity in primary human glioma cell lines

MiR-21 and miR-30c expression levels were measured by qRT-PCR in nine different human primary cell lines (Figure 6a), eight derived from glioblastoma tumors (patient no. 1 to no. 8) and one from tissue surrounding the tumor (patient no. 9), and compared with TRAIL sensitivity. As shown in Figure 6b, TRAIL sensitivity correlated with miR-21 and miR-30c expression levels in all cases analyzed, with the exception of control sample that did not respond to TRAIL. Moreover, anti-miRs expression in TRAIL-

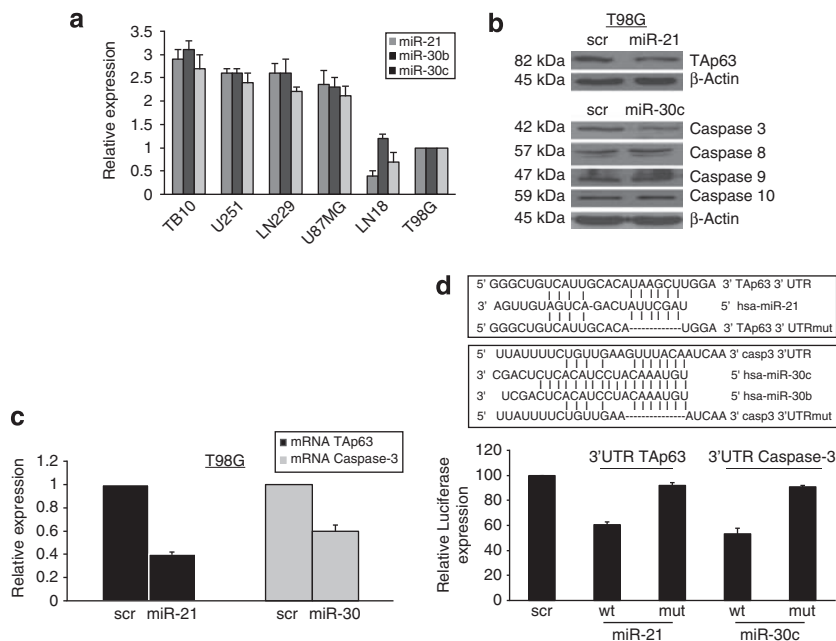


Figure 4. TAp63 and caspase-3 are targets of miR-21 and miR-30c. **(a)** qRT-PCR expression of miR-21, miR-30c and miR-30b in TB10, LN229, U251, U87MG, LN18 and T98G glioma cells. **(b)** TAp63 and caspase-3, caspase-8, caspase-9 and caspase-10 western blot analysis of T98G cells transfected with a scrambled sequence as negative control and with miR-21 and miR-30c, as indicated. **(c)** qRT-PCR of TAp63 and caspase-3 mRNA in T98G transfected with a negative control and with miR-21 and miR-30c, as indicated. **(d)** Alignment between miR-21 and 3'UTR TAp63 wild type or mutant and between miR-30c and 3'UTR caspase-3 wild type or mutant. Luciferase activity of PGL3-3'UTR TAp63 and of PGL3-3'UTR caspase-3 vector after HEK-293 transfection with scrambled miR, miR-21 and miR-30c wild type or mutated, as indicated.

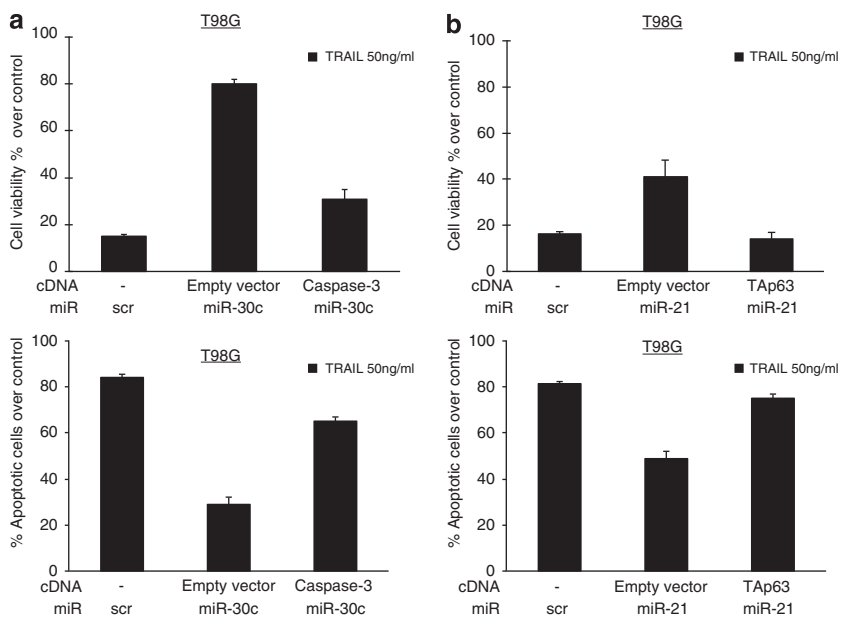


Figure 5. Validation of the involvement of caspase-3 and TAp63 in TRAIL sensitivity. Cell viability assay (upper panels) and propidium iodide staining (lower panels) of T98G cells transfected with miR-30c **(a)** and miR-21 **(b)** in the presence of cDNA for caspase-3 or TAp63.

resistant primary cultured cells (patient no. 1 and no. 2) was able to determine an increase of TRAIL sensitivity (Figure 6c) and concomitantly an increase of the levels of TAp63 and caspase-3 (Figure 6d).

DISCUSSION

Sensitization of cancer cells to apoptosis could be a valuable strategy to define new treatment options for cancer, in particular

when using agents that aim to directly activate apoptotic pathways. A promising agent is the death receptor ligand TRAIL,¹⁹ as it induces apoptosis in most cancer cells, but not in normal cells.^{20,21} Moreover, TRAIL exhibits potent tumoricidal activity *in vivo* in several xenograft models, including malignant glioma.^{22,23} Indeed, agonistic anti-TRAIL receptor monoclonal antibodies (mAbs), including mapatumumab (HGS-ETR1, anti-human DR4 mAb),²⁴ lexatumumab (HGS-ETR2, anti-human DR5 mAb)²⁵ and MD5-1 (anti-mouse DR5 mAb) are currently under

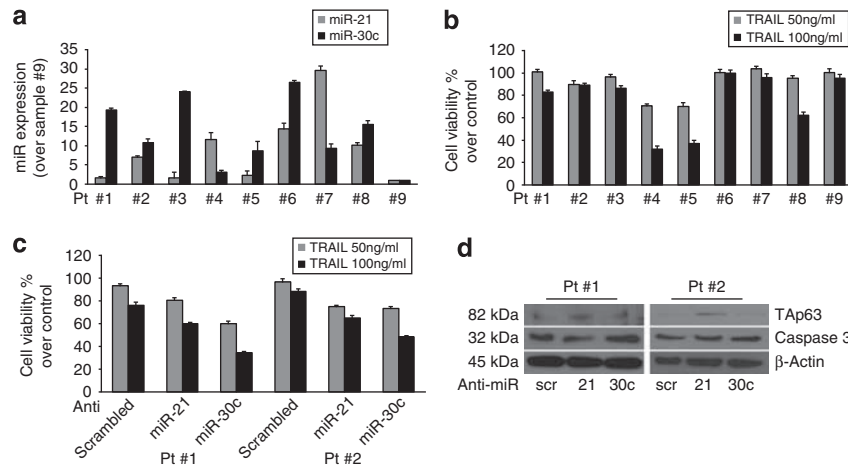


Figure 6. Effect of miR-21 and 30c on primary glioblastoma cell lines. **(a)** qRT-PCR analysis of miR-21 and miR-30c levels in eight primary glioblastoma cancer cell lines and one primary cell line derived from the surrounding tumor tissue used as control. **(b)** TRAIL sensitivity of primary cell lines (10^4 cells) treated with two different doses of SuperKiller TRAIL for 24 h, as indicated. **(c)** Cell viability assay of glioblastoma cells from two patients (#1 and #2) transfected with anti-miR-21 and anti-miR-30c and then treated with 50 ng/ml and 100 ng/ml of TRAIL for 24 h. Anti-miRs treatment sensitized glioblastoma cells to TRAIL. **(d)** Western blot analysis of TAp63 and caspase-3 after anti-miR-21 and anti-miR-30c transfection in patient #1 and #2.

intensive investigation. The former two mAbs have been tested in phase 1 clinical trials in patients with systemic malignancy, exhibiting excellent safety profiles. Anti-mouse DR5 mAb MD5-1 could also be administered safely without inducing hepatotoxicity either alone or in combination with histone deacetylase inhibitors in mice.²⁶ The induction of apoptosis by TRAIL is essentially dependent on the expression of specific TRAIL receptors and on the activation of caspases,²⁰ thus the regulation of the expression levels of those molecules is of fundamental importance.

MicroRNAs are emerging as key regulators of multiple pathways involved in cancer development and progression,^{27–29} and may become the next targeted therapy in glioma. The present study shows that microRNA expression may modulate TRAIL-induced apoptosis in glioma cells, by the regulation of caspase-3 and TAp63 levels. We analyzed the miRs profile of TRAIL-resistant compared with TRAIL-sensitive glioma cells. We then focused our attention on miR-30b/c and miR-21, as only these miRs among those identified by the array, demonstrated the ability to revert the TRAIL-sensitive phenotype. We also provided evidences that this regulation is not restricted to glioma, but it is present also in a different type of cancer such as NSCLC.

MiR-21 has been found overexpressed in high-grade glioma patients³⁰ and studies have identified different miR-21 key targets for glioma biology, such as *RECK*, *TIMP3*, *Spry2* and *Pdcd4* genes, which are suppressors of malignancy and inhibitors of matrix metalloproteinase.^{16,31–33} Moreover, levels of expression of miR-21 have been associated to patients survival.³⁴

Other studies indicate that knockdown of miR-21 in cultured glioblastoma cells triggers activation of caspases and leads to increased apoptotic cell death.³⁵ Corsten *et al.*³⁶ hypothesized that suppression of miR-21 might sensitize gliomas for cytotoxic tumor therapy. With the use of locked nucleic acid (LNA)-anti-miR-21 oligonucleotides and neural precursor cells (NPC) expressing a secretable variant of TRAIL (S-TRAIL), they showed that the combined suppression of miR-21 and NPC-S-TRAIL leads to a synergistic increase in caspase activity and a decreased cell viability in human glioma cells *in vitro* and *in vivo* in xenograft experiments. Interestingly, Papagiannakopoulos *et al.*¹⁵ described that miR-21 targets multiple important components of the p53 tumor-suppressive pathways. They showed that downregulation of miR-21 in glioblastoma cells leads to repression of growth,

increased apoptosis and cell cycle arrest, through the regulation of target proteins such as HNRPK and TAp63. Our study describes for the first time the direct link between miR-21, TAp63 and TRAIL sensitivity. We demonstrated that miR-21 targets the 3'UTR sequence of TAp63, and that transfection of miR-21 is able to downregulate TAp63 at both mRNA and protein levels. More importantly, we demonstrated that miR-21, through TAp63, is able to modulate TRAIL sensitivity, as the co-transfection of miR-21 and TAp63 cDNA renders the cells again responsive to TRAIL. TAp63 is a transcription factor that regulates the expression levels of different apoptosis-regulating genes, such as TRAIL receptors, bcl211 and Apaf1.¹⁸ Thus, it is possible that those apoptosis-regulating molecules are regulated by miR-21 through TAp63.

Several studies link miR-30 to apoptosis and human cancer. Li *et al.*³⁷ demonstrated that miR-30 family members inhibited mitochondrial fission through the suppression of the expression of p53 and its downstream target Drp1, whereas, Joglekar *et al.*³⁸ demonstrated that miR-30 may have a role in epithelial-to-mesenchymal transition. Our recent data demonstrate that miR-30 targets the anti-apoptotic protein BIM, participating to gefitinib resistance in lung cancer.³⁹ MiR-30 has been also associated with stem cell properties. Yu *et al.*⁴⁰ described that miR-30 is reduced in breast tumor stem cells (BT-ICs), and demonstrated that enforced expression of miR-30 in BT-ICs inhibits their self-renewal capacity by reducing Ubc9, and induces apoptosis through silencing ITGB3. In our hands, miR-30 overexpression inhibits TRAIL-induced apoptosis in glioma cells by targeting caspase-3. In fact, modulating the expression of either miR-30 or caspase-3, we observed a modification of TRAIL sensitivity of glioma cells. The opposing results on the role of miR-30 on cell death may be ascribed either to different cell system (breast vs glioma), or to different type of cancer cell (stem vs differentiated cells). In favour of this hypothesis, many reports describe opposing role of miRs in a different cell context.²⁸ Recently, miR-30d has been described to target caspase-3 in breast cancer cells, and thus to regulate apoptosis.⁴¹ The seed sequence recognizing the 3'UTR of caspase-3 is highly homologous within the members of the miR-30 family (miR-30b/c/d) suggesting a more generalized role of miR-30 family members in the regulation of cell death and cancer progression.

In many experiments, we observed that there is a redundancy within miR-21 and miR-30 in the regulation of TRAIL sensitivity. Our data, either in primary or in established cell lines, demonstrates that it is sufficient that one of the two miRs is highly expressed in the cells, that apoptosis resistance will manifest. We have also observed that miR-30 has a predominant effect in contrasting TRAIL-induced apoptosis. This may be related to the effect of this miR in targeting one important component of the cell death machinery, that is, caspase-3.

In conclusion, our study analyzed microRNA expression pattern in TRAIL-resistant and TRAIL-sensitive glioma cells, and identified specific miRs and their targets involved in the regulation of the apoptotic programme. This may be of relevance for future cancer therapy improvement in glioma.

MATERIALS AND METHODS

Cell culture and transfection

U87MG, T98G, U251, TB10, CALU-1 and 293 cells were grown in Dulbecco's modified Eagle's medium (DMEM). H460 were grown in RPMI. Media were supplemented with 10% heat-inactivated fetal bovine serum, 2 mM L-glutamine and 100 U/ml penicillin/streptomycin. LN229 and LN18 were grown in Advanced DMEM (Invitrogen, Milan Italy) + 2 mM Glutamine + 5% fetal bovine serum. For miRs transient transfection, cells at 50% confluency were transfected using Oligofectamine (Invitrogen) with 100 nM of pre-miR-30c, -30b, -125b, -146b, -181a, -21, miR-scrambled or anti-miR- (Applied Biosystems, Milan, Italy). For caspase-3 and TAp63 transient transfection, cells were transfected using Lipofectamine and Plus Reagent with 4 µg of caspase-3 cDNA (Origene, Rockville, MD, USA) or TAp63 cDNA for 24 h. TAp63 cDNA was obtained from Professor Viola Calabrò (Naples). SuperKiller TRAIL for cell treatment was purchased from Enzo Biochem (New York, NY, USA).

Primary cell cultures

Glioblastoma specimens were collected at neurosurgical Unit of Cardarelli hospital (Naples). All the samples were collected according to a prior consent of the donor before the collection, acquisition or use of human tissue. To obtain the cells, samples were mechanically disaggregated, then the lysates were grown in DMEM-F12 medium supplemented with 10% fetal bovine serum 1% penicillin streptomycin and 20 ng/ml EGF (Sigma-Aldrich, Milan, Italy). To exclude a fibroblast contamination, cells were stained for GFAP, a protein found in glial cells.

Protein isolation and western blotting

Cells were washed twice in ice-cold phosphate-buffered saline, and lysed in JS buffer (50 mM HEPES pH 7.5 containing 150 mM NaCl, 1% Glycerol, 1% Triton X-100, 1.5 mM MgCl₂, 5 mM EGTA, 1 mM Na₃VO₄ and 1 × protease inhibitor cocktail). Protein concentration was determined by the Bradford assay (Bio-Rad, Milan, Italy) using bovine serum albumin as the standard, and equal amounts of proteins were analyzed by SDS-PAGE (12.5% acrylamide). Gels were electroblotted onto nitrocellulose membranes (Millipore, Bedford, MA, USA). For immunoblot experiments, membranes were blocked for 1 h with 5% non-fat dry milk in Tris-buffered saline containing 0.1% Tween-20, and incubated at 4 °C over night with primary antibody. Detection was performed by peroxidase-conjugated secondary antibodies using the enhanced chemiluminescence system (GE Healthcare, Milan, Italy). Primary antibodies used were: anti-βActin from Sigma-Aldrich; anti-caspase-8, 9 and 10 were from Cell Signalling Technology (Boston, MA, USA); anti-Caspase 3 and anti-TAp63 from Santa Cruz Biotechnologies (Santa Cruz, CA, USA).

miRNA microarray experiments

From each sample, 5 µg of total RNA (from T98G, LN18, TB10, LN229 cells) was reverse transcribed using biotin-end-labelled random-octamer oligonucleotide primer. Hybridization of biotin-labelled cDNA was performed on an Ohio State University custom miRNA microarray chip (OSU_CCC version 3.0), which contains 1150 miRNA probes, including 326 human and 249 mouse miRNA genes, spotted in duplicates. The hybridized chips were washed and processed to detect biotin-containing transcripts by streptavidin-Alexa647 conjugate and scanned on an Axon 4000B microarray scanner (Axon Instruments, Sunnyvale, CA, USA).

Raw data were normalized and analyzed with GENESPRING 7.2 software (zcomSilicon Genetics, Redwood City, CA, USA). Expression data were median-centered by using both the GENESPRING normalization option and the global median normalization of the BIOCONDUCTOR package (www.bioconductor.org) with similar results. Statistical comparisons were done by using the GENESPRING ANOVA tool, predictive analysis of microarray and the significance analysis of microarray software (<http://www-stat.stanford.edu/~tibs/SAM/index.html>).

RNA extraction and real-time PCR

Total RNAs (miRNA and mRNA) were extracted using Trizol (Invitrogen) according to the manufacturer's protocol. Reverse transcription of total miRNA was performed starting from equal amounts of total RNA per sample (1 µg) using miScript reverse Transcription Kit (Qiagen, Milan, Italy), for mRNAs SuperScript III Reverse Transcriptase (Invitrogen) was used. For cultured cells, quantitative analysis of Caspase-3, TAp63, β-Actin (as an internal reference), miR-30b/c, miR-21 and RNU5A (as an internal reference) were performed by real-time PCR using specific primers (Qiagen), miScript SYBR Green PCR Kit (Qiagen) and iQ SYBR Green Supermix (Bio-Rad), respectively. The reaction for detection of mRNAs was performed as follow: 95 °C for 15', 40 cycles of 94 °C for 15', 60 °C for 30' and 72 °C for 30'. The reaction for detection of miRNAs was performed as follow: 95 °C for 15', 40 cycles of 94 °C for 15', 55 °C for 30' and 70 °C for 30'. All reactions were run in triplicate. The threshold cycle (CT) is defined as the fractional cycle number at which the fluorescence passes the fixed threshold. For relative quantization, the 2^(-ΔCT) method was used as previously described.⁴² Experiments were carried out in triplicate for each data point, and data analysis was performed by using software (Bio-Rad).

Northern blot analysis

RNA samples (30 µg) were separated by electrophoresis on 15% acrylamide, 7 mol/l urea gels (Bio-Rad, Hercules, CA, USA) and transferred onto Hybond-N+ membrane (Amersham Biosciences, Piscataway, NJ, USA). Hybridization was performed at 37 °C in 7% SDS/0.2 mol/l Na₂PO₄ (pH 7.0) for 16 h. Membranes were washed at 42 °C, twice with 2 × standard saline phosphate (0.18 mol/l NaCl/10 mmol/l phosphate (pH 7.4)), 1 mmol/l EDTA (saline-sodium phosphate-EDTA; SSPE) and 0.1% SDS and twice with 0.5 × SSPE/0.1% SDS. The oligonucleotides (PRIMM, Milan, Italy) used, complementary to the sequences of the mature miRNAs, were: miR-21-probe 5'-TCAACATCAGTCTGATAAGCTA-3'; miR-30c-probe 5'-GCTGAG AGTGTAGGATGTTTACA-3'. An oligonucleotide complementary to the U6 RNA (5'-GCAGGGCCATGCTAATCTTCTCTGTATCG-3') was used to normalize the expression levels. Totally, 100 pmol of each probe were end labelled with 50 mCi [³²P]ATP using the poly-nucleotide kinase (Roche, Basel, Switzerland). Blots were stripped by boiling in 0.1% SDS for 10 min before re-hybridization.

Luciferase assay

The 3' UTR of the human Caspase-3 genes was PCR amplified using the following primers: Caspase-3 forward: 5'-TCTAGAAGGGCGCCATCGCCAAG TAAGAAA-3', Caspase-3 reverse: 5'-TCTAGACCCGTGAAATGTCACTGA CAG-3' and cloned downstream of the Renilla luciferase stop codon in pGL3 control vector (Promega, Milan, Italy). A deletion was introduced into the miRNA-binding sites by using the QuikChange Mutagenesis Kit (Stratagene, La Jolla, CA, USA) using the following primers: Caspase-3 mut forward 5'-GCAAAATCTTAAGTATGTTATTTCTGTTGAAATCAAAGGA AAATAGTAATGTTTATACT-3'. Caspase-3mut reverse 5'-AGTATAAAACAT TACTATTTTCCTTTGATTTCAACAGAAAATAACATACTTAAGAATTTTGC-3'.

The 3' UTR of the human TAp63 gene was PCR amplified using the following primers: TAp63 forward: 5'-TCTAGAGCAAGAGATAAGTCTTT CATGGCTGCTG-3', TAp63 reverse: 5'-TCTAGATGGAAATCCCACTATCCCA AG-3', and cloned downstream of the Renilla luciferase stop codon in pGL3 control vector (Promega). A deletion was introduced into the miRNA-binding sites by using the QuikChange Mutagenesis Kit (Stratagene) using the following primers: TAp63 mut forward 5'-CTGGTCAAGGGCTGTCATTG CACTCCATTTAATTT-3' TAp63 mut reverse 5'-AAATTAATGGAGTGCAT GACGCCCTTGACCAG-3'.

Hek-293 cells were cotransfected with 1.2 µg of generated plasmid and 400 µg of a Renilla luciferase expression construct pRL-TK (Promega) with Lipofectamine 2000 (Invitrogen). Cells were harvested 24 h post transfection and assayed with Dual Luciferase Assay (Promega) according to the

manufacturer's instructions. Three independent experiments were performed in triplicate.

Cell death quantification

Cells were plated in 96-well plates in triplicate, stimulated and incubated at 37 °C in a 5% CO₂ incubator. SuperKiller TRAIL was used at final concentration of 50 or 100 ng/ml for 24 h. Apoptosis was analyzed via propidium iodide incorporation in permeabilized cells by flow cytometry. The cells (2×10^5) were washed in phosphate-buffered saline and resuspended in 200 µl of a solution containing 0.1% sodium citrate, 0.1% Triton X-100 and 50 µg/ml propidium iodide (Sigma). Following incubation at 4 °C for 30 min in the dark, nuclei were analyzed with a Becton Dickinson FACScan flow cytometer (Becton Dickinson, Milan, Italy). Cellular debris was excluded from analyses by raising the forward scatter threshold, and the DNA content of the nuclei was registered on a logarithmic scale. The percentage of elements in the hypodiploid region was calculated. Cell viability was evaluated with the CellTiter 96 AQueous One Solution Cell Proliferation Assay (Promega) according to the manufacturer's protocol. Metabolically active cells were detected by adding 20 µl of MTS to each well. After 2 h of incubation, the plates were analyzed in a Multilabel Counter (BioTek, Milan, Italy).

Colony assay

Cells were transfected with miR-scrambled, miR-30b/c or miR-21 for 24 h, then were harvested and 2.4×10^4 cells were plated in six-well plates. After 24 h, cells were treated with 50 or 100 ng/ml of superKiller TRAIL for 24 h, as indicated. Cells were transferred to 100 mm dishes and let grown for 6 days. Finally, the cells were coloured with 0.1% crystal violet dissolved in 25% methanol for 20 min at 4 °C. Dishes were washed with water and then let dry on the bench, and then photographs were taken.

ACKNOWLEDGEMENTS

This work was partially supported by funds from Associazione Italiana Ricerca sul Cancro, AIRC to GC (grant n.ro 10620), and MERIT (RBNE08E8CZ_002) to GC. CQ and MI are supported by the 'Federazione Italiana Ricerca sul Cancro' (FIRC) Post-Doctoral Research Fellowship. GR is supported by a MERIT project Fellowship.

REFERENCES

- 1 Tran B, Rosenthal MA. Survival comparison between glioblastoma multiforme and other incurable cancers. *J Clin Neurosci* 2010; **17**: 417–421.
- 2 Purow B, Schiff D. Advances in the genetics of glioblastoma: are we reaching critical mass? *Nat Rev Neurol* 2009; **5**: 419–426.
- 3 Schaefer U, Voloshanenko O, Willen D, Walczak H. TRAIL: a multifunctional cytokine. *Front Biosci* 2007; **12**: 3813–3824.
- 4 Falschlehner C, Emmerich CH, Gerlach B, Walczak H. TRAIL signalling: Decisions between life and death. *Int J Biochem Cell Biol* 2007; **39**: 1462–1475.
- 5 Younes A, Vose JM, Zelenetz AD, Smith MR, Burris HA, Ansell SM *et al*. A Phase 1b/2 trial of mapatumumab in patients with relapsed/refractory non-Hodgkin's lymphoma. *Br J Cancer* 2010; **103**: 1783–1787.
- 6 Trarbach T, Moehler M, Heinemann V, Kohne CH, Przyborek M, Schulz C *et al*. Phase II trial of mapatumumab, a fully human agonistic monoclonal antibody that targets and activates the tumour necrosis factor apoptosis-inducing ligand receptor-1 (TRAIL-R1), in patients with refractory colorectal cancer. *Br J Cancer* 2010; **102**: 506–512.
- 7 Garofalo M, Romano G, Quintavalle C, Romano MF, Chiurazzi F, Zanca C *et al*. Selective inhibition of PED protein expression sensitizes B-cell chronic lymphocytic leukaemia cells to TRAIL-induced apoptosis. *Int J Cancer* 2007; **120**: 1215–1222.
- 8 Zanca C, Garofalo M, Quintavalle C, Romano G, Acunzo M, Ragno P *et al*. PED is overexpressed and mediates TRAIL resistance in human non-small cell lung cancer. *J Cell Mol Med* 2008; **12**: 2416–2426.
- 9 Quintavalle C, Incoronato M, Puca L, Acunzo M, Zanca C, Romano G *et al*. c-FLIPL enhances anti-apoptotic Akt functions by modulation of Gsk3β activity. *Cell Death Differ* 2010; **17**: 1908–1916.
- 10 Calin GA, Croce CM. MicroRNA signatures in human cancers. *Nat Rev Cancer* 2006; **6**: 857–866.
- 11 Croce CM. Causes and consequences of microRNA dysregulation in cancer. *Nat Rev Genet* 2009; **10**: 704–714.
- 12 Garofalo M, Di Leva G, Romano G, Nuovo G, Suh SS, Ngankea A *et al*. miR-221 & 222 regulate TRAIL resistance and enhance tumorigenicity through PTEN and TIMP3 downregulation. *Cancer Cell* 2009; **16**: 498–509.

- 13 Garofalo M, Quintavalle C, Di Leva G, Zanca C, Romano G, Taccioli C *et al*. MicroRNA signatures of TRAIL resistance in human non-small cell lung cancer. *Oncogene* 2008; **27**: 3845–3855.
- 14 Incoronato M, Garofalo M, Urso L, Romano G, Quintavalle C, Zanca C *et al*. miR-212 increases tumor necrosis factor-related apoptosis-inducing ligand sensitivity in non-small cell lung cancer by targeting the antiapoptotic protein PED. *Cancer Res* 2010; **70**: 3638–3646.
- 15 Papagiannakopoulos T, Shapiro A, Kosik KS. MicroRNA-21 targets a network of key tumor-suppressive pathways in glioblastoma cells. *Cancer Res* 2008; **68**: 8164–8172.
- 16 Gaur AB, Holbeck SL, Colburn NH, Israel MA. Downregulation of Pdc4 by mir-21 facilitates glioblastoma proliferation *in vivo*. *Neuro-Oncology* 2011; **13**: 580–590.
- 17 Zhu S, Si M-L, Wu H, Mo Y-Y. MicroRNA-21 Targets the Tumor Suppressor Gene Tropomyosin 1 (TPM1). *J Biol Chem* 2007; **282**: 14328–14336.
- 18 Gressner O, Schilling T, Lorenz K, Schulze Schleithoff E, Koch A, Schulze-Bergkamen H *et al*. TAP63[alpha] induces apoptosis by activating signaling via death receptors and mitochondria. *EMBO J* 2005; **24**: 2458–2471.
- 19 Nagane M, Huang HJS, Cavenee WK. The potential of TRAIL for cancer chemotherapy. *Apoptosis* 2001; **6**: 191–197.
- 20 Gonzalez F, Ashkenazi A. New insights into apoptosis signaling by Apo2L/TRAIL. *Oncogene* 2010; **29**: 4752–4765.
- 21 Walczak H, Bouchon A, Stahl H, Krammer PH. Tumor necrosis factor-related apoptosis-inducing ligand retains its apoptosis-inducing capacity on Bcl-2- or Bcl-xL-overexpressing chemotherapy-resistant tumor cells. *Cancer Res* 2000; **60**: 3051–3057.
- 22 Balyasnikova IV, Ferguson SD, Han Y, Liu F, Lesniak MS. Therapeutic effect of neural stem cells expressing TRAIL and bortezomib in mice with glioma xenografts. *Cancer Lett* 2011; **310**: 148–159.
- 23 Unterkircher T, Cristofanon S, Vellanki SHK, Nonnenmacher L, Karpel-Massler G, Wirtz CR *et al*. Bortezomib primes glioblastoma, including glioblastoma stem cells, for TRAIL by increasing tBid stability and mitochondrial apoptosis. *Clin Cancer Res* 2011; **17**: 4019–4030.
- 24 Chuntharapai A, Dodge K, Grimmer K, Schroeder K, Marsters SA, Koepfen H *et al*. Isotype-dependent inhibition of tumor growth *in vivo* by monoclonal antibodies to death receptor 4. *J Immunol* 2001; **166**: 4891–4898.
- 25 Plummer R, Attard G, Pacey S, Li L, Razak A, Perrett R *et al*. Phase 1 and pharmacokinetic study of lexatumumab in patients with advanced cancers. *Clin Cancer Res* 2007; **13**: 6187–6194.
- 26 Ichikawa K, Liu W, Zhao L, Wang Z, Liu D, Ohtsuka T *et al*. Tumoricidal activity of a novel anti-human DR5 monoclonal antibody without hepatocyte cytotoxicity. *Nat Med* 2001; **7**: 954–960.
- 27 Garofalo M, Condorelli G, Croce CM. MicroRNAs in diseases and drug response. *Curr Opin Pharmacol* 2008; **8**: 661–667.
- 28 Garofalo M, Quintavalle C, Romano G, Croce CM, Condorelli G. miR221/222 in cancer: their role in tumor progression and response to therapy. *Curr Mol Med* 2012; **12**: 27–33.
- 29 Garofalo M, Condorelli GL, Croce CM, Condorelli G. MicroRNAs as regulators of death receptors signaling. *Cell Death Differ* 2010; **17**: 200–208.
- 30 Malzkorn B, Wolter M, Liesenberg F, Grzendowski M, Stühler K, Meyer HE *et al*. Identification and functional characterization of microRNAs involved in the malignant progression of gliomas. *Brain Pathol* 2009; **20**: 539–550.
- 31 Gabriely G, Wurdinger T, Kesari S, Esau CC, Burchard J, Linsley PS *et al*. MicroRNA 21 promotes glioma invasion by targeting matrix metalloproteinase regulators. *Mol Cell Biol* 2008; **28**: 5369–5380.
- 32 Kwak HJ, Kim YJ, Chun KR, Woo YM, Park SJ, Jeong JA *et al*. Downregulation of Spry2 by miR-21 triggers malignancy in human gliomas. *Oncogene* 2011; **30**: 2433–2442.
- 33 Moore LM, Zhang W. Targeting miR-21 in glioma: a small RNA with big potential. *Expert Opin Therap Targets* 2010; **14**: 1247–1257.
- 34 Lakomy R, Sana J, Hankeova S, Fadrus P, Kren L, Lzicarova E *et al*. miR-195, miR-196b, miR-181c, miR-21 expression levels and O-6-methylguanine-DNA methyltransferase methylation status are associated with clinical outcome in glioblastoma patients. *Cancer Sci* 2011; **102**: 2186–2190.
- 35 Chan JA, Krichevsky AM, Kosik KS. MicroRNA-21 is an antiapoptotic factor in human glioblastoma cells. *Cancer Res* 2005; **65**: 6029–6033.
- 36 Corsten MF, Miranda R, Kasmieh R, Krichevsky AM, Weissleder R, Shah K. MicroRNA-21 knockdown disrupts glioma growth *in vivo* and displays synergistic cytotoxicity with neural precursor cell delivered S-TRAIL in human gliomas. *Cancer Res* 2007; **67**: 8994–9000.
- 37 Li J, Donath S, Li Y, Qin D, Prabhakar BS, Li P. miR-30 regulates mitochondrial fission through targeting p53 and the dynamin-related protein-1 pathway. *PLoS Genet* 2010; **6**: e1000795.
- 38 Joglekar MV, Patil D, Joglekar VM, Rao GV, Reddy ND, Mitnala S *et al*. The miR-30 family microRNAs confer epithelial phenotype to human pancreatic cells. *Islets* 2009; **1**: 137–147.

- 39 Garofalo M, Romano G, Di Leva G, Nuovo G, Jeon Y-J, Ngankea A *et al*. EGFR and MET receptor tyrosine kinase-altered microRNA expression induces tumorigenesis and gefitinib resistance in lung cancers. *Nat Med* 2011; **18**: 74–82.
- 40 Yu F, Deng H, Yao H, Liu Q, Su F, Song E. Mir-30 reduction maintains self-renewal and inhibits apoptosis in breast tumor-initiating cells. *Oncogene* 2010; **29**: 4194–4204.
- 41 Li N, Kaur S, Greshock J, Lassus H, Zhong X, Wang Y *et al*. A combined array-based comparative genomic hybridization and functional library screening approach identifies mir-30d as an oncomir in cancer. *Cancer Res* 2011; **72**: 154–164.
- 42 Livak KJ, Schmittgen TD. Analysis of relative gene expression data using real-time quantitative PCR and the $2^{-\Delta\Delta C(T)}$ Method. *Methods* 2001; **25**: 402–408.

Supplementary Information accompanies the paper on the Oncogene website (<http://www.nature.com/onc>)

Electrochemical detection of miRNA-222 by use of a magnetic bead-based bioassay

Francesca Bettazzi · Ezat Hamid-Asl ·
Carla Lucia Esposito · Cristina Quintavalle ·
Nello Formisano · Serena Laschi · Silvia Catuogno ·
Margherita Iaboni · Giovanna Marrazza ·
Marco Mascini · Laura Cerchia · Vittorio De Franciscis ·
Gerolama Condorelli · Ilaria Palchetti

Received: 6 July 2012 / Revised: 18 September 2012 / Accepted: 2 October 2012 / Published online: 26 October 2012
© Springer-Verlag Berlin Heidelberg 2012

Abstract MicroRNAs (miRNAs, miRs) are naturally occurring small RNAs (approximately 22 nucleotides in length) that have critical functions in a variety of biological processes, including tumorigenesis. They are an important target for detection technology for future medical diagnostics. In this paper we report an electrochemical method for miRNA detection based on paramagnetic beads and enzyme amplification. In particular, miR 222 was chosen as model sequence, because of its involvement in brain, lung, and liver cancers. The

proposed bioassay is based on biotinylated DNA capture probes immobilized on streptavidin-coated paramagnetic beads. Total RNA was extracted from the cell sample, enriched for small RNA, biotinylated, and then hybridized with the capture probe on the beads. The beads were then incubated with streptavidin–alkaline phosphatase and exposed to the appropriate enzymatic substrate. The product of the enzymatic reaction was electrochemically monitored. The assay was finally tested with a compact microfluidic device which enables multiplexed analysis of eight different samples with a detection limit of 7 pmol L⁻¹ and RSD=15 %. RNA samples from non-small-cell lung cancer and glioblastoma cell lines were also analyzed.

Published in the special issue *Analytical Science in Italy* with guest editor Aldo Roda.

F. Bettazzi · E. Hamid-Asl · S. Laschi · G. Marrazza ·
M. Mascini · I. Palchetti (✉)
Dipartimento di Chimica “Ugo Schiff”,
Università degli Studi di Firenze,
Via della Lastruccia 3,
50019 Sesto Fiorentino (Fi), Italy
e-mail: ilaria.palchetti@unifi.it

C. L. Esposito · L. Cerchia · V. De Franciscis
Istituto di Endocrinologia e Oncologia Sperimentale, CNR,
80138 Napoli, Italy

C. Quintavalle · N. Formisano · S. Catuogno · M. Iaboni ·
G. Condorelli
Dipartimento di Biologia e Patologia Cellulare e Molecolare,
Università degli Studi di Napoli Federico II,
80138 Napoli, Italy

E. Hamid-Asl
Department of Analytical Chemistry,
Faculty of Chemistry, University of Mazandran,
Babolsar, Iran

S. Catuogno · G. Condorelli
Dipartimento di Biologia e Patologia Cellulare e Molecolare,
Università degli Studi di Napoli Federico II and Istituto di
Endocrinologia e Oncologia Sperimentale, CNR,
80138 Napoli, Italy

Keywords MicroRNA · Magnetic beads · Electrochemical assay · miRNA-222

Introduction

MicroRNAs (miRNAs, miRs) are naturally occurring small RNAs (approximately 22 nucleotides in length) that act as regulators of protein translation. Because many diseases are caused by the misregulated activity of proteins, miRNAs have also been implicated in a number of diseases including different kinds of cancer [1], heart disease [2], and immunological and neurological diseases [3–5]. Expression of miRNAs controls a number of physiological and pathological responses [6, 7]. Consequently, miRNAs are intensely studied as candidates for diagnostic and prognostic biomarkers. Moreover, the ability to selectively regulate protein activity through miRNAs could enable treatment of many forms of cancer [8] and other serious illness. Standardized methods for detection of miRNAs, all relying on hybridization [9], are northern blotting, microarray, and real-time PCR (RT-PCR).

Biosensors are emerging options for miRNA detection [10–16]. Electrochemistry is regarded as one of the most appealing techniques in term of cost, ease of operation and automation. Recently, some examples of sensitive electrochemical miRNA biosensing have been reported in the literature [17–26]. Pohlmann and Sprinzl [24] used a four-component hybridization assay for sensitive and specific detection of miR 16 based on an enzymatic electrochemical signal; the detection limit was 2 pmol L^{-1} . The crucial feature of this method was the generation of base stacking between immobilized capture DNA, miRNA, a complementary RNA probe, and the enzyme–DNA conjugate. An electrochemical sensing technique for miR 21 detection is reported in Ref. [25]; functionalized gold nanoparticles were used to increase the amount of enzymatic label on the electrode surface and thus the sensitivity of the method.

In all the references cited, however, the electrode surface was used both as solid support for the hybridization and as the surface for the electrochemical measurement.

Bead-based hybridization has the theoretical advantage that it might more closely approximate hybridization in solution [27–31]. Beads are disposable, which enables one to consider irreversible binding chemistry on bead surfaces for sensing with concomitant improvements in binding specificity. Moreover, magnetic beads enable easy separation and washing steps. Indeed, beads-based miRNA detection is both feasible and attractive because of its high speed and relatively low cost. Bead-based optical microarrays for miRNA analysis have been reported in the literature [29].

In this paper, two electrochemical methods based on paramagnetic beads for multiplexing miRNA detection are reported. In the first approach disposable screen-printed electrodes were used as transducers. Biotinylated DNA capture probes were immobilized on streptavidin-coated paramagnetic beads. Total RNA was extracted from the sample, enriched in the small fragments, biotinylated, and then hybridized with the beads. The beads were then incubated with streptavidin alkaline phosphatase (AP) and exposed to the enzymatic substrate (α -naphthyl phosphate). The product of the enzymatic reaction (α -naphthol) was electrochemically monitored by differential pulse voltammetry. To improve the analytical performance, this bead-based assay was also integrated into a microfluidic device. Microfluidic systems are well recognized for their ability to move small volumes of fluids through different processes and over a sensing surface.

The core of the system used in this study is an electrochemical chip containing eight polymer microchannels. The presence of microelectrodes in each channel enables direct quantification of the hybridization reaction by conducting eight electrochemical measurements in parallel. In this approach, magnetic beads are modified and hybridized with sample containing the target miRNA, as described above. They are introduced into the microchannel inlet of a chip, and accumulated on nearby electrode surfaces, by virtue of a magnetic holder positioned above

the microchannels. A solution of the enzymatic substrate (*p*-aminophenyl phosphate) is added for in-situ signal detection. After readout, the magnet array is flipped away, the beads are removed by addition of regeneration buffer, and the chip is ready for other assays. The detection step is particularly rapid, because the extent of the hybridization reaction is followed by real-time measurement of the AP enzyme kinetics, without the need to wait for a longer incubation time. High sensitivity can be achieved, because of the concentration of the product of the enzymatic reaction, which increases rapidly because of the small size of the microchannels.

Previously, we described a microfluidic-based electrochemical assay coupled to magnetic beads for analysis of DNA sequences of *Legionella pneumophila* [36]. Here, we apply the bead-based method for electrochemical detection of miRNAs and demonstrate the feasibility of the assay for sensitive and specific detection of synthetic miRNAs. In particular, we used the developed method for detection of miRNAs from lung and brain cancer cell lines known to express different levels of miR 222. miR 222 is markedly upregulated in aggressive non-small-cell lung cancer, hepatocarcinoma [6, 7, 33, 34], and glioblastoma–astrocytoma [35] cells, as compared with less invasive and/or normal brain, lung, and liver cells.

The experimental results obtained are discussed in the following sections.

Materials and methods

Reagents

Streptavidin–alkaline phosphatase-conjugated (strp-AP), α -naphthyl phosphate, diethanolamine, *d*-biotin, bovine serum albumin (BSA), diethyl pyrocarbonate (DEPC), 97 % by NMR, and polyoxyethylene-20-sorbitan monolaurate (Tween 20) were obtained from Sigma–Aldrich (Italy). Disodium hydrogen phosphate, potassium chloride, magnesium chloride, sodium chloride, Tris HCl, and EDTA were purchased from Merck (Italy). *p*-Aminophenyl phosphate was purchased from Diagnoswiss (Switzerland).

MilliQ-grade water was used throughout this work. DEPC was added to water. DEPC treatment of solutions is accomplished by adding 1 mL DEPC per liter of water, stirring overnight, autoclaving for 1 h to hydrolyze any remaining DEPC, and then passing the solution through a 0.2- μm RNase-free filter (Sarstedt, Germany). Dynabeads Myone streptavidin C1 10 mg mL^{-1} were purchased from Dynal Biotech (Milan, Italy).

Synthetic oligonucleotides were purchased from Eurofins MWG Operon (www.eurofinsdna.com). The sequences are reported below:

- Mature miRNA 222 (Target) sequence: 5'-AGC UAC AUC UGG CUA CUG GGU CUC-biotin TEG-3'

- Capture probe sequence: 5'-GAG ACC CAG TAG CCA GAT GTA GCT-biotin TEG-3'
- Non complementary sequence (a 16-mer sequence of miRNA-16): 5'-UAG CAG CAC GUA AAU A-biotin TEG-3'
- Three base mismatch sequence of miRNA 222 (mismatch): 5'-AGC UAC AUC UUC UUA CUG GGU CU-biotin TEG-3'
- Mature miRNA-221: 5'-AGC UAC AUU GUC UGC UGG GUU UC-biotin TEG-3'

The RNA pre-miR sequence was obtained by transcription with T7 polymerase of the PCR amplified sequence. RNA concentration was measured with NanoDrop (Thermo Scientific). The sequence:

- Pre-miRNA-222: 5' GCU GCU GGA AGG UGU AGG UAC CCU CAA UGG CUC AGU AGC CAG UGU AGA UCC UGU CUU UCG UAA UCA GCA GCU ACA UCU GGC UAC UGG GUC UCU GAU GGC AUC UUC UAG CU 3'

The compositions of the buffers are:

- PB-T: phosphate buffer 0.5 mol L⁻¹, pH 7.4, containing 0.05 % Tween 20
- DEA: diethanolamine 0.1 mol L⁻¹ pH 9.6, 0.1 mol L⁻¹ KCl, 1 mmol L⁻¹ MgCl₂, 0.05 % Tween 20
- 2×W&B (washing and binding buffer): 10 mmol L⁻¹ Tris HCl, 1 mmol L⁻¹ EDTA, 2.0 mol L⁻¹ NaCl, 0.05 % Tween 20
- 1×W&B (washing and binding buffer): 5 mmol L⁻¹ Tris HCl, 0.5 mmol L⁻¹ EDTA, 1.0 mol L⁻¹ NaCl, 0.05 % Tween 20
- Substrate buffer: 0.10 mol L⁻¹ 2-methylaminoethanol at pH 9 (recipe for 200 mL: 1.60 mL 2-methylaminoethanol and 81 mg magnesium chloride in distilled water)
- Regeneration solution: Diagnoswiss proprietary solution of dimethyl sulfoxide (Sigma–Aldrich)

Analytical method

Experimental conditions, for example beads modification, and hybridization and labeling conditions have already been optimized as described in our previous papers [36, 37]. In this paper, application of the method to real samples, and in particular to small miRNA sequences, and integration of the procedure in to a microfluidic device is presented (Fig. 1). The method is based on biotinylated DNA capture probes (CPs) immobilized on streptavidin-coated paramagnetic beads (Fig. 1a). Total RNA is extracted from the cell samples (Fig. 1b), enriched for small species and biotinylated, and then hybridized with the modified beads. The beads were then incubated with streptavidin alkaline phosphatase (AP) and exposed to α -naphthyl-phosphate (Fig. 1c). The product of

the enzymatic reaction was electrochemically monitored by use of a disposable screen-printed electrochemical cell (SPEC) (Fig. 1d). Moreover, a compact microfluidic device (Gravi-Cell), which enables multiplexed analysis of eight different samples, was tested (Fig. 1e). To perform the measurement with the Gravi-Cell, beads are passed through the microchannels of a suitable miniaturized chip and a magnet array is placed on the channels to block the functionalized beads along the embedded microelectrodes contained in each microchannel (Fig. 1f). The enzyme substrate is then added for in-situ signal detection. Upon readout, the magnet array is flipped away, the beads are removed by addition of regeneration buffer, and the so-regenerated chip is ready for further analysis [36].

Fitting of calibration curves was performed by use of Origin Software version 8.1.

Disposable screen-printed electrodes

The screen-printed electrochemical cell (SPEC) consists of a carbon working electrode, a carbon counter electrode, and a silver pseudoreference electrode. Materials and procedures used to screen-print the transducers and to couple the cell with a magnet (to collect the beads for the measurement) are described elsewhere [38, 39]. Electrochemical measurements were performed using a μ Autolab type II potentiostat/galvanostat with the GPES 4.9 software package (Ecochemie, The Netherlands). All potentials were referred to the Ag/AgCl screen-printed pseudo-reference electrode. All electrochemical experiments were carried out at room temperature (25 °C).

To perform electrochemical measurement using magnetic beads, SPECs were kept horizontal and a magnet holding block was placed on the bottom part of the electrode, to better localize the beads on to the working surface. A known volume of a solution containing the enzymatic substrate was then placed on the SPEC surface to close the electrochemical cell.

Biomodification of paramagnetic and streptavidin-coated beads

Functionalization with the biotinylated capture probe was carried out on aliquots of 0.1 mL, containing 10 mgmL⁻¹ beads. The beads were washed three times with 250 μ L 2×W&B buffer solution and re-suspended in 200 μ L of the same buffer. DEPC water (200 μ L) containing 5 μ mol L⁻¹ capture probe was added to the suspension of the beads. After incubation for 15 min with continuous mixing, the beads were washed three times with 1×W&B. Finally, modified beads were incubated for 30 min with 100 μ L of a 1 mmol L⁻¹ solution of biotin in 1×W&B, to block remaining streptavidin active sites on the probe-functionalized surface and thus prevent the undesired binding of other biotinylated oligonucleotides. The probe-modified and biotin-blocked beads were then

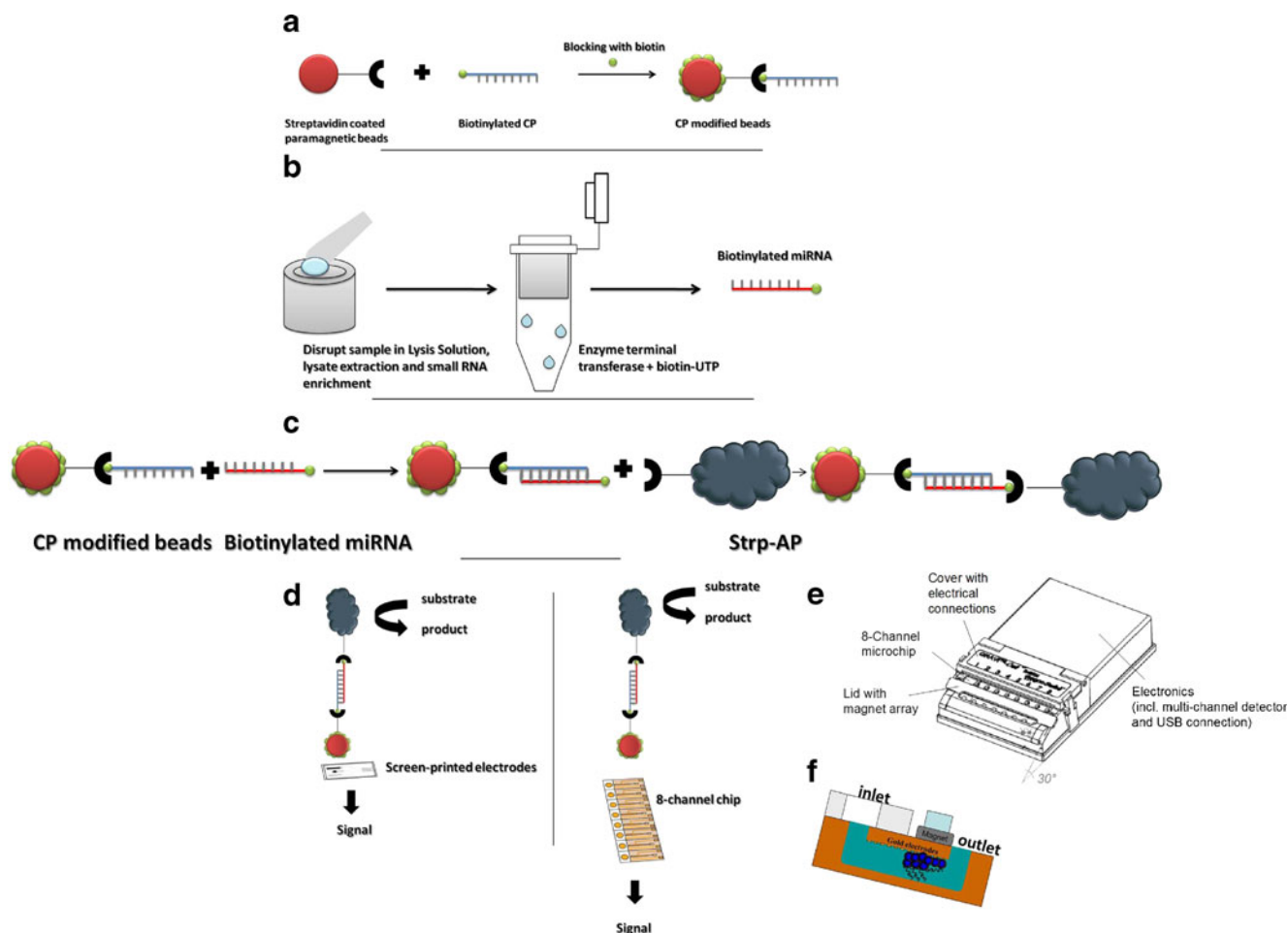


Fig. 1 Schematic diagram of the assay. **(a)** Biotinylated DNA capture probes are immobilized on streptavidin-coated magnetic beads. **(b)** Cell samples are lysed in a denaturing lysis solution. The total RNA is extracted from the lysate is purified and enriched in miRNAs. The enriched fraction is then terminal-conjugated with biotin using enzyme terminal transferase. **(c)** Probe-modified and biotin-blocked beads are incubated with the biotinylated miRNA targets (diluted to the desired concentration in PB-T). Both the blank and non-complementary

strands are used as negative controls. **(d)** The biotinylated hybrids are labeled with a streptavidin–alkaline phosphatase conjugate. The particles are then magnetically entrapped on to a screen-printed electrode. The substrate is added and the enzymatic product is measured by DPV. **(e)** The assay has also been integrated into a microfluidic device that enables multiplexed analysis. Reprinted with permission from Ref. [36]. **(f)** Schematic diagram of beads blocked within the microchannel, on the electrode surface, by the magnet

washed three times with $1\times$ W&B and re-suspended in $500\ \mu\text{L}$ $1\times$ W&B. Every aliquot, stored at $4\ ^\circ\text{C}$, can be used for several experiments.

Hybridization procedure

Biotinylated targets (oligonucleotides and samples) were diluted to the desired concentration in PB-T. Both the blank and non-complementary strands were used as negative controls. For every assay $20\ \mu\text{L}$ probe-modified beads was used. After magnetic separation of the beads, using a magnetic particle concentrator (MagneSphere Magnetic Separation Stand, Promega), the buffer was removed carefully and the beads were then incubated with $50\ \mu\text{L}$ of the target solution for 30 min. When real samples were analyzed, a thermal

denaturation procedure (5 min in boiling water and 1 min in ice bath) was used before hybridization. After hybridization, the beads were washed three times with $250\ \mu\text{L}$ DEA, to remove non-specifically adsorbed sequences.

After the hybridization and washing steps, beads were then incubated with $50\ \mu\text{L}$ of a solution containing $0.75\ \text{U mL}^{-1}$ streptavidin–alkaline conjugate and $10\ \text{mg mL}^{-1}$ BSA in DEA buffer. After 20 min beads were washed three times with $250\ \mu\text{L}$ DEA buffer. After washing, beads were re-suspended in $50\ \mu\text{L}$ DEA buffer.

Electrochemical measurement of miRNA using a SPEC

The electrochemical measurements were performed by placing the magnetic particles concentrator under the SPEC. The

bead suspension (10 μL) was deposited on the working electrode surface; the electrochemical cell was then covered with 60 μL of 1 mg mL^{-1} α -naphthyl phosphate in DEA buffer. After 5 min of incubation, the electrochemical signal of the enzymatically produced α -naphthol was measured by DPV.

Electrochemical measurements of mature miRNA using the microfluidic-based device

The Gravi-Cell (DiagnoSwiss, Monthey, Switzerland) microfluidic device was used. The Gravi-Cell is a USB powered, microfluidic-based immunoassay device for running bead procedures with standard immunology reagents. The instrument works with Gravi-Chip, a chip containing eight microchannels of ~ 300 nL volume with integrated gold microelectrodes. The main advantages of this device are that, because the fluidics are driven solely by natural forces, there are no serviceable pumps, tubes, or valves.

A highly detailed description of the system and its software control can be found elsewhere [36]. The procedure ends with the electrochemical detection step, in which the kinetics of the enzyme-label reaction are followed by real-time chronoamperometry, by measuring the current alternately on each channel and then reporting it vs. time [36]. The time evolution of the measured current follows Michaelis–Menten kinetics, so that the concentration of the target analyte is given by the current slope at the origin in the individual microchannels. The analytical signal is reported as the linear slope of the current (current per unit time) relative to analyte concentration. Once terminated, the program automatically applies a chip-regeneration procedure that must be followed by the user. The measured electrical current is directly linked to the concentration of the product of the enzyme reaction, and thus to the concentration of the enzyme and hence of the complex within the microchannels. Just after electrochemical measurements, the beads are released by removing the magnet array. Another advantage is that each Gravi-Chip can be regenerated for multiple uses. This can be achieved by washing the microchannels and reservoirs several times with the appropriate buffers. In this manner, the chip can be used for up to 100 analyses. For working with Gravi-Chip, some pretreatments are necessary. The microchannels should be wet three times by alternately filling the bottom and the upper reservoirs with ethanol and waiting each time for 30 s. The microchannels are then washed with washing buffer, by filling the upper and the bottom reservoirs and aspirating the solution with a pipette. The bottom reservoirs are then filled with 15 μL washing buffer before starting the experiment. This procedure enables wetting of the microchannels to ensure appropriate filling with aqueous solutions, and prevents air bubble formation that could partially block the fluid flows. To perform

the measurements the magnetic holder of the Gravi-Cell should be on; thus a 15- μL aliquot of modified beads is added simultaneously to each of the eight upper reservoirs of the chip, to accumulate the magnetic particles within the microchannels in the vicinity of the electrode surface. The beads flow down the microchannels for 4 min. The electrochemical detection step was finally carried out. To this end, 15 μL substrate buffer was introduced into the upper reservoirs and maintained for 30 s. Subsequently, 15 μL 12.0 mmol L^{-1} *p*-aminophenyl phosphate (pAPP) solution (in this approach the electrochemical substrate for detection by use of AP) prepared in the substrate buffer was dispensed in the upper reservoirs and removed after 20 s. This step was repeated once again, and electrochemical detection of the enzymatic reaction product starts. Finally, the regeneration procedure for reusing the Gravi chip is performed. For this step, 10 μL regeneration solution is dispensed into the top reservoirs.

Sample preparation for analysis with the electrochemical method

Cell culture

Human non-small-cell lung cancer Calu 1 cell line, and glioblastoma U87MG and T98G cell lines were grown in Dulbecco's modified Eagle medium (DMEM). Human non-small-cell lung cancer H460 cell line was grown in Roswell Park Memorial Institute medium (RPMI). Both media were supplemented with 10 % heat-inactivated fetal bovine serum (FBS) with 2 mmol L^{-1} L-glutamine and 100 U mL^{-1} penicillin–streptomycin.

RNA extraction

Total RNA was extracted with Trizol Reagent in accordance with the manufacturer's instructions (Invitrogen), while RNA enriched in small molecules was obtained with the *mir*Vana miRNA isolation kit in accordance with the manufacturer's instructions (Applied Biosystems). RNA concentration was measured with NanoDrop (Thermo Scientific).

RNA ligation: procedure and control

Total RNA or RNA enriched in small molecules (200 pmol) was terminal conjugated with biotin with 400 $\text{U } \mu\text{L}^{-1}$ of the enzyme terminal transferase (Roche) in accordance with the manufacturer's procedure.

RT-PCR procedure for mature miRNA analysis

Total RNAs (miRNA and mRNA) were extracted using Trizol (Invitrogen) in accordance with the manufacturer's procedure. Reverse transcription of total miRNA was performed starting from equal amounts of total RNA/sample (1 μg) using the

miScript reverse transcription kit (Qiagen). For cultured cells, quantitative analysis of miR 222 and RNA-U6B (as an internal control of the measurement [40]) were performed by real-time PCR with specific primers (Qiagen) with miScript SYBR green qPCR kit (Qiagen). The reaction for detection of miRNAs was performed as follow: 95 °C for 15 min, 40 cycles of 94 °C for 15 s, 55 °C for 30 s, and 70 °C for 30 s. All reactions were run in triplicate. The threshold cycle (CT) is defined as the fractional cycle number at which the fluorescence passes the fixed threshold. For relative quantification the $2^{(-\Delta CT)}$ method was used as described elsewhere [40]. Experiments were performed in triplicate for each data point, and data analysis was performed by use of software (Bio-Rad).

Results and discussion

Calibration curves of mature miRNA

To test the sensitivity and analytical performance of the assay and to check reliability of the chosen capture probe, a calibration experiment was designed using a synthetic biotinylated miRNA target. The results are reported in Fig. 2. The DPV response increased with the target concentration up to 50 nmol L⁻¹. Detection limits, calculated considering the slope of the linear portion of the calibration curve in the range 0–1 nmol L⁻¹ ($y=3 \times 10^{-6}x+2 \times 10^{-7}$, $r^2=0.995$), and fitting to the respective linear equation the mean of the blank solution response plus three times its standard deviation, were found to be 12 pmol L⁻¹. The reproducibility of the analysis, calculated as average RSD, was 9.6 % and the sensitivity was 3 μ A nmol⁻¹L. This detection limit is better than those of other electrochemical methods for miRNA detection [26].

The selectivity of the assay was monitored by use of two miRNA sequences (miR 16 and miR 221). As for miR 222,

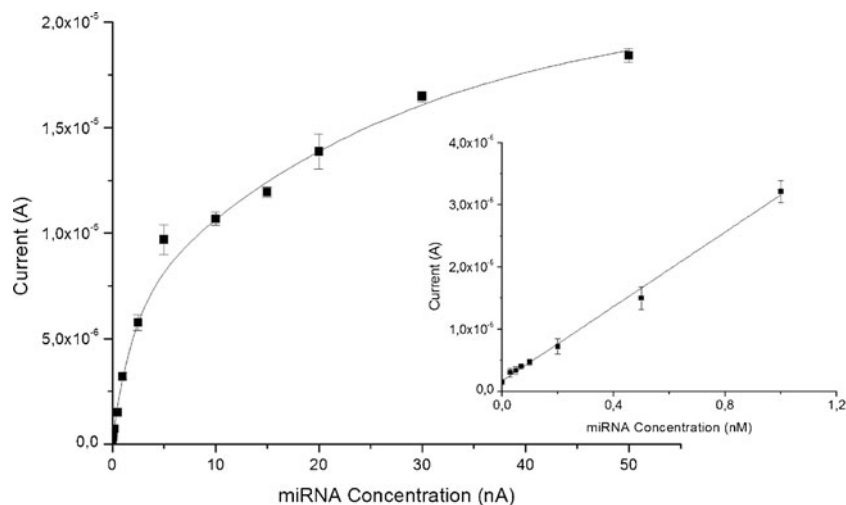
miR 16 is also associated with many tumors (i.e. it is deregulated in B-cell chronic lymphocytic leukemia). However, its sequence markedly differs from that of miR 222. It can, therefore, be regarded as a fully non-complementary sequence. In contrast, miR 221 is structurally closely related to miR 222, and both are frequently overexpressed in human malignancies.

To further test the selectivity, a synthetic sequence (called “mismatch”) was designed with three central bases mismatched compared with miR 222. Thus, beads modified with miR 222 complementary CPs were incubated with different concentrations of miR 222, miR 16, mismatch, and miR 221. Results are reported in Fig. 3. The signal observed with the complementary sequence (miRNA-222) is always higher than that obtained with the other sequences, for all the concentrations tested. It should, moreover, be pointed out that the current signal for miR 16 (the fully non-complementary sequence) is of the same order of magnitude as that for the blank. Assuming the complementary hybridization efficiency is 100 %, the hybridization efficiency was approximately 30 % for miR 221 as compared with that of miR 222 (100 %), for all the concentrations tested.

The signals for the mismatch sequence were 24 %, 21 %, and 24 % of that for miR 222 (100 %) at 0.5, 1, and 2.5 nmol L⁻¹, respectively. Similar values of efficiency of discrimination between closely related and mismatch miRNA sequences have previously been reported for other electrochemical assays [23, 24]. Thus, these results demonstrated that the bioassay was able to discriminate complementary miR-222. Nevertheless, improvement of mismatch discrimination and thus of selectivity can possibly be achieved by introducing modified nucleotides (for example LNA) in the capture probe sequence [41].

Selectivity was also monitored versus pre-miR 222. Pre-miR 222 is the 110-oligonucleotide stem-loop precursor of mature miR 222, and thus contains the sequence of mature miR 222. We investigated the selectivity of the assay for mature miRNA

Fig. 2 Calibration curve for mature miR 222. Error bars are standard deviations from three replicates. Disposable screen-printed electrochemical cells were used as transducers. *Inset:* The calibration curve at the low concentration end



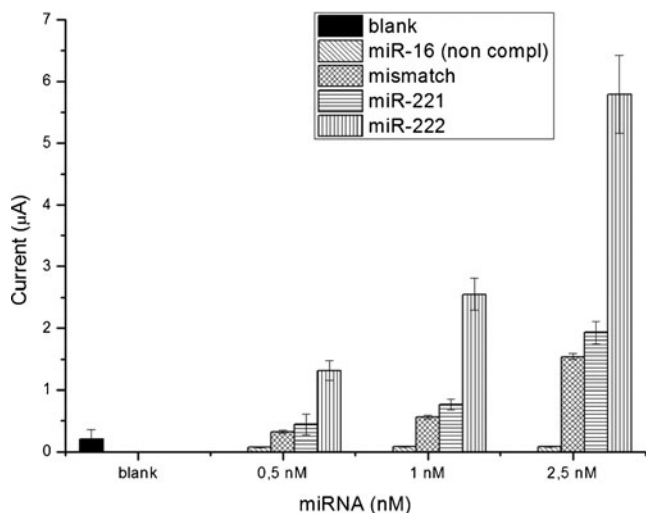


Fig. 3 Analysis of non-complementary (miR 16), miR 221, mismatch, and complementary (miR 222) sequences by use of miR 222 CP-modified beads. Error bars are standard deviations from three replicates. Disposable screen-printed electrochemical cells were used as transducer

by analyzing signal changes observed when beads were exposed to solution containing the pre-miRNA, the mature miRNA, and an equimolar mixture of both, as reported in Fig. 4. The DPV current signal of the pre-miRNA ($0.20 \pm 0.10 \mu\text{A}$) is only slightly different from that of the blank ($0.18 \pm 0.02 \mu\text{A}$); this could be related to non-specific adsorption. However the signal of mature miRNA ($0.99 \pm 0.11 \mu\text{A}$) is significantly higher than that of pre-miRNA, and when mixtures of miRNA-222 and pre-miRNA were analyzed the current signal ($1.0 \pm 0.1 \mu\text{A}$) was comparable with the electrochemical signal in the presence of miRNA-222 only.

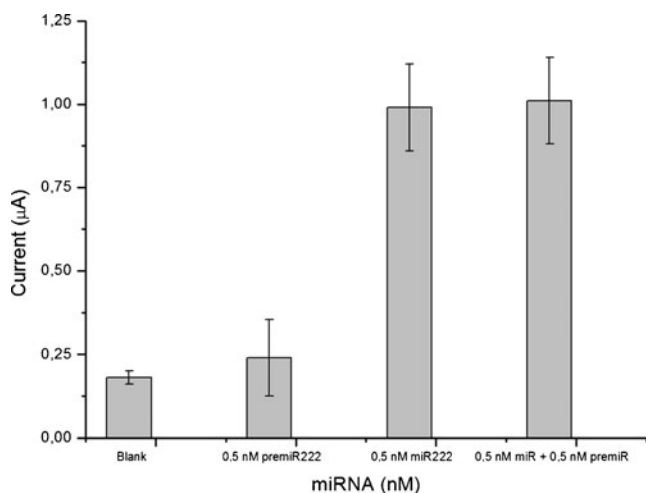


Fig. 4 Analysis of samples containing pre-miR 222, mature miR 222, and a equimolar mixture of 0.5 nmolL^{-1} pre-miR and 0.5 nmolL^{-1} mature miR 222, using miR 222 CP-modified beads. Error bars are standard deviations from three replicates. Disposable screen-printed electrochemical cells were used as transducer

Having confirmed the analytical performance for the miRNA target, the method was tested by using RNA samples extracted from cell lines. Levels of miRNA-222 have been shown to be increased in brain (glioblastoma), lung, and liver cancers [31–35]. For this reason the cell lines Calu 1, H460, U87MG, and T98G were studied. Calu1 and H460 cells are well-characterized non-small-cell lung cancer (NSCLC) cell lines and are regarded as an in-vitro model of lung cancer. In the literature [31–35], it is reported that miRNA-222 is overexpressed in Calu1, as compared with H460. Therefore, we used Calu1 cells to determine their levels of miRNA-222, and compared these levels with that for H460 cells. Similarly we tested the level of miRNA-222 in human U87MG glioblastoma-astrocytoma cells, which are known to express higher levels of miRNA-222 than human T98G glioblastoma cells [31–35].

Several independent samples of Calu1, H460, U87 MG, and T98G cells were evaluated for miRNA-222 levels by use of the electrochemical bioassay. The same samples were also analyzed by qRT-PCR. As reported in the “Materials and methods” section, total RNA was extracted from the cell sample, enriched for small RNA, ligated with biotin at the 3’ terminus (to introduce the enzymatic label), and then hybridized with the capture probe on the beads. The results of the electrochemical bioassay are shown in Fig. 5. For glioblastoma cells, the signal obtained for U87MG is higher than the signal obtained for T98G. Similarly, for NSCLC cells, Calu1 gave a signal higher than that obtained for the H460 cell line. In particular, a current increase of approximately twofold was observed for Calu1 and U87MG cells compared with H460

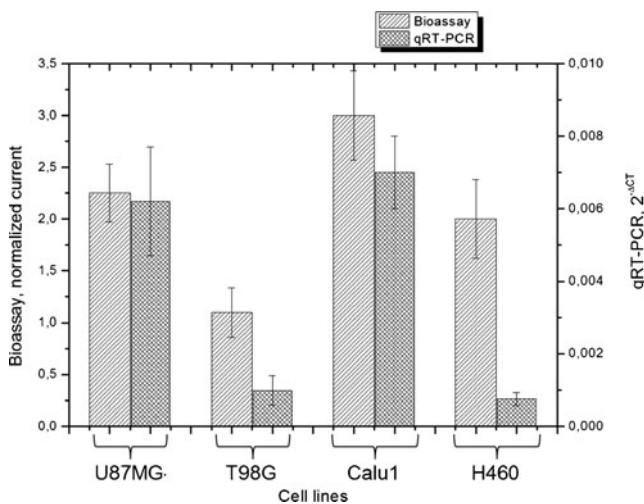


Fig. 5 Analysis of cell samples. The total RNA is extracted from U87MG and T98G glioblastoma cells and from Calu1 and H460 NSCLC cells. After extraction RNA was purified, enriched in small fragments and biotinylated in vitro. Before analysis, each sample was diluted 1:3 in PB-T containing CP-modified beads. Disposable screen-printed electrochemical cells were used as transducer. Error bars are standard deviations from three independent samples. The same samples were also analyzed by RT-PCR, which revealed that miR-222 is up-regulated in U87MG versus T98G cells and in Calu1 vs. H460 cells

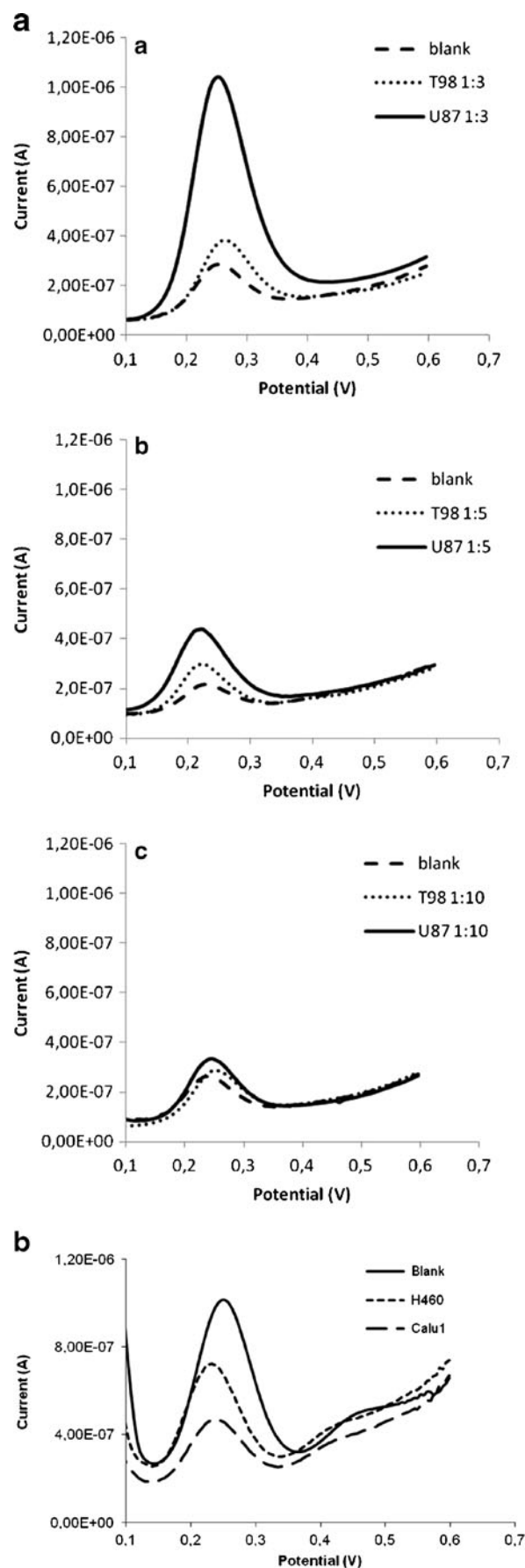
and T98G cells, respectively. The normalized current value reported in Fig. 5 is the ratio of the current signal for the sample to the current signal for the blank (in this way fluctuations of signal values because of enzymatic activity are controlled). The qRT-PCR results are also reported in Fig. 5. As can be seen, the relative threshold cycle (CT) values were reported. The CT is the cycle number at which the fluorescence associated with a particular amplicon crosses a threshold line [40]. To study the amount of an amplified target, the CT absolute value is not meaningful. CT values are only used in comparative methods when normalized to an endogenous reference (Δ CT) and relative to a calibrator sample [40]. By comparing the Δ CT for Calu1 with that for H460, it was confirmed that levels of the miRNA amplicons of Calu1 samples were higher than those for H460. qRT-PCR data also confirmed overexpression of miR-222 in U87MG samples compared with T98G.

Because of the limited dynamic range of the assay ($0.01\text{--}1\text{ nmol L}^{-1}$), multiple analyses of unknown RNA extracted from the cell samples at different dilutions were performed. The voltammetric profiles of the different dilutions of miRNA extracted from glioblastoma cells are reported in Fig. 6. The signals for both the glioblastoma cell lines decreased as the dilution factor was increased, with higher signals being obtained for a dilution of 1:3 (Fig. 6a). Decrease in current signal was observed for both cell lines, but it was more important for U87MG than for T98G. This is possibly because the T98G miRNA current signal is low and, on increasing the dilution factor, this current signal is leveled by the blank signal. The dilution factor 1:3 was also used to analyze Calu1 and H460 samples (Fig. 6b).

Analysis with the microfluidic device

The assay scheme was also integrated into a microfluidic device. The commercially available device used (Fig. 1e), combines a special chip containing eight polymer microchannels with a PC-controlled instrument. The presence of microelectrodes in each channel enables eight parallel electrochemical measurements. To perform the measurements, beads are passed through the microchannels of the chip and a magnet array is placed on the channels to block the functionalized beads along the embedded microelectrodes contained in each microchannel. The substrate is then added for chronoamperometric measurement of the enzyme kinetics. The eight channels were sequentially measured, each 2 s, at a potential of +250 mV vs. Ag/AgCl, for a total

Fig. 6 Voltammetric scans obtained from analysis of samples extracted from the cell lines. (a) U87MG and T98G glioblastoma cell lines at different dilutions. Before analysis each sample was diluted with PB-T. (a) dilution 1:3; (b) dilution 1:5; (c) dilution 1:10. Other conditions as reported in Fig. 5. (b) Calu1 and H460 cell lines at dilution 1:3. Other conditions as reported in Fig. 5



acquisition time of 90 s; in this way many measurement cycles are recorded, and a plot of current as a function of time is obtained for each channel. The slope of the linear portion of the plot is a direct measure of the *p*-aminophenol concentration and, hence, of the enzyme concentration.

The calibration curve, with the synthetic target, are reported in Fig. 7. The electrochemical response rapidly increased with increasing sample concentration up to 2.5 nmol L⁻¹ then decreased slowly; the trend observed could not be explained in terms of saturation of all available bead-immobilized capture probes. Future experiments will be devoted to better analysis of this behavior and extending the range of concentration analyzed at higher concentrations. The detection limit, calculated by considering the slope of the linear portion of the calibration curve in the range 0–1 nmol L⁻¹ ($y=0.4831x$, $r^2=0.998$) and fitting, with the respective linear equations, the mean of the blank solution response plus three times its standard deviation, was found to be 7 pmol L⁻¹, coupled with reproducibility of the analysis of 15 %, calculated as average RSD %, and sensitivity of 0.4831 nAs⁻¹nmol⁻¹L. This detection limit is even better than that obtained with the first approach based on screen-printed electrodes and DPV measurements.

RNA samples from the cell lines of glioblastoma and lung cancer were also tested (Fig. 8). In Fig. 8a are reported the current profiles vs. time for samples from the different cell lines. For the glioblastoma cells, the slope values obtained for U87MG are higher than the values obtained for T98G. Similarly, for NSCLC cells, the slope for Calu1 was steeper than that obtained for the H460 cell line. The slopes are reported in Fig. 8b. The expression levels measured with the microfluidic-based electrochemical assay confirmed that miR-222 is more highly expressed in Calu1 and U87MG cells than in H460 and T98G cells. It should, however, be noted that all the samples analyzed are independent samples and thus can express different levels of miRNA. Thus, the absolute value of analytical signal can

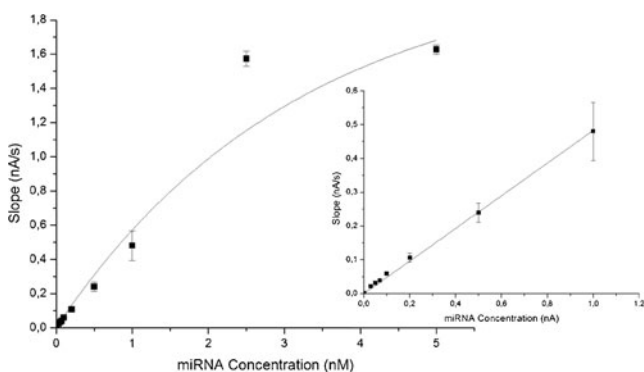


Fig. 7 Electrochemical detection using the Gravi-Cell microfluidic device—calibration curve for mature miR 222. *Error bars* are standard deviations from three experiments. *Inset*: the calibration curve at the low concentration end

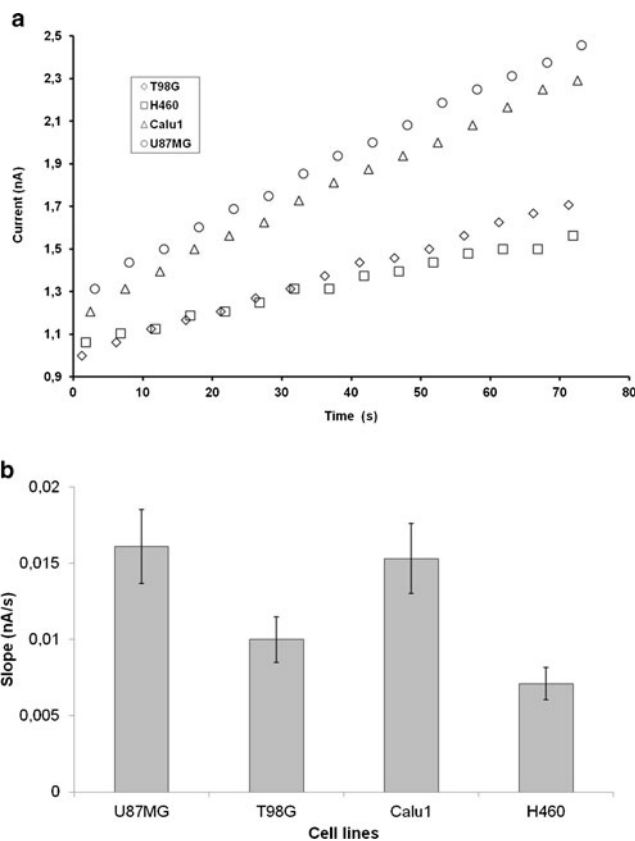


Fig. 8 Electrochemical analysis of the miRNAs extracted from cell samples using the Gravi-Cell microfluidic platform. After extraction, RNA was purified, enriched in small fragments, and biotinylated *in vitro*. Before analysis each sample was diluted 1:3 with PB-T. *Error bars* are standard deviations from three replicates on the same samples. **(a)** Chronoamperometric detection of enzyme kinetics in a chip for the different samples. Each *symbol* represents a single current acquisition value. Data were then processed using a fitting tool; for each channel a plot of current as a function of time was obtained. The slope of the linear portion of the plot, which is a direct measure of the *p*-aminophenol concentration, was used as analytical data. The chronoamperometric detection was performed at +250 mV vs. Ag/AgCl. **(b)** the corresponding analytical signal

vary among samples of the same cell line. Nevertheless, the behavior among U87G and T98 cells and among Calu1 and H460 is consistent.

Conclusions

Small non-coding RNA species, known as microRNAs, have critical functions in a variety of biological processes, including development, cell growth, differentiation, apoptosis, and tumorigenesis. Recent studies have revealed the value of miRNA expression patterns for diagnostic, prognostic, and therapeutic uses, thus heightening interest in miRNAs' potential as biomarkers of tumor development, progression, and chemosensitivity. Some unique features of miRNAs, for example their small total number and short length, have created

technical obstacles to direct application in a variety of procedures, leading to a need to develop novel methods designed to measure miRNA with high specificity and sensitivity.

The method reported in this paper is based on magnetic beads coupled to enzymatic amplification. The assay was also integrated into a compact, commercially available, microfluidic device. Given desktop dimensions and USB powering, the microfluidic device is highly portable. Its portability leads to a very interesting approach to monitoring miRNA expression profiles with eight samples processed simultaneously, in accordance with the concept of multiplexed point of care testing. The detection limit of the proposed method (7 pmol L^{-1}) was better than that in a recently published paper [26] or for those for other methods [17, 18, 24]. The results reported indicate the method can be used to discriminate among different cell lines which express different amounts of miRNA-222. Moreover, the method can be easily multiplexed—merely by using beads modified with different CPs and using the microfluidic device, analyses of eight different samples can be performed simultaneously. In our opinion this method is of promise for discriminating upregulated mature miRNA levels (i.e. in some human malignancies) from normal levels in cell samples.

References

- Calin GA, Croce CM (2006) *Nat Rev Cancer* 6:857–866
- Quintavalle C, Garofalo M, Croce CM, Condorelli G (2011) *Vascul Pharmacol* 55:87–91
- Luo X, Lin H, Pan Z, Xiao J, Zhang Y, Lu Y, Yang B, Wang Z (2008) *J Biol Chem* 283:20045–20052
- Lukiw WJ, Zhao Y, Cui JG (2008) *J Biol Chem* 283:31315–31322
- Xiao C, Rajewsky K (2009) *Cell* 136:26–36
- Garofalo M, Condorelli GL, Croce CM, Condorelli G (2009) *Cell Death Differ* 17:200–208
- Garofalo M, Condorelli G, Croce CM (2008) *Curr Opin Pharmacol* 8:661–667
- Zhang G, Wang Q, Xu R (2010) *Current Genomics* 11:311–325
- Cissell KA, Deo SK (2009) *Anal Bioanal Chem* 394:1109–1116
- Cissell KA, Rahimi Y, Shrestha S, Junt EA, Deo SK (2008) *Anal Chem* 80:2319–2325
- Cissell KA, Campbell S, Deo SK (2008) *Anal Bioanal Chem* 391:2577–2580
- Hartig JS, Grune I, Najafi-Shoushtari SH, Famulok M (2004) *J Am Chem Soc* 126:722–723
- Sipova H, Zhang S, Dudley AM, Galas D, Wang K, Homola J (2010) *Anal Chem* 82:10110–10115
- Fang S, Lee HJ, Wark AW, Corn RM (2006) *J Am Chem Soc* 128:14044–14046
- Min Lee J, Cho H, Jung Y (2010) *Angew Chem* 49:8662–8665
- Driskell JD, Seto AG, Jones LP, Jokela S, Dluhy RA, Zhao YP, Tripp RA (2008) *Biosens Bioelectron* 24:923–928
- Gao Z, Yu YH (2007) *Biosens Bioelectron* 22:933–940
- Gao Z, Yu YH (2007) *Sensor Actuator B* 121:552–559
- Fan Y, Chen X, Trigg AD, Tung C, Kong J, Gao Z (2007) *J Am Chem Soc* 129:5437–5443
- Peng Y, Gao Z (2011) *Anal Chem* 83:820–827
- Peng Y, Yi G, Gao Z (2010) *Chem Commun* 46:9131–9133
- Zhang GJ, Chua JH, Chee RE, Agarwal A, Wong S (2009) *Biosens Bioelectron* 24:2504–2508
- Yang H, Hui A, Pampalakis G, Soleymani L, Liu FF, Sargent EH, Kelley SO (2009) *Angew Chem* 48:8461–8464
- Pohlmann C, Sprinzl M (2010) *Anal Chem* 82:4434–4440
- Yin H, Zhou Y, Chen C, Zhu L, Ai S (2012) *Analyst* 137:1389–1395
- Lusi EA, Passamano M, Guarascio P, Scarpa A, Schiavo L (2009) *Anal Chem* 81:2819–2822
- Palecek E, Fojta M (2007) *Talanta* 74:276–290
- Wang J, Kawde A, Erdem A, Salzar M (2001) *Analyst* 126:2020–2024
- Lu J, Getz G, Miska EA, Alvarez-Saavedra E, Lamb J, Peck D, Sweet-Cordero A, Ebert BL, Mak RH, Ferrando AA, Jacks T, Horvitz HR, Golub TR (2005) *Nature* 435:834–838
- Wang B, Howel P, Bruheim S, Ju J, Owen LB, Fodstad O, Xi Y (2011) *PLoS ONE* 6(2): e17167
- Jin J, Cid M, Poole CB, McCreynolds LA (2010) *Biotechniques* 48:17–22
- Garofalo M, Quintavalle C, Di Leva G, Zanca C, Romano G, Taccioli C (2008) *Oncogene* 27:3845–3855
- Garofalo M, Di Leva G, Romano G, Nuovo G, Suh SS, Ngankee A (2009) *Cancer Cell* 16:498–509
- Garofalo M, Quintavalle C, Romano G, Croce CM, Condorelli G (2012) *Curr Mol Med* 12:27–33
- Quintavalle C, Garofalo M, Zanca C, Romano R, Iaboni M, DelBassoDeCaro M, Martinez-Montero JC, Incoronato M, Nuovo G, Croce CM, Condorelli G (2012) *Oncogene* 31:858–868
- Laschi S, Miranda-Castro R, González-Fernández E, Palchetti I, Raymond F, Rossier JS, Marrazza G (2010) *Electrophoresis* 31:1–10
- Laschi S, Palchetti I, Marrazza G, Mascini M (2009) *Bioelectrochemistry* 76:214–220
- Laschi S, Palchetti I, Marrazza G, Mascini M (2006) *J Electroanal Chem* 593:211–218
- Centi S, Silva E, Laschi S, Palchetti I, Mascini M (2007) *Anal Chim Acta* 594:9–16
- Livak KJ, Schmittgen TD (2001) *Methods* 25:402–408
- You Y, Moreira BG, Behlke MA, Owczarzy R (2006) *Nucleic Acids Res* 34:e60